REDUCED DENSITY MATRICES: DEVELOPMENT AND CHEMICAL APPLICATIONS

Mauricio Rodríguez Mayorga

Doctoral Thesis:

Reduced Density Matrices: Development and Chemical Applications.

Mauricio Antonio Rodríguez Mayorga

2018

Doctoral Programme in Chemistry

Supervised by: Dr. Eduard Matito i Gras and Prof. Miquel Solà Puig

Tutor: Prof. Miquel Solà Puig

Presented in partial fulfillment of the requirements for a doctoral degree from the University of Girona

Universitat de Girona

Dr. Eduard Matito i Gras and Prof. Dr. Miquel Solà Puig, from University of Girona,

WE DECLARE:

That this thesis entitled "Reduced density matrices: Development and Chemical Applications.", presented by Mauricio Rodríguez Mayorga to obtain the doctoral degree, has been completed under our supervision.

For all intents and purposes, we hereby sign this document.

Signature

Dr. Eduard Matito i Gras

Prof. Dr. Miquel Solà Puig

Girona, 25 June, 2018

"If then you do not make yourself equal to God, you cannot apprehend God; for like is known by like. Leap clear of all that is corporeal, and make yourself grown to a like expanse with that greatness which is beyond all measure; rise above all time and become eternal; then you will apprehend God. Think that for you too nothing is impossible; deem that you too are immortal, and that you are able to grasp all things in your thought, to know every craft and science; find your home in the haunts of every living creature; make yourself higher than all heights and lower than all depths; bring together in yourself all opposites of quality, heat and cold, dryness and fluidity; think that you are everywhere at once, on land, at sea, in heaven; think that you are not yet begotten, that you are in the womb, that you are young, that you are old, that you have died, that you are in the world beyond the grave; grasp in your thought all of this at once, all times and places, all substances and qualities and magnitudes together; then you can apprehend God.

But if you shut up your soul in your body, and abase yourself, and say 'I know nothing, I can do nothing; I am afraid of earth and sea, I cannot mount to heaven; I know not what I was, nor what I shall be,' then what have you to do with God?"- Hermes Trismegistus.

To GAOTU,

Acknowledgments

This thesis has been funded by Spanish MINECO Project No. CTQ2014-52525-P, the Basque Country Consolidated Group Project No. IT588-13 and specially by the doctoral grant FPU-2013/00176 from the Spanish Ministry of Educuation, Culture and Sports (MECD).

Además de los agradecimientos económicos, quiero agradecer a mis directores de tesis, Eduard Matito y Miquel Solà. Ha sido un gusto recorrer este camino con vosotros. Quiero agradeceros lo que he aprendido de vosotros científicamente y de la vida del investigador (hacer informes, montar proyectos, hacer clubs, preparar material para seminarios, etc). Siempre os habéis asegurado que vaya a conferencias y cursos de formación gracias a los que pude conocer a muchos colegas y a los grandes 'gurus' del campo (por no decir que también he conocido ciudades y países gracias a dichos viajes). Especialmente quiero agradecer a Eduard porque además de cargar con el día a día, fue un gran amigo que incluso intentó enseñarme lo que es una buena birra pero acabé bebiendo lámbicas...sorry :P! Incluyo aquí al Dr. Eloy Ramos-Cordoba, pues si bien es cierto que no figuras como un director, durante el primer año y medio casi fuiste uno, desde aquellos días en *Canpre* con las discusiones de cuadraturas (pidiendo comida al Multani) hasta nuestra invasión a Euksadi y las nuevas discusiones que surgieron sobre matrices de orden 2. ¡Gracias!

En segundo lugar quiero agradecer a mi familia: mi madre, mi padre y mi hermano. Siempre me han apoyado desde la elección de la carrera, para poder continuar la misma en Granada, para animarme durante la vida universitaria (y post-universitaria ahora), etc. ¡Muchas gracias! Y sabéis que mucha de esta tesis es vuestra.

En tercer lugar quiero agradecer a todos los maestros que me han enseñado sobre

ciencia (en especial sobre matemáticas, programación y cuántica). La lista es muy larga pero trataré de ponerlos a todos (ordenados cronológicamente): Jaime Cárdenas(Col. San José), Elard Gutierrez(UNSA), Dante Góngora(UNSA), Sergio Aquise(UNSA), Felix Cuadros(UNSA), José M. Sanchez Ruiz(UGR), Elvira Romera(UGR), Emilio San Fabián(UA), Antonio Ureña(UGR), Juan Carlos Angulo(UGR), Francisco Gálvez(UGR), David Peralta(UGR), Rosa Caballol(URV), Miquel Solà(UdG), Juan Carlos Paniagua(UB), Sergei Vyboishchikov(UdG), Jose Español(UNED) y Carlos Ferdandez(UNED).

Luego quiero agradecer a los compañeros del IQC/UdG con los que tuve placer de compartir despacho y buenas discusiones de ciencia y de la vida :). Agradecer a Marc, Yevhen, Sergi, Albert, Silvia, Ferran, Quim, Abril, Pedro, Josep Maria, Carme, Rafael Islas, Adrià, Luis (perroflauta), Ouissam y Vero (desde hace nada doctora). Así como a todos los amigos que hice en Girona del IQCC (extended version of IQC) como de fuera.

En enero del 2015 el Matito's group nos mudamos a Donostia (tres personas por ese entonces) y al primero que quiero agradecer por haberme hecho un hueco en su grupo de Kimika Teorikoa (KT) es al Prof. Jesus Ugalde, ¡Eskerrik asko! y ya sabes Jesus si necesitas sacudir a alguien me avisas :P. Quiero agradecer a los colegas del grupo KT por haberme recibido. Gracias a los que conocí al principio: Txema, Elena, Prof. Lopez, Txema, Txoni, Slawek, Jon I., David Casanova, Dr. Grande (mi gran amigo estos anõs en Donostia, compi de piso y colega de Ricky Pollo) y Jon Uranga (y a su cuadrilla, vaya findes de fiesta por parte vieja ¡Gracias Jon!). El grupo, cual gas en una habitación, sufrió los efectos de la termodinámica y se expandió. De esa expansión quiero agradecer a los "nuevos" miembros: Maru(también mi gran compi de piso), Olatz, Irene (y su horno XD), Ewa, Eli, Abel, Elisa, Telleria, Mikel (grumitos), Lanuza y Xiang. Así como los "anexionados" DIPC/CFM: Dani, Diego, Jorge, Cris, Sofi, Mikel$n$ ($n = 1, 2$), Raul(chileno), María y Alejandro (que la fuerza os acompañe a los dos últimos!).

Mario y Mitxe no me olvidé de vosotros, sólo que quiero hacerles un agradecimiento especial por ser grandes colaboradores y amigos! NOFT nos unió y gracias a ello os tendré para siempre muy alta estima ;) (pese a que no hay Fockiano, **que es funcional de la matriz de orden dos**, que si sólo recupera la nodinámica, etc. Al menos cumpliremos la P, la G y la Q). Mireia, si con alguien he tenido el *privilegio* de ensayar llevar a alguien es contigo, muchas gracias por permitirme ese honor (arigato gozaimasu). Sebastian, como sé que aprenderás español porque eres un tío "super listo", te agradezco en español mi gran amigo y colaborador. Que disfrutes mucho del doctorado, no te estreses y recuerda: siempre tortilla de patatas con cebolla.

Alors, c'est le moment remercie a mes amis de Strasbourg. Merci beaucoup Manu Fromager pour m'avoir accueilli dans votre group! Va être une experience incroyable avoir travaillé avec vous. Merci à Killian (qui m'a fait connaitre Claude François!), Laurent (qui m'a enseigné le model Hubbard et le 21 pour les shots) et Bruno (qui m'a aussi enseigné le model Hubbard, le ponch du Noël et les filles iraniennes). Aussi, je vais remercie à tout les membres du Laboratoire de Strasbourg!

También quiero agradecer a mis amigos de la Universidad de Granada, a los que visitaba en cada verano de vacaciones para recargar pilas. Especialmente a Sabri y a Lu (gracias Lu por mostrarme las comparsas que me han acompañado en la escritura). Así también quiero agradecer a los amigos del bar Pin Txop (donde comí mientras escribía la tesis).

Finalmente, creo que la tesis no hubiera sido lo mismo estos años si no la hubiera complementado con el Kendo (sino me hubiera vuelto loco creo). Por eso, quiero agradecer en primer lugar a mi sensei Jose Antonio Perez, a mi sempai Aitor, a mi gran amigo Luis (con el que nos hemos apuntado a todo curso), a Imanol (que hizo la cubierta de la tesis), a Mikel, a Borja, a Ibai, a Canino, a Yasushi, a

Naiara y a Hugo (que como dice un amigo, menos mal cuando crezcas ya estaré en arbitraje para no hacer ridículo contra ti). También a todos los compañeros con los que compartí este arte marcial en España y en Francia (en especial en Bayonne y en Strasbourg); este arte que me ha ayudado tanto a crecer como persona y que se ha reflejado en mi trabajo (i.e. en mi doctorado) y en mi vida. ¡Gracias!

Full list of publications

This thesis is presented as a compendium of publications.

Published and submitted articles included in the thesis :

1. Feixas F., Rodríguez-Mayorga M., Matito E., Solà M.; **Three-center bonding analyzed from correlated and uncorrelated third-order reduced density matrices.** *Comp. Theor. Chem.* 1053, 173 (2015) doi:10.1016/j.comptc.2014.09.030 (JCR Impact Factor= 1.549, SJR= 101/146 in Physical Chemistry, 3^{rd} quartile)

2. Rodríguez-Mayorga M., Ramos-Cordoba E., Salvador P., Solà M., Matito. E.; **Bonding description of the Harpoon Mechanism.** *Mol. Phys.* 114, 1345 (2016) doi:10.1080/00268976.2015.1121297 (JCR Impact Factor= 1.87, SJR= 17/36 in Physics, atomic, molecular and chemical, 2^{nd} quartile)

3. Mercero J.M., Mayorga-Rodríguez M., Matito E., Lopez X., Ugalde J.; **The Electron-pair Density Distribution of the $^{1,3}\Pi_u$ Excited States of H_2.** *Can. J. Chem.* 94, 998 (2016) doi:10.1139/cjc-2016-0203 (JCR Impact Factor= 1.08, SJR= 119/166 in Chemistry multidisciplinary, 3^{rd} quartile)

4. Rodríguez-Mayorga M., Ramos-Cordoba E., Feixas F., Matito E.; **Electron Correlation Effects in Third-Order Densities.** *Phys. Chem. Chem. Phys.* 19, 4522 (2017) doi:10.1039/C6CP07616E (JCR Impact Factor= 4.123, SJR= 6/36 in Physics, atomic, molecular and chemical, 1^{st} quartile)

5. Rodríguez-Mayorga M., Ramos-Cordoba E., Via-Nadal M., Piris M., Matito E.; **Comprehensive Benchmarking of Density Matrix Functional**

Approximations. *Phys. Chem. Chem. Phys.* 19, 24029 (2017) doi:10.1039/C7CP03349D (JCR Impact Factor= 4.123, SJR= 6/36 in Physics, atomic, molecular and chemical, 1^{st} quartile)

6. Rodríguez-Mayorga M., Via-Nadal M., Solà M., Ugalde J. M., Lopez X., Matito E.; **Electron-Pair Distribution in Chemical Bond Formation.** *J. Phys. Chem. A* 122, 1916 (2018) doi:10.1021/acs.jpca.7b12556 (JCR Impact Factor= 2.847, SJR= 13/36 in Physics, atomic, molecular and chemical, 2^{nd} quartile)

7. Rodríguez-Mayorga M., Ramos-Cordoba E., Lopez X., Solà M., Ugalde J., Matito. E.; **The Coulomb hole of the Ne atom.** (submitted) arXiv:1712.01789

Other published articles not included in the thesis :

8. Mitxelena I., Piris M., Rodríguez-Mayorga M.; **On the performance of Natural Orbital Functional Approximations in Hubbard Model.** *J. Phys. Condens. Matter.* 29, 425602 (2017) doi:10.1088/1361-648X/aa80ca (JCR Impact Factor= 2.678, SJR= 23/67 in Physics, condensed matter, 2^{nd} quartile)

9. Via-Nadal M., Rodriguez-Mayorga M., Matito E.; **A Salient Signature of van der Waals interactions.** *Phys. Rev. A* rapid comm. 96, 050501(R) (2017) doi:10.1103/PhysRevA.96.050501 (JCR Impact Factor= 2.925, SJR=11/36 in Physics, atomic, molecular and chemical, 2^{nd} quartile)

10. Mitxelena I., Rodríguez-Mayorga M., Piris M.; **Phase Dilemma in Natural Orbital Functional Theory from the N-representability Perspective.** *Eur. Phys. J. B* doi:10.1140/epjb/e2018-90078-8 (JCR Impact Factor= 1.436, SJR=45/67 in Physics, condensed matter, 3^{rd} quartile)

List of Abbreviations

Abbreviation	Description
E_{corr}	Correlation energy
HF	Hartree-Fock
CI	Configuration Interaction
FCI	Full-Configuration Interaction
CC	Coupled-cluster
CCSD	Coupled-cluster including only singles and doubles
CASSCF	Complete active space self consistent field
MP2	Second order Møller-Plesset perturbation theory
DFT	Density functional theory
RDM	Reduced density matrix
1-RDM	First order reduced density matrix
2-RDM	Second order reduced density matrix
3-RDM	Third order reduced density matrix
RDMFT	Reduced density matrix functional theory
2-PPD	Two-particle probability density
DI	Delocalization Index
QTAIM	Quantum Theory of Atoms in Molecules
TFVC	Topological Fuzzy Voronoi Cells
nc-ESI	n-center Electron Sharing Index
ELF	Electron Localization Function
CP	Conditional probability
IPD	Intracule Probability Density
FP	Fixed-Phases functional
MBB	Müller and Barends-Buijse functional
BBC2	Gritsenko, Pernal and Baerends functional
ML	Marques and Lathiotakis functional

MLSIC	Marques and Lathiotakis functional including self-interaction correction
CA	Csányi and Arias functional
CGA	Csányi, Goedecker and Arias functional
GU	Goedecker and Umrigar functional
F_L	Fermi level
PNOF	Piris natural orbital functional

List of Figures

List of Tables

Contents

Abstract

Quantum chemistry deals with the analysis of the electronic structure of molecules. Unfortunately, the exact electronic structure requires the solution of the Schrödinger equation, which can only be exactly solved for hydrogen atom. A practical solution of the Schrödinger equation is performed using finite basis sets and building approximated wavefunctions, which are optimized according to the variational principle. Another approach is based on the reformulation of the problem where instead of solving the Schrödinger equation, energy expressions in terms of reduced quantities (the electronic density and reduced density matrices) are assumed. Density functional theory is probably the most famous methodology within the last approach, where the reduced quantity used is the electronic density. Nevertheless, some other less familiar approaches can be found in the literature. Among these approximations, reduced density matrix functional theory and the Contracted Schrödinger equation are the genesis of the present thesis.

In the Contracted Schrödinger equation methodology up to fourth-order reduced density matrices are required for the computation of the electronic energy. Nevertheless, to reduce the computational cost high-order reduced density matrices are approximated from lower order ones. In this thesis, we have focused on the approximations suggested for the reconstruction of third-order reduced density matrices from the second- and first-order ones. There was not any exhaustive benchmark in the literature that focused on how electron correlation affects these approximations, thus we have developed it in order to improve the approximations suggested up to now. For the first study, we worked with the three-electron Harmonium atom (in the ^2P and ^4P states) and tuned correlation effects by playing with the ω parameter (i.e. with the confinement). In this study, we analyzed how electron correlation affects some properties with respect to the exact results. We have studied: a) electron sharing indexes, b)

N-representability conditions, and c) the sum rule, among others. Our study revealed that Valdemoro approximation is an excellent approximation for computing electron sharing indexes, but it was closely followed by the approximation suggested by Matito and coworkers. Secondly, we have seen that Fermi correlation seems to be easier to model than the Coulomb one (which is obviously much more convoluted). From this study, we have also gathered information about the importance of the Fermi level in the definition of σ_p phase factors of Nakatsuji and Mazziotti approximations. In our second study, we have also tested how well these approximations perform for the computation of electron sharing indexes in three-center two electrons and three-center four electron bonds. From the last study, we observed that Valdemoro and Matito and coworkers approximations provide the most accurate results when compared to the reference values.

In reduced density matrix functional theory, the energy expression is an explicit functional of the first-order reduced density matrix, and therefore the second-order reduced density needed for the computation of the Coulomb electron-electron interaction is reconstructed from the first-order one. Usually, the first-order reduced density matrix is taken in the diagonal representation, where the basis are the natural orbitals and the diagonal elements of the matrix are the natural orbital occupancies. In reduced density matrix functional theory the reconstructed second-order reduced density matrix elements are built as functions of the natural orbital occupancies. In the same spirit as we did for third-order reduced density matrices, we have studied how electron correlation affects these approximations. To that end, we have worked with the two-electron Harmonium atom in the ^1S state (the ground state) and tuned correlation effects by playing with the ω parameter. The benchmark that we have developed is based on the analysis of several properties of the reconstructed matrices, and provides new insights for the development of more robust approximations. In this study, we have also analyzed how electron correlation affects some properties, namely we have studied: a) delocalization index, b) N-representability condi-

tions, c) the sum rule, d) intracule probability densities, and e) the Coulomb electron-electron repulsion energy, among others. Our results have proven that the Fixed-Phases approximation is almost exact for any correlation regime, and only deviates from the exact result in the strong-correlation limit. In this study we have worked with PNOFi and JK-only approximations, where the latter only produce the second-order reduced density matrix elements which are accompanied by the Coulomb (J) or the exchange (K) integrals. We have also proven that PNOFi approximations perform better than JK-only approximations in the majority of tests (specially for the N-representablity conditions and the antisymmetry tests). We have also analyzed how some JK-only approximations produce unphysical elements for the reconstructed matrices that account for some properties (like the sum rule) but fail to many other properties (e.g. they introduce self-interaction errors). Besides, we have also proven that a self-interaction correction applied *a posteriori* is not the best way to avoid the introduction of unphysical elements (see the *Results and Discussions* section for more details). Finally, our results demonstrated that more robust approximations can be obtained by imposing as many conditions as possible from the beginning (i.e. in the construction of the approximation).

In this thesis, we have also worked with the radial intracule probability density obtained from the second-order reduced density matrix, actually, from the diagonal part of this matrix (i.e. the two-particle probability density). The two-particle probability density provides the probability density to find electron pairs, where one electron is placed at $\mathbf{r}_1$ and another is placed at $\mathbf{r}_2$, and it represents a 6D-function that cannot be reproduced in 2D or 3D plots unless some coordinates are fixed. The intracule coordinate $\mathbf{r}_{12} = \mathbf{r}_2 - \mathbf{r}_1$ allows us to fix some coordinates and gather some of the information contained in the two-particle probability density. The radial intracule probability density is obtained by selecting all possible pairs at a given interelectronic distance, $|\mathbf{r}_{12}|$, and after performing the spherical average. In this thesis, we have analyzed how the latter evolves during the bond dissociation/formation process of some diatomic

molecules. In our first study, we focused on $^{1,3}\Pi_u$ excited states of H_2. Tal and Katriel, and Colbourn found and reported the counterintuitive non-monotonic behavior of the electron repulsion energy in the $^3\Pi_u$ excited state of H_2 as a function of the internuclear separation. It was observed an increase of the V_{ee} at Hartree-Fock level, accompanied by a decrease of the $\langle r_{12} \rangle$, when the H-H bond is stretched; we have confirmed this effect using FCI calculations. From Hund's rule, the triplet should be much more stable than the singlet due to the reduction of repulsion as a consequence of the Pauli principle. We have observed that the electronic cloud is more compact for the triplet state and the screening of the external potential produced by the nuclei is less effective, thus the electron-nucleus attraction is much larger in this state than in the singlet. The larger electron-nucleus attraction obtained for the triplet state compensates the unexpected larger V_{ee} of the triplet state, and makes the triplet state more stable (in good agreement with Hund's rule). In our second study, we focused on the electron rearrangements that occur in the bond formation of some diatomic molecules. In this study, we analyzed the difference between the exact radial intracule probability density and the non-relaxed one. Our results provide a classification of the bonds in single and double bonds according to the profile obtained along the bond formation, and we could also observe the formation of electrons pairs in Li_2 between the electrons localized in the nuclei and the electron at the non-nuclear attractor. Unfortunately, it was impossible to track the harpoon mechanism followed by LiH, nevertheless, we could observe that a covalent bond profile is obtained at large interatomic distances whereas at small interatomic distances the ionic profile was recovered. In this work, we also suggested an approximation to the exact and usually expensive radial intracule probability density by using CCSD natural occupancies and the Müller or Buijse and Baerends approximation for the second-order reduced density matrix. This study demonstrated that the approximation suggested produces results comparable to the exact ones and reduces the computational cost. Lastly, we used the radial intracule probability density for the description of a shoulder observed in the Coulomb hole of Neon atom. We constructed a set of even-tempered

basis and used CISD calculations (that retrieved more than 95% of the electron correlation) to prove that the shoulder was not an artifact but a real effect produced by the electron correlation of the core electrons. We also proved in this work that there was not an important transfer of the electronic density between the K and L shells, which suggetss that there is only an electron rearrangement within the K shell that produces the shoulder observed.

Finally, in the last work of this thesis we have studied the harpoon mechanism, which is observed in gas phase for some molecules formed by atoms that present a small difference between ionization potential and the electron affinity. The Potential Energy Surface (PES) for molecules formed by the harpoon mechanism changes the character from covalent to ionic when the bond is formed, which occurs by means of an electron transfer. The change of character on the PES is very fast and, therefore, this mechanism presents an Avoided Crossing (AC) at the geometry where the electron transfer takes place. In this work, we used chemical descriptors applied to some diatomic molecules in an attempt to characterize this mechanism within the Born-Oppenheimer approximation. The set of diatomic molecules chosen for this study includes LiH, BH, BeH, LiF, CO, N_2, He_2, H_2 and F_2 (the last five species were taken as counterexamples). We have proven that the analysis of the atomic population is not enough to characterize this mechanism. Our study showed that only the delocalization index is able to recognize the harpoon mechanism (if we use Quantum Theory of Atoms in Molecules (QTAIM) or Topological Fuzzy Voronoi Cells (TFVC) atomic partitions). The electron localization function and the Laplacian of the electron density provided means to visualize the electron transfer that happens due to the harpoon mechanism. Actually, the scan of these quantities along the interatomic axis permits the visualization of the transfer. Finally, among the information theory quantities, only the Fisher informations (in position and momentum spaces) were able to distinguish between the systems that follow the harpoon mechanism and the other systems (only H_2 was incorrectly assigned by the Fisher informations as a system formed by the harpoon mechanism).

Resum

La química quàntica tracta el problema de l'anàlisi de l'estructura electrònica de les molècules. Malauradament, un anàlisi rigurós de l'estructura electrònica requereix la solució exacta de l'equació d'Schrödinger, que només es pot resoldre exactament per a l'àtom d'hidrogen. Una solució pràctica per resoldre l'equació d'Schrödinger consisteix en emprar un conjunt finit de funcions de base per construir funcions d'ona aproximades, que s'optimizen d'acord amb el principi variacional. Un altre procediment planteja la reformulació del problema en termes de densitats reduïdes (com la densitat electrònica o les matrius reduïdes de la densitat), en comptes d'intentar resoldre directament l'equació d'Schrödinger en termes de la funció d'ona del sistema. Probablement, la metodologia més famosa d'aquest tipus la coneguda com a teoria del funcional de la densitat (DFT), que utiliza una formulació en termes de la densitat electrònica. Així mateix, existeixen altres procediments menys coneguts, com la teoria del funcional de la matriu reduïda de la densidad de segon order i l'equació d'Schrödinger contreta, que són part de la motivació d'aquesta tesi.

La teoria de l'equació d'Schrödinger contreta emprea matrius reduïdes de la densidad fins a quart ordre per tal de calcular l'energia electrònica d'un sistema. No obstant, les matrius reduïdes d'ordre més gran són freqüentment aproximades a partir de les matrius d'ordre més petit. En aquesta tesi ens hem centrat bàsicament en les aproximacions de la matriu reduïda de la densitat de tercer ordre, a partir de les matrius de primer i segon ordre. Fins ara, no existia un estudi exhastiu que permetés calibrar les aproximacions existents en funció de la correlació electrònica del sistema. Per aquesta raó, hem realitzat aquest anàlisi per tal d'avaluar totes les aproximacions de la matriu de la densitat reduïda a tercer ordre que s'han proposat fins ara. Com a estudi pilot, primer hem analitzat els estats electrònics ${}^2P$ i ${}^4P$ de l'àtom harmònic de tres electrons jugant amb els efectes de correlació a partir de la modificació del

paràmetre de confinament, ω. S'ha analitzat com la correlació afecta algunes propietats comparant-les amb el resultat exacte. S'ha estudiat entre d'altres: a) els índexs de compartició electrònica, b) les condicions de N-representabilitat, i c) la regla de la suma. El nostre estudi mostra que l'aproximació de Valdemoro dóna resultats excel·lents en el càlcul d'índexs de compartició electrònica, quasi tan bons com els obtinguts amb l'aproximació de Matito i col·laboradors. Tant mateix, hem comprovat que la correlació de Fermi és més fàcil de tractar que la correlació de Coulomb (que, òbviament, és molt més complexa). També hem obtingut informació sobre la importància del nivell de Fermi en la definició del factors de fase, σ_p, de les aproximacions de Nakatuji i Mazziotti. En un segon treball, hem testat les esmentades aproximacions de la matriu reduïda de la densitat a tercer ordre en el càlcul dels índexs de compartició electrònica en molècules amb enllaços de tres centres i dos electrons, així com de tres centres i quatre electrons. D'aquest estudi se'n desprèn que la aproximació de Valdemoro i, la de Matito i col·laboradors donen els millors resultats.

En la teoria del funcional de la matriu reduïda de la densidad, l'expressió de l'energia és un funcional explícit de la matriu reduïda de la densitat a primer ordre i, per tant, la matriu reduïda de la densitat a segon ordre (que cal per a fer el càlcul de l'interacció Coulòmbica entre electrons) es reconstrueix a partir matriu reduïda de la densitat a primer ordre. Normalment, es pren la representació diagonal de la matriu reduïda a primer ordre en termes dels orbitals naturals i les seves ocupacions. En la teoria del funcional de la matriu reduïda de la densitat, els elements de la matriu reduïda a segon ordre es construeixen en termes de les ocupacions dels orbitals na- turals. En línia amb l'estudi anterior sobre les matrius reduïdes a tercer ordre, hem analitzat com la correlació electrònica afecta a aquestes aproximacions. Amb aquest objectiu, hem treballat amb l'estat fonamental (^{1}S) de l'atòmic harmòmic de dos electrons i hem modificat els efectes de correlació electrònica jugant amb el paràmetre de confinament, ω. S'ha avaluat vàries propietats de les matrius reconstruïdes amb l'objectiu de donar vàries claus per a la construcció d'aproximacions més robustes. En

aquest estudi també hem analitzat com la correlació electrònica afecta a certes propietats. S'ha estudiat entre d'altres: a) l'índex de deslocalització, b) vàries condicions de N-representabilitat, c) la regla de la suma, d) la densitat intracular de probabilitat, i e) l'energia de repulsió Coulòmbica entre electrons. Els nostres resultats mostren que l'aproximació de les fases fixes és pràcticament exacta, independentment del règim de correlació del sistema, només presenta lleugeres desviacions en la regió de correlació forta. En aquest article, hem emprat les aproximacions dels funcionals PNOFi i les basades només en integrals J i K (Coulomb i intercanvi, respectivament), conegudes com a JK. També hem demostrat que les aproximacions PNOFi donen millors resultats que les JK en la majoria de tests (especialment en aquells on es proven les condicions de N-representabilitat i d'antisimetria). Així mateix, en aquesta tesi es mostra que les aproximacions JK produeixen matrius amb elements mancats de sentit físic que, malgrat donar resultats positius en alguns tests (com la regla de la suma), fallen en molts altres tests (per exemple, aquests elements introdueixen importants errors d'auto-interacció electrònica). D'altra banda, hem pogut comprovar que la correcció de l'error d'autointeracció electrònica *a posteriori*, no és la millor manera d'evitar la introducció d'elements de matriu mancats de sentit físic (veure la secció *Resultats* i *Discussió* per a més detalls). Finalment, els nostres resultats mostren que la imposició de vàries condicions exactes, porta a la construcció d'aproximacions de les matrius de segon ordre que són molt més robustes.

També hem treballat amb la densitat de probabilitat intracular radial, que s'obté a partir de la diagonal de la matriu reduïda de la densitat a segon ordre, és a dir, de la densitat de probabilitat de dues partícules (o densitat de parells). La densitat de parells dóna la probabilitat de trobar parells d'electrons, amb un electró col·locat a la posició $\mathbf{r}_1$, i l'altre a la posició $\mathbf{r}_2$. És una funció de sis coordenades que no es pot representar en gràfiques de dues i tres dimensions, llevat que es fixin algunes d'aquestes coordenades. La coordenada intracular, $\mathbf{r}_{12} = \mathbf{r}_1 - \mathbf{r}_2$, permet fixar unes coordenades i obtenir part de la informació con-

tinguda en la densitat de parells. La densitat de probabilitat intracular radial s'obté seleccionant tots els possibles parells a una certa distància electrònica, $|\mathbf{r}_{12}|$, i després realizant un promig esfèric. S'ha analitzat com aquesta quantitat canvia durant el procés de formació/dissociació de l'enllaç d'algunes molècules diàtomiques. En un primer treball hem centrat els esforços en l'estudi dels estats excitats $^{1,3}\Pi_u$ de la molècula d'hidrogen. Tal i Katriel, així com Colbourn i col·laboradors, van trobar un comportament contraintuïtiu (no monotòn) de l'energia de repulsió electrònica en l'estat $^3\Pi_u$ de la molècula d'hidrogen respecte a la distància interatòmica. Van observar un increment de la repulsió electrònica que venia acompanyat d'una disminució de la distància interelectrònica promig a l'allargar la distànca entre els àtoms d'hidrogen en un càlcul Hartree-Fock. A partir de càlculs FCI, hem pogut confirmar aquests resultats. D'acord amb la regla de Hund, el triplet hauria de ser molt més estable que el singlet degut a la reducció de la repulsió electrònica imposada pel principi de Pauli. En el triplet, el núvol electrònic és més compacte i l'apantallament del potencial extern produït pels nuclis és menys eficient. En altres paraules, l'atracció electró-nucli és molt més gran en el triplet que en el singlet, compensant la gran repulsió electrònica del triplet en comparació al singlet i fent el triplet més estable que el singlet (d'acord amb la regla de Hund). En un segon estudi, ens hem centrat en els reordenaments electrònics que succeixen en el procés de formació de l'enllaç de molècules diatòmiques. En concret, ens centrem en la diferència entre la densitat de probabilitat intracular radial exacta i la seva anàloga no relaxada. Els nostres resultats permeten donar una classificació dels enllaços en dobles i simples, d'acord amb el perfil obtingut al llarg de la formació de la molècula i, observar la formació de parells d'electrons en la molècula de Li_2 entre un àtom de liti i l'atractor no nuclear. Malauradament, no ha estat possible seguir el mecanisme tipus arpó que es dóna en la formació de la molècula de LiH usant aquesta eina. No obstant, sí que es reconeix el perfil d'enllaç covalent a distàncies llargues, i iònic a distàncies curtes, en la molèula de LiH. En aquest mateix treball també hem suggerit una aproximació a l'exacta i sovint costosa (computacionalment) probabilitat de densitat intracular radial utilizant ocupa-

cions dels orbitals naturals d'un càlcul CCSD i l'aproximació de Müller (també coneguda com a Baerends-Buijse) pel càlcul de la matriu reduïda de la densitat a segon ordre. Els resultats mostren que l'aproximació proporciona resultats comparables als exactes i redueix el cost computacional del càlcul. Finalment, hem emprat la probabilitat densitat intracular radial per analitzar el colze que s'observa en el forat de Coulomb de l'àtom de neó. S'ha construït un conjunt de funcions de base emprant exponents variables que depenen només de dos paràmetres (es coneixen en anglès com a *even-tempered*) i les hem utilitzat en càlculs CISD (permetent recuperar més d'un 95% de l'energia de correlació del sistema) per demostrar que el colze no és artificial, sinó un efecte real produït per la correlació dels electrons interns del neó. En aquest estudi també s'ha pogut mostrar que no hi ha una transferència important d'electrons entre les capes K i L de l'àtom i, per tant, el colze observat és degut a un procés de reorganització dels electrons de la capa K.

Per acabar, en l'últim treball d'aquesta tesii, hem estudiat el mecanisme de l'arpó que s'observa en la formació en fase gas d'algunes molècules que presenten dos atòms amb diferències molt petites entre el potencial de ionització de l'un i l'afinitat electrònica de l'altre. Les superfícies d'energia potencial (PES, de les sigles en anglès) de molècules formades per un mecanisme de tipus arpó, canvien el caràcter covalent de l'enllaç a iònic durant el procés de formació(el de la molècula en el seu estat fonamental). Aquest procés de canvi és molt ràpid i està caracterizat per la presència d'un punt de creuament evitable en la zona on hi ha el canvi de caràcter de l'enllaç. En aquest treball hem utilizat descriptors químics en molècules diàtomiques per tal de caracteritzar el mecanisme dins de l'aproximació de Born-Oppenheimer. El conjunt de molècules que hem escollit per aquest estudi inclou LiH, BH, BeH, LiF, CO, N_2, He_2, H_2 i F_2 (les últimes cinc espècies s'han escollit com a contraexemples del mecanisme de l'arpó). S'ha pogut demostrar que l'anàlisi de les poblacions electròniques dels àtoms no és suficient per tal de caracteritzar aquest mecanisme. Els resultats mostren que només l'índex de deslocalització pot reconèixer el mecanisme de l'arpó dels

altres casos (sempre i quan utilitzem les particions àtomiques QTAIM o TFVC). La funció de localització electrònica i la Laplaciana de la densitat electrònica permeten visualitzar la tranferència de l'electró que té lloc degut al mecanisme de l'arpó. De fet, el perfil d'aquesta quantitat al llarg de l'eix interatòmic mostra la transferència de l'electró d'un àtom a l'altre. Per últim, de totes les eines basades en la teoria de la informació, només la informació de Fischer (en l'espai de posicions i de moments) permet distingir entre molècules que segueixen el mecanisme de l'arpó i les altres espècies (d'acord amb la informació de Fischer, només la molècula H_2 s'assigna incorrectament com a molècula formada pel mecanisme de l'arpó).

Resumen

La química cuántica se ocupa del análisis de la estructura electrónica de las moléculas. Desafortunadamente, la estructura electrónica requiere la solución exacta de la ecuación de Schrödinger, que solo se puede resolver analíticamente para el átomo de hidrógeno. A nivel práctico la solución de la ecuación de Schrödinger se suele realizar usando bases finitas y mediante la construcción de funciones de onda aproximadas, que son optimizadas de acuerdo con el principio variacional. Otro enfoque se basa en la reformulación del problema, donde en lugar de resolver la ecuación de Schrödinger se usan expresiones de energía en términos de cantidades reducidas (e.g la densidad y las matrices densidad), siendo la teoría del funcional de la densidad probablemente la metodología más famosa dentro del último enfoque (donde la cantidad reducida utilizada es la densidad electrónica). Sin embargo, otros enfoques menos familiares se pueden encontrar en la literatura. Entre las aproximaciones menos familiares, la teoría del funcional de la matriz densidad y la ecuación de Schrödinger contraída son el génesis de la presente tesis.

En la metodología de la ecuación de Schrödinger contraída se requieren matrices densidad de hasta cuarto orden para el cálculo de la energía. Sin embargo, para reducir el coste computacional, las matrices densidad de alto orden se aproximan a partir de las de orden inferior. En esta tesis, nos hemos centrado en las aproximaciones sugeridas para la reconstrucción de matrices densidad de tercer orden, construídas a partir de las de segundo y de primer orden. No existía en la literatura un estudio detallado sobre cómo la correlación electrónica afecta a estas aproximaciones. Por tal motivo, hemos llevado a cabo dicho estudio para mejorar las aproximaciones sugeridas hasta ahora. Para el primer estudio, trabajamos con el átomo armónico de tres electrones (en los estados ${}^2P$ y ${}^4P$) y modificamos los efectos de correlación usando el parámetro ω (i.e. el confinamiento). En este estudio, analizamos cómo la correlación afecta al-

gunas propiedades con respecto a los resultados exactos. Se ha estudiado: a) índices de compartición de electrones, b) condiciones de N-representabilidad, y c) la regla de la suma, entre otras. Nuestro estudio reveló que la aproximación de Valdemoro es excelente para calcular índices de compartición de electrones, pero es seguida de cerca por la aproximación sugerida por Matito y sus colaboradores. En segundo lugar, hemos visto que la correlación de Fermi parece ser más fácil para modelar que la de Coulomb (que obviamente es mucho más complicada). A partir de este estudio, también hemos recopilado información sobre la importancia del nivel de Fermi en la definición del factor de fase, σ_p, de las aproximaciones de Nakatsuji y de Mazziotti. En nuestro segundo estudio, hemos analizado la exactitud que se puede obtener con las aproximaciones para el cálculo de los índices de compartición de electrones para sistemas de tres centros con dos electrones y de tres centros con cuatro electrones. Del último estudio, observamos que las aproximaciones de Valdemoro y de Matito y sus colaboradores proporcionan los resultados más cercanos a los de referencia.

En teoría funcional de la matriz densidad, la expresión de energía es una función explícita de la matriz densidad de primer orden, y por lo tanto la densidad de segundo orden necesaria para el cálculo de la repulsión interelectrónica se reconstruye a partir de la de primer orden. Usualmente, la matriz densidad de primer orden se toma en la representación diagonal, donde la base son los orbitales naturales y los elementos diagonales de la matriz son las ocupaciones de los orbitales naturales. Los elementos de la matriz densidad de segundo orden son reconstruídos como funciones de las ocupaciones de los orbitales naturales. Tal y como hicimos para las matrices densidad de tercer orden, nuestro estudio se basó en ver cómo la correlación electrónica afecta a estas aproximaciones. Con este fin, hemos trabajado con el átomo armónico de dos electrones en el estado ^1S (el estado fundamental) y modificamos los efectos de correlación por medio del parámetro ω. Para el presente estudio, hemos llevado a acabo el análisis de varias propiedades de las matrices reconstruidas. Esperamos que nuestro estudio proporcione nuevos conocimientos para el de-

sarrollo de aproximaciones más robustas. En este estudio, se analizó cómo la correlación electrónica afecta algunas propiedades, es decir, hemos estudiado: a) el índice de deslocalización, b) condiciones de N-representabilidad, c) la regla de suma, d) las probabilidades intraculares, y e) la repulsión interelectrónica, entre otros. Nuestros resultados han demostrado que la aproximación de fases fijas es casi exacta para cualquier régimen de correlación, y solo se desvía del resultado exacto en el límite de fuerte correlación. En este estudio hemos trabajado con las aproximaciones PNOFi y JK, donde las últimas solo producen los elementos de matriz densidad de segundo orden que están acompañados por las integrales Coulomb (J) o de intercambio (K). Se ha demostrado que las aproximaciones PNOFi producen mejores resultados que las JK en la mayoría de las pruebas (especialmente para las condiciones de N-representabilidad y la prueba de antisimetría). También hemos analizado cómo algunas aproximaciones JK producen elementos no físicos al reconstruir las matrices, que si bien es cierto que corrigen algunas propiedades (como la regla de suma) deterioran muchas otras propiedades (por ejemplo, introducen errores de autointeracción). Además, hemos demostrado que la corrección de auto interacción aplicada *a posteriori*, no es la mejor manera de evitar la generación de elementos no físicos (ver la sección de *Resultados* y *Discusiones* para más detalles). Finalmente, nuestros resultados han demostrado que se pueden obtener aproximaciones más robustas imponiendo tantas condiciones como sea posible desde el principio (es decir, en la construcción de la aproximación).

En esta tesis también hemos trabajado con la densidad de probabilidad intracular radial obtenida de la matriz densidad de segundo orden, específicamente, de la parte diagonal de esta matriz (es decir, la densidad de probabilidad de dos partículas). La densidad de probabilidad de dos partículas proporciona la densidad de probabilidad para encontrar pares de electrones, donde un electrón se coloca en $\mathbf{r}_1$ y otro se coloca en $\mathbf{r}_2$, y representa una función 6D que no se puede representar en gráficos 2D o 3D a menos que se fijen algunas coordenadas. La coordenada intracular, $\mathbf{r}_{12} = \mathbf{r}_2 - \mathbf{r}_1$, nos permite fijar algunas

coordenadas y recopilar algo de la información de la densidad de probabilidad de dos partículas. La densidad de probabilidad intracular radial se obtiene al seleccionar de todos los pares posibles, los que se encuentran a una distancia interelectrónica dada, $|\mathbf{r}_{12}|$, y después llevar a cabo un promedio esférico. En esta tesis, se ha analizado cómo evoluciona este último durante la disociación /formación del enlace de algunas moléculas diatómicas. En nuestro primer estudio, nos enfocamos en los estados excitados $^{1,3}\Pi_u$ del H_2. Tal y Katriel, y Colbourn encontraron y reportaron un comportamiento contraintuitivo no monotónico de la repulsión de electrones en el estado excitado $^3\Pi_u$ de la molécula de hidrógeno respecto a la distancia inter atómica. Se observó un aumento del V_{ee} a nivel de Hartree-Fock, acompañado por una disminución de la $\langle r_{12} \rangle$, cuando el enlace se estira; hemos confirmado este efecto usando cálculos FCI. La regla de Hund establece que el triplete debería ser mucho más estable que el singlete debido a la reducción de la repulsión como consecuencia del principio de Pauli. Se ha observado que la nube electrónica es más compacta para el triplete y el apantallamiento del potencial externo producido por los núcleos es menos efectivo, por lo que la atracción electrón-núcleo es mucho más grande en este estado que en el singlete. La energía de atracción núcleo-electrón obtenida para el estado triplete compensa el mayor (e inesperado) V_{ee} del estado triplete, y hace que el estado del triplete sea más estable (de acuerdo con la regla de Hund). En nuestro segundo estudio, nos centramos en los reordenamientos que occurren con los electrones durante la formación de enlaces de algunas moléculas diatómicas. En este estudio, analizamos la diferencia entre la densidad de probabilidad intracular radial exacta y la no relajada. Nuestros resultados proporcionan una clasificación de los tipos de enlaces en simples y dobles de acuerdo con el perfil obtenido a lo largo de la formación de enlaces, y también podemos observar la formación de pares de electrones en la molécula de Li_2 entre los electrones localizados en los núcleos y el electrón en el atractor no nuclear. Desafortunadamente, fue imposible rastrear el mecanismo del arpón seguido por las molécula de LiH, sin embargo, pudimos observar que un perfil de enlace covalente se obtiene a grandes distancias interatómicas mientras que a pequeñas distancias

interatómicas se recuperó el perfil iónico. En este trabajo también sugerimos una aproximación a la exacta y generalmente costosa densidad de probabilidad intracular radial mediante el uso de las ocupaciones de los orbitales naturales CCSD y la aproximación de Müller o Buijse y Baerends para la matriz densidad de segundo orden. Este estudio demostró que la aproximación sugerida produce resultados comparables a los exactos y reduce el tiempo del cálculo computacional. Por último, utilizamos la densidad de probabilidad intracular radial para el estudio de un hombro observado en el agujero de Coulomb del átomo de Neón. Construímos para este estudio un conjunto de bases *even-tempered* y usamos cálculos CISD (que recuperan más del 95% de la correlación electrónica) para demostrar que el codo no es un error de las bases, sino un efecto real producido por la correlación electrónica que afecta a los electrones de la capa K. También demostramos en este trabajo que no había un transferencia importante de la densidad electrónica entre las capas K y L, lo que sugiere que solo hay una reorganización de electrones dentro de la capa K que produce el hombro reportado.

Finalmente, en el último trabajo de esta tesis hemos estudiado el mecanismo del arpón, que se observa en fase gaseosa para algunas moléculas formadas por átomos que presentan una pequeña diferencia entre el potencial de ionización y la electroafinidad. La superficie de energía potencial para moléculas formadas por el mecanismo del arpón cambia el carácter de covalente a iónico cuando se forma un enlace, que ocurre por medio de una transferencia de electrones. El cambio de carácter en el superficie de energía potencial es muy rápido y, por lo tanto, este mecanismo presenta un cruce evitado en la geometría donde tiene lugar la transferencia de electrones. En este trabajo, utilizamos descriptores químicos aplicados a algunas moléculas diatómicas en un intento de caracterizar este mecanismo dentro de la aproximación de Born-Oppenheimer. El conjunto de moléculas diatómicas elegidas para este estudio incluye LiH, BH, BeH, LiF, CO, N_2, He_2, H_2 y F_2 (las últimas cinco especies fueron tomadas como contraejemplos). Se ha demostrado que el análisis de la población atómica no es suficiente para caracterizar este mecanismo. Nuestro estudio mostró también

que solo el índice de deslocalización es capaz de reconocer el mecanismo del arpón (si usamos particiones atómicas QTAIM o TFVC). La función de localización de electrones y el Laplaciano de la densidad de electrones proporcionan medios para visualizar la transferencia de electrones. En realidad, el escaneo de estas cantidades a lo largo del eje interatómico permite la visualización de la transferencia de electrones. Finalmente, de las cantidades de la teoría de la información, solo las informaciones de Fisher (en el espacio de posiciones y en el espacio de momentos) fueron capaces de distinguir entre los sistemas que siguen el mecanismo del arpón y los otros sistemas (lamentablemente, la molécula de H_2 fue incorrectamente clasificada por la información de Fisher como una molécula formada por el mecanismo del arpón).

I) Introduction

1.1) From Classical Mechanics to Quantum Mechanics

By the beginning of the 20^{th} century a new discipline was born in physics. It was proposed to explain some fundamental questions which arose from some experiments that could not be explained with classical mechanics [5, 6] and Maxwell's equations [7]. Experiments such as: a) the spectroscopic series of Hydrogen [8–11], b) the black body radiation [12], c) the photoelectric effect [13], and d) the double-slit experiment [14], made physics (and our conception of the nature) change because new concepts such as the *energy quantization* [15] were needed to explain them. A new era of advances in physics followed the introduction of the *energy quantization*, that also changed what we knew in many other sciences such as chemistry, biology, and medicine, among others. In 1901, Planck [15] introduced the concept of *energy quantization* to explain the black-body radiation experiment, and the application of this concept to describe matter and light was achieved some years later (mid-1920s) by Schrödinger [16] and Heisenberg [17, 18] with the development of quantum mechanics. Schrödinger's approach to quantum mechanics was based on the usage of partial differential equations, while Heisenberg's approach employed matrices. The algebra of matrices with infinite rows and columns was not known by physicists at that time, therefore, Schrödinger's approach eventually got more adepts and it is nowadays the most common approach used when we apply quantum mechanics to study matter and light. **Nevertheless, we would like to remark at this point that matrices have accompanied quantum mechanics development throughout this time**.

In 1920 Bohr published his work about the "Correspondence Principle" [19] which states the relationship between quantum mechanics and classical mechanics, where the latter is retrieved from the first one in the limit of large

quantum numbers. The limit of large quantum numbers is always produced by macroscopic systems, therefore, we only require quantum mechanics for studying small particles such as molecules, atoms, and electrons, among others. The advent of quantum mechanics changed our conception of nature by introducing unexpected properties of matter and light such as: a) Tunneling energy barriers, which is fundamental in biological processes (see for example Ref. [20]), b) Entanglement between particles, that has changed our way of coding information (see for example Ref. [21]), c) Uncertainty relations (e.g. Heisenberg's uncertainty principle[1]), and d) That particles may behave like waves [23] (e.g photons), among others.

1.2) From Chemistry to Quantum Chemistry

Chemistry is an old science derived from the ancient alchemy, it separated from alchemy in 1661 when Boyle published his work "The Sceptical Chymist" [24] that settle the difference between chemistry and alchemy by making the first one be based on the scientific method. By the end of the 18^{th} century, chemistry became a science thanks to the works of Lomonosov[2] and Lavoisier.[3] At the beginning of the 19^{th} century, Dalton [27] recovered Democritus' [28] ideas and proposed the Modern Atomic Theory.[4] The application of the Schrödinger equation in 1926 for the description of the spectroscopic series of Hydrogen atom [16] changed what we knew about the structure of atoms. One year later, Walter Heitler and Fritz London published the first application of quantum mechanics to study a diatomic hydrogen molecule [29], which provided a new vision of the chemical bond concept. Thus, the proper description of the structure of molecules and the changes that occur during the *chemical reaction* is only

[1] Heisenberg's uncertainty principle [22] states that the more precisely the position of some particle is determined, the less precisely its momentum (speed) can be known, and vice versa.

[2] He presented the law of conservation of mass in 1756 [25].

[3] Due to his outstanding work, people gave him the appellation of the "father of modern chemistry". He also produced the first modern chemistry textbook [26].

[4] He suggested that in order to study the matter, one has to first understand its constituents (the atoms).

possible using quantum mechanics. **The application of quantum mechanics in chemistry is, hence, called quantum chemistry.** In the following years, quantum chemistry expanded thanks to the works of Mulliken [30, 31], Hund [32], Born [18, 33], Born-Oppenheimer [34], Hückel [35–38], and specially Pauling [39–43],[5] among others. The application of quantum chemistry as a routine methodology was only possible with the advent of more powerful computers and the works of Pople [44–51] and Kohn [52–55], who introduced the efficient implementation of Gaussian type orbitals and foundations of the Density Functional Theory, respectively.[6]

1.3) Quantum Chemistry

The starting point to apply quantum chemistry for studying any system, is usually to write the non-relativistic time-dependent Schrödinger [16] equation,

$$i\hbar\frac{\partial\psi(\mathbf{X},t)}{\partial t} = \widehat{H}(\mathbf{X})\psi(\mathbf{X},t), \tag{1}$$

where $i = \sqrt{-1}$ is the imaginary unit, $\hbar = \frac{h}{2\pi}$ (where h is Planck's constant [15]), $\mathbf{X}$ represents all the spatial coordinates of all nuclei and electrons of the system, $\widehat{H}(\mathbf{X})$ is known as the Hamiltonian operator[7] and $\psi(\mathbf{X},t)$ is known as the wavefunction of the system. In order to solve Eq. 1, which is a partial differential equation, we could apply the usual method of separation of variables and suggest a solution of the form $\psi_i(\mathbf{X},t) = \Phi_i(t)\varphi_i(\mathbf{X})$. Applying the separation of variables yields

$$\Phi_i(t) = \exp\left[\frac{-iE_it}{\hbar}\right], \tag{2}$$

[5] Pauling is seen as one of the founders of quantum chemistry and was awarded with the Nobel Prize in chemistry (in 1954) for his contribution to the field.

[6] Their advances made quantum chemistry become a routine methodology. They were awarded with the Nobel Prize in chemistry (in 1998) for their work.

[7] Considered to be independent of time in this case when we are interested in the structure of the system. In many other situations, like in the interaction between light and matter, the Hamiltonian also depends on time $\widehat{H}(\mathbf{X},t)$ and we can not use the separation of variables method.

where the particular set of energies ($\{E_i\}_{i=0}^{\infty}$) is said to produce an stationary state.[8] For stationary states Eq. 1 reduces to the time-independent Schrödinger equation [16],

$$\widehat{H}(\mathbf{X})\varphi_i(\mathbf{X}) = E_i\varphi_i(\mathbf{X}), \tag{3}$$

where the Hamiltonian for molecular systems takes the form

$$\widehat{H}(\mathbf{X}) = \widehat{H}(\mathbf{R}_1, \mathbf{R}_2, ..., \mathbf{R}_{N_a}, \mathbf{r}_1, \mathbf{r}_2, ..., \mathbf{r}_N) \tag{4}$$

$$= -\sum_{i}^{N_a} \frac{\nabla^2_{\mathbf{R}_i}}{2} - \sum_{i}^{N} \frac{\nabla^2_{\mathbf{r}_i}}{2} - \sum_{i}^{N_a}\sum_{j}^{N} \frac{Z_i}{|\mathbf{R}_i - \mathbf{r}_j|} \tag{5}$$

$$+ \sum_{i,j<i}^{N_a} \frac{Z_i Z_j}{|\mathbf{R}_i - \mathbf{R}_j|} + \sum_{i,j<i}^{N} \frac{1}{|\mathbf{r}_i - \mathbf{r}_j|},$$

where N_a is the number of nuclei, N is the number of electrons, and the operators of Eq. 5 correspond to: a) the kinetic energy of the nuclei, b) the kinetic energy of the electrons, c) the Coulomb interaction between the electrons and the nuclei, d) the Coulomb interaction between the nuclei, and e) the Coulomb interaction between the electrons, respectively. In order to solve Eq. 3, we usually apply the Born-Oppenheimer approximation [34].[9] Using this approximation, the wavefunction is written as a product

$$\varphi_i(\mathbf{R}_1, \mathbf{R}_2, ..., \mathbf{R}_{N_a}, \mathbf{r}_1, \mathbf{r}_2, ..., \mathbf{r}_N) = \vartheta_i(\mathbf{R}_1, \mathbf{R}_2, ..., \mathbf{R}_{N_a})\Psi_i(\mathbf{r}_1, \mathbf{r}_2, ..., \mathbf{r}_N), \tag{6}$$

where $\vartheta_i(\mathbf{R}_1, \mathbf{R}_2, ..., \mathbf{R}_{N_a})$ corresponds to the nuclear wavefunction and $\Psi_i(\mathbf{r}_1, \mathbf{r}_2, ..., \mathbf{r}_N)$ corresponds to the electronic wavefunction (the subindex i is omitted hereafter to simplify the notation). Within this approximation the Hamiltonian is decoupled in two operators

$$\widehat{H}(\mathbf{R}_1, \mathbf{R}_2, ..., \mathbf{R}_{N_a}, \mathbf{r}_1, \mathbf{r}_2, ..., \mathbf{r}_N) = \widehat{H}_{nuc}(\mathbf{R}_1, \mathbf{R}_2, ..., \mathbf{R}_{N_a}) + \widehat{H}_{el}(\mathbf{r}_1, \mathbf{r}_2, ..., \mathbf{r}_N), \tag{7}$$

[8] A state is stationary when all observable properties of the state are constant in time (e.g. the energy E_i, the probability distribution $|\psi_i(\mathbf{X}, t)|^2 = |\varphi_i(\mathbf{X})|^2$, among others).

[9] It consists in the assumption that the motion of atomic nuclei and electrons in a molecule can be separated. This is often justified by stating that "the heavy nuclei move more slowly than the light electrons".

where

$$\widehat{H}_{el}(\mathbf{r}_1, \mathbf{r}_2, ..., \mathbf{r}_N) = -\sum_i^N \frac{\nabla^2_{\mathbf{r}_i}}{2} - \sum_i^{N_a}\sum_j^N \frac{Z_i}{|\mathbf{R}_i - \mathbf{r}_j|} + \sum_{i,j<i}^{N_a} \frac{Z_i Z_j}{|\mathbf{R}_i - \mathbf{R}_j|} + \sum_{i,j<i}^{N} \frac{1}{|\mathbf{r}_i - \mathbf{r}_j|}, \tag{8}$$

which satisfies the electronic Schrödinger equation: $\widehat{H}_{el}\Psi = E_{el}\Psi$ (from now on we will use E and $\widehat{H}$ to refer to E_{el} and $\widehat{H}_{el}$, respectively), and $\widehat{H}_{nuc} = -\sum_i^{N_a} \frac{\nabla^2_{\mathbf{R}_i}}{2} + E(\mathbf{R}_1, \mathbf{R}_2, ..., \mathbf{R}_{N_a})$, that satisfies the nuclear Schrödinger equation: $\widehat{H}_{nuc}\vartheta = E_i\vartheta$. From the nuclear Schrödinger equation we notice that the Born-Oppenheimer approximation gives rise to the Potential Energy Surface (PES) concept, which is crucial in modern quantum chemistry to study, among others, reaction mechanisms [29, 56, 57].[10] Notice that E_i is the total energy of the system (see Eq. 3) which contains the electronic energy, the vibrational energy, the rotational energy and the nuclear kinetic energy. The Born-Oppenheimer approximation can only be trusted when the energy levels obtained from solving the electronic Schrödinger equation, $\{E_n\}_{n=0}^{\infty}$, are well separated between each other for any atomic configuration, which is not always the case (e.g. systems formed by the harpoon mechanism [58]). However, in this thesis we have used Born-Oppenheimer electronic wavefunctions (and some chemical descriptors) in an attempt to track the harpoon mechanism from the sudden changes that occur to these wavefunctions in the region where the energy levels get close to each other (see chapter VIII for more details).

In quantum chemistry we usually work with Born-Oppenheimer approximation and the problem reduces in most of the cases to find E for a given atomic configuration, because E can be used to: a) compare the stability between systems, b) characterize energy barriers, c) find reaction paths, among other applications. In order to find E we need to solve the electronic Schrödinger equation (from now on we will refer to it as the Schrödinger equation). Since

[10] Notice that $E = E(\mathbf{R}_1, \mathbf{R}_2, ..., \mathbf{R}_{N_a})$ and the PES only depend on the coordinates of the nuclei (i.e. on a given configuration of the atoms).

the problem in quantum chemistry is to find E and therefore the problem is fully defined, Paul A. M. Dirac suggested 1929 that [59]: *"The fundamental laws necessary for the mathematical treatment of a large part of physics and the whole of chemistry are thus completely known, and the difficulty lies only in the fact that application of these laws leads to equations that are too complex to be solved"*. The Schrödinger equation is a complicated partial differential equation and two families of approaches have been suggested to find E.

1.3.1) Wavefunction Methods

The solution of the Schrödinger equation can be attempted by suggesting a trial wavefunction, $\widetilde{\Psi}$, and optimize some parameters attending to the variational principle.[11] This trial wavefunction is usually expressed using some basis functions of Hilbert's space [60]. Nonetheless, electrons are fermionic particles which imposes that Ψ must be antisymmetric with respect to the exchange of the coordinates of two electrons. To satisfy the antisymmetry condition, the first approximation suggested (using some basis functions) for a $\widetilde{\Psi}$ was to use a Slater determinant (Ξ) [61], which introduced the Hartree-Fock approximation [62] (also known as the self-consistent field method). Within this approximation, the basis is optimized in order to minimize the energy which produces an orthonormal basis that is known as the canonical orbitals basis. Unfortunately, the optimized wavefunction obtained from Hartree-Fock approximation (constructed using the canonical orbitals) treats the opposite-spin electrons as independent particles and lacks the *correlation energy* (E_{corr}) [63],[12] **which**

[11] Which states that for any given trial wavefunction, $\widetilde{\Psi}$, $E_0 \leq \frac{\int \widetilde{\Psi}^* \widehat{H} \widetilde{\Psi} d\mathbf{r}_1 d\mathbf{r}_2 \ldots d\mathbf{r}_N}{\int \widetilde{\Psi}^* \widetilde{\Psi} d\mathbf{r}_1 d\mathbf{r}_2 \ldots d\mathbf{r}_N}$, where E_0 is the ground state energy and the equality is attained for the ground state wavefunction ($\widetilde{\Psi} \equiv \Psi_0$).

[12] The term *correlation energy* was coined by Löwdin as the difference between the exact energy and the restricted Hartree-Fock energy [63], some other authors take the unrestricted Hartree-Fock energy as reference [64] but in this thesis we have worked with Löwdin's definition. In Löwdin's definition, the E_{corr} is essentially a measure of the error in the Hartree-Fock method [65]. In Hartree-Fock the instantaneous electron-electron repulsion is replaced by the repulsion of each electron with an average electron charge cloud, thus, the electron correlation

is usually small but an important component of E. In order to have a proper description of any system of interest, E_{corr} must be accurately calculated [66–68]. **Actually, the problem in quantum chemistry relies essentially in providing an accurate value for the** E_{corr}. The Hartree-Fock wavefunction can be improved by adding to it all possible Slater determinants that we can construct for a given basis function,

$$\widetilde{\Psi}= \sum_i C_i \Xi_i, \tag{9}$$

where the C_i coefficients are then optimized using the variational principle. The trial wavefunction given by Eq. 9 is known as the Full-Configuration Interaction (FCI) wavefunction.[13] FCI wavefunctions require important computational resources and are in most cases impractical [66–68], despite the important advances that computers have experienced in the last decades. As an alternative to the FCI wavefunction, two types of approximations have been suggested in quantum chemistry (see Ref. [67]).

- The first group of methods is based on using only some Slater determinants of Eq. 9. In this group we have: a) methods based on the truncation the FCI wavefunction by fixing the maximum number of excitations with respect to the Hartree-Fock wavefunction (e.g including only singles and doubles excitations we obtain the CISD wavefunction), b) the coupled-cluster (CC) methods,[14] which use the operator e^T (see Ref. [67] for more details) and also restrict the number of excitations (e.g the CC including only singles and doubles excitations (CCSD)), and c) methods based on

is a measure of how much the movement of one electron is influenced by the presence of the rest of electrons.

[13]The FCI wavefunction provides the exact E for the system if an infinite basis set is used. Unfortunately, we can only work with finite basis functions, thus, the E obtained is said to be the exact energy within the given finite basis.

[14]It is worth to mention that CC methods are based on generating a wavefunction using the e^T operator, nevertheless, the wavefunction is not optimized attending to the variational principle. The problem is solved using a projection (see Ref. [67] for more details) and the energy obtained might not be variational but it is size-consistent.

the multiconfiguration self-consistent field, which generate a qualitatively correct reference state when Hartree-Fock approximation is a poor reference due to near degeneracies of the orbitals (e.g. CASSCF).[15]

In the first two methods the Hartree-Fock Slater determinant is the most important contribution to the CI expansion, thus the E_{corr} retrieved is said to be of *dynamic type*. For the last family of methods (which are employed when the Hartree-Fock wavefunction is a poor reference) the E_{corr} retrieved is said to be of *nondynamic type*.[16]

- The second group is based on Perturbation theory [71], where the missing E_{corr} is assumed to be a small perturbation to the reference energy (usually the Hartree-Fock wavefunction is taken as reference). In this group the most important approach in quantum chemistry is the Møller-Plesset (MPi) approach [72], where i is the order of the perturbation correction considered. In practical applications, MP2 is the most usual approach, where only up to second-order corrections to the Hartree-Fock wavefunction are included. When MP2 calculations are performed, the E_{corr} retrieved is known to be of *dynamic type* (e.g. a first approximation for the description of weak interactions can be obtained from MP2 results (see for example Ref. [73])). Thus, MP2 is usually applied as an on top correction to the Hartree-Fock wavefunction or to the CASSCF wave function (CASPT2), in an attempt to retrieve the missing *dynamic* correlation.

The approximations already introduced are based on suggesting a $\widetilde{\Psi}$ that is as close as possible to the exact FCI wavefunction (Eq. 9), however, usually

[15] $\widetilde{\Psi}$ must be constructed including as many Slater determinants as needed in order to treat in a proper way the near degeneracies of the canonical orbitals.

[16] Dynamic correlation is retrieved by CI expansions where the Hartree-Fock Slater determinant is the most important contribution to the CI expansion (e.g. *dynamic* correlation is fundamental for the description of weak interactions [69,70] (van der Waals interactions)). On the other hand, *nondynamic* correlation is present due to near degeneracies (e.g. it appears in the description of the bond dissociation process due to the degeneracies observed between the bonding and antibonding orbitals [68]).

the number of Slater determinants required by these approximations is still very large. Consequently, these methods still require important computational resources and, therefore, they are not feasible when the number of electrons and basis functions increases. Let us mention that most of these methods were developed in the last century and they belong to the consolidated methods of quantum chemistry. Nowadays, the research within these methods is mostly devoted to reduce the computational resources needed (see for example Ref. [74]).

1.3.2) Reduced Quantities Methods

As we have mentioned, the proper description of the E_{corr} is the fundamental search of quantum chemistry. The reduction of the computational cost with respect to the wavefunction methods when computing E, which includes an accurate E_{corr}, can be performed by using reduced quantities. Reduced quantities are obtained from the wavefunction upon integration of some coordinates, hence for example we could obtain the electronic density,

$$\rho(\mathbf{r}) = N \int \Psi^*(\mathbf{r}, \mathbf{r}_2, ..., \mathbf{r}_N)\Psi(\mathbf{r}, \mathbf{r}_2, ..., \mathbf{r}_N) d\mathbf{r}_2 d\mathbf{r}_3 ... d\mathbf{r}_N, \tag{10}$$

where an N factor is being introduced to make $\rho(\mathbf{r})$ integrate to the number of electrons. The electronic density is the key ingredient of Density Functional Theory [53, 75–77] (DFT), which is the most popular alternative to wavefunction methods for the computation of E. DFT is based on Hohenberg and Kohn theorems [53], which state the existence of an energy functional that explicitly depends on the electronic density $E = E[\rho(\mathbf{r})]$. The $E[\rho(\mathbf{r})]$ functional is valid for the ground state energy (E_0) for local external potentials (see the *Methodology* section for more details) and when the ground state is not degenerated.[17] In DFT, the unknown functionals are kinetic energy functional ($T[\rho]$)

[17] An electronic energy level E_i is degenerated when more that one Ψ produces the same energy for the same system. Some approaches, like Levy's constrained-search formulation, permit the application of DFT to degenerated states [78].

and the electron-electron repulsion functional $V_{ee}[\rho(\mathbf{r})]$.

In 1965, Kohn-Sham provided a practical way to calculate E_0 in DFT [54], they proposed to use a reference system of noninteracting particles subject to some external potential, $v_s(\mathbf{r})$, so that its density, $\rho_s(\mathbf{r})$, should be the same as the ground state density of the actual system ($\rho_s(\mathbf{r}) = \rho(\mathbf{r})$). In Kohn-Sham scheme, the $E_{xc}[\rho(\mathbf{r})]$ functional accounts for the exchange, correlation and the correlation kinetic energy.[18] (see Ref. [77] for more details). Since the reference system is composed of noninteracting particles, a Slater determinant is an exact solution of the Kohn-Sham system. Hence, the density $\rho_s(\mathbf{r})$ is defined from a Slater determinant wavefunction.

Several approximations to $E_{xc}[\rho(\mathbf{r})]$ can be found in the literature (see Refs. [75–77, 79]). Some approximations rely on strong-theoretical grounds and attempt to fulfill as many constraints as possible, where the constraints are imposed from physical and mathematical conditions that the exact functional must attain (being the SCAN functional [80] probably the most representative functional of this group). On the other hand, some functionals [81–83] use a large number of parameters that are fitted to minimize the mean absolute error in the computation of properties (e.g. atomization energies, ionization potentials, electron affinities, energy barriers, among others.) for large sets of molecules, being the Minnesota family of functionals probably the most representative functionals of this group. The development of new $E_{xc}[\rho(\mathbf{r})]$ functionals is always accompanied by an exhaustive benchmark, where people usually compare the mean absolute error of energy related properties obtained with some previous functionals and the new properties obtained with the new approximation suggested. Nevertheless, some authors [84] have recently pointed out the importance of include in the analysis some other properties when we present a benchmark of

[18] The kinetic energy of the noninteracting system is not the same as for the interacting one. Therefore, we can define the correlation kinetic energy as $T_c = T[\rho] - T_s[\rho]$, where $T[\rho]$ is the exact kinetic energy and $T_s[\rho]$ is the kinetic energy of the noninteracting system.

functional approximations. **In this vein, the usage of model systems opens an avenue for developing and benchmarking new functionals, because for model systems highly accurate results (FCI results in most of the cases) can be obtained and later used as reference**. In previous works [85], we used FCI results obtained for the Harmonium atom model [86] as reference for benchmarking some of the most popular DFT functionals, and then we analyzed how to reparameterize the famous B3LYP functional in order to provide an accurate description of the Harmonium atom model.

DFT is the most common reduced quantity methodology used as an alternative to wavefunction methods, nonetheless, DFT is not the only method based on reduced quantities available. Some other approaches rely on the first-order reduced density matrix (1-RDM) or even in higher order reduced density matrices. When the reduced quantity used is the 1-RDM the works of Gilbert [87], Donnelly and Parr [88], Levy [89] and Valone [90] provided the basis of Reduced Density Matrix Functional Theory (RDMFT), within this theory the existence of a universal functional of the energy that depends only on the 1-RDM is the equivalent to the DFT universal functional. The most important advantage with respect to DFT is that the kinetic energy functional is fully determined in RDMFT ($T = T\,[\text{1-RDM}]$), hence **only the Coulomb electron-electron repulsion remains unknown in terms of the 1-RDM**. RDMFT has not been so extensively studied and only a few reduced density matrix approximations can be found in the literature (see the *Methodology* section for more details). On the other hand, some other methodologies require higher order reduced density matrices like: a) variational 2-reduced density matrix [91], b) the Contracted Schrödinger Equation [92–98] and, c) the Antihermitian Contracted Schrödinger Equation [99]. All these methodologies are based on the **reconstruction** of high-order reduced density matrices from lower order ones. In this thesis, we have focus on the development of some comprehensive benchmarks for reconstructions of second- and third-order reduced density matrices

(see chapters IV and V). These benchmarks consist of a battery of tests[19] where we analyze how the properties obtained from the reconstructed matrices match the exact results. This kind of benchmarks were not available,[20] thus the importance of our work (and this thesis) is to provide the scientific community with new tools that can be use in the development of more robust approximations. In chapters IV and V, we have used the Harmonium atom model system to tune correlation effects in order to study how electron correlation affects the reconstructed matrices. Moreover, for third-order reduced density matrices we have also analyze how the reconstructed matrices perform for the computation of electron sharing indices [102–104].

Reduced quantities give access to many physical properties that in some cases can even be compared with experiments, e.g. the radial intracule probability density (see the section 2.2.4 for more details). Therefore, in this thesis we have also focused on understanding the features of these properties. To that end, in chapters VI and VII we have studied how the radial intracule probability density evolves due to the electron rearrangements that occur in the bond formation/dissociation process. In section 6.2 we have suggested a new approximation to the exact (obtained from FCI wave functions) radial intracule probability density, there we used CCSD results and one of the reconstructions of second-order reduced density matrices that we analyzed in the chapter V. In chapter VII, we have also used the radial intracule probability density to understand the electron rearrangements that happen to the core electrons of Neon atom, which lead to a certain feature of the Coulomb hole of this system.

Finally, in chapter VIII, we have used Born-Oppenheimer FCI wavefunctions in

[19] In accordance with recent studies [84] which suggest that several properties should be used when we present a benchmark and not only focus on the energy E obtained.

[20] To our knowledge, the most complete benchmark for second-order reduced density matrix approximations available in the literature was done by Cioslowski and coworkers [100]. Nevertheless, they only focused on the energy and did not analyze other properties of the reconstructed matrices, which is usually what some other authors do (see for example Ref. [101]).

order to describe the harpoon mechanism. Recall that systems formed by the harpoon mechanism should be studied without using the Born-Oppenheimer approximation, notwithstanding, in this chapter we have analyzed how some chemical descriptors allow us to follow this mechanism from Born-Oppenheimer FCI wavefunctions. The chemical descriptors used in chapter VIII are all based in reduced quantities: a) the electronic density, and b) the second-order reduced density matrix.

So, this thesis has been entirely focused on reduced quantities and properties that we can obtain from them. We covered **from benchmarking reconstructions to applications**. **Our benchmarks can be used in the development of more robust approximations to second- and third-order reduced density matrices**. We have also provided manners to obtain approximated electron sharing indices (chapters IV and V) and radial intracule probability densities (chapter VI) by using reconstructed density matrices. **In all the applications we used chemical descriptors, based on reduced quantities, to study some problems of chemical interest** such as: a) the analysis of how the electron rearrangements that occur in the bond formation/dissociation process affect the radial intracule probability density, b) the correlation effects in the core electrons of the Neon atom (with special attention to how these effects modify the Coulomb hole), and c) the qualitative description of the harpoon mechanism from highly accurate wavefunctions.

II) Methodology

This section is organized in three parts. In the first part, we introduce the concept of Density Matrices and Reduced Density Matrices (RDMs), discussing in detail the probabilistic information contained within density matrices. In addition, we discuss how the energy is actually a functional of the 2-RDM. Secondly, we introduce some magnitudes widely used in quantum chemistry: a) the Electron Sharing Index, b) the Electron Localization Function, c) the radial intracule probability density, and d) Information Theory Quantities. On the second section, we introduce approximate 3- and 2-order density matrices from lower-order matrices, with special attention to the N-representability problem of 1-, 2-, and 3-order RDMs. In the last section, we introduce the model system which we have used to test how electron correlation affects these approximations. This model system is more than a simple model because it can be used to study quantum dots and Wigner crystals, among other systems. Therefore, is actually a realistic playground, and its simplicity allows us to easily interpret how electron correlation affects these approximations, and gather fundamental hints for the development of RDM approximations. We also cover the systems which served as a yardstick to understand the approximations and tools analyzed in this thesis.

2.1) Density Matrices

Quantum systems are known to exist in nature either as pure states or mixed states. Pure states are solutions to the Schrödinger equation,

$$\widehat{H}\Psi(\mathbf{x}_1, \mathbf{x}_2, ..., \mathbf{x}_N) = E\Psi(\mathbf{x}_1, \mathbf{x}_2, ..., \mathbf{x}_N), \tag{11}$$

which in the case of dealing with electrons, $\mathbf{x}_i$ variables correspond to the 3D spatial coordinates plus the spin ($\mathbf{x}_i \equiv \mathbf{r}_i, s_i$). The wavefunction Ψ is therefore a function in the coordinate space and in the spin space. Since the Hamiltonian

operator used in most of the electronic structure calculations only involves the spatial coordinates (i.e. the Hamiltonian does not depend on the spin), Eq. 11 represents a partial differential equation of $3N$ coordinates. Clearly, it is a very complicated problem from the mathematical perspective; only solvable with numerical methods in the majority of cases.

For an N electron system, the N-order density matrix can be constructed from the N-electron wavefunction in the following manner:

$$\gamma_N(\mathbf{x}'_1,...,\mathbf{x}'_N;\mathbf{x}_1,...,\mathbf{x}_N) = \Psi^*(\mathbf{x}'_1,...,\mathbf{x}'_N),\Psi(\mathbf{x}_1,...,\mathbf{x}_N) \tag{12}$$

which depends on $8N$ variables. m-order RDMs are obtained from the $N-m$ partial trace (integration) of Eq. 12:

$$\gamma_m(\mathbf{x}'_1,...,\mathbf{x}'_m;\mathbf{x}_1,...,\mathbf{x}_m) = \binom{N}{m} m! \int \gamma_N(\mathbf{x}'_1,...,\mathbf{x}'_N;\mathbf{x}_1,...,\mathbf{x}_N) \times \Delta^N_{m+1} d\mathbf{x}_{m+1}...d\mathbf{x}_N d\mathbf{x}'_{m+1}...d\mathbf{x}'_N, \tag{13}$$

where $\Delta^N_{m+1} = \prod_{i=m+1}^{N} \delta(\mathbf{x}'_i - \mathbf{x}_i)$, ($\delta(\mathbf{x}'_i - \mathbf{x}_i)$ being the usual Dirac delta function) and the factor $\binom{N}{m}m!$ is being introduced for normalization in order to account for all possible groups of electrons of size m that can be produced (which is known as McWeeny's normalization [105]). Fortunately, the reduction of order gives rise to functions that still contain most of the information needed for calculating physical magnitudes of interest. For instance, using RDMs we can compute the probability of the m-electron distribution, given by setting $\mathbf{x}'_1 = \mathbf{x}_1$, $\mathbf{x}'_2 = \mathbf{x}_2$,...,$\mathbf{x}'_m = \mathbf{x}_m$ in Eq. 13. Notice that the probabilistic character attributed to density matrices comes from Born's interpretation [106] of the wavefunction which states that for one-particle systems, the square modulus of the wavefunction, $|\Psi(\mathbf{x})|^2$, is proportional to the probability of finding the particle at any particular point $\mathbf{x}$ (i.e. $|\Psi(\mathbf{x})|^2$ is thus a probability density).

As first example, let us introduce the 3-order RDM (3-RDM) obtained from an N-particle RDM ($N > 3$)

$$\gamma_3(\mathbf{x}'_1, \mathbf{x}'_2, \mathbf{x}'_3; \mathbf{x}_1, \mathbf{x}_2, \mathbf{x}_3) = N(N-1)(N-2) \times \int \gamma_N(\mathbf{x}'_1, ..., \mathbf{x}'_N; \mathbf{x}_1, ..., \mathbf{x}_N) \Delta_4^N d\mathbf{x}_4 ... d\mathbf{x}_N d\mathbf{x}'_4 ... d\mathbf{x}'_N. \tag{14}$$

Integration over spin coordinates produces the spinless 3-RDM,

$$\rho_3(\mathbf{r}'_1, \mathbf{r}'_2, \mathbf{r}'_3; \mathbf{r}_1, \mathbf{r}_2, \mathbf{r}_3) = \int \gamma_3(\mathbf{x}'_1, \mathbf{x}'_2, \mathbf{x}'_3; \mathbf{x}_1, \mathbf{x}_2, \mathbf{x}_3)|_{s_1=s'_1, s_2=s'_2, s_3=s'_3} ds_1 ds_2 ds_3. \tag{15}$$

The diagonal part of the 3-RDM (Eq. 14) provides the probability of finding three electrons at $\mathbf{r}_1$, $\mathbf{r}_2$ and $\mathbf{r}_3$ with spin σ_1, σ_2 and σ_3, respectively. The 3-RDM is given by

$$\gamma_3(\mathbf{x}_1, \mathbf{x}_2, \mathbf{x}_3) = \int \gamma_3(\mathbf{x}'_1, \mathbf{x}'_2, \mathbf{x}'_3; \mathbf{x}_1, \mathbf{x}_2, \mathbf{x}_3) \times \delta(\mathbf{x}'_1 - \mathbf{x}_1)\delta(\mathbf{x}'_2 - \mathbf{x}_2)\delta(\mathbf{x}'_3 - \mathbf{x}_3) d\mathbf{x}'_1 d\mathbf{x}'_2 d\mathbf{x}'_3, \tag{16}$$

which is known as the (spin-with) 3-particle probability density. Integration over spin coordinates produces the spinless 3-particle probability density,

$$\rho_3(\mathbf{r}_1, \mathbf{r}_2, \mathbf{r}_3) = \int \gamma_3(\mathbf{x}_1, \mathbf{x}_2, \mathbf{x}_3) ds_1 ds_2 ds_3. \tag{17}$$

As we did for the 3-RDM (Eq. 14), we can obtain the 2-RDM using Eq. 13 on its corresponding spinless RDM,

$$\rho_2(\mathbf{r}'_1, \mathbf{r}'_2; \mathbf{r}_1, \mathbf{r}_2) = \int \gamma_2(\mathbf{x}'_1, \mathbf{x}'_2; \mathbf{x}_1, \mathbf{x}_2)|_{s_1=s'_1, s_2=s'_2} ds_1 ds_2. \tag{18}$$

Also, we may define the probability of finding electron pairs, with any given spin, using the (spin-with) 2-particle probability density obtained from the diagonal part of the 2-RDM,

$$\gamma_2(\mathbf{x}_1, \mathbf{x}_2) = \int \gamma_2(\mathbf{x}'_1, \mathbf{x}'_2; \mathbf{x}_1, \mathbf{x}_2) \times \delta(\mathbf{x}'_1 - \mathbf{x}_1)\delta(\mathbf{x}'_2 - \mathbf{x}_2) d\mathbf{x}'_1 d\mathbf{x}'_2, \tag{19}$$

Integration over spin coordinates produces the spinless 2-particle probability density (or simply the 2-particle probability density (2-PPD)),

$$\rho_2(\mathbf{r}_1, \mathbf{r}_2) = \int \gamma_2(\mathbf{x}_1, \mathbf{x}_2) ds_1 ds_2. \tag{20}$$

In this vein, we can finally introduce the (spin-with) 1-particle probability density from the 1-RDM

$$\gamma(\mathbf{x}) = \gamma_1(\mathbf{x}'; \mathbf{x}), \tag{21}$$

which is usually normalized to the number of electrons (N). Upon integration over the spin coordinate, Eq. 21 produces the electronic density or simply the density, usually written as $\rho(\mathbf{r})$.

It is possible to express all previous quantities using some basis of atomic or molecular orbitals $\{\phi_i\}_{i=1}^{M}$ (where M is the size of the basis). For example, the spinless 2-RDM can be expressed as

$$\rho_2(\mathbf{r}'_1, \mathbf{r}'_2; \mathbf{r}_1, \mathbf{r}_2) = \sum_{ijkl}^{M} {}^2D_{ij,kl} \phi_i(\mathbf{r}'_1) \phi_j(\mathbf{r}'_2) \phi_k(\mathbf{r}_1) \phi_l(\mathbf{r}_2) \tag{22}$$

where the set of all ${}^2D_{ij,kl}$ elements (i.e. ${}^2\mathbf{D}$ matrix) is also usually known as the 2-RDM. In the same manner, the spinless 1-RDM can also be expressed on an orbital basis as

$$\rho_1(\mathbf{r}'; \mathbf{r}) = \sum_{ij}^{M} {}^1D_{i,j} \phi_i(\mathbf{r}') \phi_j(\mathbf{r}), \tag{23}$$

likewise, the set of elements ${}^1D_{i,j}$ is also usually known as the 1-RDM. The density written in this basis is $\rho(\mathbf{r}) = \sum_{ij}^{M} {}^1D_{i,j} \phi_i(\mathbf{r}) \phi_j(\mathbf{r})$. The matrix that contains all ${}^1D_{i,j}$ elements (i.e. ${}^1\mathbf{D}$ matrix) can be brought to a diagonal form through an unitary transformation,

$$\rho_1(\mathbf{r}'; \mathbf{r}) = \sum_{i}^{M} n_i \chi_i(\mathbf{r}') \chi_i(\mathbf{r}), \tag{24}$$

where the n_i elements are known as the natural orbital occupancies and the $\{\chi_i\}_{i=1}^{M}$ as the natural orbitals, being the latter formed as a linear combination of the ϕ_i.

The wavefunction (Ψ in Eq. 11) is a function of $4N$ coordinates (including the spin), thus storing it and computing magnitudes of physical interest from it is usually expensive (from the computational perspective). On the contrary, using RDMs requires less stored information and computation of physical magnitudes is, therefore, much more convenient from them. Also, reduced density matrices can be used to describe mixed states (where there is an statistical mixture of pure states that can not be described by a single wavefunction) [107], making density matrices more versatile than wavefunctions.

Moreover, one of the most coveted quantities of interest, the energy, only depends on the 2-RDM when electrons interact via Coulomb forces. The energy is calculated as an expectation value $E = \frac{\langle\Psi|\widehat{H}|\Psi\rangle}{\langle\Psi|\Psi\rangle}$ and is one of the most important quantities in chemistry because it determines the most stable structure, energy barriers, etc. The energy can be considered as an explicit functional of the spinless 2-RDM

$$E[\rho_2(\mathbf{r}_1', \mathbf{r}_2'; \mathbf{r}_1, \mathbf{r}_2)] = T[\rho_1(\mathbf{r}_1'; \mathbf{r}_1)] + V_{\text{ext}}[\rho_1(\mathbf{r}_1'; \mathbf{r}_1)] + V_{ee}[\rho_2(\mathbf{r}_1, \mathbf{r}_2)] \tag{25}$$

where

$$T[\rho_1(\mathbf{r}_1'; \mathbf{r}_1)] = -\frac{1}{2}\int \nabla^2_{\mathbf{r}_1}\rho_1(\mathbf{r}_1'; \mathbf{r}_1)|_{\mathbf{r}_1'=\mathbf{r}_1} d\mathbf{r}_1' \tag{26}$$

is the kinetic energy,

$$V_{\text{ext}}[\rho_1(\mathbf{r}_1'; \mathbf{r}_1)] = \int \rho_1(\mathbf{r}_1'; \mathbf{r}_1) v_{\text{ext}}(\mathbf{r}_1', \mathbf{r}_1) d\mathbf{r}_1' d\mathbf{r}_1 \tag{27}$$

is the interaction between the electrons and the external potential (which in the case of a local external potential is simply $V_{\text{ext}}[\rho(\mathbf{r})] = \int \rho(\mathbf{r}) v_{\text{ext}}(\mathbf{r}) d\mathbf{r}$) and

$$V_{ee}[\rho_2(\mathbf{r}_1, \mathbf{r}_2)] = \frac{1}{2}\int \frac{\rho_2(\mathbf{r}_1, \mathbf{r}_2)}{|\mathbf{r}_2 - \mathbf{r}_1|} d\mathbf{r}_1 d\mathbf{r}_2, \tag{28}$$

the usual Coulomb electron-electron interaction. Eqs. 25 and 27 are valid for any local (e.g. produced by the nuclei) or non-local external potential that does not introduce interactions between the electrons. The advantage of using Eq. 25 over Eq. 11 is clear, noticing that the evaluation of the energy only requires the 2-RDM which is less expensive to store and use than the total wavefunction.

2.2) Statistical Quantities Based on Density Matrices

In this section we introduce: the Delocalization Index, the Electron Sharing Index, the Electron Localization Function and the Intracule Probability Density. These four quantities require the probabilistic interpretation of RDMs and some concepts/definitions borrowed from statistics. These quantities are used either as benchmark tools or as chemical descriptors in the present thesis.

2.2.1) The Delocalization Index

In 1807 Dalton [27] recovered Democritus' [28] ideas and proposed the Modern Atomic Theory. Dalton suggested that in order to study the matter, one has to first understand its constituents (the atoms). Actually, he assumed that atoms retained their identity even as constituents of larger structures. Later, in 1916 Lewis [108] suggested that atoms are held by sharing a pair of electrons between them, giving a first definition of the chemical bond. Hence, chemistry was born with the idea of an *atom in a molecule* (AIM) where the electronic structure of molecules is given by the role of the constituent atoms. Characterizing atoms inside a molecule requires the introduction of an *atomic partition*. An atomic partition subdivides the atoms in a molecule and there are two ways to define an atomic partition: a) by partitioning the Hilbert space (the mathematical space where the wavefunction is defined) or b) by partitioning the Cartesian space. The most famous Cartesian space partition was proposed by R. F. W. Bader and gives rise to the Quantum Theory of Atoms in Molecules(QTAIM) [109], where the atomic domains are contoured by the so-called zero-flux regions. The integration of the atomic density within the atomic domain A provides the number of electrons (or population) in that region,

$$N(A) = \langle \widehat{N}_A \rangle = \int_A \gamma(\mathbf{x}) d\mathbf{x} = \overline{N}_A, \tag{29}$$

where $\widehat{N}_A$ is the particle operator applied on atom A and $N(A)$ (sometimes written as $\overline{N}_A$) is the atomic population of atom A. Analogously, the integration

of the pair density using two atomic domains A and B defines pair populations,

$$N(A,B) = \langle \widehat{N}_A \widehat{N}_B \rangle = \int_A \int_B \gamma_2(\mathbf{x}_1, \mathbf{x}_2) d\mathbf{x}_1 d\mathbf{x}_2. \tag{30}$$

The difference between the pair population and the product of independent monoelectronic densities is known as the covariance. The covariance, defined in statistics, is the measure of the joint variability of two variables. From the covariance we define the Delocalization Index (DI) [110–115]

$$\begin{aligned} \delta(A,B) &= -2\mathrm{cov}(N(A), N(B)) \\ &= -2\langle (\widehat{N}_A - \overline{N}_A)(\widehat{N}_B - \overline{N}_B) \rangle \\ &= 2[N(A)N(B) - N(A,B)]. \end{aligned} \tag{31}$$

The DI is a measure of the number of electrons pairs shared between two centers; it provides non-integer values closely related somewhat to the concept of bond order. From Eq. 30, we notice that the DI depends on the (spin-with) 2-particle probability density defined in Eq. 19. Therefore, the DI can be written in terms of the (spin-with) 2-particle probability density expressed using some basis (in analogy to Eq. 22) as

$$\delta(A,B) = -2 \sum_{\substack{ijkl \\ \sigma\sigma'}}^{M} {}^2D^{\sigma\sigma'}_{ij,kl} S_{ik}(A) S_{jl}(B) + 2N(A)N(B), \tag{32}$$

where $\sigma, \sigma' \in \{\alpha, \beta\}$ and $S_{ab}(X) = \int_X \phi_a(\mathbf{r})\phi_b(\mathbf{r})d\mathbf{r}$ is the overlap between orbitals a and b in the domain defining atom X. We can also define the localization index as

$$\lambda(A) = \int_A \int_A \left[\gamma(\mathbf{x}_1)\gamma(\mathbf{x}_2) - \gamma_2(\mathbf{x}_1, \mathbf{x}_2)\right] d\mathbf{x}_1 d\mathbf{x}_2. \tag{33}$$

It is straight-forward to prove that

$$N = \sum_A N(A) = \sum_{B, A<B} \delta(A,B) + \sum_A \lambda(A) \tag{34}$$

An electron totally localized within an atom contributes 1 to the localization index. A localized pair of electrons contributes 2 to the localization index and an electron shared between two atoms contributes 1/2 to the localization index

and 1/2 to the delocalization index [116]. For example, in Fig. 1 we observe that for N_2 at Hartree-Fock equilibrium distance ($R_{NN} = 1.0783$ Å) using aug-cc-pVDZ basis a DI of $\delta(N_1, N_2) = 3.040$ and two equal localization indexes of $\lambda(N_1) = \lambda(N_2) = 5.480$ are obtained. We know that N has a configuration like this: $1s^2 2s^2 2p^3$ and N_2 shows a triple bond ($2 \times 2p^3$). Each N has a lone pair ($2s^2$) and two core electrons $1s^2$. There is a total of 14 electrons distributed as 3 delocalized (each of the 3 electrons shared by each N contribute 1/2) and 11 localized (5.5 per N atom: two from the core electrons, two from the lone pair and $3 \times 1/2$ from each electron shared). The computed numbers match well with this counting.

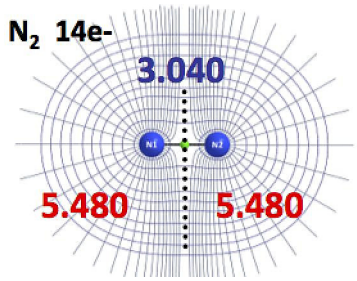

Figure 1 – Delocalization Index for N_2 at the Hartree-Fock equilibrium distance ($R_{NN} = 1.078$ Å) computed with aug-cc-pVDZ basis (Fig. taken from Ref. [1]).

Finally, the total delocalization in a given atom is defined as

$$\delta(A) = \sum_{B \neq A} \delta(A, B), \tag{35}$$

which has been related to the valence of an atom [117], providing a division of the electrons localized and delocalized in an atom,

$$N(A) = \frac{1}{2}\delta(A) + \lambda(A). \tag{36}$$

2.2.2) The Electron Sharing Index

In chemistry, Lewis theory is still widely used to describe and rationalize many bonds. The DI introduced in the previous section is a modern tool, based

on the idea of pairs of electrons, to characterize the bonding between two atoms. Nevertheless, a number of molecular species do not fit the model suggested by Lewis. Most of them include more than two atoms such as B_2H_6 ring that is held by 4 electrons forming two 3-center 2-electrons bonds. Some other examples are: agostic bonds, organic/inorganic aromaticity, hyperconjugation/conjugation and 3-center 4-electrons bonds (like allyl-anion). In all those cases, the electron sharing is described with the n-center Electron Sharing Index (nc-ESI), which is defined as

$$\delta(A_1, A_2, ..., A_n) = \frac{(-2)^{n-1}}{(n-1)!} \langle \prod_{i=1}^{n} (\widehat{N}_{A_i} - \overline{N}_{A_i}) \rangle, \tag{37}$$

which reduces to Eq. 32 for $n = 2$. This generalization was introduced by Giambiagi [118] in 1994. For the $n = 3$ case, we have

$$\begin{aligned} \delta(A_1, A_2, A_3) &= 2\langle \widehat{N}_{A_1} \widehat{N}_{A_2} \widehat{N}_{A_3} \rangle - 2\langle \widehat{N}_{A_1} \widehat{N}_{A_2} \rangle \overline{N}_{A_3} \\ &- 2\langle \widehat{N}_{A_2} \widehat{N}_{A_3} \rangle \overline{N}_{A_1} - 2\langle \widehat{N}_{A_1} \widehat{N}_{A_3} \rangle \overline{N}_{A_2} \\ &+ 4\overline{N}_{A_1} \overline{N}_{A_2} \overline{N}_{A_3} \end{aligned} \tag{38}$$

the evaluation of the first term of Eq. 38:

$$\langle \widehat{N}_{A_1} \widehat{N}_{A_2} \widehat{N}_{A_3} \rangle = \int_{A_1} \int_{A_2} \int_{A_3} \gamma_3(\mathbf{x}_1, \mathbf{x}_2, \mathbf{x}_3) d\mathbf{x}_1 d\mathbf{x}_2 d\mathbf{x}_3 \tag{39}$$

requires up to the 3-RDM. The 3c-ESI, $\delta(A_1, A_2, A_3)$, gives a measure of how the electron distribution is skewed from its mean, which may be related to the simultaneous electron fluctuation among the atomic population of the atomic domains (A_1, A_2, A_3).

Up to now we have introduced the mean value of the number of electrons of an atom, $N(A)$ (see Eq. 29), the DI related to the fluctuation of electrons between two atoms (see Eq. 32), the localization index $\lambda(A)$ on the number of electrons of an atom (see Eq. 33) and the 3c-ESI (see Eq. 38) related to the fluctuation among three atoms. From statistics we know that $N(A)$ is the first cumulant of the distribution of the number of electrons in the atom A

and $\delta(A)$ (see Eqs. 35 and 36) corresponds to the variance (also known as the second cumulant). We also know that cumulants and moments are intimately related through their corresponding generating functions (see Ref. [119] for more details). Actually, it can be proven that a moment of n-th order is an nth-degree polynomial in the first n cumulants [119]. Thus, from the relationship between moments and cumulants, and the definition given for the nc-ESI (see Eqs. 37 and 38) is easy to relate these indices to the n-th order cumulants. As we have seen, cumulants appeared naturally in this context. Therefore, it is not surprising that lower-order cumulants have also been used as building blocks to construct approximations to higher-order n-order RDMs (see below the *Approximate density matrices* section).

2.2.3) The Electron Localization Function

The next physical magnitude of interest that we want to introduce, arising from the probabilistic nature of density matrices is the Electron Localization Function (ELF). The ELF [120] was introduced by Becke and Edgecombe in 1990 as a measure of the likelihood of finding an electron in the neighborhood space of a reference electron located at a given point and with the same spin. In order to define it, we need to split the pair density into the following spin cases:

$$\rho_2(\mathbf{r}_1,\mathbf{r}_2) = \sum_{\sigma} \rho_2^{\sigma\sigma}(\mathbf{r}_1,\mathbf{r}_2) + \sum_{\sigma\neq\sigma'} \rho_2^{\sigma\sigma'}(\mathbf{r}_1,\mathbf{r}_2) \qquad \sigma,\sigma' \in \{\alpha,\beta\} \tag{40}$$

where $\rho_2^{\sigma\sigma}(\mathbf{r}_1,\mathbf{r}_2)$ ($\rho_2^{\sigma\sigma'}(\mathbf{r}_1,\mathbf{r}_2)$) represents the contribution from the same (opposite) spin elements to the 2-PPD. Since the pair density contains information about electron pairs, correlation effects are also contained within it. For the same spin case, the so-called Coulomb and Fermi correlations are included whereas for the opposite pair density only the Coulomb correlation is present.[21] Here we also need to split the density in spin cases: $\rho(\mathbf{r}) = \rho_\alpha(\mathbf{r}) + \rho_\beta(\mathbf{r})$. Again,

[21] The Fermi correlation prevents two same-spin electrons from being found at the same point in space while Coulomb correlation describes the correlation between the spatial position of electrons due to their Coulomb repulsion.

borrowing a concept from statistics, we can define the *conditional probability* density as

$$P(\mathbf{r}_1, \mathbf{r}_2) = \frac{\rho_2(\mathbf{r}_1, \mathbf{r}_2)}{\rho(\mathbf{r}_1)}, \tag{41}$$

which provides the probability of finding electron 2 nearby $\mathbf{r}_2$ when electron 1 is at $\mathbf{r}_1$. Using the *conditional probability*, Becke and Edgecombe defined the ELF in order to account for the Fermi contribution to the *conditional probability* (CP), $P^{\sigma\sigma}(\mathbf{r}_1, \mathbf{r}_2) = \frac{\rho_2^{\sigma\sigma}(\mathbf{r}_1, \mathbf{r}_2)}{\rho_\sigma(\mathbf{r})}$. In Hartree-Fock approximation, the 2-RDM depends only on the 1-RDM, defined from the determinant:

$$\gamma_2^{\mathrm{HF}}(\mathbf{x}_1', \mathbf{x}_2'; \mathbf{x}_1, \mathbf{x}_2) = \begin{vmatrix} \gamma_1(\mathbf{x}_1'; \mathbf{x}_1) & \gamma_1(\mathbf{x}_1'; \mathbf{x}_2) \\ \\ \gamma_1(\mathbf{x}_2'; \mathbf{x}_1) & \gamma_1(\mathbf{x}_2'; \mathbf{x}_2) \end{vmatrix}. \tag{42}$$

For $\mathbf{x}_1' = \mathbf{x}_1$ and $\mathbf{x}_2' = \mathbf{x}_2$, the product of the two diagonal elements produces the Coulomb term (i.e. the term formed by two independent one-electron densities repealing through a Coulomb interaction component of the V_{ee} energy). On the other hand, the product of off-diagonal elements produces the so-called exchange contribution. The corresponding spinless 2-RDM is obtained from $\rho_2^{\mathrm{HF}}(\mathbf{r}_1', \mathbf{r}_2'; \mathbf{r}_1, \mathbf{r}_2) = \int \gamma_2^{\mathrm{HF}}(\mathbf{x}_1', \mathbf{x}_2'; \mathbf{x}_1, \mathbf{x}_2)_{s_1 = s_1', s_2 = s_2'} ds_1 ds_2$ which in the $\mathbf{r}_1' = \mathbf{r}_1$ and $\mathbf{r}_2' = \mathbf{r}_2$ case, produces the 2-PPD. From HF approximation we know that only same spin electrons produce exchange contributions. Thus, for the HF same spin CP (obtained after spin integration) we have

$$P^{\sigma\sigma}(\mathbf{r}_1, \mathbf{r}_2) = \frac{\rho_\sigma(\mathbf{r}_1)\rho_\sigma(\mathbf{r}_2) - \rho_x(\mathbf{r}_1, \mathbf{r}_2)}{\rho_\sigma(\mathbf{r}_1)}, \tag{43}$$

where $\rho_x(\mathbf{r}_1, \mathbf{r}_2) = \rho_1(\mathbf{r}_1; \mathbf{r}_2)\rho_1(\mathbf{r}_2; \mathbf{r}_1)$ is known as the exchange density. Becke developed the Taylor series expansion for this function. In fact, he worked with $P^{\sigma\sigma}(\mathbf{r}, \mathbf{r} + \mathbf{s})$ expansion at $\mathbf{s} = \mathbf{0}$ using the $e^{\mathbf{s}\cdot\nabla}$ operator to produce the Taylor series expansion. Then, he performed the spherical average for any given scalar s distance, and arrived to the following expression for the CP [121]:

$$\overline{P}^{\sigma\sigma}(\mathbf{r}, s) = \frac{1}{3}\left[\tau_\sigma(\mathbf{r}) - \frac{1}{4}\frac{|\nabla\rho_\sigma(\mathbf{r})|^2}{\rho_\sigma(\mathbf{r})}\right] s^2 + ..., \tag{44}$$

where $\tau_\sigma(\mathbf{r}) = \sum_i |\nabla\phi_i(\mathbf{r})|^2$ is the kinetic energy density, $\mathbf{r}$ are the coordinates of the reference electron and s is the radius of the shell where the second electron

is located after the spherical average (the overline over $P^{\sigma\sigma}$ indicates that a spherical average is being performed). The smaller the probability of finding an electron near the reference point $\mathbf{r}$, the more localized the reference electron is. Thus, electron localization is related to $D_\sigma = \tau_\sigma(\mathbf{r}) - \frac{1}{4}\frac{|\nabla\rho_\sigma(\mathbf{r})|^2}{\rho_\sigma(\mathbf{r})}$. D_σ vanishes for one-electron systems and also for many-electron systems with regions dominated by one single σ orbital. It is important to notice that the relationship with localization is inverse with respect to D_σ. Hence the ELF is finally given by the ratio:

$$ELF(\mathbf{r}) = \frac{1}{1+\chi_\sigma^2(\mathbf{r})}, \tag{45}$$

where $\chi_\sigma^2(\mathbf{r}) = D_\sigma(\mathbf{r})/D_\sigma^0(\mathbf{r})$, $D_\sigma^0(\mathbf{r}) = \frac{3}{5}(6\pi^2)^{2/3}\rho_\sigma^{5/3}(\mathbf{r})$, being $D_\sigma^0(\mathbf{r})$ the reference taken from the uniform electron gas. The ELF as defined in Eq. 45 is bounded between $[0,1]$, being 1 for perfect localization and $1/2$ in the electron-gas-like case. The ELF for BH at the equilibrium distance is shown as an example in Fig. 2, where we observe that the ELF is highly localized on top of H atom and on the atomic domain of B atom but it is negligible along the bond. We know that BH is formed through a covalent bond that is highly polarized, that is why the ELF is almost zero in the bond region but large in the atomic domains because the electrons are mostly localized on the atomic domain of B and H atoms.

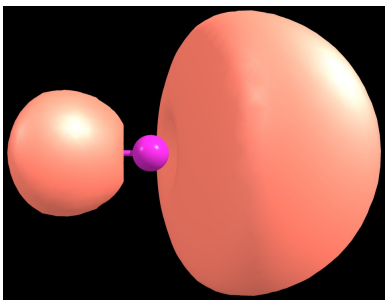

Figure 2 – Full configuration interaction contour plot of ELF for BH at the equilibrium distance with the aug-cc-pVDZ basis computed with our **RHO_OPS** [2] program (isocontour=0.8).

2.2.4) The Intracule Probability Density

The next magnitude related to the probabilistic nature that we want to introduce is the Intracule Probability Density (IPD). From the 2-PPD defined in Eq. 20, the analysis is still complicated because it represents a 6D-function that cannot be represented in 2D or 3D plots unless some coordinates are fixed. The usage of the intracule coordinate $\mathbf{r}_{12} = \mathbf{r}_2 - \mathbf{r}_1$ in the IPD provides a 3D representation of part of the information contained in the 2-PPD. Let us define the IPD as

$$I(\mathbf{s}) = \frac{1}{2} \int \rho_2(\mathbf{r}_1, \mathbf{r}_2) \delta(\mathbf{s} - \mathbf{r}_{12}) d\mathbf{r}_1 d\mathbf{r}_2, \tag{46}$$

where the Dirac delta function excludes all possibilities except those where $\mathbf{s} = \mathbf{r}_2 - \mathbf{r}_1$, which are the only ones that contribute for a given $\mathbf{s}$. The spherical integration of the IPD

$$I(s) = s^2 \int I(\mathbf{s}) d\Omega_s, \tag{47}$$

where $d\Omega_s = \sin\theta_s d\theta_s d\phi_s$ produces the radial IPD. The radial IPD is a fundamental function because the V_{ee} can be written as an explicit functional of the radial intracule probability density,

$$V_{ee}[I(s)] = \int \frac{I(s)}{s} ds. \tag{48}$$

The difference between the exact (full configuration interation) $I(s)$ and the Hartree-Fock $I(s)$ provides information about correlation effects and is known as Coulson's Coulomb hole [122]

$$h(s) = I^{\mathrm{FCI}}(s) - I^{\mathrm{HF}}(s). \tag{49}$$

Actually, for any method which includes electron correlation, it is possible to define the corresponding Coulomb hole,

$$h(s) = I^{\mathrm{X}}(s) - I^{\mathrm{HF}}(s), \tag{50}$$

which can be used to analyze the treatment of electron correlation from different methods, and can also be used to classify and quantify electron correlation by

introducing the concept of range separation [70,123,124].[22] Hence, some authors based the development of new electron correlation methods on the reconstruction of Coulomb holes (see for example Refs. [125, 126]). It is worth to mention that the radial IPD can actually be obtained experimentally from X-Ray scattering cross-sections [127–129]. Thus, the radial IPD is actually an observable based on the probabilistic nature of the 2-PPD, which we can compare with experiments (see for example Fig. 3). In Fig. 3 we observe that the maximum of the radial IPD lies near the interatomic distance (R_{CO}) because the nuclei gather the electronic density and many pairs of electrons can be formed from electrons separated by R_{CO}.

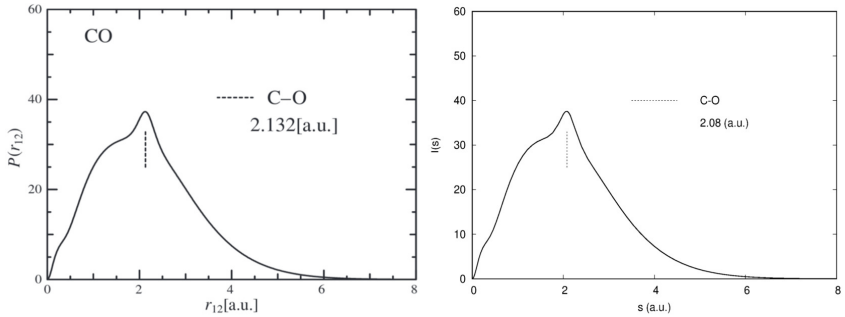

Watanabe et al., *Mol Phys,* **102,** 649 (2004) M. Rodríguez-Mayorga **RHO2_OPS** code

Figure 3 – On the l.h.s the experimental (obtained from X-Ray scattering cross-sections) and on the r.h.s. the computational (obtained with CASSCF(6,6) and **RHO2_OPS** [3] code) radial IPD.

2.2.5) Information Theory Quantities

Finally, the last quantities we want to introduce are based on the electronic density $\rho(\mathbf{r})$ but also on the electronic density in the momentum space $\pi(\mathbf{p})$. The first magnitude has already been introduced but, the momentum space density requires some explanation. The Schrödinger equation as written in

[22] The range separation concept is based on the interactions between the electrons, and it is used to classify them as short- and long-range interactions (i.e. attending to the interelectronic distance where the interactions take place).

Eq. 11 is in spatial coordinates if we set $\mathbf{x}_i = (\mathbf{r}_i, s_i)$. But, if we replace $\mathbf{x}_i \rightarrow \mathbf{y}_i = (\mathbf{p}_i, s_i)$ with $\mathbf{p}_i$ defined as the momentum vector of electron i whose components are $\mathbf{p}_i = (p_{x_i}, p_{y_i}, p_{z_i})$ in Cartesian coordinates and rewrite the operators of the Hamiltonian in momentum space, the wavefunction obtained from the Schrödinger equation is $\Psi(\mathbf{p}_1, \mathbf{p}_2, ..., \mathbf{p}_N)$. The transformation from spatial coordinates to momentum space coordinates is performed through a Fourier transformation, that is to say,

$$\Psi(\mathbf{p}_1, \mathbf{p}_2, ..., \mathbf{p}_N) = (2\pi)^{-3N/2} \int \exp\left[-i(\mathbf{p}_1 \cdot \mathbf{r}_1 + \mathbf{p}_2 \cdot \mathbf{r}_2 + ... + \mathbf{p}_N \cdot \mathbf{r}_N)\right] \times \Psi(\mathbf{r}_1, \mathbf{r}_2, ..., \mathbf{r}_N) d\mathbf{r}_1 d\mathbf{r}_2 ... d\mathbf{r}_N. \tag{51}$$

Setting $\mathbf{y}_i = (\mathbf{p}_i, s_i)$ allows us to define equations completely equivalent to Eqs. 12-19, for instance the 2-PPD is defined as

$$\pi_2(\mathbf{p}_1, \mathbf{p}_2) = \int \gamma_2(\mathbf{y}_1; \mathbf{y}_2) ds_1 ds_2, \tag{52}$$

which represents the probability of finding an electron with momentum $\mathbf{p}_1$ and a second electron with momentum $\mathbf{p}_2$ regardless the momentum of the other electrons. In the same manner, we may write an expression completely equivalent to Eq. 21 which upon spin integration produces the electronic density in the momentum space $\pi(\mathbf{p})$. When transforming n-order RDMs from spatial space to the momentum space through a Fourier transform, we must perform a transformation of $2N$ $\mathbf{x}_i$ coordinates (for an N-electron system) because coordinates and primed coordinates are changed independently. Only after computing the $2N$ Fourier transform, we set primed coordinates equal to the non-primed ones in order to obtain Eq. 52 and $\pi(\mathbf{p})$. The Fourier transform of the position-space electronic density does not produce the momentum space one,

$$\pi(\mathbf{p}) \neq (2\pi)^{-3/2} \int \rho(\mathbf{r}) \exp\left[-i\mathbf{p} \cdot \mathbf{r}\right] d\mathbf{r}. \tag{53}$$

Following the orbital expansions introduced in Eqs. 22-24 for the spinless 2-order and 1-order RDMs, it is easy to prove using Plancherel's theorem [130] that any orthonormal basis in the position space ($\{\phi_i(\mathbf{r})\}_{i=1}^{M}$) transforms into

an orthonormal basis ($\{\eta_i(\mathbf{p})\}_{i=1}^{M}$) in the momentum space. With a one-to-one correspondence between these two basis (e.g. the ϕ_1 orbital transforms into the η_1 one).

From information theory, it is possible to define the entropy of any distribution. This entropy measures the unpredictability of a certain distribution i.e., the spread of the distribution. Hence, we may define the Shannon entropy for the electronic densities as

$$S[\rho(\mathbf{r})] = -\int \overline{\rho}(\mathbf{r}) \ln \overline{\rho}(\mathbf{r}) d\mathbf{r}, \tag{54}$$

and

$$S[\pi(\mathbf{p})] = -\int \overline{\pi}(\mathbf{p}) \ln \overline{\pi}(\mathbf{p}) d\mathbf{p}, \tag{55}$$

where $\overline{\rho}(\mathbf{r})$ and $\overline{\pi}(\mathbf{p})$ are the electronic densities normalized to 1. These entropies play an important role quantum mechanics because the uncertainty principle can be written using them as $S[\rho(\mathbf{r})] + S[\pi(\mathbf{p})] \geq 3(1 + \ln \pi)$ which was proven by Hirschman [131], Beckener [132], Bialynicki-Birula and Mycielski [133]. Another quantity borrowed from information theory is the Fisher information. The Fisher informations for our density distributions are

$$F[\rho(\mathbf{r})] = \int \frac{|\nabla \overline{\rho}(\mathbf{r})|^2}{\overline{\rho}(\mathbf{r})} d\mathbf{r}, \tag{56}$$

and

$$F[\pi(\mathbf{p})] = \int \frac{|\nabla \overline{\pi}(\mathbf{p})|^2}{\overline{\pi}(\mathbf{p})} d\mathbf{p}, \tag{57}$$

which measure local changes of the electron densities (i.e. mostly the sharpness of $\overline{\rho}(\mathbf{r})$ and $\overline{\pi}(\mathbf{p})$). The position space entropy is closely related to the Weizsäcker kinetic energy (only differing from it by a multiplicative constant $\frac{1}{8N}$). Information theory quantities have been previously used to characterize some bonding patterns and we used them in chapter VIII in an attempt to characterize the harpoon mechanism.

2.3) Approximate Density Matrices

Using density matrices, we reduce the cost of storage and managing information compared to wavefunction methods. Nevertheless, in many cases density matrices are still large objects that are not easy to store and use. As an example, consider a system with 300 basis, thus 300^4 2-RDM elements (${}^2D_{ij,kl}$) are produced.[23] Taking into account that double precision numbers require 8 bytes, already 64.8 gigabytes are needed for storing this matrix. On the other hand, for the same system the 1-RDM would only require 720 megabytes.[22] Therefore, is much more convenient to try to approximate high-order RDMs from lower-order ones.

2.3.1) N-Representability

Reconstruction of higher order RDMs from lower order ones is not a trivial task. The partial trace (integration) reduces the order of density matrices but there is no recipe to recover the information lost during the integration process and it is thus recommendable to impose physical requirements on the reconstruction of approximate RDMs. One physical requirement to impose is the N-representability, which imposes that the reconstructed n-RDM must correspond to an antisymmetric wavefunction for fermionic systems. Unfortunately, all the necessary and sufficient conditions are not known in general for all n-RDMs. Only the whole set of conditions is known for 2-RDMs but they are not practical [134], because this set requires for $N > 2$ the knowledge of all higher order density matrices from 3- up to N-order.

Some N-representability conditions rely on the fact that the whole spectrum of some operators must be positive semidefinite (all their eigenvalues must be greater or equal to 0). The set of conditions related to these operators are

[23] Assuming that no symmetry and/or antisymmetry properties of the 2-RDM are considered. For instance, when symmetry is taken into account savings of the order of $\sim 2n!$ are produced for an n-RDM.

called *positivity* conditions. If we define an operator $\widehat{A}$ as a linear combination of strings of creation ($a^{\dagger}_{a\sigma'}$) and/or annihilation ($a_{a\sigma'}$) operators, with $\widehat{A}^{\dagger}$ being its corresponding adjoint counterpart, the expectation value of

$$\langle\Psi|\widehat{A}^{\dagger}\widehat{A}|\Psi\rangle \geq 0 \tag{58}$$

must hold when $\widehat{A}$ is not a singular operator because then $\widehat{A}^{\dagger}\widehat{A}$ is a Hermitian operator (is actually a hermitian non-negative operator). The $a^{\dagger}_{a\sigma}$ ($a_{a\sigma}$) is the usual creation (annihilation) operator acting over orbital ϕ_a with spin σ.
By setting $\widehat{A} = \sum_{\sigma'}\sum_{j} x_{j\sigma'}a_{j\sigma'}$ in Eq. 58 we get the ${}^{1}\mathbf{D}$ matrix elements,

$${}^{1}D^{\sigma\sigma'}_{i,j} = \langle\Psi|a^{\dagger}_{i\sigma}a_{j\sigma'}|\Psi\rangle. \tag{59}$$

Then, we proceed to diagonalize this matrix (as we did in Eq. 24) and we have to prove that the eigenvalues (the natural orbital occupancies $\{n_i\}_{i=1}^{M}$) must be greater or equal to 0. Setting $\widehat{A} = \sum_{\sigma'}\sum_{j} x_{j\sigma'}a^{\dagger}_{j\sigma'}$ in Eq. 58, we produce the ${}^{1}\mathbf{Q}$ matrix elements

$${}^{1}Q^{\sigma\sigma'}_{i,j} = \langle\Psi|a_{i\sigma}a^{\dagger}_{j\sigma'}|\Psi\rangle, \tag{60}$$

where we can use the anticonmutation relation $\{a_{i\sigma}, a^{\dagger}_{j\sigma'}\} = \delta_{i\sigma j\sigma'}$ to write the ${}^{1}\mathbf{Q}$ matrix as

$${}^{1}\mathbf{Q} = \mathbf{I} - {}^{1}\mathbf{D}, \tag{61}$$

that after diagonalization leads to the conclusion that the occupancies should be lower or equal to 1. Therefore, the *positivity* conditions impose that the whole set of occupancies must be in the interval $[0, 1]$. This condition is enough to ensure that the matrix is N-representable [107]. Nevertheless, this condition only ensures N-representability but not that the 1-RDM corresponds to a pure state; mixed states may arise if we only impose this condition. Recently, some authors have suggested the usage of the so-called Generalize Pauli constraints to ensure that only pure states are generated (see Refs. [135–137]). Nonetheless, we have not considered these constraints in the present thesis, and we only mention their existence for completeness.

In the case of the 2-RDM, the P (Löwdin), Q (Garrod and Percus) and G (Weinhold and Wilson) conditions define strong constraints for the diagonal elements (also known as the (2,2)-positivity conditions). These three conditions require only the 2-RDM; they arise naturally from setting $\widehat{A} = \sum_{\sigma\sigma'} \sum_{lk} x_{l\sigma' k\sigma} a_{l\sigma'} a_{k\sigma}$, $\widehat{A} = \sum_{\sigma\sigma'} \sum_{lk} x_{l\sigma' k\sigma} a^\dagger_{l\sigma'} a^\dagger_{k\sigma}$ and $\widehat{A} = \sum_{\sigma\sigma'} \sum_{lk} x_{l\sigma' k\sigma}\ a^\dagger_{l\sigma'} a_{k\sigma}$ in Eq. 58, respectively. Using these operators we build the following matrices **P**, **Q** and **G**:

$$P^{\sigma\sigma'}_{ij,kl} = \langle \Psi | a^\dagger_{i\sigma} a^\dagger_{j\sigma'} a_{l\sigma'} a_{k\sigma} | \Psi \rangle \,, \tag{62}$$

$$Q^{\sigma\sigma'}_{ij,kl} = \langle \Psi | a_{i\sigma} a_{j\sigma'} a^\dagger_{l\sigma'} a^\dagger_{k\sigma} | \Psi \rangle \,, \tag{63}$$

$$G^{\sigma\sigma'}_{ij,kl} = \langle \Psi | a_{i\sigma} a^\dagger_{j\sigma'} a^\dagger_{l\sigma'} a_{k\sigma} | \Psi \rangle \,, \tag{64}$$

that must be diagonalized in order to analyze their positive semidefinite character (by checking that all eigenvalues produced are greater or equal to zero). The first matrix coincides with the ${}^2\mathbf{D}$, thus proving the P condition is equivalent to prove that geminal occupancies are non-negative. The **Q** matrix involves the positive semidefinite character of the holes while the **G** matrix involves the positive semidefinite character of particle-hole probabilities. Notice that all possible permutations between creation and annihilation operators that generate independent positivity conditions have been taken into account in Eqs. 62-64 [138]. These conditions have been analyzed in detail for many approximations to the 2-RDM in chapter V.

Finally, for 3-RDMs, employing creation and annihilation operators, it is possible to produce the corresponding **P** and **Q** matrices. Additionally, two **G**-like matrices involving particle-hole probabilities can be constructed. The positive semidefinite character of these matrices must be proved upon diagonalization and analysis of their eigenvalues. Notwithstanding, the 3-order matrices to diagonalize are in general extensive, making it computational unaffordable for large systems. For this reason, it is convenient to express these matrices in terms of the n-RDMs, generating expressions that can be checked in a given basis. Upon direct usage of the $\widehat{A}$ string operators, we obtain the following inequalities which

must be satisfied in any basis set,

$$ {}^3D_{ijk,ijk} \geq 0 \tag{65} $$

$$ 1 - {}^1D_{i,i} - {}^1D_{j,j} - {}^1D_{k,k} + {}^2D_{ij,ij} + {}^2D_{ik,ik} + {}^2D_{jk,jk} - {}^3D_{ijk,ijk} \geq 0 \tag{66} $$

$$ {}^2D_{ij,ij} - {}^3D_{ijk,ijk} \geq 0 \tag{67} $$

$$ {}^1D_{i,i} - {}^2D_{ij,ij} - {}^2D_{ik,ik} + {}^3D_{ijk,ijk} \geq 0 \tag{68} $$

These conditions correspond to P-, Q-, G- and G-like conditions and are related to the particles, holes and particle-hole conditions. Since they must hold for any basis, they are also valid within the canonical basis (or the natural orbitals basis if preferred). Obviously, the analysis of these inequalities only with the canonical orbitals is a condition much more relaxed than the conditions obtained from the full diagonalization of **P**, **Q** and **G** matrices. Nevertheless, if any approximated 3-RDM does not satisfy these inequalities in any given basis, there will always be violations of the more stringent conditions obtained upon diagonalization.

All *positivity* conditions that we have introduced are necessary but unfortunately not sufficient to ensure that an 1-, 2- or 3-RDM is N-representable and it is recommendable to impose other known necessary conditions (for instance for 2-RDM see Ref. [138]).

2.3.2) The Sum Rule

Additionally, RDMs must fulfill the sum rule (i.e. appropriate normalization), which is written as

$$ \mathrm{Tr}[{}^1\mathbf{D}] = \sum_i {}^1D_{i,i} = N, \tag{69} $$

$$ \mathrm{Tr}[{}^2\mathbf{D}] = \sum_{ij} {}^2D_{ij,ij} = N(N-1) \tag{70} $$

and

$$ \mathrm{Tr}[{}^3\mathbf{D}] = \sum_{ijk} {}^3D_{ijk,ijk} = N(N-1)(N-2). \tag{71} $$

where Tr stands for the trace of these matrices.

2.3.3) Symmetry Properties

n-order RDMs must present some symmetry properties. The 1-RDM is hermitian with respect to the exchange of indices

$$ {}^1D^{\sigma\sigma'}_{i,j} = \langle\Psi|a^\dagger_{i\sigma'}a_{j\sigma}|\Psi\rangle = \langle\Psi|a^\dagger_{j\sigma}a_{i\sigma'}|\Psi\rangle^* = {}^1D^{\sigma'\sigma *}_{j,i} \tag{72} $$

where the $*$ denotes complex conjugated, which for real ${}^1\mathbf{D}$ matrices implies that ${}^1D^{\sigma\sigma'}_{i,j} = {}^1D^{\sigma'\sigma}_{j,i}$. In the same fashion, it can be proved that the equalities:

$$ {}^2D^{\sigma\sigma'}_{ij,kl} = {}^2D^{\sigma\sigma'}_{kl,ij} \tag{73} $$

and

$$ {}^3D^{\sigma\sigma'\sigma''}_{ijk,lmn} = {}^3D^{\sigma\sigma'\sigma''}_{lmn,ijk} \tag{74} $$

where $\sigma'' \in \{\alpha, \beta\}$ hold for real 2- and 3-RDMs, respectively. Equivalent symmetry properties can be written for higher order RDMs.

2.3.4) Antisymmetry Properties

Due to the fermionic nature of the electrons, which imposes that the wavefunction Ψ must be antisymmetric, n-order RDMs ($n \geq 2$) must fulfill some antisymmetry conditions. For the same spin elements of the 2-RDM, the following equalities

$$ {}^2D^{\sigma\sigma}_{ij,kl} = -{}^2D^{\sigma\sigma}_{ji,kl} = {}^2D^{\sigma\sigma}_{ji,lk} = -{}^2D^{\sigma\sigma}_{ij,lk}. \tag{75} $$

must hold. In the same manner, 3-RDM elements of the same spin also meet the antisymmetry condition with respect to the exchange of indices. The exchange of indices leads to the following equalities

$$ {}^3D^{\sigma\sigma\sigma'}_{ijk,lmn} = -{}^3D^{\sigma\sigma\sigma'}_{jik,lmn} = {}^3D^{\sigma\sigma\sigma'}_{ijk,mln} = ..., \tag{76} $$

notice that σ' can be equal or not to σ. If it is equal to σ, we can also permute it with the rest of indices and the antisymmetry condition must hold; otherwise,

if it is not equal to σ we have no information when we permute it with the rest of indices.

We have used the sum rule and the symmetry conditions to analyze the goodness of RDM approximations available in the literature in chapters IV and V. Violations of these conditions produces spurious results when using these matrices.

2.3.5) n-RDM Approximations

Approximations to matrices of 2- and 3-order were tested in the present thesis, being in all cases built from lower order matrices. That is to say, the 2-RDM is approximated from the 1-order one and the 3-RDM is approximated from the 2-order and the 1-order ones. Most of these approximations were developed in order to provide methodologies for solving the Schrödinger equation (see Refs. [93, 94, 96, 139–146] for some examples).

2.3.5.a) 2-RDM Approximations

2-RDM approximations are used in RDMFT [145,146]. RDMFT was brought to light in 1975 by Gilbert's theorem [87] which is an extension of the Hohenberg-Kohn theorem [53] for nonlocal external potentials. In his work Gilbert demonstrated the existence of an energy functional of the 1-RDM, $E[^1\mathbf{D}]$, which along with the works of Donnelly and Parr [88], Levy [89] and Valone [90] established the foundations of RDMFT. As we have shown in Eq. 25, the energy is an explicit functional of the 2-RDM but only the V_{ee} depends explicitly on the 2-RDM (the rest of energy components depend only on the 1-RDM)

$$E[^1\mathbf{D}] = T[^1\mathbf{D}] + V_{\text{ext}}[^1\mathbf{D}] + V_{ee}[^2\mathbf{D}]. \tag{77}$$

In order to write Eq. 77 as a functional of the 1-RDM we need to express the 2-RDM as a functional of the 1-RDM ($^2\mathbf{D}[^1\mathbf{D}]$). The functional $E[^1\mathbf{D}]$, that exists

according to Gilbert's theorem, must be independent of the basis used to expand the 1-RDM. Thus far, most of the approximations to the 2-RDM are only given in terms of the natural orbitals and natural orbital occupancies. However, many approximations employ expressions that are non orbital invariant[24] and thus, one cannot reconstruct the actual 1-RDM, which is need to guarantee the existence of $E[^1\mathbf{D}]$. Consequently, most energy functionals of the 1-RDM are actually just functional approximations of the 2-RDM ($^2\mathbf{D}[\{n_i\}_{i=1}^M, \{\chi_i\}_{i=1}^M]$).

Before we introduce the 2-RDM approximations analyzed in this thesis, it is worth to mention that in 1956 Löwdin and Shull [148] noticed that the wavefunction for a closed-shell two-electron system can be written in the basis of natural orbitals as

$$\Psi(\mathbf{x}_1, \mathbf{x}_2) = \frac{1}{\sqrt{2}}(\alpha_1\beta_2 - \alpha_2\beta_1)\sum_k c_k\chi_k(\mathbf{r}_1)\chi_k(\mathbf{r}_2) \tag{78}$$

where the coefficients $c_k = \pm n_k^{1/2}$, n_k being the natural orbital occupancy of orbital χ_k. Notice that there is a $\pm$ sign which is sometimes called the phase factor [149]. From Eq. 78, we obtain the 2-RDM

$$\begin{aligned}\gamma_2(\mathbf{x}_1', \mathbf{x}_2'; \mathbf{x}_1, \mathbf{x}_2) = &\frac{1}{2}(\alpha_1'\beta_2' - \alpha_2'\beta_1')(\alpha_1\beta_2 - \alpha_2\beta_1) \\ &\times \sum_{kl} c_k c_l \chi_k(\mathbf{r}_1')\chi_k(\mathbf{r}_2')\chi_l(\mathbf{r}_1)\chi_l(\mathbf{r}_2)\end{aligned} \tag{79}$$

where the product of coefficients $c_k c_l = \Phi_{kl}\sqrt{n_k n_l}$ includes undetermined phase factors, Φ_{kl}. Therefore, two-electron system wavefunctions and 2-RDMs are completely determined by natural orbital occupancies except for some phase factors, $\Phi_{kl} = \{-1, 1\}$. This expression was used by some authors [125,143,150] to define the Fixed-Phases (FP) functional from the phases of some two-electron systems. It was observed that in most cases if natural orbitals are ordered according to their occupancy in most two-electron systems: $\Phi_{1k} = -1$ ($k \neq 1$)

[24] It was proven by Lathiotakis and coworkers [147] that for many approximations to the 2-RDM, unitary transformations in the subspace of degenerate occupation numbers produce changes in the energy.

and all other phases were positive. Thus, it is possible to define the Fermi level which only has one orbital, the χ_1, below it. The FP functional defined by fixing $\Phi_{lk} = -1$ (if $l = 1 \wedge k \neq 1$) and equal to $+1$ otherwise, recovers the exact wavefunction in the weak-correlation regime of closed-shell two-electron systems. Nevertheless, some studies have proven that these phases do not remain fixed and for example, some authors obtained that in the strong-correlation regime for the 2e-Harmonium atom, phases change signs and there is not a fixed pattern [151–154].

The starting point of many 2-RDM approximations is the Hartree-Fock expression for the 2-RDM (Eq.42) which in terms of natural orbitals is written as

$$ {}^2D^{\sigma\sigma'}_{ij,kl} = n_i^\sigma n_j^{\sigma'} \delta_{ik}\delta_{jl} \qquad \sigma \neq \sigma' \tag{80} $$

for the opposite-spin components (where only Coulomb interactions are present), whereas, for the same-spin components we have

$$ {}^2D^{\sigma\sigma}_{ij,kl} = n_i^\sigma n_j^\sigma (\delta_{ik}\delta_{jl} - \delta_{il}\delta_{jk}) \tag{81} $$

for which Coulomb and exchange interactions are taken into account. For any Hartree-Fock energy calculation, the starting point is to define an *ansatz* formed by one single Slater determinant as a trial wavefunction. Using a single-determinant approach implies that the final 1-RDM contains only diagonal elements which are either one (for the occupied orbitals) or zero (for the unoccupied ones). Moreover, the orbitals that minimize the Hartree-Fock energy expression are the canonical orbitals but, since in the canonical basis the 1-RDM is already diagonal, the canonical orbitals and the natural orbitals coincide. It is well known that the single-determinant approach ignores all correlation effects between the electrons of the opposite spin because these electrons are treated as independent particles (i.e. using Eqs. 24 and 80 in Eq. 22, makes the opposite-spin component of the 2-PPD be: $\rho_2^{HF,\sigma\sigma'}(\mathbf{r}_1, \mathbf{r}_2) = \rho^\sigma(\mathbf{r}_1)\rho^{\sigma'}(\mathbf{r}_2)$ for the Hartree-Fock approximation). Thus, in an attempt to retrieve correlation effects, some authors have suggested to modify the exchange component of the

functional expression [125, 155] (arguing that Fermi and Coulomb holes can be modeled by tuning only the exchange effects). That is to say, work with the following modified expression for the same-spin component,

$$^2D^{\sigma\sigma}_{ij,kl} = n^\sigma_i n^\sigma_j \delta_{ik}\delta_{jl} - f(n_i, n_j)\delta_{il}\delta_{jk}, \tag{82}$$

where the whole set of $f(n_i, n_j)$ functions used in the present thesis is collected in Table 1. These approximations of the 2-RDM give rise to approximated functionals of the energy, $\tilde{\mathrm{E}}[^1\mathbf{D}]$, through Eq. 77. The energy functionals that we analyze in chapter V are:

2.3.5.a.1) **MBB:**

Introduced independently by Müller and by Buijse and Baerends [125, 155, 156], it produces an approximated functional which fulfills the sum rule, Eq. 70. This functional was derived from the requirement of minimal violation of the Pauli principle and from the analysis of Fermi and Coulomb holes. Notice that the term $-\sqrt{n_i n_j}$ has to take care of all exchange and correlation effects and make the MBB resemble the FP functional. This functional performs well if the natural orbitals and natural orbital occupancies are not used in a self-consistent procedure. Otherwise, non-variational energies can be obtained (see for example Ref. [157]). Since this functional performs relatively well when applied in a non-self-consistent manner, it has been used for computing approximate properties such as DIs [158], studying interacting quantum atoms electronic energy partitions [159], among others.

2.3.5.a.2) **POWER:**

The POWER functional was introduce by Cioslowski and Pernal [160] to study the properties of the $(n_i n_j)^\alpha$ expression that generalizes the Hartree-Fock and the MBB approximations. It was first proven that $\alpha \geq 0.5565$ was needed to produce admissible densities (i.e. solutions that are: stable with respect to

the corresponding Euler equations, N-representable and whose V_{ee} satisfies the Lieb-Oxford bound [161]). The POWER functional is mostly used in solid state physics and, according to Sharma et al. [162], the MBB overcorrelates the electrons and, thus, the POWER functional mediates with the overcorrelation of the electrons by using a parameter $\alpha > 1/2$. Notice that in some applications, the bound $\alpha \geq 0.5565$ is not fixed and values like 0.53 are used [163].

2.3.5.a.3) **BBC2:**

It is based on physically motivated corrections to the MBB approximation. BBC2 was developed by Gritsenko and coworkers [164], it requires a definition of the Fermi level (F_L) as: the last orbital whose occupancy is greater or equal to $N/2$. It contains corrections to restore the positive sign for cross products between weakly correlated orbitals but also to recover the exchange-type interaction for the strongly occupied natural orbitals. It only keeps the $-\sqrt{n_i n_j}$ to account for the Coulomb correlation between the weakly and strongly occupied orbitals.

2.3.5.a.4) **CA:**

Csányi and Arias functional [165] is based on the framework of tensor-product expansions of the 2-RDM. This functional was developed as a correction to the Hartree-Fock approximation in order to better describe a wide range of density regimes of the homogeneous electron gas, retain the sum rule and exploit the particle-hole symmetry. It clearly improves over the MBB approximation for a wide range of densities of the homogeneous electron gas.

2.3.5.a.5) **CGA:**

Csányi, Goedecker and Arias functional [166] was developed in the same spirit as CA functional using tensor-product expansions of the 2-RDM. It was developed

as an intermediate case of HF and CA approaches. This functional dramatically improves over the previous ones for high densities of the homogeneous electron gas, it significantly improves the correlation energies at typical valence densities, and according to the authors it is comparable to the generalized-gradient approximation performance in atoms [166].

2.3.5.a.6) **ML:**

Marques and Lathiotakis functional [167] was developed using a Padé approximant from a fully empirical approach. This functional was built with three parameters that were fitted to reproduce the correlation energy of the G2 set and to recover the Hartree-Fock limit for integer occupation numbers.

2.3.5.a.7) **MLSIC:**

Marques and Lathiotakis functional corrected for self-interaction [167] is an improvement of the previous one, it was developed to correct the self-interaction error produced by ML approximation but keeping the same structure of a Padé approximant but reoptimizing the parameters.

2.3.5.a.8) **GU:**

Goedecker and Umrigar functional [150] only corrects the self-interaction error present in MBB. It removes the elements producing the self-interaction error but the rest of elements are completely equivalent to the MBB ones.

The eight functionals already introduced are known as JK-only functionals because the 2-RDM elements produced are ${}^2D^{\sigma\sigma'}_{ij,ij}(\sigma,\sigma' \in \{\alpha,\beta\})$ and ${}^2D^{\sigma\sigma}_{ij,ji}(\sigma \in \{\alpha,\beta\})$, which are either accompanied by the Coulomb integrals ($J_{ij} = \langle ij|ij\rangle$) or by exchange integral ($K_{ij} = \langle ij|ji\rangle$) respectively. In the description of BBC2

we have introduced the F_L which is used in solid state physics to analyze the energy levels. The F_L can be considered to be an energy level of an electron, such that at thermodynamic equilibrium this energy level would have a 50% probability of being occupied at any given time ($n_{F_L} \geq 0.5$) [168]. Unfortunately, the inclusion of the F_L in the definition of the approximation can also thwart the orbital invariance and make the approximation not truly a functional of the 1-RDM.

Table 1 – $f(n_i, n_j)$ functions (see Eq. 82) that define the JK-only functionals, where F_L is the Fermi level defined as $F_L = N/2$.

Functional	$f(n_i, n_j)$	parameters	Ref.
MBB	$(n_i n_j)^{1/2}$		[125, 156]
POWER	$(n_i n_j)^{\alpha}$		[160, 162, 169]
BBC2	n_i $\quad i = j$ $-(n_i n_j)^{1/2}$ $\quad i \neq j \wedge i \in (F_L; \infty) \wedge j \in (F_L; \infty)$ $n_i n_j$ $\quad i \neq j \wedge i \in [1; F_L] \wedge j \in [1; F_L]$ $(n_i n_j)^{1/2}$ $\quad$ otherwise		[164]
CA	$[n_i(1-n_i)n_j(1-n_j)]^{1/2} + n_i n_j$		[165]
CGA	$\frac{n_i n_j + [n_i(2-n_i)n_j(2-n_j)]^{1/2}}{2}$		[166]

ML	$n_i n_j \frac{a_0+a_1 n_i n_j}{1+b_1 n_i n_j}$		$a_0 = 126.3101$ $a_1 = 2213.33$ $b_1 = 2338.64$	[167]
MLSIC	$n_i n_j \frac{a_0+a_1 n_i n_j}{1+b_1 n_i n_j}$	$i \neq j$	$a_0 = 1298.78$ $a_1 = 35114.4$ $b_1 = 36412.2$	[167]
	$n_i n_j$	$i = j$		
GU	$(n_i n_j)^{1/2}$	$i \neq j$		[150]
	$n_i n_j$	$i = j$		

Another approach for building approximated 2-RDMs is based on the cumulant expansion. By adding to the Hartree-Fock expression of the 2-RDM, Eq. 42, a cumulant matrix Γ is defined:

$$ {}^2D^{\sigma\sigma'}_{ij,kl} = n^\sigma_i n^{\sigma'}_j \delta_{ik}\delta_{jl} + {}^2\,\Gamma^{\sigma\sigma'}_{ij,kl} \qquad \sigma \neq \sigma' \tag{83} $$

and

$$ {}^2D^{\sigma\sigma}_{ij,kl} = n^\sigma_i n^\sigma_j (\delta_{ik}\delta_{jl} - \delta_{il}\delta_{jk}) + {}^2\,\Gamma^{\sigma\sigma}_{ij,kl}. \tag{84} $$

Cumulants gather all correlation effects not contained in the Hartree-Fock approximation (recall that Hartree-Fock only treats correctly Fermi correlation). Hence, the two matrices (${}^2\Gamma^{\sigma\sigma'}_{ij,kl}$ and ${}^2\Gamma^{\sigma\sigma}_{ij,kl}$) should contain all the missing correlation effects to construct the exact 2-RDM. We have seen that cumulants appear naturally from the statistical nature of density matrices when we introduced the nc-ESI. Actually, it is well known that n-order RDMs can be expressed from lower order ones by employing approximations to the cumulant

matrices [170].

2.3.5.a.9)**PNOF Functionals:**

To keep the approximations simple, instead of producing four index approximated matrices, it is much more suitable to stick to only two indices and set to zero all elements that differ in three and four indices. Therefore, the cumulants are approximated by means of the auxiliary matrices $\mathbf{\Delta}$ and $\mathbf{\Pi}$ in the following manner

$$^2\Gamma^{\sigma\sigma'}_{ij,kl} = -\Delta^{\sigma\sigma'}_{ij}\delta_{ik}\delta_{jl} + \Pi_{ik}\delta_{ij}\delta_{kl} \qquad \sigma \neq \sigma' \tag{85}$$

and

$$^2\Gamma^{\sigma\sigma}_{ij,kl} = -\Delta^{\sigma\sigma}_{ij}\delta_{ik}\delta_{jl} + \Delta^{\sigma\sigma}_{ij}\delta_{il}\delta_{jk}, \tag{86}$$

where the $\mathbf{\Delta}$ and $\mathbf{\Pi}$ matrices are constructed attending to the P-, Q-, and G-N-representability conditions (when possible), to attain the sum rule and to keep some fundamental properties of fermionic particles ($\langle S^2\rangle$, antisymmetry). Different definitions of these matrices produce different implementations of the PNOFi ($i = 2, .., 7$) functionals. The $\mathbf{\Delta}$ matrix is taken equal for both spin cases (i.e. $\Delta^{\sigma\sigma}_{ij} = \Delta^{\sigma\sigma'}_{ij}$), except for PNOF3 where $\Delta^{\sigma\sigma}_{ij} = 0$. The whole family of $\mathbf{\Delta}$ and $\mathbf{\Pi}$ matrices is collected in Table 2.

Table 2 – Δ and Π non-zero matrix elements. The diagonal elements coincide for all functionals: $\Delta_{ii} = n_i^2$ and $\Pi_{ii} = n_i$. $S_F = \sum_{i=1}^{F_L} h_i$, $T_{ij} = n_i n_j - \Delta_{ij}$, $h_i = 1 - n_i$, and S_γ^x and γ_i are defined in Eqs. 88 and 89, respectively. Ω_g is the subspace containing orbital g, which is below the Fermi level, and several orbitals above the Fermi level.

	Δ_{ij}	Π_{ij}	cases ($i \neq j$)	Ref.
PNOF2	$h_i h_j$	$\sqrt{n_i n_j} + \sqrt{h_i h_j} + T_{ij}$	$i \wedge j \in [1, F_L]$	[171]
	$n_j h_i \left(\frac{1-S_F}{S_F}\right)$	$\sqrt{n_i n_j} - \sqrt{n_j h_i} + T_{ij}$	$i \in [1, F_L] \wedge j \in (F_L, M]$	
	$n_i h_j \left(\frac{1-S_F}{S_F}\right)$	$\sqrt{n_i n_j} - \sqrt{n_i h_j} + T_{ij}$	$j \in [1, F_L] \wedge i \in (F_L, M]$	
	$n_i n_j$	T_{ij}	$i \wedge j \in (F_L, M]$	
PNOF3	$h_i h_j$	$n_i n_j - \sqrt{n_i n_j}$	$i \wedge j \in [1, F_L]$	[172]
	$n_j h_i \left(\frac{1-S_F}{S_F}\right)$	$n_i n_j - \sqrt{n_i n_j} - \sqrt{n_j h_i}$	$i \in [1, F_L] \wedge j \in (F_L, M]$	
	$n_i h_j \left(\frac{1-S_F}{S_F}\right)$	$n_i n_j - \sqrt{n_i n_j} - \sqrt{n_i h_j}$	$j \in [1, F_L] \wedge i \in (F_L, M]$	
	$n_i n_j$	$n_i n_j + \sqrt{n_i n_j}$	$i \wedge j \in (F_L, M]$	

PNOF4	$h_i h_j$	$-\sqrt{h_i h_j}$	$i \wedge j \in [1, F_L]$	[173]
	$n_j h_i \left(\frac{1-S_F}{S_F}\right)$	$-\sqrt{\left(\frac{h_i n_j}{S_F}\right)\left(n_i - n_j + \frac{h_i n_j}{S_F}\right)}$	$i \in [1, F_L] \wedge j \in (F_L, M]$	
	$n_i h_j \left(\frac{1-S_F}{S_F}\right)$	$-\sqrt{\left(\frac{h_j n_i}{S_F}\right)\left(n_j - n_i + \frac{h_j n_i}{S_F}\right)}$	$j \in [1, F_L] \wedge i \in (F_L, M]$	
	$n_i n_j$	$\sqrt{n_i n_j}$	$i \wedge j \in (F_L, M]$	
PNOF5	$n_i n_j$	$-\sqrt{n_i n_j}$	$(i \wedge j \in \Omega_g) \wedge (i = g \vee j = g)$	[174]
	$n_i n_j$	$\sqrt{n_i n_j}$	$(i \wedge j \in \Omega_g) \wedge (i \wedge j \in (F_L, M])$	
PNOF6x	$e^{-2S_F} h_i h_j$	$-e^{-S_F}\sqrt{h_i h_j}$	$i \wedge j \in [1, F_L]$	[175]
	$\gamma_i \gamma_j / S^x_\gamma$	$-\sqrt{\left(n_i h_j + \frac{\gamma_i \gamma_j}{S^x_\gamma}\right)\left(n_j h_i + \frac{\gamma_i \gamma_j}{S^x_\gamma}\right)}$	$i \in [1, F_L] \wedge j \in (F_L, M]$	
$x = d,\ u,\ h$	$\gamma_i \gamma_j / S^x_\gamma$	$-\sqrt{\left(n_i h_j + \frac{\gamma_i \gamma_j}{S^x_\gamma}\right)\left(n_j h_i + \frac{\gamma_i \gamma_j}{S^x_\gamma}\right)}$	$j \in [1, F_L] \wedge i \in (F_L, M]$	
	$e^{-2S_F} n_i n_j$	$e^{-S_F}\sqrt{n_i n_j}$	$i \wedge j \in (F_L, M]$	
PNOF7	$n_i n_j$	$-\sqrt{n_i n_j}$	$(i \wedge j \in \Omega_g) \wedge (i = g \vee j = g)$	[176]
	$n_i n_j$	$\sqrt{n_i n_j}$	$(i \wedge j \in \Omega_g) \wedge (i \wedge j \in (F_L, M])$	
	0	$-\sqrt{n_i h_i n_j h_j}$	$(i \vee j) \in [1, F_L] \wedge ((i \in \Omega_g \wedge j \notin \Omega_g) \vee (j \in \Omega_g \wedge i \notin \Omega_g))$	
	0	$\sqrt{n_i h_i n_j h_j}$	$(i \wedge j) \in (F_L, \infty) \wedge ((i \in \Omega_g \wedge j \notin \Omega_g) \vee (j \in \Omega_g \wedge i \notin \Omega_g))$	

In Table 2 we have collected all non-zero elements of $\mathbf{\Delta}$ and $\mathbf{\Pi}$ matrices. PNOF5 was originally based on a perfect pairing approach. The perfect pairing approach is given by the occupancies as

$$n_i + n_j = 1, \tag{87}$$

where the occupancy n_i of an orbital $\chi_i \in [1, F_L)$ is coupled to the occupancy n_j of only one orbital $\chi_j \in (F_L, \infty)$. Later, PNOF5 was extended to produce the PNOF5e functional, where the occupancy of an orbital $\chi_i \in [1, F_L)$ is coupled to the occupancies of a set of orbitals $\{\chi_j\} \in (F_L, \infty)$. PNOF6 was also conceived in a perfect pairing approach but it has also been used in a extended version (PNOF6e) for calculations. In this thesis, we used PNOF5e and PNOF6e functionals but **we kept the names PNOF5 and PNOF6 for them**. PNOF6 requires the definition of S_γ^x (see Table 2 for more details), thus, beyond the perfect pairing approach (i.e. for the extended version of PNOF6) three different definitions of S_γ^x can be proposed. The three S_γ^xs used in this thesis are defined as

$$S_\gamma^d = \sum_{i=1}^{F_L} \gamma_i, \qquad S_\gamma^u = \sum_{i>F_L}^{M} \gamma_i, \qquad S_\gamma^h = \frac{S^d + S^u}{2}, \tag{88}$$

where

$$\gamma_i = n_i(1 - n_i) + \kappa_i^2 - \kappa_i \sum_{i=j}^{F_L} \kappa_j, \tag{89}$$

and

$$\kappa_i = \begin{cases} (1 - n_i)e^{-S_F} & i \in [1, F_L] \\ n_i e^{-S_F} & i \in (F_L, M] \end{cases} \tag{90}$$

F_L being the last occupied orbital below the Fermi level and $S_F = \sum_{i=1}^{F_L}(1-n_i)$. PNOF$i$ approximations are known as JKL-only approximations because they include Coulomb (J_{ij}), exchange (K_{ij}) and the exchange and time-inversion integrals (i.e. $L_{ij} = \langle ii|jj\rangle$ in the usual bra-ket notation). All approximations here introduced, rapidly approach to the Hartree-Fock approximation in the weak-correlation regime. Thus, our concern about how correlation affects 2-RDM approximations is clarified in chapter V, where we analyze ten properties

of 2-RDM approximations (see below) at different correlation regimes of the two-electron Harmonium atom.

Finally, let us mention that the formal cost of RDMFT calculations is of M^4 (where M is the size of the basis) when the 2-RDM approximations are employed. RDMFT calculations require the transformation of the integrals from the atomic orbital basis to the molecular orbital basis, which implies an additional cost of M^5. Nevertheless, the self-consistent procedure used by RDMFT calculations optimizes orbitals and occupancies, thus, the prefactor of the self-consistent procedure is very large, resulting in a very large number of iterations. Since many iterations are required, in practice the cost is much higher than the formal M^5 scaling.

2.3.5.b) **3-RDM Approximations**

High order approximations to n-RDMs also start from the corresponding n-order Hartree-Fock RDMs, adding all missing correlation effects beyond the Hartree-Fock approximation through the corresponding n-order cumulants. In the present thesis, we worked with up to 3-RDMs approximations. Thus, the starting point is a Slater determinant, and for this wavefunction, the HF 3-RDM reads,

$$\gamma_3^{\mathrm{HF}}(\mathbf{x}_1', \mathbf{x}_2', \mathbf{x}_3'; \mathbf{x}_1, \mathbf{x}_2, \mathbf{x}_3) = \begin{vmatrix} \gamma_1(\mathbf{x}_1'; \mathbf{x}_1) & \gamma_1(\mathbf{x}_1'; \mathbf{x}_2) & \gamma_1(\mathbf{x}_1'; \mathbf{x}_3) \\ \gamma_1(\mathbf{x}_2'; \mathbf{x}_1) & \gamma_1(\mathbf{x}_2'; \mathbf{x}_2) & \gamma_1(\mathbf{x}_2'; \mathbf{x}_3) \\ \gamma_1(\mathbf{x}_3'; \mathbf{x}_1) & \gamma_1(\mathbf{x}_3'; \mathbf{x}_2) & \gamma_1(\mathbf{x}_3'; \mathbf{x}_3) \end{vmatrix} . \qquad (91)$$

In order to simplify the notation, let us introduce the Grassmann product also known as wedge product [177]. This product allows the formation of an m-dimensional matrix from permutations of indices of several q_i-dimensional matrices, so that $\sum_i q_i = m$ and the antisymmetry of the formed matrix is preserved. The Grassmann product of a and b matrices of dimension q and $m - q$

is:

$$(a \wedge b)^{i_1,i_2,\ldots,i_m}_{j_1,j_2,\ldots,j_m} = a^{i_1,i_2,\ldots,i_q}_{j_1,j_2,\ldots,j_q} \wedge b^{i_{q+1},i_{q+2},\ldots,i_m}_{j_{q+1},j_{q+2},\ldots,j_n} \tag{92}$$

$$= \left(\frac{1}{n!}\right)^2 \sum_{\pi} \sum_{\sigma} \widehat{\pi}\widehat{\sigma}\epsilon(\pi)\epsilon(\sigma) a^{i_1,i_2,\ldots,i_q}_{j_1,j_2,\ldots,j_q} b^{i_{q+1},i_{q+2},\ldots,i_m}_{j_{q+1},j_{q+2},\ldots,j_n} \tag{93}$$

where $\widehat{\pi}$ permutes all superindices, $\widehat{\sigma}$ permutes all subindices, $\epsilon(\pi)$ and $\epsilon(\sigma)$ return 1 [-1] for even [odd] permutations. Within this notation, the Hartree-Fock 2-RDM is simply ${}^2\mathbf{D}^{\mathrm{HF}} = {}^1\mathbf{D} \wedge {}^1\mathbf{D} = {}^1\mathbf{D}^2$. Notice that the correct symmetry is generated thanks to the $\epsilon(\pi)$ and $\epsilon(\sigma)$ functions. Considering the cumulant matrix (${}^2\mathbf{\Gamma}$), any 2-RDM is written as ${}^2\mathbf{D} = {}^1\mathbf{D}^2 + {}^2\mathbf{\Gamma}$ using the Grassmann product. It is easy to demonstrate that for the Hartree-Fock approximation the two cumulants: ${}^2\mathbf{\Gamma}$ and ${}^3\mathbf{\Gamma}$ are set to zero. Therefore, the Hartree-Fock expression for the 3-RDM is simply

$${}^3\mathbf{D}^{\mathrm{HF}} = {}^1\mathbf{D}^3. \tag{94}$$

In this vein, any 3-RDM can be written using the Grassmann product, the exact 1-RDM and the exact 2-RDM as

$${}^3\mathbf{D} = -3\ {}^1\mathbf{D}^3 + 9\ {}^2\mathbf{\Gamma} \wedge {}^1\mathbf{D} + {}^3\mathbf{\Gamma} \tag{95}$$

where ${}^1\mathbf{D}^3 = {}^1\mathbf{D} \wedge {}^1\mathbf{D} \wedge {}^1\mathbf{D}$,${}^2\mathbf{\Gamma}$ is the cumulant matrix for the 2-RDM and ${}^3\mathbf{\Gamma}$ is the cumulant matrix for the 3-RDM. The last term collects only third-order correlation effects, the rest of effects are captured by $9\ {}^2\mathbf{\Gamma} \wedge {}^1\mathbf{D}$. The next approximation that we want to introduce is Valdemoro's approximation [95], where the ${}^3\mathbf{\Gamma} = \mathbf{0}$. This approximation is based on the relationship between particles and holes. Within this approximation, all correlation effects introduced are only captured through the ${}^2\mathbf{\Gamma}$ matrix. By setting ${}^3\mathbf{\Gamma} = \mathbf{0}$ in Eq. 95, we obtain

$${}^3\mathbf{D}^{\mathrm{VAL}} = 9\ {}^2\mathbf{D} \wedge {}^1\mathbf{D} - 12\ {}^1\mathbf{D}^3. \tag{96}$$

In order to improve over Valdemoro's approximation, Mazziotti [178] and Nakatsuji [179] proposed some approximations to the missing ${}^3\mathbf{\Gamma}$ cumulant. Mazziotti and Nakatsuji proposed the usage of the ${}^2\mathbf{\Gamma}$ matrix in the following manner

$$\left[{}^3\mathbf{D}^{\mathrm{MAZ}}\right]_{ijk,lmn} = \left[{}^3\mathbf{D}^{\mathrm{VAL}}\right]_{ijk,lmn} - \frac{1}{\xi^{lmn}_{ijk} - 3} \sum_{p} \widehat{A}\left({}^2\Gamma_{ij,lp}\ {}^2\Gamma_{pk,mn}\right) \tag{97}$$

and

$$\left[{}^3\mathbf{D}^{\mathrm{NAK}}\right]_{ijk,lmn} = \left[{}^3\mathbf{D}^{\mathrm{VAL}}\right]_{ijk,lmn} + \sum_p \sigma_p \widehat{A}\left({}^2\Gamma_{ij,lp}\ {}^2\Gamma_{pk,mn}\right) \tag{98}$$

where $\widehat{A}$ performs the antisymmetric summation of i, j and k indices, and l, m and n indices (without mixing them) excluding the p index from the permutations, for orbitals below the Fermi level and $\sigma_p = -1$ otherwise, $\sigma_p = 1$, and $\xi_{ijk}^{lmn} = {}^1D_{i,i} + {}^1D_{j,j} + {}^1D_{k,k} + {}^1D_{l,l} + {}^1D_{m,m} + {}^1D_{n,n}$. These approximations are commonly used in solving the Contracted Schrödinger Equation[25] [92–98] and the Antihermitian Contracted Schrödinger Equation formalisms [99].

Matito and coworkers [102] have developed an approximation to the diagonal elements of the ${}^3\mathbf{D}$ matrix. Their starting point is a reformulation of Eq. 95 only in terms of the ${}^2\mathbf{D}$,

$${}^3\mathbf{D} = -2{}^1\mathbf{D}^3 + 3\ {}^2\mathbf{D} \wedge {}^1\mathbf{D} + {}^3\mathbf{\Gamma}, \tag{99}$$

from Eq. 99, we could collect all diagonal elements and write

$$\begin{aligned} {}^3D_{ijk,lmn} = &-2{}^1D_{i,l}{}^1D_{j,m}{}^1D_{k,n} + {}^2D_{ij,lm}{}^1D_{k,n} + {}^2D_{ik,ln}{}^1D_{j,m} \\ &+ {}^2D_{jk,mn}{}^1D_{i,l} + {}^3\Delta_{ijk,lmn} \end{aligned} \tag{100}$$

where ${}^3\Delta_{ijk,lmn}$ contains all missing terms needed to recover the appropriate antisymmetry but also the ${}^3\Gamma_{ijk,lmn}$ elements. They suggested the construction of some of these elements (in the natural orbital basis) as

$${}^3\Delta_{ijk,lmn} = 2\delta_{in}\delta_{jl}\delta_{km}(n_i n_j n_k)^a, \tag{101}$$

where $a = 1$, $1/2$ or $1/3$. Notice that the Kronecker delta forces that only ${}^3\Delta_{ijk,jki}$ elements are non zero. Therefore, not all elements are reconstructed within this approximation. Nevertheless, it can be easy proven that the ${}^3\mathbf{D}$ constructed taking $a = 1/3$ attains the correct normalization. The justification of this approximation relies on simple and cheap approximation for the evaluation of the 3c-ESI that generalizes Müller approximation for the DI. With this

[25] Actually, for the Contracted Schrödinger Equation we also need the 4-RDM.

approximation, the 3c-ESI is simply

$$\delta(A_1, A_2, A_3) = 4\sum_{ijk}(n_i n_j n_k)^a S_{ij}(A_1) S_{jk}(A_2) S_{ki}(A_3) \tag{102}$$

in the natural orbital basis. In consequence, the missing elements needed to build the total ${}^3\mathbf{\Delta}$ matrix have not been provided up to now because they are not needed for the evaluation of the 3c-ESI.

All ${}^2\mathbf{D}$ and ${}^3\mathbf{D}$ approximations here presented have been put to the test with the 2- and 3-electrons Harmonium atom models because of the simplicity to tune correlation effects within these systems. In chapters IV and V the corresponding studies are presented and the most important conclusions are presented in the *Results and Discussions*, and *Conclusions* sections.

2.4) The Harmonium Atom Model

The harmonium atom model is obtained by replacing the Coulomb electron-nucleus attraction by a parabolic confinement $-\frac{Z}{|\mathbf{r}|} \rightarrow \frac{1}{2}\omega^2\mathbf{r}^2$ [86]. Hence, the Hamiltonian for this system is

$$\widehat{H} = \sum_i \left(-\frac{\nabla_i^2}{2} + \frac{1}{2}\omega^2\mathbf{r}_i^2\right) + \sum_{i>j}\frac{1}{|\mathbf{r}_i - \mathbf{r}_j|} \tag{103}$$

Notice that the usual Coulomb electron-electron repulsion remains unchanged. The ω parameter is called the confinement strength. This parameter allows to easily tune correlation effects. For large ω values the electrons are strongly confined and the kinetic energy dominates over the electron-electron repulsion; thus electrons behave almost like independent particles in this region and any mean field theory (like Hartree-Fock) is good enough for describing the system. Thus large ω values define the low-correlation regime. The strong-correlation regime is thus produced by small ω values and the multiconfiguration character of the wavefunction in this region makes the occupancies of the natural orbitals tend to zero. Small ω values introduce strong-correlation effects by reducing the

kinetic energy of the system making the V_{ee} dominant in this region. Actually, in the $\omega \to \infty$ limit a Wigner crystallization of the electrons is produced [180].

This model system is widely used for method benchmarking as well as developing new methods (specially for developing density functional approximations in DFT). The 2-electron Harmonium atom is especially interesting since it was proven by Santos [181] and later by Taut [182] that is analytically solvable for an infinite set of ω values. That is to say, closed-form expressions for the wavefunctions can be found for the singlet and the triplet states for an infinite set of ω values, making this system an excellent candidate for understanding correlation effects because correlation effects seem to be independent of the external potential as P. M. W. Gill and coworkers recently pointed out from his work with Spherium atom model [183]. Therefore, the information gathered from this system should be easily transferable to real atoms and molecules. It is worth to mention that because of the nature of the external parabolic potential, this model cannot ionize (i.e. all energy levels are quantized).

In this thesis, we have worked with the 2- and 3-electron harmonium atoms. For the 2-electron case we worked with the ^1S state (see chapter V) whereas for the 3-electron case we worked with the ^2P and ^4P states in chapter IV. We have used this model system as a benchmark tool for analyzing how correlation effects affect 2-RDM and 3-RDM approximations. To do so, we used a set of 20 ω values [184], ranging between 0.03 and 1000, for the 2-electron Harmonium atom and with 12 ω values for the 3-electron case (ranging from 0.1 to 1000) [185], covering a large spectrum of the strong- and weak-correlation regimes. In previous works, Cioslowski and coworkers developed a set of even-tempered basis functions, ranging from 4SP to 8SPDF basis functions, for the set of ω values that were also used in the present thesis [186–189]. In chapters IV and V we used the 7SPDF even-tempered basis, which consists of 7s, 7p, 7d and 7f orbitals.

2.5) Chemical Models

The chemical descriptors (e.g. the DI) are used to study properties such as: electron delocalization [190–192], aromaticity [115, 193–196], characterize agostic bonds [197], among others. We have used some of these chemical descriptors (i.e. the DI, the ESI and the radial IPD) as benchmark tools of 2- and 3-RDM matrices in chapters IV and V. Nevertheless, we also used them in this thesis for chemical purposes to: a) visualize electron rearrangements (through the analysis of the $I(s)$), b) understand a certain feature of the Coulomb hole of Ne atom and c) to characterize the so-called harpoon mechanism.

In chapter VI we analyze the changes in $I(s)$ (Eq. 47) along the dissociation process in order to understand the electronic rearrangements during the bond formation/dissociation process. To this end, we worked with H_2 in its ground state and some excited states ($^{1,3}\Pi$), HeH^+, LiH, BH, LiF, F_2, CO and N_2. In this chapter we proposed a simple approximation to the usually expensive exact radial intracule probability density using an approximate wavefunction and a MBB reconstruction for the 2-RDM. Finally, we also tested the goodness and advantages of using MBB approximation for computing the $I(s)$ by comparing the approximate $I(s)$ with the exact one.

Next, we used the $I(s)$ to study of the Coulomb hole of the Neon atom. It was previously observed that in this Coulomb hole there is a shoulder for small r_{12} values (around 0.1 Å). In chapter VII we study the nature of Ne atom's Coulomb hole and unveil the reason for the existence of this shoulder from highly accurate CISD wavefunctions. Some fundamental questions about the importance of the basis functions needed to observe this shoulder are addressed and also discussed in this chapter.

Finally, in chapter VIII we worked with some diatomic systems H_2, He_2, LiH, BeH, BH, LiF, F_2, CO and N_2 to study the harpoon mechanism. In this mecha-

nism, during the formation of the molecule, there is at least one avoided crossing at some geometry R_{AB} between two diabatic states one ionic and another covalent, resulting into two Potential Energy Curves (PECs) of two adiabatic states with varying ionic/covalent character. The resulting PEC for the ground-state shows a change of character from ionic (at the equilibrium distance) to covalent (at the dissociated limit where neutral atoms are formed), which occurs around avoided crossing geometry R_{AB}. We have worked with the Shannon entropies (Eqs. 54 and 55), Fisher integrals (Eqs. 56 and 57), DI (Eq. 32), ELF (Eq. 45) and $-\nabla^2\rho(\mathbf{r})$ (this is known as an indicator of density concentration [109, 198]). In order to find a chemical descriptor able to recognize this change in the ground-state wavefunction for systems expected to be formed by the harpoon mechanism, LiH, BH, BeH and LiF. H_2, F_2, CO, N_2 and He_2 molecules were taken as counterexamples since the first four are formed by covalent bonds (formed by single or triple bonds) and the last one is formed by dispersion forces (van der Waals interactions).

III) Objectives

The main objective of this thesis is the development and application of RDMs (and reduced quantities), focusing on the development of benchmarks to analyze many properties that we can compute using RDMs. We have introduced n-RDMs and the properties that we used in the development of the benchmarks in the *Methodology* section. Moreover, we have also used some properties that depend on n-RDMs to give new insights of chemical reactions and the electronic structure of Ne atom. In this chapter the detailed objectives of the thesis will be presented.

The emerging methodologies that use reduced quantities other than the electronic density for the computation of the energy (e.g. RDMFT, variational-2RDM, CSE, among others.) have led to the development of functionals of the energy in terms of the 1-RDM and the 2-RDM. These methodologies provide alternatives to the widely used DFT method, usually improving DFT description of strongly-correlated systems. Contrary to DFT, for which many benchmarks are available, exhaustive benchmarks for approximations to the 2-RDM and 3-RDM were not available. Thus, one of the objectives of this thesis is to produce them. According to recent studies [84], benchmarks should include as many properties as possible, thus we have proceed in consequence and evaluated many properties of the approximate matrices (e.g. N-representability properties, symmetry properties, 3c-ESI, DI, radial IPDs, among others). The Hartree-Fock approximation is an excellent approximation when electron-correlation effects are negligible and, therefore, many 2-RDM and 3-RDM approximations retrieve the Hartree-Fock approximation in the weak-correlation limit. Nevertheless, the information of how electron correlations affects them was missing in the literature. In order to study how electron correlations affects the 2- and 3-RDM approximations, we propose to work with the 2- and the 3-electron Harmonium atoms, which allow an easy tunning of correlation effects. The benchmarks pro-

posed in this thesis consist on a battery of tests, where the properties chosen are easy to assess and not expensive (from the computational perspective). **Our benchmarks should not only serve as pure calibration tools for the available approximations, they should also bring light on the drawbacks present in the available approximations and provide clues to develop better approximations in the future.** The benchmarks should be easily extended to molecular systems, where we will also use some properties like the 3c-ESI to evaluate the performance of the approximations in these systems.

Another objective is to adquire a broader view of the radial IPD which depends on density matrices. The radial IPD is used as a benchmark tool in the first objective of this thesis but we need to understand the information contained within this magnitude. Therefore, we propose to compute it along the bond formation process of some simple but representative diatomic molecules (H_2, LiH, BH, Li_2, F_2, CO, among others) in order to analyze how electron rearrangements can be visualize using it. The computation of the radial IPD is usually expensive, thus, we will also try to propose some alternative to the exact radial IPD. Secondly, the next objective was to **analyze how electron correlation affects the shell structure of atoms**, thus Neon's atom Coulomb hole is an excellent candidate because it presents some shoulder in the small interelectronic region that needs to be studied in detail. We will understand what correlation effects of the K-shell electrons produce the shoulder and we will also analyze how electron correlation affects the different shells by studying the K and L shells separately.

Our last objective is to **describe the harpoon mechanism using chemical descriptors** based on reduced quantities. This work must be carried out using small diatomic systems that follow the mechanism and using also some counterexamples, LiH being the simplest and most representative system formed by this mechanism. This study should also provide a detailed analysis of the ability of the chemical descriptors to track the electron transfer. The chemical

descriptors proposed for the analysis are the ELF, the Laplacian of the electronic density, the analysis of the population and information theory quantities. This study should also serve to test the ability to track the electron transfer of descriptors proposed in the future. We also want to know how the atomic partition affects the values obtained for the descriptors in this analysis.

IV) Benchmarking 3-RDM Approximations

4.1) Electron Correlation Effects in Third-Order Densities

Rodríguez-Mayorga M., Ramos-Cordoba E., Feixas F., Matito E. “Electron correlation effects in third-order densities”. *Phys. Chem. Chem. Phys*. Vol. 19 (2017) : 4522-4529.

https://doi.org/10.1039/C6CP07616E

PCCP

PAPER

View Article Online
View Journal | View Issue

Cite this: *Phys. Chem. Chem. Phys.*, 2017, **19**, 4522

Electron correlation effects in third-order densities†

Mauricio Rodriguez-Mayorga,[ab] Eloy Ramos-Cordoba,[ac] Ferran Feixas[b] and Eduard Matito*[ad]

Received 7th November 2016,
Accepted 4th January 2017

DOI: 10.1039/c6cp07616e

rsc.li/pccp

The electronic energy of a system of fermions can be obtained from the second-order reduced density matrix through the contracted Schrödinger equation or its anti-Hermitian counterpart. Both energy expressions depend on the third-order reduced density matrix (3-RDM) which is usually approximated from lower-order densities. The accuracy of these methods depends critically on the set of *N*-representability conditions enforced in the calculation and the quality of the approximate 3-RDM. There are no benchmark studies including most 3-RDM approximations and, thus far, no assessment of the deterioration of the approximations with correlation effects has been performed. In this paper we introduce a series of tests to assess the performance of 3-RDM approximations in a model system with varying electron correlation effects, the three-electron harmonium atom. The results of this work put forward several limitations of the currently most used 3-RDM approximations for systems with important electron correlation effects.

1 Introduction

The equations to calculate the electronic energy of an *N*-electron system have been known for a long time, however, their exact application leads to equations much too complicated to be solved.[1] Indeed, the energy is a well-known functional of the wavefunction and there exist a plethora of methods to construct increasingly accurate wavefunctions leading to corresponding approximations of the electronic energy. The complex structure of a wavefunction complicates the practical solutions of the underlying mathematical equations and, therefore, many wavefunction methods can only be applied to molecules of modest size. Conversely, there are robust theorems assessing the existence of energy functionals of the density[2] and the first-order reduced density matrix (1-RDM),[3] however, the exact functional is not known and the accuracy of the corresponding approximations is not so easily assessed.

A completely different set of approximations is obtained if the working ansatz is the second-order reduced density matrix (2-RDM). For a system of fermions subject to one and two-particle forces the exact energy can be completely expressed in terms of the 2-RDM.[4–7] Many authors have attempted the calculation of the ground-state energy from the 2-RDM because it is a much simpler object than the electronic wavefunction and, therefore, it entails a reduced computational cost. The use of the variational method to calculate the energy of a system involves the modification of the 2-RDM subject to the *N*-representability conditions (see Section 2.2). Although a complete set of *N*-representability conditions of the 2-RDM is nowadays known,[8] a practical solution to the problem remains to be found. Besides, the *N*-representability problem of *n*-order reduced density matrices (*n*-RDM), for $n > 2$, is still unsolved.

Notwithstanding, the contracted Schrödinger equation (CSE)[9–17] and the anti-Hermitian counterpart (ACSE)[18] have rekindled the interest in methods that use the 2-RDM and higher-order densities.[19] Both CSE and ACSE energy expressions depend on the 3-RDM (the CSE depends also on the 4-RDM),[20,21] which is usually approximated from lower-order densities.[22–24] The accuracy of these methods depends critically on the set of *N*-representability conditions enforced in the calculation and the quality of the approximate 3-RDM.[7,19] There are not many approximations to the 3-RDM,[18,22,23,25] and, to our knowledge, very few benchmark tests have been performed in order to compare these approximations.[24,26–29] Moreover, no assessment of the deterioration of the approximations upon inclusion of electron correlation has been carried out.

n-RDMs are also used in the context of density matrix functional theory (DMFT)[30,31]—where the 2-RDM is approximated from the exact 1-RDM—and in some variations of the density matrix renormalization group (DMRG) that use up to the 5-RDM.[32]

[a] *Kimika Fakultatea, Euskal Herriko Unibertsitatea UPV/EHU, and Donostia International Physics Center (DIPC), P.K. 1072, 20080 Donostia, Euskadi, Spain. E-mail: ematito@gmail.com*
[b] *Institut de Química Computacional i Catàlisi (IQCC) and Departament de Química, University of Girona, 17071 Girona, Catalonia, Spain*
[c] *Department of Chemistry, University of California Berkeley, 94720, Berkeley, CA, USA*
[d] *IKERBASQUE, Basque Foundation for Science, 48011 Bilbao, Spain*

† Electronic supplementary information (ESI) available. See DOI: 10.1039/c6cp07616e

The 3-RDM and higher orders are also used to calculate particle number distributions in domains[33–37] and to construct several electronic structure descriptors such as multicenter indices[38] and aromaticity descriptors.[39–43]

In this paper we submit the four most employed 3-RDM approximations (the single-determinant approximation,[44] Valdemoro's,[22] Nakatsuji's[23] and Mazziotti's[24]) to a series of constrictive tests that will put forward some important limitations of these approximations and suggest new means to construct more robust ones. We will employ highly-accurate full-configuration-interaction (FCI) benchmark data for the three-electron harmonium atom, a model system that permits us to test methods under varying electron correlation regimes and has been successfully used in the past to test DMFT[45] and DFT methods.[46–49] The present set of tests does not involve electronic energies and, therefore, it is not biased towards providing most accurate energies. In this sense, they add to the list of benchmark tests that assess the other properties of RDMs[50] and can be used to complement the many existing energy-based benchmarking tools.

2 Methodology

2.1 Density matrices

The n-order reduced density matrix (n-RDM) of an N-electron system is obtained from the wavefunction upon integration over $N-n$ coordinates (see ref. 51 for notation),[6]

$$\rho(\mathbf{1}',\ldots,\mathbf{n}';\mathbf{1},\ldots,\mathbf{n}) = \binom{N}{n} n! \int \mathrm{d}_{\mathbf{n+1}} \ldots \int \mathrm{d}_{\mathbf{N}} \times \Psi(\mathbf{1}',\ldots,\mathbf{n}',\mathbf{n}+\mathbf{1}\ldots,\mathbf{N})\Psi^*(\mathbf{1},\ldots,\mathbf{N}). \quad (1)$$

where Ψ is the wavefunction describing the system and we have assumed the McWeeny normalization.[52] The n-density function (n-DF, hereafter) corresponds to the diagonal part of the n-RDM, *i.e.*,

$$\rho_n(\mathbf{1},\ldots,\mathbf{n}) = \int \mathrm{d}_{\mathbf{1}'} \ldots \int \mathrm{d}_{\mathbf{n}'} \rho(\mathbf{1}',\ldots,\mathbf{n}';\mathbf{1},\ldots,\mathbf{n})\delta(\mathbf{1}'-\mathbf{1})\ldots\delta(\mathbf{n}'-\mathbf{n}) \quad (2)$$

The n-RDM can be expanded in terms of a set of M orbitals, $\{\phi_i(\mathbf{1})\}_{i=1,M}$, giving

$$\rho(\mathbf{1}',\ldots,\mathbf{n}';\mathbf{1},\ldots,\mathbf{n}) = \sum_{\substack{i_1\ldots i_n \\ j_1\ldots j_n}}^{M} {}^nD^{i_1\ldots i_n}_{j_1\ldots j_n} \phi_{i_1}{}^*(\mathbf{1}')\ldots\phi_{i_n}{}^*(\mathbf{n}') \times \phi_{j_1}(\mathbf{1})\ldots\phi_{j_n}(\mathbf{n}) \quad (3)$$

where ${}^nD^{i_1\ldots i_n}_{j_1\ldots j_n}$ are the elements of ${}^n\mathbf{D}$, which is the n-th order density matrix (n-DM hereafter). In the following we will assume that n-DM is expressed on the basis of canonical molecular orbitals obtained from a Hartree–Fock calculation, unless otherwise specified.

In practice, the calculation of the n-DM carries a large computational cost and it is common to resort to approximate n-DM constructed from lower-order matrices. Namely, for the 3-DM there exist four well-known approximations: the single-determinant (SD) approximation (also referred as $n=1$, *vide infra*),

$${}^3\mathbf{D}^{\mathrm{SD}} = {}^1\mathbf{D}\wedge{}^1\mathbf{D}\wedge{}^1\mathbf{D} = {}^1\mathbf{D}^3, \quad (4)$$

Valdemoro's approximation,[22]

$${}^3\mathbf{D}^{\mathrm{VAL}} = 3!\left[\frac{3}{2}{}^2\mathbf{D} - 2{}^1\mathbf{D}^2\right]\wedge{}^1\mathbf{D} = 9{}^2\mathbf{D}\wedge{}^1\mathbf{D} - 12{}^1\mathbf{D}^3, \quad (5)$$

Nakatsuji's approximation,[23]

$$\left[{}^3\mathbf{D}^{\mathrm{NAK}}\right]^{pqs}_{ijk} = \left[{}^3\mathbf{D}^{\mathrm{VAL}}\right]^{pqs}_{ijk} + \sum_l \sigma_l \hat{A}\left({}^2\Delta^{pl}_{ij}\,{}^2\Delta^{qs}_{lk}\right), \quad (6)$$

and Mazziotti's approximation,[18]

$$\left[{}^3\mathbf{D}^{\mathrm{MAZ}}\right]^{pqs}_{ijk} = \left[{}^3\mathbf{D}^{\mathrm{VAL}}\right]^{pqs}_{ijk} - \frac{1}{\chi^{pqs}_{ijk}-3}\sum_l \hat{A}\left({}^2\Delta^{pl}_{ij}\,{}^2\Delta^{qs}_{lk}\right) \quad (7)$$

where ${}^2\Delta = {}^2\mathbf{D} - {}^1\mathbf{D}^2$ is the cumulant of the 2-DM,[53] $\hat{A}$ performs the antisymmetric summation of all superindices and all subindices (without mixing superindices and subindices) excluding l, $\sigma_l = 1$ for orbitals below the Fermi level and -1 otherwise, and $\chi^{pqs}_{ijk} = {}^1D^i_i + {}^1D^j_j + {}^1D^k_k + {}^1D^p_p + {}^1D^q_q + {}^1D^s_s$. The latter expressions (eqn (4)–(7)) use Grassmann algebra (notice the wedge product, $\wedge$),[54] as introduced by Mazziotti to provide a compact representation of these approximations.[24,55–58]

2.2 *N*-Representability conditions

For a quantum-mechanical system of N identical fermions, the N-representability problem is the problem of recognizing whether, for a given n-RDM, there exists an antisymmetric N-particle wavefunction fulfilling eqn (1). The N-representability problem, therefore, concerns the determination of conditions (constraints), the N-representability conditions, to be imposed on the approximate n-RDM to guarantee the fulfillment of eqn (1).[5] If the equality holds the n-RDM is said to be N-representable. The full set of sufficient conditions for N-representability of the n-RDM is only known for the 1-RDM[5] and the 2-RDM,[8] the latter set carrying a large computational cost.

The use of non-N-representable n-RDM can lead to spurious results such as non-variational electronic energies.[6] Therefore, methods that use approximate 2-RDM and higher-order densities such as DMFT, CSE, ACSE or DMRG need to impose the necessary N-representable conditions that are available. In this work we are concerned with the assessment of the 3-RDM, and therefore we will consider the following N-representability conditions that the 3-DM should satisfy:[6,59]

D (or P) condition:

$${}^3D^{ijk}_{ijk} \geq 0 \quad (8)$$

G condition (I):

$${}^2D^{ij}_{ij} - {}^3D^{ijk}_{ijk} \geq 0 \quad (9)$$

G condition (II):

$${}^1D^i_i - {}^2D^{ij}_{ij} - {}^2D^{ik}_{ik} + {}^3D^{ijk}_{ijk} \geq 0 \quad (10)$$

Q condition:

$$1 - {}^1D^i_i - {}^1D^j_j - {}^1D^k_k + {}^2D^{ij}_{ij} + {}^2D^{ik}_{ik} + {}^2D^{jk}_{jk} - {}^3D^{ijk}_{ijk} \geq 0 \quad (11)$$

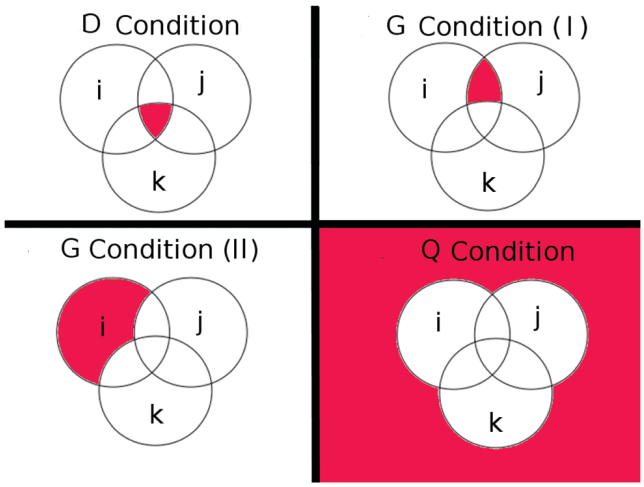

Fig. 1 Venn diagrams representing the probabilities of occupying orbitals *i*, *j* and *k*, according to the D, G-I, G-II and Q conditions of the 3-DM.

These *N*-representability conditions are related to the probability of finding groups of three electrons in different orbitals and, therefore, they can be easily illustrated with Venn diagrams (see Fig. 1). D condition accounts for the probability of finding three electrons occupying orbitals *i*, *j* and *k*, Q condition is related to the probability that neither *i*, *j* nor *k* are occupied, whereas G conditions I and II concern the probability of finding the three electrons in *i* and *j* but not in *k* and the probability of finding the electrons in *i* but not in *j* or *k*, respectively. These conditions hold for an arbitrary orthonormal orbital basis and, therefore, the full validation of eqn (8)–(11) involves the positive definiteness condition of the underlying operators.[60] The simplest way to check these conditions consists in finding the diagonal form of the corresponding operators and check that each associated eigenvalue is nonnegative. For a 3-DM this procedure involves the very costly procedure of constructing the natural 3-states.[6] In this paper we restrict ourselves to a less constrictive test that consists in checking the D, G-I, G-II and Q conditions on the basis of canonical molecular orbitals. 3-DM approximations that fail to fulfill a given condition on this basis set obviously fail to satisfy the most general condition.

Apart from these conditions, the 3-DM should satisfy the symmetry

$$ {}^3D^{ijk}_{lmn} = {}^3D^{lmn}_{ijk} \tag{12}$$

and antisymmetry conditions

$$ {}^3D^{ijk}_{lmn} = -{}^3D^{jik}_{lmn} = {}^3D^{kij}_{lmn} = \ldots \tag{13}$$

as well as the sum rule imposed by eqn (1), *i.e.*,

$$ \mathrm{Tr}\left[{}^3\mathbf{D}\right] = \sum_{ijk} {}^3\mathbf{D}^{ijk}_{ijk} = N(N-1)(N-2) \tag{14}$$

2.3 Multicenter indices

The *n*-DF can be used to calculate the so-called *n*-center electron sharing indices (*n*c-ESI),[61] through the following formula:

$$ \delta(\mathrm{A}_1, \mathrm{A}_2, \ldots, \mathrm{A}_n) = \frac{(-2)^{n-1}}{(n-1)!} \int_{\mathrm{A}_1} \mathrm{d}_{\mathbf{1}} \int_{\mathrm{A}_2} \mathrm{d}_{\mathbf{2}} \cdots \int_{\mathrm{A}_n} \mathrm{d}_{\mathbf{n}} \gamma(\mathbf{1}, \mathbf{2}, \ldots, \mathbf{n}), \tag{15}$$

where

$$ \gamma(\mathbf{1},\mathbf{2},\ldots,\mathbf{n}) = \langle (\hat{\rho}_1 - \bar{\rho}_1)(\hat{\rho}_2 - \bar{\rho}_2)\ldots(\hat{\rho}_n - \bar{\rho}_n) \rangle, \tag{16}$$

$\hat{\rho}$ stands for the density operator[6] (see eqn (17) and (19)) and $\bar{\rho}$ is its average value, *i.e.*, $\bar{\rho}_{\mathrm{A}} = \langle \hat{\rho} \rangle_{\mathrm{A}}$. From $\gamma(\mathbf{1},\mathbf{2},\ldots,\mathbf{n})$, 2^n terms arise and the computationally most expensive one involves the *n*-DF,

$$ \langle \hat{\rho}_1 \ldots \hat{\rho}_n \rangle_{\mathrm{A}_1 \ldots \mathrm{A}_n} = \int_{\mathrm{A}_1} \mathrm{d}_{\mathbf{1}} \ldots \int_{\mathrm{A}_n} \mathrm{d}_{\mathbf{n}} \rho_n(\mathbf{1}, \ldots, \mathbf{n}), \tag{17}$$

and the lower-order DF in a set of three-dimensional space regions. $\delta(\mathrm{A}_1,\ldots,\mathrm{A}_n)$ is invariant with respect to the order of the atoms in the string and is proportional to the *n*-central moment of the *n*-variate probability distribution, *n*-DF, integrated into the atomic basins $\mathrm{A}_1,\ldots,\mathrm{A}_n$:[62]

$$ \delta(\mathrm{A}_1, \ldots, \mathrm{A}_n) = \frac{(-2)^{n-1}}{(n-1)!} \left\langle \prod_{i=1}^{n} \left(\hat{N}_{\mathrm{A}_i} - \bar{N}_{\mathrm{A}_i} \right) \right\rangle \tag{18}$$

where $\hat{N}_{\mathrm{A}}$ is the particle operator applied to region A and $\bar{N}_{\mathrm{A}}$ is the average number of electrons in A (or population of A):

$$ \bar{N}_{\mathrm{A}} = \langle \hat{\rho}_1 \rangle_{\mathrm{A}} = \int \mathrm{d}_{\mathbf{1}} \hat{N}_{\mathrm{A}} \rho(\mathbf{1}) \equiv \int_{\mathrm{A}} \mathrm{d}_1 \rho(\mathbf{1}). \tag{19}$$

The large cost associated with the 3c-ESI is mostly due to the computation of the exact 3-DF, which by itself is a huge computational task for non-single-determinant wavefunctions. The 3c-ESI is thus often computed from approximate 3-DF.[43,63,64] In a recent work[65] we have put forward two new approximations to the 3-DF that have been used to calculate the 3c-ESI in a series of molecules. Our approximations were compared against the Valdemoro,[22] Nakatsuji[23] and Mazziotti[24] approximations, showing that one of our proposals was clearly superior to the others.[65,66] This 3-DF expression was named cube root (CR) or $n = 1/3$ approximation, it is exact for single-determinant wavefunctions and is the only approximation to satisfy the sum rule, eqn (14). It can be obtained by setting $a = 1/3$ in the following general expression

$$ \rho_3^a(\mathbf{1},\mathbf{2},\mathbf{3}) = \gamma^a(\mathbf{1},\mathbf{2},\mathbf{3}) - 2\rho(\mathbf{1})\rho(\mathbf{2})\rho(\mathbf{3}) + \hat{\pi}_1^3 \rho_2(\mathbf{1},\mathbf{2})\rho(\mathbf{3}), \tag{20}$$

where $\hat{\pi}_1^3$ is an operator which generates the two possible subsets of indices of sizes 1 and 2 from the elements in the set $\{\mathbf{1},\mathbf{2},\mathbf{3}\}$, ρ_2 is the 2-density function (2-DF) and

$$ \gamma^a(\mathbf{1},\mathbf{2},\mathbf{3}) = 2 \sum_{ijk} \left(n_i n_j n_k \right)^a \eta_i^*(\mathbf{1}) \eta_j(\mathbf{1}) \eta_k(\mathbf{2}) \eta_j^*(\mathbf{2}) \eta_i(\mathbf{3}) \eta_k^*(\mathbf{3}), \tag{21}$$

where $\eta_i(\mathbf{1})$ is a natural orbital and n_i its occupation number. The CR approximation of the 3-DF bears a close resemblance with Müller's approximation of the 2-DF[67] and provides a simple expression to calculate the 3c-ESI only in terms of natural orbitals:

$$ \tilde{\delta}^{\mathrm{CR}}(\mathrm{A}_1, \mathrm{A}_2, \mathrm{A}_3) = 4 \sum_{ijk} \left(n_i n_j n_k \right)^{1/3} S_{ij}(\mathrm{A}_1) S_{jk}(\mathrm{A}_2) S_{ki}(\mathrm{A}_3), \tag{22}$$

where $S_{ij}(A_1)$ is the atomic overlap matrix (AOM) of atom A_1,

$$S_{ij}(A_1) = \int_{A_1} d_{\mathbf{1}} \eta_i^*(\mathbf{1})\eta_j(\mathbf{1}). \quad (23)$$

In the tests of this paper we include the 3c-ESI using two approximations we have recently suggested,[65,66] the latter eqn (22) and

$$\widetilde{\delta}^{SR}(A_1, A_2, A_3) = 4\sum_{i,j,k}(n_i n_j n_k)^{1/2} S_{ij}(A_1)S_{jk}(A_2)S_{ki}(A_3). \quad (24)$$

which is also indicated as $n = 1/2$. These approximations, as well as the single-determinant approximation ($n = 1$), *i.e.*, eqn (4) substituted in eqn (15),

$$\widetilde{\delta}^{SD}(A_1, A_2, A_3) = 4\sum_{i,j,k} n_i n_j n_k S_{ij}(A_1)S_{jk}(A_2)S_{ki}(A_3), \quad (25)$$

only require the calculation of the natural orbitals and their occupancies and, therefore, bear a very reduced computational cost (unlike the 3-DM formulations of Valdemoro, Mazziotti and Nakatsuji that generate 3c-ESI approximations that implicitly depend on the exact 2-DM). Conversely, the 3-DF approximations in eqn (20) for $a = 1$, $a = 1/2$ and $a = 1/3$ are referred to as SD ($n = 1$), SR ($n = 1/2$) and CR ($n = 1/3$), and depend on natural orbitals and the 2-DF. Except in the case of the SD approximation, no 3-DM can be constructed from the latter formulae and, therefore, some of the benchmark tests suggested in this paper cannot be applied. For single-determinant wavefunctions all the approximations analyzed in this study reduce to the exact formulation.

2.4 Harmonium atom

Our working system is the harmonium atom (HA),[68] where the electrons are confined on a parabolic potential, $\frac{1}{2}\omega^2\mathbf{r}^2$, and whose Hamiltonian reads

$$\hat{H} = \sum_i^N \left(-\frac{1}{2}\hat{\nabla}^2_{\mathbf{r}_i} + \frac{1}{2}\omega^2\mathbf{r}_i^2\right) + \sum_{i<j}^N \frac{1}{r_{ij}} \quad (26)$$

where ω is the confinement strength. This model allows an easy tuning of the amount of correlation by playing with the ω parameter. For large values of ω electrons are in a low-correlation regime, whereas the small-ω region corresponds to highly correlated systems. The two-electron harmonium has been widely used in calibration and benchmarking of electronic structure methods[45–49,69–75] due to the availability of analytical[76–78] and very accurate results.[79–82]

In the present study we have taken the lowest-lying quartet ($S = 3/2$) and doublet ($S = 1/2$) states of the three-electron HA for several values of the ω parameter ($\omega \in [0.1,1000]$). FCI calculations of quartet and doublet 3e-HA from a previous study[49] have been used to generate the exact 3-DM and various approximations. For the reader's reference, let us note that the correlation energy of the helium atom is very similar to the correlation energy of two-electron harmonium at $\omega = 1/2$.

3 Computational details

FCI calculations were performed on the two lowest-lying states (doublet and quartet) of the three-electron HA for 12 values of the confinement parameter, ω, namely 0.1, 0.15, 0.2, 0.3, 0.4, 0.5, 1.0, 2.0, 5.0, 10.0, 100.0, and 1000.0. We used a modified version of the code developed by Knowles[83,84] and a variationally-optimized even-tempered basis set consisting of seven S, P, D and F Gaussian functions, amounting a total of 112 basis functions.[49] 1-DM, 2-DM and 3-DM were calculated from the FCI expansion coefficients using the DMN code[85] developed in our group. The approximate 3-DMs were also generated with the DMN code.

In this work we will test four 3-DM expressions, namely, Valdemoro's (eqn (5)), Nakatsuji's (eqn (6)), Mazziotti's (eqn (7)), and the single-determinant approximation (eqn (4)). A series of four tests will be used to analyze the performance of these 3-DM approximations: (i) fulfillment of the sum rule, eqn (14), (ii) attainment of the D-, G-I, G-II and Q conditions of the 3-DM, eqn (8)–(11) (see Fig. 1), (iii) calculation of the 3c-ESI between three regions of the Cartesian space and (iv) a termwise assessment, *i.e.*,

$$Tw\left[{}^3\mathbf{D}^{\mathbf{X}}\right] = \sum_{(i<j<k)\leq(l<m<n)} \left|\left[{}^3D^X\right]^{ijk}_{lmn} - {}^3D^{ijk}_{lmn}\right|. \quad (27)$$

For the sake of completeness, in tests (i) and (iii) we have also included the calculation of the two approximate 3-DF obtained from eqn (20) by setting $a = 1/2$ and $a = 1/3$ (*vide supra*).

The 3c-ESI calculations were performed over several three-region partitions of the Cartesian space occupied by the HA. In the end, among many partitions tested we have decided for the partition that was most affected by correlation effects and, therefore, poses the most stringent test to the 3-DM approximations. Namely, the Cartesian space is partitioned by two concentric spheres with radii r_1 and r_2, which are selected in such a way that there is one electron in each of the three resulting regions. Obviously, r_1 and r_2 vary for each value of ω and each spin state, their values being collected in Table 1. The calculation of the corresponding overlap matrices, eqn (23), was performed with the in-house RHO_OPS code.[86] The 3c-ESI values were computed with the ESI-3D[87–89] code developed in our group.

Table 1 Values of r_1 and r_2 that define the partition of the 3e-HA in three regions of the Cartesian space

	$S = 1/2$		$S = 3/2$	
ω	r_1/a.u.	r_2/a.u.	r_1/a.u.	r_2/a.u.
0.10	4.03	5.66	4.35	5.92
0.15	3.25	4.54	3.45	4.70
0.20	2.75	3.86	2.93	4.03
0.30	2.17	3.07	2.33	3.21
0.40	1.84	2.62	1.99	2.74
0.50	1.62	2.31	1.76	2.43
1.0	1.10	1.59	1.21	1.68
2.0	0.76	1.10	0.84	1.17
5.0	0.47	0.68	0.52	0.73
10.0	0.33	0.47	0.37	0.52
100.0	0.10	0.15	0.11	0.16
1000.0	0.03	0.04	0.04	0.05

4 Results

4.1 The sum rule

The plots in Fig. 2 correspond to the difference between the trace of $^3\mathbf{D}$ obtained from the different approximations *via* eqn (14) and the trace of the exact 3-DM (which for a three-electron system equals six) against the inverse of the confinement strength, ω. The $n = 1/3$ approximation has not been included because it satisfies the sum rule. The smaller the ω value, the more important the correlation effects in the HA. For large values of ω, all the approximations provide trace values very close to the exact result. However, as ω decreases, most approximations show significant deviations. The single-determinant approximation gives a very poor estimate of the trace with more than 50% of the error for the doublet state at $\omega = 0.1$. Mazziotti's 3-DM only performs marginally better than the single-determinant approximation in this case. Valdemoro's approximation systematically underestimates the value of the trace, but provides very accurate results. On the other hand, Nakatsuji's 3-DM and $n = 1/2$ (eqn (24)) approximation also provide quite accurate trace values but show larger errors than Valdemoro's. The quartet state poses a less serious test for the approximations, giving significantly smaller errors in the calculation of the trace. In this case, Mazziotti's 3-DM provides quite accurate results, improving Nakatsuji's values. Again, the Valdemoro approximation provides trace values systematically below the exact ones but more accurate than any other approximation.

4.2 *N*-Representability

We have assessed the deviation from the *N*-representability conditions introduced in Section 2.2 by summing the l.h.s. of eqn (8)–(11) on the basis of canonical molecular orbitals. The resulting numbers are plotted against ω^{-1} in Fig. 3. As expected, a more significant deviation from the *N*-representability conditions is observed as the confinement strength is weakened.

The single-determinant approximation of the 3-DM satisfies the D condition, however, it presents significant errors in the other *N*-representability conditions for low values of ω. Valdemoro's 3-DM presents the largest deviations from the D condition for both states, in line with the fact that it is the only approximation that underestimates the trace value of $^3\mathbf{D}$. In addition, it presents non-negligible deviations in the G conditions for the doublet state. Mazziotti's approximation shows the smallest errors in the D condition upon inclusion of electron correlation and, with the exception of the G-I condition in the doublet state, it presents the smallest deviations from *N*-representability conditions. Therefore, in the case of Mazziotti's approximation, the large errors in the sum rule (eqn (14)) seem to be connected to the satisfaction of the G-I condition. Interestingly, Nakatsuji's 3-DM presents the smallest deviations in the G-I condition for the doublet state and it does not perform better than Mazziotti's approximation in the other *N*-representability conditions. Although there is no apparent reason for that, on the basis of canonical molecular orbitals, the Q condition is attained by all the approximate 3-DM, excepting the single-determinant formulation.

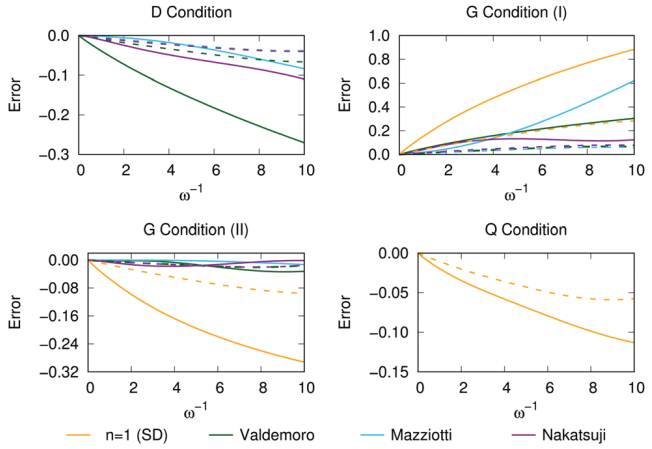

Fig. 3 Errors associated with the *N*-representability conditions. Solid lines are used for the doublet state and dashed lines are used for the quartet state.

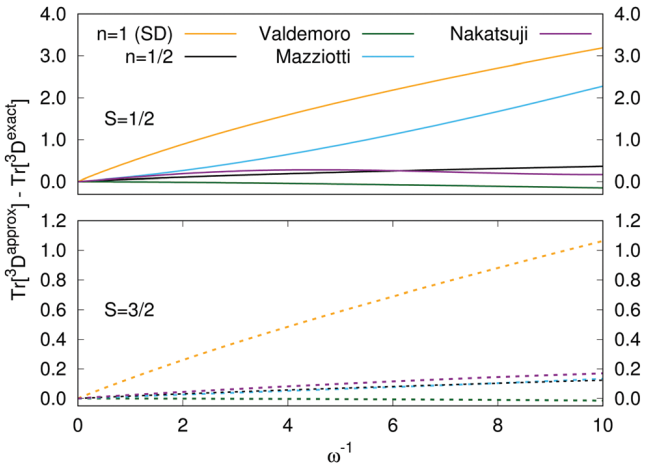

Fig. 2 Error in the trace of the 3-DM against the inverse of ω for the doublet (top) and quartet (bottom) states of three-electron harmonium.

4.3 3c-ESI

The 3c-ESI between regions A, B and C is a measure of the simultaneous electron sharing between these regions.[38,88] The partition has been constructed to contain one electron in each of its parts. Upon reduction of the confinement parameter the electron distribution spreads and, consequently, regions A and B increase their size. The 3c-ESI decreases with ω, showing values between 0.38 and 0.33 for both spin states, which indicate that there is substantial electron sharing between the three regions.

The difference between the approximate 3c-ESI and the exact ones is plotted against the logarithm of the confinement parameter in Fig. 4. In general, the approximations correctly provide the gross electron sharing, with the exception of Mazziotti's in the doublet state. The latter always overestimates the actual 3c-ESI and, as we have seen in previous tests, it presents a very large error for low-ω values of the doublet state, whereas it gives very good estimates of the quartet state. For both states, Valdemoro's approximation systematically underestimates the 3c-ESI but it provides the most accurate values. Excepting the doublet state at the strong correlation regime, Nakatsuji's 3-DM

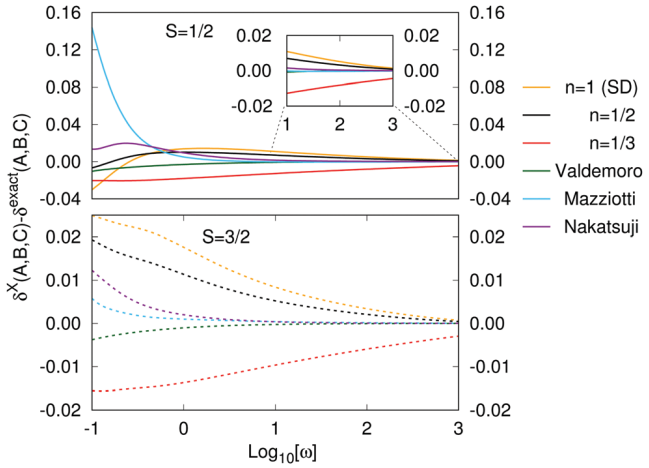

Fig. 4 3c-ESI errors of the approximate 3-DM for the doublet (above) and quartet (below) states of 3e-HA plotted against the logarithm of ω.

provides results that are usually worse than Mazziotti's. The 3-DF obtained from $a = 1/3$ and $a = 1/2$ gives better results than the single-determinant approximation ($a = 1$) and, for both states, the $n = 1/3$ approximation error seems to reach an asymptotic value.

4.4 Termwise error

Thus far, we have examined the performance of 3-DM approximations in the properties that depend only on the diagonal part of the 3-DM. In Fig. 5 we find the accumulated termwise error of the $^3\mathbf{D}$, eqn (27), for the different 3-DM used in this work. Upon decrease of the confinement strength, the electron correlation enhances (especially in the doublet state) and the matrices present larger termwise deviations, as expected. Indeed, for the quartet state, the single-determinant approximation shows the worst results, while the other three approximations show similar errors. Surprisingly, the largest deviations (even larger than the single-determinant approximation for low-ω values) of the doublet state are presented by Valdemoro's formulation. Mazziotti's 3-DM performs only marginally better and Nakatsuji's provides the

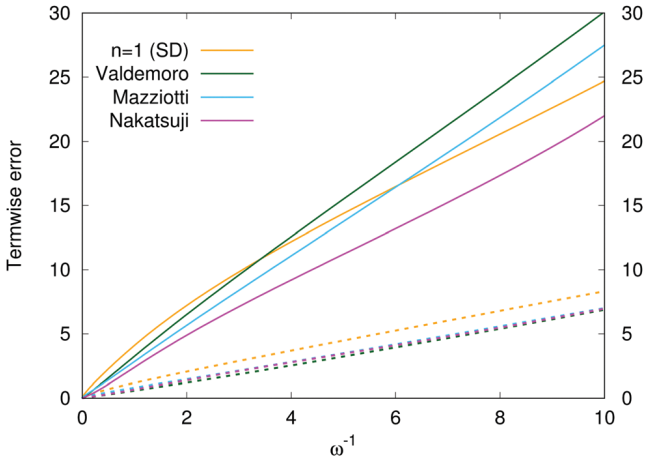

Fig. 5 Termwise errors of the 3-DM approximations for the doublet (solid) and quartet (dashed) states plotted against the inverse of ω.

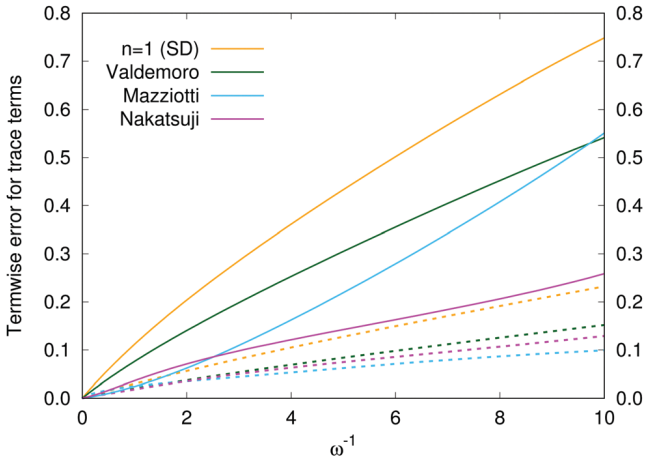

Fig. 6 Termwise errors of the diagonal elements of the 3-DM approximations for the doublet (solid) and quartet (dashed) states plotted against the inverse of ω.

best results for the range of ω values considered in this work. However, the trends in Fig. 5 suggest that for very low ω values the total errors will be worse than the poor single-determinant approximation. Finally, it is worth mentioning that the termwise error increases as ω^{-1} in all cases. On the other hand, the termwise error of the diagonal elements of the 3-DM is not too large in most approximations, except for the single-determinant one (see Fig. 6). Nakatsuji's approximation shows the smallest errors at the weak confinement regime.

5 Conclusions

We have introduced a series of four tests for 3-DM approximations that can be readily computed in a model three-electron system with varying electron correlation effects. The results of this work put forward several limitations of the currently most used 3-DM approximations for systems with important electron correlation effects. Our results show that most of the properties evaluated show errors of the 3-DM approximations that increase as ω^{-1} in the three-electron harmonium atom. Although the approximations perform reasonably well in accounting for the 3c-ESI, they fail to satisfy several N-representability conditions. In addition, they also show significant deviations from the trace numbers upon inclusion of electron correlation.

The comparison of the quartet and doublet states permits the analysis of the Coulomb correlation, which is only present in the doublet state. For this reason, this state poses a most serious challenge for the 3-DM approximations. Indeed, Mazziotti's 3-DM performs remarkably bad for the low-spin state if we compare it against Nakatsuji's approximation, which provides better 3c-ESI values and trace numbers for small values of the confinement parameter. Since Mazziotti's approximation gives small deviations for all the tested N-representability conditions but G-I, one is prompted to attribute the erratic behavior of this 3-DM approximation to the violation of the G-I condition. Furthermore, Nakatsuji's approximation performs reasonably well for this state and, therefore, one is tempted to conclude that the phase

factor σ_l of eqn (6) is responsible for this fact. Investigation along these lines is currently being pursued in our laboratory.

Finally, one should mention that analytical solutions of two- and three-electron harmonium atoms at $\omega \to 0$ have recently become available and could be used to calibrate 3-DM approximations at this highly correlated limit.[90]

In general, it is advisable to use approximations other than the single-determinant formulations, which provide the largest errors for most tests. However, for large correlation effects, all approximations fail to satisfy at least one of the tests, suggesting caution when using the current 3-DM approximations in this context. In this sense, we expect that the construction of new 3-DM approximations will benefit from the deficiencies shown by the present test set.

Acknowledgements

This research has been funded by Spanish MINECO Project No. CTQ2014-52525-P and the Basque Country Consolidated Group Project No. IT588-13. M. R. M. acknowledges the doctoral grant FPU-2013/00176 from the Spanish Ministry (MEC). The authors acknowledge the computational resources and technical and human support provided by SGI/IZO-SGIker UPV/EHU, especially from Txema Mercero who provided valuable technical assistance.

References

1 P. A. M. Dirac, *Proc. R. Soc. London, Ser. A*, 1929, **123**, 714–733.
2 P. Hohenberg and W. Kohn, *Phys. Rev.*, 1964, **136**, B864–B871.
3 T. Gilbert, *Phys. Rev. B: Solid State*, 1975, **12**, 2111.
4 K. Husimi, *Nippon Sugaku-Buturigakkwai Kizi Dai 3 Ki*, 1940, **22**, 264–314.
5 A. J. Coleman, *Rev. Mod. Phys.*, 1963, **35**, 668–687.
6 A. J. Coleman and V. I. Yukalov, *Reduced density matrices: Coulson's challenge*, Springer Verlag, Berlin, 2000, vol. 72.
7 D. A. Mazziotti, *Chem. Rev.*, 2012, **112**, 244–262.
8 D. A. Mazziotti, *Phys. Rev. Lett.*, 2012, **108**, 263002.
9 H. Nakatsuji, *Phys. Rev. A: At., Mol., Opt. Phys.*, 1976, **14**, 41–50.
10 F. Colmenero, C. P. del Valle and C. Valdemoro, *Phys. Rev. A: At., Mol., Opt. Phys.*, 1993, **47**, 971.
11 F. Colmenero and C. Valdemoro, *Phys. Rev. A: At., Mol., Opt. Phys.*, 1993, **47**, 979.
12 C. Valdemoro, L. Tel and E. Pérez-Romero, *Adv. Quantum Chem.*, 1997, **28**, 33–46.
13 K. Yasuda and H. Nakatsuji, *Phys. Rev. A: At., Mol., Opt. Phys.*, 1997, **56**, 2648–2657.
14 M. Ehara, M. Nakata, H. Kou, K. Yasuda and H. Nakatsuji, *Chem. Phys. Lett.*, 1999, **305**, 483–488.
15 M. Nakata, M. Ehara, K. Yasuda and H. Nakatsuji, *J. Chem. Phys.*, 2000, **112**, 8772–8778.
16 J. Cioslowski, *Many-electron densities and reduced density matrices*, Kluwer Academic, New York, 2000.
17 B. Verstichel, H. van Aggelen, D. Van Neck, P. W. Ayers and P. Bultinck, *Phys. Rev. A: At., Mol., Opt. Phys.*, 2009, **80**, 032508.
18 D. A. Mazziotti, *Phys. Rev. Lett.*, 2006, **97**, 143002.
19 D. A. Mazziotti, *Acc. Chem. Res.*, 2006, **39**, 207–215.
20 J. J. Foley IV, A. E. Rothman and D. A. Mazziotti, *J. Chem. Phys.*, 2011, **134**, 034111.
21 J. W. Snyder Jr and D. A. Mazziotti, *J. Chem. Phys.*, 2011, **135**, 024107.
22 F. Colmenero and C. Valdemoro, *Int. J. Quantum Chem.*, 1994, **51**, 369–388.
23 H. Nakatsuji and K. Yasuda, *Phys. Rev. Lett.*, 1996, **76**, 1039–1042.
24 D. A. Mazziotti, *Phys. Rev. A: At., Mol., Opt. Phys.*, 1999, **60**, 4396.
25 D. R. Alcoba, C. Valdemoro and L. M. Tel, *Comput. Theor. Chem.*, 2013, **1003**, 55–61.
26 C. Valdemoro, L. Tel and E. Pérez-Romero, *Many-Electron Densities and Reduced Density Matrices*, Springer, 2000, pp. 117–137.
27 H. Nakatsuji, *Many-Electron Densities and Reduced Density Matrices*, Springer, 2000, pp. 85–116.
28 D. A. Mazziotti, *Many-Electron Densities and Reduced Density Matrices*, Springer, 2000, pp. 139–163.
29 G. Gidofalvi and D. A. Mazziotti, *J. Chem. Phys.*, 2007, **126**, 024105.
30 M. Piris and J. Ugalde, *Int. J. Quantum Chem.*, 2014, **114**, 1169–1175.
31 K. Pernal and K. J. H. Giesbertz, *Top. Curr. Chem.*, 2015, **368**, 125.
32 T. Yanai, Y. Kurashige, W. Mizukami, J. Chalupsky, T. N. Lan and M. Saitow, *Int. J. Quantum Chem.*, 2015, **115**, 283–299.
33 C. Aslangul, R. Constanciel, R. Daudel and P. Kottis, *Advances in Quantum Chemistry*, Academic Press, New York, 1972, vol. 6, pp. 93–141.
34 R. Daudel, R. F. W. Bader, M. E. Stephens and D. S. Borrett, *Can. J. Chem.*, 1974, **52**, 1310–1320.
35 P. Ziesche, *Many-Electron Densities and Reduced Density Matrices*, Springer, 2000, pp. 33–56.
36 E. Francisco, A. M. Pendás and M. A. Blanco, *J. Chem. Phys.*, 2007, **126**, 094102.
37 A. M. Pendás, E. Francisco and M. Blanco, *Phys. Chem. Chem. Phys.*, 2007, **9**, 1087–1092.
38 K. C. Mundim, M. Giambiagi and M. S. de Giambiagi, *J. Phys. Chem.*, 1994, **98**, 6118–6119.
39 M. Giambiagi, M. S. de Giambiagi, C. D. dos Santos Silva and A. P. de Figuereido, *Phys. Chem. Chem. Phys.*, 2000, **2**, 3381–3392.
40 P. Bultinck, R. Ponec and S. Van Damme, *J. Phys. Org. Chem.*, 2005, **18**, 706–718.
41 F. Feixas, E. Matito, J. Poater and M. Solà, *Chem. Soc. Rev.*, 2015, **44**, 6389–6646.
42 E. Matito and M. Solà, *Coord. Chem. Rev.*, 2009, **253**, 647–665.
43 J. Cioslowski, E. Matito and M. Solà, *J. Phys. Chem. A*, 2007, **111**, 6521–6525.
44 P.-O. Löwdin, *Phys. Rev.*, 1955, **97**, 1474–1489.
45 J. Cioslowski, M. Piris and E. Matito, *J. Chem. Phys.*, 2015, **143**, 214101.
46 S. Ivanov, K. Burke and M. Levy, *J. Chem. Phys.*, 1999, **110**, 10262.
47 Z. Qian and V. Sahni, *Phys. Rev. A: At., Mol., Opt. Phys.*, 1998, **57**, 2527.

48 M. Taut, A. Ernst and H. Eschrig, *J. Phys. B: At., Mol. Opt. Phys.*, 1998, **31**, 2689.
49 J. Cioslowski and E. Matito, *J. Chem. Theory Comput.*, 2011, **7**, 915.
50 E. Ramos-Cordoba, P. Salvador, M. Piris and E. Matito, *J. Chem. Phys.*, 2014, **141**, 234101.
51 In the following we will indicate the coordinates of the electron using the short-hand notation $\mathbf{1} \equiv (\vec{r}_1, \sigma_1)$ and $\mathrm{d}_\mathbf{1} \equiv \mathrm{d}\vec{r}_1\mathrm{d}\sigma_1$ for the derivatives. A semicolon (;) will be used to separate l.h.s. coordinates from r.h.s. coordinates. The absence of the semicolon indicates the diagonal elements of the matrix.
52 R. McWeeny, *Rev. Mod. Phys.*, 1960, **32**, 335–369.
53 W. Kutzelnigg and D. Mukherjee, *J. Chem. Phys.*, 1999, **110**, 2800–2809.
54 The Grassman or wedge product between two tensors a and b is given by

$$(a \wedge b)^{i_1 i_2 i_3 \ldots i_n}_{j_1 j_2 j_3 \ldots j_n} = \left(\frac{1}{n!}\right)^2 \sum_{\pi} \sum_{\sigma} \varepsilon(\pi)\varepsilon(\sigma)\hat{\pi}\hat{\sigma} a^{i_1 \ldots i_p}_{j_1 \ldots j_p} b^{i_{p+1} \ldots i_n}_{j_{p+1} \ldots j_n} \quad (28)$$

where $\hat{\pi}$ permutes all the superindices, $\hat{\sigma}$ permutes all the subindices, $\varepsilon(\pi)$ and $\varepsilon(\sigma)$ return 1 (-1) for even (odd) permutations.
55 D. A. Mazziotti, *Phys. Rev. A: At., Mol., Opt. Phys.*, 1998, **57**, 4219–4234.
56 D. A. Mazziotti, *Chem. Phys. Lett.*, 1998, **289**, 419–427.
57 A. E. DePrince III and D. A. Mazziotti, *J. Chem. Phys.*, 2007, **127**, 104104.
58 D. A. Mazziotti, *Chem. Phys. Lett.*, 2000, **326**, 212–218.
59 P. W. Ayers and E. R. Davidson, *Adv. Chem. Phys.*, 2007, **134**, 443–483.
60 D. A. Mazziotti and R. M. Erdahl, *Phys. Rev. A: At., Mol., Opt. Phys.*, 2001, **63**, 042113.
61 M. Giambiagi, M. S. de Giambiagi and K. C. Mundim, *Struct. Chem.*, 1990, **1**, 423–427.
62 The expectation values do not include the self-pairing of electrons (explicitly forbidden by Pauli's exclusion principle).
63 J. M. Mercero, E. Matito, F. Ruipérez, I. Infante, X. Lopez and J. M. Ugalde, *Chem. – Eur. J.*, 2015, **21**, 9610–9614.
64 F. Feixas, J. Vandenbussche, P. Bultinck, E. Matito and M. Solà, *Phys. Chem. Chem. Phys.*, 2011, **13**, 20690–20703.
65 F. Feixas, M. Solà, J. M. Barroso, J. M. Ugalde and E. Matito, *J. Chem. Theory Comput.*, 2014, **10**, 3055–3065.
66 F. Feixas, M. Rodrguez-Mayorga, E. Matito and M. Solà, *Comput. Theor. Chem.*, 2015, **1053**, 173–179.
67 A. M. K. Müller, *Phys. Lett.*, 1984, **105A**, 446–452.
68 N. R. Kestner and O. Sinanoglu, *Phys. Rev.*, 1962, **128**, 2687.
69 P. M. Laufer and J. B. Krieger, *Phys. Rev. A: At., Mol., Opt. Phys.*, 1986, **33**, 1480–1491.
70 S. Kais, D. R. Hersbach, N. C. Handy, C. W. Murray and G. J. Laming, *J. Chem. Phys.*, 1993, **99**, 417.
71 C. Filippi, C. J. Umrigar and M. Taut, *J. Chem. Phys.*, 1994, **100**, 1290.
72 C.-J. Huang and C. J. Umrigar, *Phys. Rev. A: At., Mol., Opt. Phys.*, 1997, **56**, 290.
73 P. Hessler, J. Park and K. Burke, *Phys. Rev. Lett.*, 1999, **82**, 378.
74 W. M. Zhu and S. B. Trickey, *J. Chem. Phys.*, 2006, **125**, 094317.
75 E. V. Ludeña, V. Karasiev, A. Artemiev and D. Gómez, in *Functional N*-representability in density Matrix and Density Functional Theory: An illustration for Hooke's Atom, ed. J. Cioslowski, Kluwer Academic/Plenum Publishers, New York, 2000, ch. 10.
76 E. Santos, *An. R. Soc. Esp. Fis. Quim.*, 1968, **64**, 177.
77 M. Taut, *Phys. Rev. A: At., Mol., Opt. Phys.*, 1993, **48**, 3561.
78 J. Cioslowski and E. Matito, *J. Chem. Phys.*, 2011, **134**, 116101.
79 J. Cioslowski and K. Pernal, *J. Chem. Phys.*, 2000, **113**, 8434.
80 E. Matito, J. Cioslowski and S. F. Vyboishchikov, *Phys. Chem. Chem. Phys.*, 2010, **12**, 6712.
81 J. Cioslowski, K. Strasburger and E. Matito, *J. Chem. Phys.*, 2012, **136**, 194112.
82 J. Cioslowski, K. Strasburger and E. Matito, *J. Chem. Phys.*, 2014, **141**, 044128.
83 P. J. Knowles and N. C. Handy, *Comput. Phys. Commun.*, 1989, **54**, 75.
84 P. J. Knowles and N. C. Handy, *Chem. Phys. Lett.*, 1984, **111**, 315–321.
85 E. Matito and F. Feixas, *DMn program*, University of Girona (Spain) and University of Szczecin (Poland), 2009.
86 M. Rodríguez-Mayorga, *RHO-OPS: Density Operations*, Institute of Computational Chemistry and Catalysis, University of Girona, Catalonia, Spain, 2015.
87 E. Matito, *ESI-3D: Electron Sharing Indices Program for 3D Molecular Space Partitioning*, Institute of Computational Chemistry and Catalysis, University of Girona, Catalonia, Spain, 2015.
88 E. Matito, M. Solà, P. Salvador and M. Duran, *Faraday Discuss.*, 2007, **135**, 325–345.
89 E. Matito, M. Duran and M. Solà, *J. Chem. Phys.*, 2005, **122**, 014109.
90 J. Cioslowski, *J. Chem. Phys.*, 2015, **142**, 114104.

4.2) Three-Center Bonding Analyzed from Correlated and Uncorrelated Third-Order Reduced Density Matrices

Computational and Theoretical Chemistry 1053 (2015) 173–179

Contents lists available at ScienceDirect

Computational and Theoretical Chemistry

journal homepage: www.elsevier.com/locate/comptc

Three-center bonding analyzed from correlated and uncorrelated third-order reduced density matrices

Ferran Feixas, Mauricio Rodríguez-Mayorga, Eduard Matito *, Miquel Solà *

Institut de Química Computacional i Catàlisi and Departament de Química, Universitat de Girona, Campus Montilivi, 17071 Girona, Catalonia, Spain

ARTICLE INFO

Article history:
Received 21 August 2014
Accepted 28 September 2014
Available online 7 October 2014

Keywords:
Three-center electron sharing indices (3c-ESI)
Three-center bonding
Three-center two-electron (3c-2e) bonds
Three-center four-electron (3c-4e) bonds
Third-order reduced density matrix (3-RDM)
Average number of three particles (3-AN)

ABSTRACT

Several approximations to the third-order reduced density matrices (3-RDM) are applied to compute approximate three-center electron sharing indices (3c-ESI) and average number of three particles (3-AN) for correlated and uncorrelated wave functions with different atomic partition schemes. Exact and approximated 3c-ESI are calculated for a set of molecules with three-center two-electron (3c-2e) and three-center four-electron (3c-4e) bonding. Results show that 3c-2e bonding is associated with positive values of 3c-ESI irrespective of the method of calculation, atomic partition employed, and approximation to the third-order density matrix used. Single-determinant calculations yield negative 3c-ESI values for 3c-4e bonds, whereas the exact CASSCF 3c-ESIs are positive or close to zero. Some approximations to the 3-RDM preserve the negative sign of the 3-ESI for 3c-4e bonds, however they perform poorly on the calculation of 3-AN. The adequacy of the 3-RDM approximation to calculate 3-AN is also analyzed, revealing that Valdemoro's approximation to the 3-RDM is the best approximation while Mazziotti's and natural-orbital based approximations yield the lowest maximum errors.

Published by Elsevier B.V.

1. Introduction

The importance of the electron pair bond concept was recognized by Lewis already in 1916 [1]. Most chemical interactions in molecules can be described with a set of localized two-center two-electron bonds (2c-2e). Although these 2c-2e bonds are certainly able to describe the molecular structure of most of molecules, some molecules have more complicated bonding patterns involving interactions between more than two atoms that result in multicenter bonds. One of the paradigmatic cases is diborane that contains a B_2H_2 ring that is held by four electrons forming two 3-center 2-electron (3c-2e) bonds as described first by Lipscomb [2,3]. 3c-2c bonds are present not only in boranes but also in a number of non-classical systems such as metal clusters, distorted lithiocarbons, etc. [4,5]. Apart from the 3c-2e bonds, 3c-4e chemical interactions are needed to interpret the bonding in hypervalent systems like XeF_2, PF_5 or SF_4 and in electron-rich orbital-deficient molecules such as the trihalide anions X_3^- or hydrogen bihalide anions XHX^- [4] as well as in more special bonding situations like in Fischer carbenes [6]. According to Bridgeman and Empson [5], although a number of 4-, 5-, and 6-center bonds have been described [4,7–14], the 3-center bonding interactions represent by far the most significant multicenter bonding situations found in molecular systems.

There are several ways to analyze multicenter bonding in quantum chemistry [15–18]. Probably one of the most widely used is the calculation of multicenter electronic indices (*n*c-ESIs). The 3c-ESI was defined for the first time in 1990 by Giambiagi et al. [19]. Using this definition several authors found that, for single-determinant wave functions, 3c-2e bonds are characterized by positive values of the 3c-ESI whereas 3c-4e bonding yield negative values. On the other hand, the absence of 3c-bonding is reflected by low values of the 3c-ESI [20–22]. The integrations over atomic basins in the first 3c-ESI calculations were performed with a Mulliken-like partitioning of the molecular space [23]. Later on, 3c-ESI calculations were also carried out using Bader's quantum theory of atoms in molecules (QTAIM) [24–26] and fuzzy atom [27] topological partitions. It was found that the qualitative results obtained do not depend on the partition used [28–30], except in very few cases (the 3c-ESI of N_3^- with the D95++ basis set changes of sign when going from Mulliken to QTAIM partition [30]). The qualitative results are not dependent on the basis set either, especially in the case of QTAIM partitioning [30]. Another aspect that has been investigated is the effect of electron correlation on 3c-ESI values. Previous results at the correlated level show that 3c-ESI in 3c-2e bonds keep the positive sign when going from single-determinant to multi-determinant wave functions [31,32]. For 3c-4e bonding the results are less conclusive. In most reported cases, 3c-ESIs for

* Corresponding authors.
E-mail addresses: ematito@gmail.com (E. Matito), miquel.sola@udg.edu (M. Solà).

http://dx.doi.org/10.1016/j.comptc.2014.09.030
2210-271X/Published by Elsevier B.V.

3c-4e bonds remain negative but their absolute values are drastically reduced at the correlated level [32–34], whereas in other reported examples 3c-ESIs become positive, changing their expected negative sign [35]. According to Ponec and coworkers [32], the reason for the change of sign is that electron correlation transforms the 3c-4e bonding scheme into a pattern of two very polar 2c-2e bonds. The 3c-4e molecular orbital (MO) bonding mechanism described by Rundle [36,37] and Pimentel [38] is depicted in Scheme 1 for F_3^- and CO_2 that have σ and π 3c-4e bonds, respectively. From this mechanism, one can already anticipate relatively large 2c-ESI between the two nonbonded atoms and this is actually what is found [29,39,40].

Average number of *s* particles (*s*-AN) in a given domain is a relevant quantity for the calculation of many-particle distributions and probabilities [41–44]. These quantities have been used for a wide variety of purposes linked one way or another to the electronic characterization of molecular structures. In particular, from the 1-AN and *N*-AN one can calculate the probability of finding only a given number of electrons in a given molecular region [41,45], from these probabilities one can also try to find the best three-dimensional decomposition of the molecular structure into regions (loges) [41,46,47] with the most probable division into localized groups of electrons. In addition, the *s*-AN from *s* lower or equal to *n* are used to calculate *n*c-ESI [35]. The *s*-AN are computed from the *s*-order reduced density matrices (*s*-RDM) and, therefore, they can be used to assess the goodness of a given *s*-RDM approximation.

In this work we analyze a large set of molecules with 3c-bonding at the single-determinant and correlated level with the exact 3-RDM (at the CASSCF level) and different approximations to the 3-RDM using CASSCF lower-order RDMs, natural orbitals and their occupancies. We will use the many instances of 3-AN needed to compute the 3c-ESI from Ref. [35] to analyze the accuracy of several 3-RDM approximations. We aim at four objectives: first, to examine the 3c-ESIs computed from correlated and uncorrelated wave functions of a relatively large set of molecules with and without 3c-bonding; second, to discuss whether the changes in 3c-ESI values when going from HF to correlated wave functions are accounted by the approximate 3-RDMs; third, to report for the first time 3c-ESI values calculated with the exact and approximate 3-RDMs using the topological fuzzy Voronoi cells (TFVC); and finally, to analyze the accuracy of the 3-RDM approximations by assessment of the 3-AN values.

2. Computational details

2.1. Methods

All molecules were optimized at the full valence CASSCF/6-311G(d,p) level [48]. The correlated 3-RDMs were computed from the CASSCF expansion coefficients using an algorithm implemented in our own program [49]. The deviation from idempotency was calculated using the natural occupancies of the CASSCF calculations. In addition, we performed single-point B3LYP [50–52], Hartree–Fock (HF), MP2 [53], and CCSD [54] using 6-311G(d,p) with the Gaussian 03 software [55] for a series of molecules with 3c-bonds of different nature, as well as for some molecules without 3c-bonds. Atomic overlap matrices (AOM) were computed with the QTAIM partition [24–26] using the AIMPAC collection of programs [56]. The numerical integrations over the atomic domains to obtain AOM were also carried out within the "fuzzy atom" framework [27] using the topological fuzzy Voronoi cells (TFVC) partitioning scheme [57] with the APOST-3D program [58]. These AOM and the exact and approximate 3-RDMs were used by ESI-3D [59–61] to calculate 3c-ESIs.

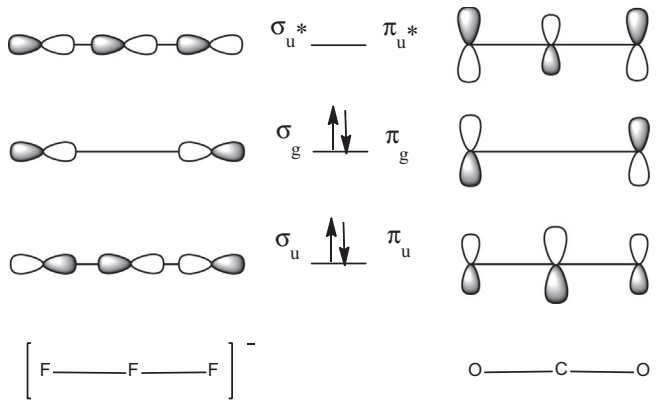

Scheme 1. Schematic molecular orbitals for the 3c-4e bond model of $[F_3]^-$ and CO_2 molecules.

2.2. Multicenter Indices

The 3-RDM was used to calculate the 3c-ESI through the following expression [35]:

$$\delta(A,B,C) = 2\iiint_{ABC} \gamma(\vec{r}_1,\vec{r}_2,\vec{r}_3)d\vec{r}_1 d\vec{r}_2 d\vec{r}_3, \tag{1}$$

where γ reads

$$\gamma(\vec{r}_1,\vec{r}_2,\vec{r}_3) = \langle(\hat{\rho}_1-\bar{\rho}_1)(\hat{\rho}_2-\bar{\rho}_2)(\hat{\rho}_3-\bar{\rho}_3)\rangle, \tag{2}$$

and the expected number of n particles, n-AN, is calculated as follows

$$\langle\hat{\rho}_1\ldots\hat{\rho}_n\rangle = \int_{A_1} d\vec{r}_1\ldots\int_{A_n} d\vec{r}_n\rho_n(\vec{r}_1,\ldots,\vec{r}_n), \tag{3}$$

$\rho_n(\vec{r}_1,\ldots,\vec{r}_n)$ being the n-RDM. Therefore the exact calculation of $\gamma(\vec{r}_1,\vec{r}_2,\vec{r}_3)$ involves the computation of the exact 3-, 2-, and 1-RDMs. For the case of closed-shell single-determinant wave functions, Eq. (1) can be written as:

$$\delta(A,B,C) = 4\sum_{i_1,i_2,i_3}^{occ} S_{i_1i_2}(A)S_{i_2i_3}(B)S_{i_3i_1}(C), \tag{4}$$

where $S_{ij}(A)$ is the atomic overlap matrix (AOM) of atom A that is given by:

$$S_{ij}(A) = \int_A \varphi_i^*(\vec{r})\varphi_j(\vec{r})d\vec{r}, \tag{5}$$

$\varphi_i(\vec{r})$ being an occupied molecular spin–orbital. $\delta(A,B,C)$ is a measure of how electron density is skewed from its mean, which may be related to simultaneous electron fluctuation between the atomic basins of atoms *A*, *B*, and *C*. In the particular case of the 2c-ESI, $\delta(A,B)$, values are usually positive, whereas $\delta(A,B,C)$ can take positive and negative values as pointed out in the Introduction.

Apart from the exact expression of 3c-ESI, in this work we have used three different approximations to the 3-RDM [35] that leads to following three approximate formulas for the calculation of 3c-ESI in correlated wave functions in terms of the AOM of the natural orbitals and their occupations n_i:

$$\delta^{SD}(A,B,C) = 4\sum_{i_1,i_2,i_3} n_{i_1}n_{i_2}n_{i_3}S_{i_1i_2}(A)S_{i_2i_3}(B)S_{i_3i_1}(C) \tag{6}$$

$$\delta^{MUL}(A,B,C) = 4\sum_{i_1,i_2,i_3} (n_{i_1}n_{i_2}n_{i_3})^{1/2}S_{i_1i_2}(A)S_{i_2i_3}(B)S_{i_3i_1}(C) \tag{7}$$

$$\delta^{CR}(A,B,C) = 4\sum_{i_1,i_2,i_3} (n_{i_1}n_{i_2}n_{i_3})^{1/3}S_{i_1i_2}(A)S_{i_2i_3}(B)S_{i_3i_1}(C), \tag{8}$$

where SD, MUL, and CR stands for single determinant, Müller-like [62], and cube root approximations [35], respectively. Among the approximations used in this work, only the CR approach fulfills the sum rule. The sum rule can be straightforwardly enforced by using an appropriate scaling of the 3-RDM components, however, the 3c-ESI thus obtained do not improve significantly compared to the unscaled values (in this work we have included normalized values for Eqs. (6)–(8)). These methods provide an inexpensive means to calculate the 3c-ESI analysis and avoid the computationally demanding calculation of the 3-RDM. In a previous work, we showed that for a collection of molecules the CR approximation gives the closest numbers to the ones obtained with the *exact* 3-RDM [35]. In the current paper we will study the effect of the type of correlated wave function and the atomic partition used on these quantities.

Finally, to calculate AOM with the TFVC partition of the molecular space [57], one defines at every point $\boldsymbol{r}$ of the space a weight factor $w_A(\boldsymbol{r})$ for each atom A to measure to which extent the given point belongs to atom A. These atomic weight factors are chosen to be non-negative and satisfy the following condition when summing over all atoms of the system:

$$\sum_A w_A(\vec{r}) = 1. \tag{9}$$

There is many different ways to choose these weights, in this work we will use a variant of Becke's multicenter integration technique known as TFVC. This method uses information on the topology of the electron density and provide results close to Bader's quantum theory of atoms in molecules (QTAIM) partition [57]. With this integration procedure, the AOM elements for an atom A are obtained as:

$$S_{ij}(A) = \int_A \varphi_i^*(\vec{r}) w_A(\vec{r}) \varphi_j(\vec{r}) d\vec{r}. \tag{10}$$

3. Results and discussion

Table 1 lists the 3c-ESI values for the set of molecules calculated with HF, CASSCF, and CCSD with the QTAIM partition. For HF and CASSCF the 3c-ESI results using TFVC partition are also included. On the other hand, B3LYP and MP2 3c-ESI values are given in the Supporting Information. The CASSCF 3c-ESIs were obtained from the exact 3-RDM and with the various approximations to the 3-RDM abovementioned. CCSD and MP2 results are obtained only with the approximations of the 3-RDM because these methodologies do not provide an unambiguous means to obtain the 3-RDM [59].

As found in previous works [5,21,22,28,30], at single-determinant level 3c-2e bonds are characterized by relatively large and positive 3c-ESI values with values larger than 0.1 for 3c-bonds containing three heavy atoms and larger than 0.04 if the 3c-2e bonds involve H atoms. For the systems without 3c-bonding one gets values in between zero and 0.04. Finally for the species having 3c-4e bonds the 3c-ESI values are negative. CH_2Li_2 is a very particular case. It is a planar molecule with a lone pair occupying the $2p_z$ orbital of C perpendicular to the molecular plane. The C–H bonds are regular 2c-2e bonds and the remaining two valence electrons participate in the C–Li bonds. The Li–C–Li interaction is usually discussed in terms of a 3c-2e bond [31]. For this particular 3c-2e interaction, Ponec and Cooper reported that, contrary to what is usually found, correlation increases the value of the 3-ESI. They attributed this increase to the polarity of the C–Li interaction. Our calculations also show an increase of the 3-ESI when going from HF to CASSCF but values of 3-ESI below 0.02 do not support the presence of a 3c-2e Li–C–Li bond. The values of 3c-ESI notably increase when TFVC partition is used for this molecule (see Table 1).

With some exceptions, for most of the molecules there is a reduction in the absolute value of the 3c-ESI when correlation is included at the CASSCF level. This is not unexpected taking into account that the same reduction is observed in the case of the 2c-ESI [59,63]. The exceptions in the reduction of the 3c-ESI at the CASSCF level correspond basically to molecules without 3c-bonding, for which the 3c-ESI is close to zero. Another important difference between the HF and CASSCF values is that 3c-ESI computed at the CASSCF level are all positive with only the exception of FHF^- that has a negative 3c-ESI although with a value very close to zero. Results in Table 1 show that 3c-2e bonding is associated with positive values of 3c-ESI at both HF and CASSCF levels of theory. Moreover, for molecules without 3c-bonding such as BH_3, CH_4, NH_3, H_2O and BeH_2, the HF and CASSCF 3c-ESI values are for the two methods close to zero. On the other hand, for 3c-4e bonding, whereas HF yield negative 3c-ESI values, the exact CASSCF 3c-ESIs are positive or close to zero. Ponec and coworkers [31,32] found an important reduction in the absolute value of the 3c-ESI of the 3c-4e bonds in SF_4, PF_5, F_3^-, FHF^-, and CH_2N_2 when electron correlation is included in the calculation via the spin-coupled valence bond method. The authors attributed this change to the transformation of the 3c-4e bonds into two very polar 2c-2e bonds. We have not investigated this point further because this would require a deep analysis of the nature of the bonding that is out of the scope of this work.

Let us now consider the results of the three different approximations to calculate the CASSCF 3c-ESI that have been used: (i) SD approximation (Eq. (6)), (ii) the Müller-like approach (MUL, Eq. (7)), and (iii) the CR (Eq. (8)) approximation. The 3c-ESI results obtained with the SD approximation are closer to the HF results than to the exact CASSCF results. In fact, with this approach the sign of all 3c-ESIs is the same as that found at the HF level. Therefore, the effect of electron correlation contained in the CASSCF wave function is not reflected in the 3c-ESIs obtained with the SD approximation. For the MUL approximation, the 3c-ESIs become more similar to the exact CASSCF results but still the sign of all 3c-ESIs is the same as that found at the HF level. The best estimates when compared to the exact 3-ESI values are obtained with the CR approximation [35]. There are four molecules ($C_3H_5^-$, F_3^-, N_2O, and N_3^-) for which the sign given by the CR approximation is incorrect, but the 3c-ESI for these molecules is close to zero.

When the three approximations are applied to methods that incorporate dynamic correlation such as CCSD and MP2, the results obtained show similar trends (MP2 results are qualitatively similar to CCSD ones and are included in Table S1 in the Supporting Information). The SD approximation yields CCSD 3c-ESI values that are not only qualitatively but also quantitatively very close to the values obtained at the HF level and also to the CASSCF values obtained with the same SD method. For the MUL approximation, the CCSD and MP2 3c-ESI become more similar to the CASSCF result but still the sign of all 3c-ESI is the same as that found at the HF level with the exception of the FHF^- species that has a 3c-ESI very close to zero. As before, the CR approximation is the one that provides closer values to the exact CASSCF results. Still, we find six molecules that do not have the correct sign when compared to exact CASSCF results, but as before the 3c-ESI for these molecules is close to zero. For all approximations, the MP2 3c-ESI values are very similar to those obtained at the CCSD level (see Table S1), the signs being the same (SO_2 with the CR approximation is the only exception) and differences being not larger than a few hundredths or even a few thousandths of an a.u. From the results of Tables 1 and S1, we can conclude that 3c-ESIs calculated with the CR approximation are a good and cheaper alternative to exact and expensive 3c-ESI using the 3-RDM, regardless the computational method used.

Finally, if we compare the results of the two different atomic partitions used, we find that the use of TFVC atomic partition gives

Table 1
Deviation from idempotency (for the CASSCF wave function) and 3c-ESI values calculated exactly at the HF and CASSCF levels together with CASSCF, and CCSD values calculated using the three approximations (SD, MUL, and RC) tested that avoid explicit computation of the 3-RDM.[a]

Species	3c-ESI	CAS (n,m)	Dev. Idemp.[b]	HF	CAS	CAS^{SD}	CAS^{MUL}	CAS^{CR}	$CCSD^{SD}$	$CCSD^{MUL}$	$CCSD^{RC}$	HF[c]	CAS[c]	$CAS^{SD,c}$	$CAS^{MUL,c}$	$CAS^{CR,c}$
$C_3H_3^+$	C–C–C	2,3	0.007	0.3936	0.2499	0.3647	0.3140	0.2544	0.3491	0.2866	0.2128	0.4079	0.2735	0.3797	0.3326	0.2761
SiC_3	C–C–C	8,8	0.045	0.3430	0.2712	0.3138	0.2732	0.2323	0.3125	0.2558	0.1908	0.3656	0.2935	0.3359	0.2982	0.2588
$C_3H_5^+$	C–C–C	6,7	0.034	0.2559	0.0801	0.2114	0.1584	0.1091	0.2168	0.1649	0.1132	0.2723	0.0934	0.2403	0.1776	0.1252
$C_2B_2H_4$	C–B–B	8,8	0.040	0.1309	0.1452	0.1266	0.1310	0.1369	0.1179	0.1118	0.0967	0.1423	0.1658	0.1467	0.1515	0.1577
H_2S	H–S–H	8,8	0.008	0.0709	0.0549	0.0596	0.0567	0.0519	0.0425	0.0390	0.0329	0.1797	0.1359	0.1499	0.1462	0.1383
CH_2Li_2	H–C–H	8,8	0.023	0.0598	0.0477	0.0457	0.0442	0.0413	0.0470	0.0432	0.0360	0.0534	0.0546	0.0433	0.0434	0.0498
SiC_3	Si–C–C	8,8	0.045	0.0566	0.0465	0.0484	0.0412	0.0347	0.0575	0.0445	0.0307	0.0626	0.0520	0.0539	0.0465	0.0396
B_2H_6	B–H–B	4,6	0.005	0.0391	0.0259	0.0418	0.0363	0.0286	0.0459	0.0384	0.0287	0.0392	0.0259	0.0401	0.0352	0.0282
BH_3	H–B–H	8,7	0.004	0.0377	0.0314	0.0346	0.0375	0.0407	0.0350	0.0376	0.0378	0.0483	0.0439	0.0463	0.0494	0.0529
CH_4	H–C–H	8,8	0.007	0.0355	0.0285	0.0304	0.0287	0.0260	0.0306	0.0279	0.0232	0.0490	0.0351	0.0414	0.0393	0.0358
NH_3	H–N–H	8,8	0.008	0.0217	0.0449	0.0213	0.0207	0.0196	0.0214	0.0194	0.0158	0.0312	0.0517	0.0300	0.0292	0.0279
CH_2Li_2	Li–C–H	8,8	0.023	0.0173	0.0211	0.0152	0.0155	0.0155	0.0156	0.0146	0.0121	0.0613	0.0880	0.1154	0.1249	0.1350
H_2O	H–O–H	8,8	0.007	0.0112	0.0411	0.0123	0.0127	0.0131	0.0128	0.0120	0.0102	0.0139	0.0450	0.0152	0.0156	0.0160
BeH_2	H–Be–H	6,7	0.004	0.0104	0.0164	0.0109	0.0145	0.0192	0.0105	0.0140	0.0182	−0.0037	0.0015	−0.0044	−0.0019	0.0057
CH_2Li_2	Li–C–Li	8,8	0.023	0.0082	0.0127	0.0088	0.0108	0.0135	0.0086	0.0095	0.0092	0.0986	0.0638	0.0579	0.0543	0.0498
FHF^-	F–H–F	8,8	0.002	−0.0030	−0.0028	−0.0029	−0.0028	−0.0026	−0.0037	0.0076	0.0175	0.0047	0.0046	0.0045	0.0046	0.0048
CO_2	O–C–O	8,6	0.020	−0.0380	0.0635	−0.0582	−0.0088	0.0307	−0.0712	−0.0227	0.0068	−0.0637	0.0781	−0.0468	0.0041	0.0435
SO_2	O–S–O	8,8	0.043	−0.0603	0.0378	−0.0778	−0.0252	0.0048	−0.0856	−0.0290	0.0048	0.0035	0.1161	0.0039	0.0533	0.0796
$C_3H_5^-$	C–C–C	8,7	0.013	−0.0725	0.0100	−0.0713	−0.0321	−0.0080	−0.0684	−0.0342	−0.0131	−0.0514	0.0175	−0.0488	−0.0169	0.0016
HCNO	C–N–O	8,6	0.045	−0.0782	0.0129	−0.0890	−0.0398	0.0119	−0.0944	−0.0348	−0.0062	−0.0535	0.0304	−0.0557	0.0046	0.0296
F_3^-	F–F–F	8,8	0.159	−0.1439	0.0216	−0.1093	−0.0468	−0.0213	−0.1320	−0.0633	−0.0304	−0.1235	0.0303	−0.1093	−0.0468	−0.0213
N_2O	N–N–O	8,6	0.051	−0.1530	0.0006	−0.1622	−0.0675	−0.0185	−0.1704	−0.0851	−0.0374	−0.1154	0.0210	−0.1142	−0.0314	0.0077
N_3^-	N–N–N	8,6	0.068	−0.2491	0.0104	−0.2076	−0.0772	−0.0118	−0.2265	−0.1139	−0.0510	−0.1207	0.0422	−0.1136	−0.0083	0.0363

[a] Units are a.u.
[b] The deviation from idempotency is calculated using the occupancies of the natural orbitals from the CASSCF wave function.
[c] All the data in this table uses the QTAIM partition except for these columns that make use of the TFVC partition.

Table 2
Average errors and maximum error for the expected number of three particles in different atomic regions: in one atom (AAA), into two atoms (AAB) and into three atoms (ABC) calculated using different 3-RDM approximations.

	Triad	SD	MUL	CR	MAZ	NAK	VAL
Average	AAA	0.343	0.163	0.094	0.057	0.035	0.028
	AAB	0.024	0.011	0.016	0.013	0.007	0.004
	ABC	0.0025	0.0014	0.0008	0.0034	0.0026	0.0010
Maximum	AAA	1.814	1.120	1.351	1.059	1.087	1.085
	AAB	0.697	0.499	0.558	0.237	0.359	0.352
	ABC	0.109	0.044	0.053	0.244	0.134	0.069

qualitatively the same results than the QTAIM one. Except for molecules containing S or Li atoms, differences are not larger than a few hundredths of an a.u. In some cases we observe a change of sign in the value of the 3c-ESI when comparing the QTAIM and TFVC results obtained at certain level of theory but, in general, these changes correspond to molecules with 3c-ESI values close to zero.

Table 2 collects the errors committed in the calculation of the expected number of particle triads using different 3-RDM approximations at the CASSCF level: Valdemoro's [64], Nakatsuji's [65,66], and Mazziotti's [67–70]. These values are calculated using Eq. (3) for $n = 3$ and different 3-RDM approximations integrated over three atomic regions. The errors are calculated as the sum of the absolute differences between the exact CASSCF value and the value obtained employing the actual 3-RDM approximation, thus being a direct evaluation of 3-RDM's accuracy. The values are separated into three groups according to the expected location of the three particles: AAA accounts for the expected number of groups of three particles in region A, AAB considers groups of three particles, two located in region A and one in region B, while ABC considers the expected number of three particles each lying in a different region. The latter quantity is a key ingredient in the calculation of 3c-ESI (see Ref. [35]). We have performed the statistical analysis from all possible permutations of the elements of a string of three atoms picked up from the target molecular set.

The first clear conclusion we can take from the data in Table 2 is the poor performance of the SD approximation, which always reports the largest average and maximum errors among all approximations with the only exception of ABC values. These results put forward the very approximate nature of the single-determinant 3-RDM expression. On the other hand, Valdemoro's approximation yields remarkably good results, giving the smallest average errors for AAA and AAB and performing reasonably well in other cases. Nakatsuji's approach for the 3-RDM affords similar errors to those reported for Valdemoro's approximation, excepting in the ABC triads that are badly estimated by this method. Mazziotti's expression for the 3-RDM gives pretty large average errors, however, it shows the smallest maximum error for AAA and AAB values. MUL approximation improves over the SD expression and obtains the smallest maximum error for ABC values. In general the CR approximation gives the best performance among the natural-orbital based approximations, showing the smallest average error and very small maximum errors for the calculation of ABC triads. The ability to reproduce ABC 3-AN is closely connected to the potential to reproduce accurate ABC 3c-ESI. Indeed, these results are in accord with the finding of Ref. [35], where 3c-ESI indices where best reproduced by the CR approximation.

Finally, to analyze the effect of electron correlation we have inspected the performance of the different 3-RDM approximation as a function of the electron correlation included in the molecule (see deviation from idempotency in Table 1). Valdemoro's and Nakatsuji's approximations performs better when the molecules do not suffer from strong correlation effects, while Mazziotti's and CR approximations improve in performance with respect to other approaches for molecules with more important correlation effects. This finding raises the question whether for highly correlated systems these approximations can actually perform much better than their competitors. Research in this line is being developed in our laboratory.

4. Conclusions

*n*c-ESI is a powerful tool to analyze the multicenter electron delocalization in molecules. In single-determinant wave functions, these indices allow for a clear separation between 3c-2e and 3c-4e bonds. However, the use of 3-RDM from correlated wave functions to calculate 3c-ESI eliminates this feature. Our results demonstrate that the single-determinant approximation to the 3-RDM permits to distinguish between the two bonding patterns. The better the approximation used, the more difficult the distinction between 3c-2e and 3c-4e becomes. Therefore, if one wants a clear-cut classification of three-center bonds into 3c-2e and 3c-4e, we recommend the calculation of the 3c-ESI using the single-determinant expression because it bears no cost (whereas the actual 3-RDM is out of reach for medium-sized molecules). Obviously, the 3c-ESI calculated in this way does not necessarily reflect the simultaneous electron fluctuation between three molecular fragments.

On the other hand, we have analyzed the accuracy of several approximate 3-RDM. To this aim, average numbers of three electrons have been computed. Our results show that in this context the single-determinant expression is far off the exact expression and should be avoided. Interestingly, Valdemoro's approximation provides the best performance among the different methods. Altogether, depending on the purpose of the calculation one should use one or another 3-RDM approximation.

Besides, we have tested the role of the atomic partition, finding that the use of TFVC atomic partition gives qualitatively the same results than the QTAIM one. The only exceptions involve S or Li atoms. In addition, the role of the source wave function in the calculation of the natural orbital approximations to the 3-RDM has been assessed. Our results indicate that MP2, CCSD, and CASSCF provide similar 3c-ESI values for the approximations tested, thus opening the door to use the approximate 3-RDM calculated from natural orbitals and occupancies of MP2 or CCSD methods, for which the calculation of 3-RDM becomes a complicated task not exempt of controversy.

Acknowledgements

The following organizations are thanked for financial support: the Spanish Ministry (MICINN, Project numbers CTQ2011-23156/BQU and CTQ2011-25086/BQU and MINECO, Europa Excelencia project CTQ2013-41236-ERC), the Generalitat de Catalunya (Projects number 2009SGR637, 2014SGR931, 2009SGR528, and Xarxa de Referència en Química Teòrica i Computacional), the Marie Curie Career Integration grant PCI09-GA-2011-294240 (E.M.), and the FEDER fund (European Fund for Regional Development) for the Grant UNGI08-4E-003. Support for the research of M. Solà was received through the ICREA Academia 2009 prize for excellence in research funded by the DIUE of the Generalitat de

Catalunya. F.F. and M.R-M, acknowledges financial support from the Beatriu de Pinós program (AGAUR) for the postdoctoral grant BP_A_00339 (F.F.) and doctoral fellowship FI-DGR2014-00003 (M.R.-M.) Excellent service by the Centre de Serveis Científics i Acadèmics de Catalunya (CESCA) is gratefully acknowledged.

Appendix A. Supplementary material

Table S1 containing 3c-ESI values calculated at the B3LYP level with the SD approximation and at the MP2 level using the three approximations (SD, MUL, and RC). Supplementary data associated with this article can be found, in the online version, at http://dx.doi.org/10.1016/j.comptc.2014.09.030.

References

[1] G.N. Lewis, The atom and the molecule, J. Am. Chem. Soc. 38 (1916) 762–785.
[2] W.N. Lipscomb, Boron Hydrides, W.A. Benjamin, New York, 1963.
[3] W.N. Lipscomb, The boranes and their relatives, Science 196 (1977) 1047–1055.
[4] O.J. Curnow, A simple qualitative molecular-orbital/valence-bond description of the bonding in main group "hypervalent" molecules, J. Chem. Educ. 75 (1998) 910–915.
[5] A.J. Bridgeman, C.J. Empson, Detecting delocalization, New. J. Chem. 32 (2008) 1359–1367.
[6] J. Poater, M. Cases, X. Fradera, M. Duran, M. Solà, Electron pairing analysis of the Fischer-type chromium-carbene complexes $(CO)_5Cr{=}C(X)R$ (X=H, OH, OCH_3, NH_2, $NHCH_3$ and R=H, CH_3, $CH{=}CH_2$, Ph, C≡CH), Chem. Phys. 294 (2003) 129–139.
[7] M.S. de Giambiagi, M. Giambiagi, M. de Souza Fortes, Multicenter bonds, bond valence and bond charge apportionment, J. Mol. Struct. (Theochem) 391 (1997) 141–150.
[8] M. Giambiagi, M.S. de Giambiagi, C.D. dos Santos Silva, A.P. de Figueiredo, Multicenter bond indices as a measure of aromaticity, Phys. Chem. Chem. Phys. 2 (2000) 3381–3392.
[9] C. Bollini, M. Giambiagi, M. de Giambiagi, A. de Figueiredo, Graphical linking of MO multicenter bond index and VB structures. II- 5-c rings and 6-c heterocyclic rings, Struct. Chem. 12 (2001) 113–120.
[10] R. Ponec, G. Yuzhakov, Evidence for 5-center 4-electron bonding in (C···H···C···H···C) array, J. Org. Chem. 68 (2003) 8284–8286.
[11] D.J. Tantillo, R. Hoffmann, Prospecting for a 5-center 4-electron $(C{\cdots}H{\cdots}C{\cdots}H{\cdots}C)^+$ bonding array, J. Am. Chem. Soc. 125 (2003) 4042–4043.
[12] A.S. Mikhaylushkin, J. Nylén, U. Häussermann, Structure and bonding of zinc antimonides: complex frameworks and narrow band gaps, Chem. Eur. J. 11 (2005) 4912–4920.
[13] R. Ponec, P. Bultinck, P. Gutta, D.J. Tantillo, Multicenter bonding in carbocations with tetracoordinate protons, J. Phys. Chem. A 110 (2006) 3785–3789.
[14] J.S. Miller, J.J. Novoa, Four-center carbon-carbon bonding, Acc. Chem. Res. 40 (2007) 189–196.
[15] A.E. Reed, L.A. Curtiss, F. Weinhold, Intermolecular Interactions from a natural bond orbital, donor–acceptor viewpoint, Chem. Rev. 88 (1998) 899–926.
[16] J. Poater, M. Duran, M. Solà, B. Silvi, Theoretical evaluation of electron delocalization in aromatic molecules by means of atoms in molecules (AIM) and electron localization function (ELF) topological approaches, Chem. Rev. 105 (2005) 3911–3947.
[17] D.Y. Zubarev, A.I. Boldyrev, Developing paradigms of chemical bonding: adaptive natural density partitioning, Phys. Chem. Chem. Phys. 10 (2008) 5207–5217.
[18] E. Matito, M. Solà, The role of electronic delocalization in transition metal complexes from the electron localization function and the quantum theory of atoms in molecules viewpoints, Coord. Chem. Rev. 253 (2009) 647–665.
[19] M. Giambiagi, M.S. de Giambiagi, K.C. Mundim, Definition of a multicenter bond index, Struct. Chem. 1 (1990) 423–427.
[20] A.B. Sannigrahi, T. Kar, Three-center bond index, Chem. Phys. Lett. 173 (1990) 569–572.
[21] T. Kar, E. Sánchez-Marcos, Three-center four-electron bonds and their indices, Chem. Phys. Lett. 192 (1992) 14–20.
[22] R. Ponec, I. Mayer, Investigation of some properties of multicenter bond indices, J. Phys. Chem. A 101 (1997) 1738–1741.
[23] R.S. Mulliken, Electronic population analysis on LCAO–MO molecular wave functions. I, J. Chem. Phys. 23 (1955) 1833–1840.
[24] R.F.W. Bader, Atoms in molecules, Acc. Chem. Res. 18 (1985) 9–15.
[25] R.F.W. Bader, Atoms in Molecules: A Quantum Theory, Clarendon, Oxford, 1990.
[26] R.F.W. Bader, A quantum theory of molecular structure and its applications, Chem. Rev. 91 (1991) 893–928.
[27] I. Mayer, P. Salvador, Overlap populations, bond orders and valences for "fuzzy" atoms, Chem. Phys. Lett. 383 (2004) 368–375.
[28] R. Bochicchio, L. Lain, A. Torre, R. Ponec, Topological population analysis from higher order densities. I. HF level, J. Math. Chem. 28 (2000) 83–90.
[29] R. Bochicchio, R. Ponec, L. Lain, A. Torre, Pair population analysis within AIM theory, J. Phys. Chem. A 104 (2000) 9130–9135.
[30] R. Bochicchio, R. Ponec, A. Torre, L. Lain, Multicenter bonding within the AIM theory, Theor. Chem. Acc. 105 (2001) 292–298.
[31] R. Ponec, D.L. Cooper, Generalized population analysis of three-center two-electron bonding, Int. J. Quantum Chem. 97 (2004) 1002–1011.
[32] R. Ponec, G. Yuzhakov, D.L. Cooper, Multicenter bonding and the structure of electron-rich molecules. Model of three-center four-electron bonding reconsidered, Theor. Chem. Acc. 112 (2004) 419–430.
[33] L. Lain, A. Torre, R. Bochicchio, Studies of population analysis at the correlated level: determination of three-center bond indices, J. Phys. Chem. A 108 (2004) 4132–4137.
[34] A. Torre, D.R. Alcoba, L. Lain, R.C. Bochicchio, Determination of three-center bond indices from population analyses: a fuzzy atom treatment, J. Phys. Chem. A 109 (2005) 6587–6591.
[35] F. Feixas, M. Solà, J.M. Barroso, J.M. Ugalde, E. Matito, New approximation to the third-order density. Application to the calculation of correlated multicenter indices, J. Chem. Theory Comput. 10 (2014) 3055–3065.
[36] R.J. Hach, R.E. Rundle, The structure of tetramethylammonium pentaiodide, J. Am. Chem. Soc. 73 (1951) 4321–4324.
[37] R.E. Rundle, On the problem structure of XeF_4 and XeF_2, J. Am. Chem. Soc. 85 (1963) 112–113.
[38] G.C. Pimentel, The bonding of trihalide and bifluoride ions by the molecular orbital method, J. Chem. Phys. 19 (1951) 446–448.
[39] J. Molina Molina, J.A. Dobado, The three-center-four-electron (3c-4e) bond nature revisited. An AIM and ELF study, Theor. Chem. Acc. 105 (2001) 328–337.
[40] X. Fradera, J. Poater, S. Simon, M. Duran, M. Solà, Electron-pairing analysis from localization and delocalization indices in the framework of the atoms-in-molecules theory, Theor. Chem. Acc. 108 (2002) 214–224.
[41] C. Aslangul, R. Constanciel, R. Daudel, P. Kottis, Aspects of localizability of electrons in atoms and molecules: loge theory and related methods, Adv. Quantum. Chem. 6 (1972) 93–141.
[42] P. Ziesche, Cumulant expansions of reduced densities, reduced density matrices, and Green's functions, in: J. Cioslowski (Ed.), Many-Electron Densities and Reduced Density Matrices, Kluwer, New York, 2000, pp. 33–56.
[43] E. Francisco, A.M. Pendás, M.A. Blanco, Electron number probability distributions for correlated wave functions, J. Chem. Phys. 126 (2007) 094102.
[44] A.M. Pendás, E. Francisco, M.A. Blanco, An electron number distribution view of chemical bonds in real space, Phys. Chem. Chem. Phys. 9 (2007) 1087–1092.
[45] R.F.W. Bader, M.E. Stephens, Fluctuation and correlation of electrons in molecular systems, Chem. Phys. Lett. 26 (1974) 445–449.
[46] J. Lopes, O. Mafra, B. Braïda, M. Causa, A. Savin, Understanding maximum probability domains with simple models, in: P. Hoggans et al. (Eds.), Advances in the Theory of Quantum Systems in Chemistry and Physics, Springer, Berlin, 2012, pp. 173–184.
[47] E. Cancès, R. Keriven, F. Lodier, A. Savin, How electrons guard the space. Shape optimization with probability distribution criteria, Theor. Chem. Acc. 111 (2004) 373–380.
[48] B.O. Roos, P.R. Taylor, P.E.M. Siegbahn, A complete active space SCF method (CASSCF) using a density matrix formulated super-CI approach, Chem. Phys. 48 (1980) 157–173.
[49] E. Matito, F. Feixas, DMn Program, University of Girona, Spain and University of Szczecin, Poland, 2009.
[50] A.D. Becke, Density-functional thermochemistry. III. The role of exact exchange, J. Chem. Phys. 98 (1993) 5648–5652.
[51] C. Lee, W. Yang, R.G. Parr, Development of the Colle–Salvetti correlation-energy formula into a functional of the electron density, Phys. Rev. B 37 (1988) 785–789.
[52] P.J. Stephens, F.J. Devlin, C.F. Chabalowski, M.J. Frisch, Ab Initio calculation of vibrational absorption and circular dichroism spectra using density functional force fields, J. Phys. Chem. 98 (1994) 11623–11627.
[53] C. Møller, M.S. Plesset, Note on an approximation treatment for many-electron systems, Phys. Rev. 46 (1934) 618–622.
[54] R.J. Bartlett, G.D. Purvis, Many-body perturbation theory, coupled-pair many-electron theory, and the importance of quadruple excitations for the correlation problem, Int. J. Quantum Chem. 14 (1978) 561–581.
[55] M.J. Frisch, G.W. Trucks, H.B. Schlegel, G.E. Scuseria, M.A. Robb, J.R. Cheeseman, J.A. Montgomery Jr., T. Vreven, K.N. Kudin, J.C. Burant, J.M. Millam, S.S. Iyengar, J. Tomasi, V. Barone, B. Mennucci, M. Cossi, G. Scalmani, N. Rega, G.A. Petersson, H. Nakatsuji, M. Hada, M. Ehara, K. Toyota, R. Fukuda, J. Hasegawa, M. Ishida, T. Nakajima, Y. Honda, O. Kitao, H. Nakai, M. Klene, X. Li, J.E. Knox, H.P. Hratchian, J.B. Cross, V. Bakken, C. Adamo, J. Jaramillo, R. Gomperts, R.E. Stratmann, O. Yazyev, A.J. Austin, R. Cammi, C. Pomelli, J.W. Ochterski, P.Y. Ayala, K. Morokuma, G.A. Voth, P. Salvador, J.J. Dannenberg, G. Zakrzewski, S. Dapprich, A.D. Daniels, M.C. Strain, O. Farkas, D.K. Malick, A.D. Rabuck, K. Raghavachari, J.B. Foresman, J.V. Ortiz, Q. Cui, A.G. Baboul, S. Clifford, J. Cioslowski, B.B. Stefanov, G. Liu, A. Liashenko, P. Piskorz, I. Komaromi, R.L. Martin, D.J. Fox, T. Keith, M.A. Al-Laham, C.Y. Peng, A. Nanayakkara, M. Challacombe, P.M.W. Gill, B. Johnson, W. Chen, M.W. Wong, C. Gonzalez, J.A. Pople, Gaussian 03, Gaussian, Inc., Pittsburgh, PA, 2003
[56] F.W. Biegler-König, R.F.W. Bader, T.-H. Tang, Calculation of the average properties of atoms in molecules. 2, J. Comput. Chem. 3 (1982) 317–328.
[57] P. Salvador, E. Ramos-Cordoba, Communication: an approximation to Bader's topological atom, J. Chem. Phys. 139 (2013) 071103.

[58] P. Salvador, E. Ramos-Córdoba, APOST-3D, Universitat de Girona, Girona, 2011.
[59] E. Matito, M. Solà, P. Salvador, M. Duran, Electron sharing indexes at the correlated level. Application to aromaticity measures, Faraday Discuss. 135 (2007) 325–345.
[60] E. Matito, Electron Sharing Indices Program for 3D Molecular Space Partitioning, Universitat de Girona, Spain and Euskal Herriko Unibersitatea, Spain, 2011.
[61] E. Matito, M. Duran, M. Solà, The aromatic fluctuation index (FLU): a new aromaticity index based on electron delocalization, J. Chem. Phys. 122 (2005) 014109; Erratum, íbid 125, 2006, 4560-4560.
[62] A.M.K. Müller, Explicit approximate relation between reduced two- and one-particle density matrices, Phys. Lett. A 105 (1984) 446–452.
[63] J. Poater, M. Solà, M. Duran, X. Fradera, The calculation of electron localization and delocalization indices at the Hartree–Fock, density functional and post-Hartree–Fock levels of theory, Theor. Chem. Acc. 107 (2002) 362–371.
[64] F. Colmenero, C. Valdemoro, Self-consistent approximate solution of the second-order contracted Schrödinger equation, Int. J. Quantum Chem. 51 (1994) 369–388.
[65] H. Nakatsuji, Equation for the direct determination of the density matrix, Phys. Rev. A 14 (1976) 41–50.
[66] H. Nakatsuji, K. Yasuda, Direct determination of the quantum-mechanical density matrix using the density equation, Phys. Rev. Lett. 76 (1996) 1039–1042.
[67] D.A. Mazziotti, Approximate solution for electron correlation through the use of Schwinger probes, Chem. Phys. Lett. 289 (1998) 419–427.
[68] D.A. Mazziotti, Comparison of contracted Schrödinger and coupled-cluster theories, Phys. Rev. A 60 (1999) 4396–4408.
[69] A.E. DePrince III, D.A. Mazziotti, Cumulant reconstruction of the three-electron reduced density matrix in the anti-Hermitian contracted Schrödinger equation, J. Chem. Phys. 127 (2007) 104104.
[70] D.A. Mazziotti, Complete reconstruction of reduced density matrices, Chem. Phys. Lett. 326 (2000) 212–218.

V) Benchmarking 2-RDM Approximations

5.1) Comprehensive Benchmarking of Density Matrix Functional Approximations

Rodríguez-Mayorga M., Ramos-Cordoba E., Via-Nadal M., Piris M., Matito E. “Comprehensive benchmarking of density matrix functional approximations. *Phys. Chem. Chem. Phys*. Vol. 19 (2017) : 24029-24041.

https://doi.org/10.1039/C7CP03349D

PCCP

PAPER

View Article Online
View Journal | View Issue

Cite this: *Phys. Chem. Chem. Phys.*, 2017, **19**, 24029

Comprehensive benchmarking of density matrix functional approximations†‡

Mauricio Rodríguez-Mayorga,[ab] Eloy Ramos-Cordoba,[ac] Mireia Via-Nadal,[a] Mario Piris[ad] and Eduard Matito *[ad]

Received 18th May 2017,
Accepted 10th August 2017

DOI: 10.1039/c7cp03349d

rsc.li/pccp

The energy usually serves as a yardstick in assessing the performance of approximate methods in computational chemistry. After all, these methods are mostly used for the calculation of the electronic energy of chemical systems. However, computational methods should be also aimed at reproducing other properties, such strategy leading to more robust approximations with a wider range of applicability. In this study, we suggest a battery of ten tests with the aim to analyze density matrix functional approximations (DMFAs), including several properties that the exact functional should satisfy. The tests are performed on a model system with varying electron correlation, carrying a very small computational effort. Our results not only put forward a complete and exhaustive benchmark test for DMFAs, currently lacking, but also reveal serious deficiencies of existing approximations that lead to important clues in the construction of more robust DMFAs.

1 Introduction

Density matrix functional theory (DMFT) is among the computational methods that have experienced a most important advance in the last years. Its foundations are more than forty years old[1] but the most important progress in the field has occurred in the last twenty years.[2,3] Namely, the use of the natural orbital representation of the first-order reduced density matrix has brought many[4–22] density matrix functional approximations (DMFAs) within the context of what is known in the literature as natural orbital functional theory. Some of these functionals provide very accurate energies, sometimes competing with high-level electronic structure methods.[23–27]

Despite the success, the account of dynamic correlation still poses a great challenge for DMFAs[2,14,23] and calls for means to separate dynamic and nondynamic correlation within DMFT.[22,28,29] The development of more accurate DMFAs also depends on appropriate benchmark tests and, to our knowledge, only a recent paper addresses the validation of most DMFAs in the literature, comparing their performance in the energy calculation of few-electron systems with different electron correlation.[23]

Since functionals are mostly used to calculate the electronic energy of chemical systems, it does not strike as a surprise that the energy usually serves as a yardstick in benchmarking DMFAs. However, it is becoming commonly accepted that energy functionals should be also aimed at reproducing other properties[30] in order to construct more robust approximations with a wider range of applicability. In this line, some of us have recently tested the spin structure of several DMFAs[27,31] using the local spin[32] as a benchmarking tool.

In the present study, we suggest a battery of ten tests to analyze DMFAs, including several properties that the exact functional should satisfy. We submit fifteen functionals to this series of constrictive tests using a model system with varying electron correlation, the two-electron harmonium atom,[33] carrying a very small computational effort.

Although the construction of computational methods that can tackle both one- and two-electron systems is relevant in other frameworks such as density functional theory,[34] it is believed that they do not pose a serious challenge in DMFT. The reason behind this idea is the existence of a quasi-exact closed-shell two-electron expression of the second-order reduced density matrix in terms of natural orbitals.[35] However, there are several facts that go against this idea. First of all, most DMFAs do not reduce to the quasi-exact expression for two-electron systems and, therefore, their calibration is justified. Second, the latter expression depends on some phase factors (*vide infra*) that change importantly under certain circumstances,[36–39] including the strong-correlation regime of

[a] *Kimika Fakultatea, Euskal Herriko Unibertsitatea UPV/EHU, and Donostia International Physics Center (DIPC), P.K. 1072, 20080 Donostia, Euskadi, Spain. E-mail: ematito@gmail.com*
[b] *Institut de Química Computacional i Catàlisi (IQCC) and Departament de Química, University of Girona, 17071 Girona, Catalonia, Spain*
[c] *Department of Chemistry, University of California Berkeley, 94720, Berkeley, CA, USA*
[d] *IKERBASQUE, Basque Foundation for Science, 48011 Bilbao, Euskadi, Spain*

† In memoriam of Jose Ignacio Eguiazabal, researcher and Director of Polymer Science and Technology Department (UPV-EHU).

‡ Electronic supplementary information (ESI) available. See DOI: 10.1039/c7cp03349d

the system studied in this work. Finally, whereas energetic differences between the quasi-exact result and the exact one are often negligible, there are several properties studied in this paper that show non-negligible differences for the quasi-exact functional.

All in all, we shall see that the set of tests suggested in this work poses a great challenge for DMFAs and reveals various defects of the approximations that were hindered by a reasonable performance in energy benchmark tests. The current strategy can be easily extended to a larger number of electrons, thus setting new challenges for the few DMFAs that reduce to the quasi-exact expression. We are confident that DMFT developers will benefit from the results obtained in this paper and will use this test set as a means to construct more robust approximations.

2 Methodology

The second-order reduced density matrix (2-RDM),[40,41]

$$\rho_2(\mathbf{x}_1,\mathbf{x}_2;\mathbf{x}_1',\mathbf{x}_2') = N(N-1)\int d\mathbf{x}_3\cdots\int d\mathbf{x}_N \times \Psi^*(\mathbf{x}_1',\mathbf{x}_2',\mathbf{x}_3,\ldots,\mathbf{x}_N)\Psi(\mathbf{x}_1,\mathbf{x}_2,\mathbf{x}_3,\ldots,\mathbf{x}_N), \quad (1)$$

where we have adopted McWeeny's normalization[41] and $\mathbf{x} = (\mathbf{r},\sigma)$, is the simplest function in terms of which the explicit expression of the electronic energy of a physical system is known.[42] Hence, approximations to the 2-RDM in terms of simpler quantities provide estimates of the energy that, in principle, should reduce the associated computational cost. Most quantum mechanical calculations employ orbital basis sets, and it is thus costumary to express the 2-RDM in a given orbital basis. In this paper, we adopt the basis of natural orbitals,

$${}^2D^{\sigma\sigma'}_{ij,kl} = \left\langle \Psi \middle| a^\dagger_{i\sigma} a^\dagger_{j\sigma'} a_{l\sigma'} a_{k\sigma} \middle| \Psi \right\rangle, \quad (2)$$

where $a^\dagger_{i\sigma}$ ($a_{i\sigma}$) is the creation (annihilation) operator acting over natural orbital i with spin σ; hereafter we will refer to ${}^2D^{\sigma\sigma'}_{ij,kl}$ as the two-density matrix (2-DM). The spinless 2-RDM is a twelve-variable function, whereas the 2-DM is a four-index tensor of dimension M^4. In the present study we focus on 2-DM approximations built from natural occupation numbers (ONs), $\{n_i\}_{i=1}^M$, where M is the size of the basis set.[1–3] The approximate 2-DMs here studied are built upon the simplification of the 2-DM being a sparse matrix with only three types of non-zero elements: ${}^2D^{\sigma\sigma}_{ij,ij}$ and ${}^2D^{\sigma\sigma'}_{ij,ij}$, ${}^2D^{\sigma\sigma}_{ij,ji}$ and ${}^2D^{\sigma\sigma'}_{ij,ji}$, and ${}^2D^{\sigma\sigma'}_{ii,jj}$. The opposite-spin elements are actually sufficient to express the exact 2-DM of a two-electron closed-shell system (see eqn (12)). Each ON-based 2-DM approximation actually provides a DMFA. Among the DMFAs, the simplest one is the single-determinant (SD) approximation, whose expression reads[40]

$${}^2D^{\mathrm{SD},\alpha\beta}_{ij,kl} = n_i^\alpha n_j^\beta \delta_{ik}\delta_{jl} \quad (3)$$

for the opposite-spin elements and

$${}^2D^{\mathrm{SD},\alpha\alpha}_{ij,kl} = n_i^\alpha n_j^\alpha(\delta_{ik}\delta_{jl} - \delta_{il}\delta_{jk}) \quad (4)$$

for the like-spin ones. Upon optimization of natural orbitals and ONs, the SD approximation produces the Hartree–Fock energy. In this work, we optimize neither the orbitals nor the occupations (*vide infra*) and, in order to avoid confusion with the Hartree–Fock method (which does not employ fractional occupancies), we have preferred to call this approximation SD. We will consider 15 DMFAs, all of which are *JKL*-only functionals, *i.e.*, functionals that only need Coulomb, exchange and time-inversion two-electron integrals.[43] We have classified them in two groups: those that only modify the exchange part of the functional and those that modify both the exchange and Coulomb parts. The latter group corresponds to the functionals developed by one of us and known as Piris natural orbital functionals (PNOFs). The first group of DMFAs uses eqn (3) and

$${}^2D^{\mathrm{X},\alpha\alpha}_{ij,kl} = n_i^\alpha n_j^\alpha \delta_{ik}\delta_{jl} - f_X(n_i^\alpha,n_j^\alpha)\delta_{il}\delta_{jk}, \quad (5)$$

the expression of $f_X(n_i,n_j)$ determining the functional.[44] These functionals are *JK*-only functionals but, in practice, they use the simple SD approximation for the terms involving two-electron Coulomb integrals (J) and, therefore, they will be referred as *K*-functionals hereafter. Their expressions are collected in Table 1.

PNOFs actually correspond to approximations to the two-particle cumulant matrix (${}^2\Gamma$),[11] which is defined as the

Table 1 $f(n_i,n_j)$ functions (see eqn (5)) that define the *K*-functionals. In a two-electron closed-shell system $F_L = 1$

DMFA	$f(n_i,n_j)$		Parameters	Ref.
SD	$n_i n_j$			40
MBB[a]	$(n_i n_j)^{1/2}$			4 and 5
BBC2[b]	n_i	$i=j$		10
	$-(n_i n_j)^{1/2}$	$i\neq j \wedge i\in(F_L;\infty)\wedge j\in(F_L;\infty)$		
	$n_i n_j$	$i\neq j \wedge i\in[1;F_L]\wedge j\in[1;F_L]$		
	$(n_i n_j)^{1/2}$	Otherwise		
CA[c]	$[n_i(1-n_i)n_j(1-n_j)]^{1/2} + n_i n_j$			7
CGA[d]	$\frac{n_i n_j + [n_i(2-n_i)n_j(2-n_j)]^{1/2}}{2}$			9
ML[e]	$n_i n_j \frac{a_0 + a_1 n_i n_j}{1 + b_1 n_i n_j}$		$a_0 = 126.3101$ $a_1 = 2213.33$ $b_1 = 2338.64$	13
MLSIC[f]	$n_i n_j \frac{a_0 + a_1 n_i n_j}{1 + b_1 n_i n_j}$	$i\neq j$	$a_0 = 1298.78$ $a_1 = 35114.4$ $b_1 = 36412.2$	13
	$n_i n_j$	$i=j$		
GU[g]	$(n_i n_j)^{1/2}$	$i\neq j$		6
	$n_i n_j$	$i=j$		
POWER[h]	$(n_i n_j)^\alpha$			15–17

[a] Introduced independently by Müller and by Buijse and Baerends.[5,8] [b] The BBC2 functional coincides with BBC1[10] for a two-electron closed-shell system. [c] Csányi and Arias functional. [d] Csányi, Goedecker and Arias functional. [e] Marques and Lathiotakis functional. [f] Marques and Lathiotakis functional corrected for self-interaction. [g] Goedecker and Umrigar functional. [h] The α parameter of the POWER functional is fitted for each ω, $\alpha(\omega)$, in order to reproduce the exact V_{ee} value (see the ESI for further details).

difference between the exact 2-DM and the SD approximation,[45]

$$^2D^{\sigma\sigma'}_{ij,kl} = {}^2D^{\mathrm{SD},\sigma\sigma'}_{ij,kl} + {}^2\Gamma^{\sigma\sigma'}_{ij,kl}. \quad (6)$$

The different PNOF expressions are constructed in terms of the auxiliary Δ and Π matrices according to the following recipe:

$$^2\Gamma^{\mathrm{PNOF}n,\alpha\beta}_{ij,kl} = -\Delta^{\alpha\beta}_{ij}\delta_{ik}\delta_{jl} + \Pi_{ik}\delta_{ij}\delta_{kl}, \quad (7)$$

$$^2\Gamma^{\mathrm{PNOF}n,\alpha\alpha}_{ij,kl} = -\Delta^{\alpha\alpha}_{ij}(\delta_{ik}\delta_{jl} - \delta_{il}\delta_{jk}). \quad (8)$$

Table 2 collects Δ and Π matrices for all PNOFs. In all PNOFs $\Delta^{\alpha\alpha}_{ij} = \Delta^{\alpha\beta}_{ij} \equiv \Delta_{ij}$ excepting PNOF3 that takes $\Delta^{\alpha\alpha}_{ij} = 0$. In this work, approximate 2-DMs are constructed from full configuration interaction (FCI) ONs and, therefore, the original PNOF5 and PNOF6,[20,21] which impose perfect-pairing constraints in the ONs, cannot be employed. Alternatively, in this paper we employ the extended versions of PNOF5[46] and PNOF6[47] that are free of these restrictions for a closed-shell two-electron system. Hereafter, the names PNOF5 and PNOF6 refer to the extended versions of these DMFAs. Unlike the original PNOF6, the extended version of PNOF6 can be actually calculated in three different ways, depending on the definition of S_γ, which will be called down (d), up (u) and average (h),

$$S^{\mathrm{d}}_\gamma = \sum_{i=1}^{F_{\mathrm{L}}}\gamma_i, \quad S^{\mathrm{u}}_\gamma = \sum_{i>F_{\mathrm{L}}}^{M}\gamma_i, \quad S^{\mathrm{h}}_\gamma = \frac{S^{\mathrm{d}}+S^{\mathrm{u}}}{2}, \quad (9)$$

where

$$\gamma_i = n_i(1-n_i) + \kappa_i{}^2 - \kappa_i\sum_{i=j}^{F_{\mathrm{L}}}\kappa_j, \quad (10)$$

Table 2 Δ and Π non-zero matrix elements. The diagonal elements coincide for all functionals: $\Delta_{ii} = n_i{}^2$ and $\Pi_{ii} = n_i$. $S_{\mathrm{F}} = \sum_{i=1}^{F_{\mathrm{L}}} h_i$, $T_{ij} = n_in_j - \Delta_{ij}$, $h_i = 1 - n_i$, and S^{x}_γ and γ_i are defined in eqn (9) and (10), respectively. Ω_g is the subspace containing orbital g, which is below the Fermi level, and several orbitals above the Fermi level. In a two-electron closed-shell system $F_{\mathrm{L}} = 1$

	Δ_{ij}	Π_{ij}	Cases ($i \neq j$)	Ref.
PNOF2	h_ih_j	$\sqrt{n_in_j} + \sqrt{h_ih_j} + T_{ij}$	$i \wedge j \in [1,F_{\mathrm{L}}]$	12
	$n_jh_i\left(\frac{1-S_{\mathrm{F}}}{S_{\mathrm{F}}}\right)$	$\sqrt{n_in_j} - \sqrt{n_jh_i} + T_{ij}$	$i \in [1,F_{\mathrm{L}}] \wedge j \in (F_{\mathrm{L}},M]$	
	$n_ih_j\left(\frac{1-S_{\mathrm{F}}}{S_{\mathrm{F}}}\right)$	$\sqrt{n_in_j} - \sqrt{n_ih_j} + T_{ij}$	$j \in [1,F_{\mathrm{L}}] \wedge i \in (F_{\mathrm{L}},M]$	
	n_in_j	T_{ij}	$i \wedge j \in (F_{\mathrm{L}},M]$	
PNOF3	h_ih_j	$n_in_j - \sqrt{n_in_j}$	$i \wedge j \in [1,F_{\mathrm{L}}]$	18
	$n_jh_i\left(\frac{1-S_{\mathrm{F}}}{S_{\mathrm{F}}}\right)$	$n_in_j - \sqrt{n_in_j} - \sqrt{n_jh_i}$	$i \in [1,F_{\mathrm{L}}] \wedge j \in (F_{\mathrm{L}}, M]$	
	$n_ih_j\left(\frac{1-S_{\mathrm{F}}}{S_{\mathrm{F}}}\right)$	$n_in_j - \sqrt{n_in_j} - \sqrt{n_ih_j}$	$j \in [1,F_{\mathrm{L}}] \wedge i \in (F_{\mathrm{L}},M]$	
	n_in_j	$n_in_j + \sqrt{n_in_j}$	$i \wedge j \in (F_{\mathrm{L}}, M]$	
PNOF4	h_ih_j	$-\sqrt{h_ih_j}$	$i \wedge j \in [1,F_{\mathrm{L}}]$	
	$n_jh_i\left(\frac{1-S_{\mathrm{F}}}{S_{\mathrm{F}}}\right)$	$-\sqrt{\left(\frac{h_in_j}{S_{\mathrm{F}}}\right)\left(n_i - n_j + \frac{h_in_j}{S_{\mathrm{F}}}\right)}$	$i \in [1,F_{\mathrm{L}}] \wedge j \in (F_{\mathrm{L}},M]$	
	$n_ih_j\left(\frac{1-S_{\mathrm{F}}}{S_{\mathrm{F}}}\right)$	$-\sqrt{\left(\frac{h_jn_i}{S_{\mathrm{F}}}\right)\left(n_j - n_i + \frac{h_jn_i}{S_{\mathrm{F}}}\right)}$	$j \in [1,F_{\mathrm{L}}] \wedge i \in (F_{\mathrm{L}},M]$	
	n_in_j	$\sqrt{n_in_j}$	$i \wedge j \in (F_{\mathrm{L}},M]$	
PNOF5	n_in_j	$-\sqrt{n_in_j}$	$(i \wedge j \in \Omega_g) \wedge (i = g \vee j = g)$	20
	n_in_j	$\sqrt{n_in_j}$	$(i \wedge j \in \Omega_g) \wedge (i \wedge j \in (F_{\mathrm{L}},M])$	
PNOF6x	$\mathrm{e}^{-2S_{\mathrm{F}}}h_ih_j$	$-\mathrm{e}^{-S_{\mathrm{F}}}\sqrt{h_ih_j}$	$i \wedge j \in [1,F_{\mathrm{L}}]$	21
	$\gamma_i\gamma_j/S^{\mathrm{x}}_\gamma$	$-\sqrt{\left(n_ih_j + \frac{\gamma_i\gamma_j}{S^{\mathrm{x}}_\gamma}\right)\left(n_jh_i + \frac{\gamma_i\gamma_j}{S^{\mathrm{x}}_\gamma}\right)}$	$i \in [1,F_{\mathrm{L}}] \wedge j \in (F_{\mathrm{L}},M]$	
x = d, u, h	$\gamma_i\gamma_j/S^{\mathrm{x}}_\gamma$	$-\sqrt{\left(n_ih_j + \frac{\gamma_i\gamma_j}{S^{\mathrm{x}}_\gamma}\right)\left(n_jh_i + \frac{\gamma_i\gamma_j}{S^{\mathrm{x}}_\gamma}\right)}$	$j \in [1,F_{\mathrm{L}}] \wedge i \in (F_{\mathrm{L}},M]$	
	$\mathrm{e}^{-2S_{\mathrm{F}}}n_in_j$	$\mathrm{e}^{-S_{\mathrm{F}}}\sqrt{n_in_j}$	$i \wedge j \in (F_{\mathrm{L}},M]$	
PNOF7	n_in_j	$-\sqrt{n_in_j}$	$(i \wedge j \in \Omega_g) \wedge (i = g \vee j = g)$	22
	n_in_j	$\sqrt{n_in_j}$	$(i \wedge j \in \Omega_g) \wedge (i \wedge j \in (F_{\mathrm{L}},M])$	
	0	$-\sqrt{n_ih_in_jh_j}$	$(i \vee j) \in [1,F_{\mathrm{L}}] \wedge ((i \in \Omega_g \wedge j \notin \Omega_g) \vee (j \in \Omega_g \wedge i \notin \Omega_g))$	
	0	$\sqrt{n_ih_in_jh_j}$	$(i \wedge j) \in (F_{\mathrm{L}},\infty) \wedge ((i \in \Omega_g \wedge j \notin \Omega_g) \vee (j \in \Omega_g \wedge i \notin \Omega_g))$	

and

$$\kappa_i = \begin{cases} (1-n_i)\mathrm{e}^{-S_\mathrm{F}} & i \in [1, F_\mathrm{L}] \\ n_i \mathrm{e}^{-S_\mathrm{F}} & i \in (F_\mathrm{L}, M] \end{cases} \quad (11)$$

F_L being the last occupied orbital below the Fermi level.

For two-electron closed-shell systems, the 2-DM in terms of ONs is known up to a phase factor, Φ_{ij},[35] the following being the only non-zero elements:

$${}^2D^{\alpha\beta}_{ii,jj} = \Phi_{ij}\sqrt{n_i^\alpha n_j^\beta} \quad (i \neq j), \quad (12)$$

where $\Phi_{ij} = \pm 1$, depending on the nature of orbitals i and j. The most convenient way to choose the phase factors is to split the set of orbitals into two groups: the orbitals above and below the Fermi level, and choose $\Phi_{ij} = 1$ for i and j belonging to the same group and $\Phi_{ij} = -1$ otherwise.[36] Let us call this approximation the fixed-phases (FP) approximation. FP is very accurate for most two-electron systems[3,36] with only a few exceptions[37,39,48] that Giesbertz *et al.* attribute to long-range Coulomb interactions.[38] For two-electron systems, PNOF4, PNOF5 and PNOF7 reduce to FP with the mentioned phase factors, *i.e.*, eqn (12) with $\Phi_{1i} = -1 (i \neq 1)$ and $\Phi_{ij} = 1$ for all other cases. Hence, hereafter we will only discuss PNOF4 results. Conversely, PNOF2, PNOF3 and PNOF6 expressions were not defined for two-electron systems and, therefore, the expression given in Table 2 does not reduce to FP.[49] In this work we have decided to study these expressions in a two-electron model.

Not all approximate 2-DMs correspond to an N-particle fermionic wavefunction. The set of 2-DMs that satisfy this condition are called N-representable 2-DMs. Non N-representable 2-DMs might lead to spurious results such as non-variational energies.[19,42] The set of conditions that guarantees the N-representability of the 2-DM is known[50] but its calculation involves higher-order density matrices. There are three conditions that only require the 2-DM for its calculation, the P-, G- and Q-conditions,[51–53] which concern the positive semidefinite character of P, Q and G matrices,[44]

$$P^{\sigma\sigma'}_{ij,kl} = \left\langle \Psi \middle| a^\dagger_{i\sigma} a^\dagger_{j\sigma'} a_{l\sigma'} a_{k\sigma} \middle| \Psi \right\rangle, \quad (13)$$

$$Q^{\sigma\sigma'}_{ij,kl} = \left\langle \Psi \middle| a_{i\sigma} a_{j\sigma'} a^\dagger_{l\sigma'} a^\dagger_{k\sigma} \middle| \Psi \right\rangle, \quad (14)$$

$$G^{\sigma\sigma'}_{ij,kl} = \left\langle \Psi \middle| a_{i\sigma} a^\dagger_{j\sigma'} a^\dagger_{l\sigma'} a_{k\sigma} \middle| \Psi \right\rangle. \quad (15)$$

In order to test these conditions, one must build these matrices and check the sign of the corresponding eigenvalues. Notice that the P matrix coincides with the 2-DM and, therefore, the P condition is equivalent to the non-negativity condition of the geminal occupancies.

The pair density, $\rho_2(\mathbf{r}_1,\mathbf{r}_2)$, is the diagonal part of the 2-RDM (*i.e.*, eqn (1) when $\mathbf{r}_1 = \mathbf{r}'_1$ and $\mathbf{r}_2 = \mathbf{r}'_2$) upon integration over spin and it is the only part of the 2-RDM needed to calculate the electron–electron repulsion energy (V_ee). Although $\rho_2(\mathbf{r}_1,\mathbf{r}_2)$ is a simpler function than the 2-RDM, it depends on six variables and it is difficult to analyze. Fortunately, there is no need of the full knowledge of $\rho_2(\mathbf{r}_1,\mathbf{r}_2)$ to compute V_ee. The calculation of the electronic repulsion only requires the radial intracule[54] density[41]

$$I(r_{12}) = r_{12}^2 \int \mathrm{d}\mathbf{r}_1' \mathrm{d}\mathbf{r}_2' \mathrm{d}\Omega_{12} \rho_2(\mathbf{r}_1', \mathbf{r}_2') \delta(\mathbf{r}_{12} - \mathbf{r}_1' + \mathbf{r}_2'), \quad (16)$$

where $\mathrm{d}\Omega_{12} = \sin\theta_{12}\mathrm{d}\theta_{12}\mathrm{d}\phi_{12}$. The radial intracule density is a one dimensional function that provides a graphical means to analyze $\rho_2(\mathbf{r}_1,\mathbf{r}_2)$ at different interelectronic separations and a simple expression to calculate V_ee,

$$V_\mathrm{ee} = \int_0^\infty \mathrm{d}r_{12} \frac{I(r_{12})}{r_{12}}. \quad (17)$$

$\rho_2(\mathbf{r}_1,\mathbf{r}_2)$ also enters the expression of the so-called delocalization index (DI),[55,56] which is a measure of covariance between the electron population of two regions, A and B,

$$\delta(A,B) = -2\int_A \int_B \mathrm{d}\mathbf{r}_1 \mathrm{d}\mathbf{r}_2 [\rho_2(\mathbf{r}_1,\mathbf{r}_2) - \rho(\mathbf{r}_1)\rho(\mathbf{r}_2)], \quad (18)$$

where $\rho(\mathbf{r})$ is the electron density. The DI has been used in the past to calibrate the performance of several approximations.[57–64] In the present work, the DMFAs use the exact natural orbitals and occupancies and, therefore, the second term in the r.h.s. of eqn (18) is identical in both the exact calculation and the DMFA. Hence, the DI difference actually measures the difference between the exact and the DMFA number of electron pairs (one in region A and another in B).

3 Computational details

We will test several DMFAs in the two-electron harmonium atom—a model system with the following Hamiltonian,[33,65,66]

$$H = -\frac{1}{2}\nabla_1^2 - \frac{1}{2}\nabla_2^2 + \frac{1}{2}\omega^2 \mathrm{r}_1^2 + \frac{1}{2}\omega^2 \mathrm{r}_2^2 + \frac{1}{|\mathbf{r}_2 - \mathbf{r}_1|}, \quad (19)$$

where the ω parameter is the confinement strength and tunes the electron correlation in a continuous manner: low-ω values correspond to a strong-correlation regime whereas weakly correlated systems are produced at large ω. The harmonium atom has been widely used for benchmarking and developing functionals[23,64,67–77] due to the availability of benchmark results.[48,78–80] The harmonium atom is one of the most difficult systems for computational methods[64,68,76,77] and, therefore, is a formidable test-bed for DMFAs. In addition to harmonium, there are other model systems that pose a great challenge for computational methods, such as the Hubbard model[81] or uniform gases of electrons trapped in rings, spheres and geometrical objects of higher dimensions.[82–85]

FCI calculations were performed for the ground-state singlet two-electron harmonium atom using 20 values of the ω parameter: 0.03, 0.033, 0.036, 0.0365373, 0.04, 0.05, 0.06, 0.08, 0.1, 0.15, 0.2, 0.3, 0.4, 0.5, 1, 2, 5, 10, 100 and 1000.[86] We used a modified version of the code developed by Knowles and Handy[87,88] and a variationally optimized even-tempered basis set of seven S, P, D and F Gaussian functions, which form a total of 112 basis functions.[86] The exact 2-DM and the ONs were

calculated from the FCI expansion coefficients using the DMN[89] in-house code. The radial intracule density was computed using RHO2_OPS[90] code which uses the algorithm proposed by Cioslowski and Liu.[91] The calculation of the DI was performed with the in-house RHO_OPS[92] and ESI-3D[57,93,94] codes.

In the current study, exact (within the given basis set) natural orbitals and occupancies are used in fifteen DMFAs (BBC2, CA, CGA, GU, MBB, POWER, ML, MLSIC, PNOF2, PNOF3, PNOF4, three PNOF6 definitions and SD) to evaluate their performance in a series of tests. Namely, we have used the expressions given in Tables 1 and 2 with FCI ONs to generate the corresponding approximate 2-DM, which are subsequently analyzed using ten different tests:

(i) calculation of the 2-DM trace, (ii) cumulative absolute error (CAE) for the diagonal elements, *i.e.*,

$$\mathrm{CAE_D}\left[{}^2\mathbf{D}^X\right] = \sum_{\substack{ij \\ \sigma\sigma'}} \left| {}^2D^{X,\sigma\sigma'}_{ij,ij} - {}^2D^{\sigma\sigma'}_{ij,ij} \right|, \tag{20}$$

(iii) CAE for all the elements of the 2-DM,

$$\mathrm{CAE}\left[{}^2\mathbf{D}^X\right] = \sum_{\substack{ijkl \\ \sigma\sigma'}} \left| {}^2D^{X,\sigma\sigma'}_{ij,kl} - {}^2D^{\sigma\sigma'}_{ij,kl} \right|, \tag{21}$$

(iv) the correct antisymmetry of the 2-DM, *i.e.*,

$$\mathrm{Err_A}\left[{}^2\mathbf{D}^{X,\sigma\sigma'}\right] = \sum_{ijkl,\sigma} \left| {}^2D^{X,\sigma\sigma}_{ij,kl} + {}^2D^{X,\sigma\sigma}_{ij,lk} + {}^2D^{X,\sigma\sigma}_{ji,lk} + {}^2D^{X,\sigma\sigma}_{ji,kl} \right|, \tag{22}$$

(v) *P*, *Q*, and *G* *N*-representability conditions, eqn (13)–(15), (vi) the DI between the two symmetric regions generated by a bisecting plane passing through the center of mass, (vii) the average interelectronic distance and (viii) its variance, (ix) the interelectronic repulsion, V_{ee}, and (x) the radial intracule density profile.

4 Results

4.1 The diagonal elements: sum rule and cumulative absolute error

The plot in Fig. 1 shows the 2-DM trace errors for several DMFAs (the exact trace equals two in McWeeny's normalization[41]). BBC2, CA, CGA, MBB, PNOF2 and PNOF4 have not been included in this plot because they satisfy the sum rule. The larger the ω value, the less important the correlation effects in the harmonium atom. Indeed, for large values of ω all approximations perform very well because correlation effects are negligible. However, when correlation increases, SD produces very poor results. GU and MLSIC have the same diagonal elements ($f(n_i,n_i) = n_i^2$) and, therefore, give exactly the same trace as the SD approximation for the two-electron case. PNOF3 coincides with SD because the former only modifies the opposite-spin elements in the cumulant construction and the opposite-spin cumulant of PNOF3 (like the exact one) does not contribute to the sum rule. ML is based on a Padé approximant including some fitted parameters that result in wrong

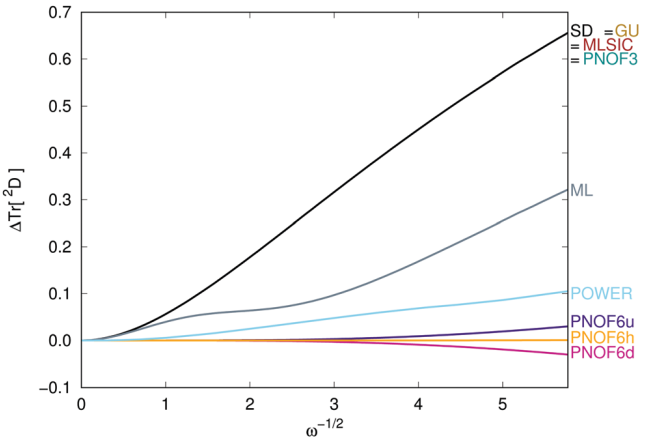

Fig. 1 2-DM trace error against $\omega^{-1/2}$. BBC2, CA, CGA, MBB, PNOF2 and PNOF4 have not been included because they satisfy the sum rule.

trace numbers. The POWER functional presents non-negligible errors in the trace as the correlation increases. PNOF6 shows small trace deviations, the three PNOF6 versions (PNOF6u, PNOF6h and PNOF6d) differing on the value of S_γ (actually, the S_γ definition, eqn (9), is responsible for the violation of the sum rule). The S_γ of PNOF6h provides the smallest error.

To get further insight about the error committed in the 2-DM diagonal elements, we have analyzed the diagonal CAE, eqn (20), as a function of $\omega^{-1/2}$ (Fig. 2). PNOF2 and PNOF4 approximations have not been included in Fig. 2 because the error produced by these approximations is lower than 10^{-4}. GU and MLSIC produce exactly the same error as the SD approximation because the self-interaction correction enforced in these approximations results in ${}^2D_{ij,ij}$ terms equal to those produced by SD. ML, which showed better trace numbers than SD for all ω values, presents a larger diagonal CAE indicating important error cancellation in the calculation of the trace. PNOF3 shows smaller diagonal CAE than SD, which necessarily come from the opposite-spin diagonal components, because the same-spin components of the 2-DM are identical in both

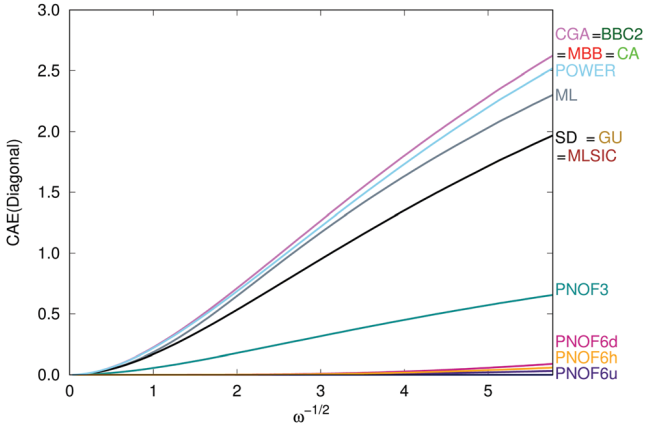

Fig. 2 Cumulative absolute error (CAE) for the diagonal elements of the 2-DM against $\omega^{-1/2}$ (eqn (20)). PNOF2 and PNOF4 approximations have not been included because they present errors lower than 10^{-4}.

approximations. All PNOF6 versions provide very small CAE, the best among the three definitions being PNOF6u (hence PNOF6h best trace numbers were due to error cancellation). BBC2, CA, CGA, MBB and POWER show larger diagonal CAE than SD due to the unphysical ${}^2D^{\sigma\sigma}_{ii,ii}$ elements that provide a correct total trace but contribute to important self-interaction errors. In fact, any *K*-functional studied in this work produces the same diagonal elements than the SD approximation (*i.e.*, $f(n_i,n_i) = n_i^2$) if we remove the unphysical elements ${}^2D^{\sigma\sigma}_{ii,ii}$ that are included in some DMFAs.

4.2 Cumulative absolute error

The total CAE (eqn (21)) is plotted against $\omega^{-1/2}$ in Fig. 3. All fifteen DMFAs provide CAE when correlation increases. A troublesome result is that all *K*-functionals perform worse than the SD approximation for all ω values. Most of the approximations show a monotonic increase of the error excepting MLSIC, probably due to the parameterization of this approximation. BBC2 and MBB values coincide for all ω and present the largest total CAE. Their 2-DMs do fully not coincide but for a closed-shell two-electron system these two DMFAs only differ in the phase of some unphysical ${}^2D^{\sigma\sigma}_{ii,ii}$ elements, which obviously contribute to the same CAE. All PNOFs perform better than SD indicating that the cumulant correction of PNOFs improves in the right direction. The most recently developed approximations, PNOF4 to PNOF7, show the best agreement with the exact 2-DM, giving only a small total CAE. Among the three PNOF6, PNOF6u performs marginally better than the rest. PNOF4 is actually exact in a wide range of ω values, only deviating at the high-correlation regime. In the high-correlation regime ($\omega \leq 0.1$) several phases of PNOF4 do not coincide with the exact ones, preventing PNOF4 from reproducing the exact elements of the 2-DM.

4.3 Antisymmetry

The electronic wavefunction must be antisymmetric due to the fermionic character of electrons. The 2-DM preserves the antisymmetric nature inherited from the wavefunction and, therefore, deviations from the antisymmetry condition, eqn (22), can be also regarded as violations of a necessary *N*-representability condition. Functionals that do not satisfy this condition fail to correctly treat the fermionic nature of electrons.

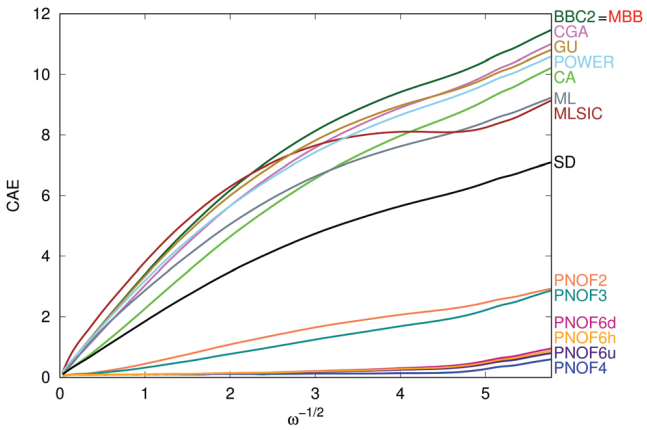

Fig. 3 Cumulative absolute error (CAE) for the whole 2-DM against $\omega^{-1/2}$ (eqn (21)).

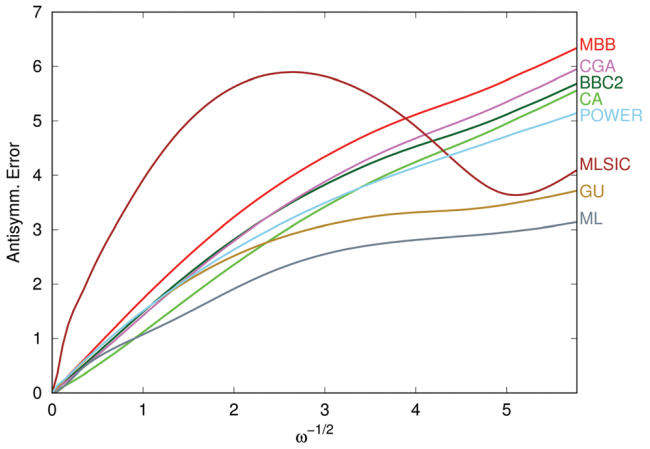

Fig. 4 Antisymmetry error of the 2-DMs (eqn (22)) against $\omega^{-1/2}$. PNOFs and SD have not been included because they satisfy the antisymmetry condition.

PNOFs were built in order to satisfy the correct antisymmetry of the 2-DM by constructing approximations from an inherently antisymmetric cumulant structure. SD is also antisymmetric by construction. Fig. 4 shows eqn (22) against $\omega^{-1/2}$ for the other DMFAs. The best *K*-functional is ML, which error is almost half the error of MBB in the high-correlation regime. The DMFAs that deviate most from the antisymmetry condition are BBC2, CA, CGA, and MBB with errors growing as $\omega^{-1/2}$. Conversely, the only DMFA that does not show a monotonic increase of the error with correlation is MLSIC, once again, putting forward the parameterized nature of this DMFA. A self-interaction correction applied to MBB produces the GU approximation,[8] resulting in smaller antisymmetry errors. One can easily prove that among all *K*-functionals that one could devise, the only one that satisfies the antisymmetric condition is SD. This result evinces the need for designing functionals that, at least, include *J* and *K* components, beyond the SD approximation.

4.4 *N*-Representability

In order to check the deviation from the *N*-representability conditions, we have computed the eigenvalues of matrices *P*, *Q* and *G* (eqn (13)–(15)) and summed all negative ones. In Fig. 5 we have plotted the result of the sum against $\omega^{-1/2}$.

The 2-DMs of PNOFs give rise to non-negative basis-set-independent eigenvalues associated to *P*-, *Q*- and *G*-conditions (see Appendix I for the basis-set dependent and independent eigenvalues). However, one cannot anticipate the conditions that the basis-set-dependent eigenvalues might impose in the functional structure and only PNOF2, PNOF4 and SD satisfy the *N*-representability conditions studied in this work. PNOF3 and PNOF6 perform very well even in the high-correlation regime with the only exception of PNOF3 that shows significant deviations in the *G*-condition when correlation increases, in line with previous findings.[19] PNOF6 shows small negative

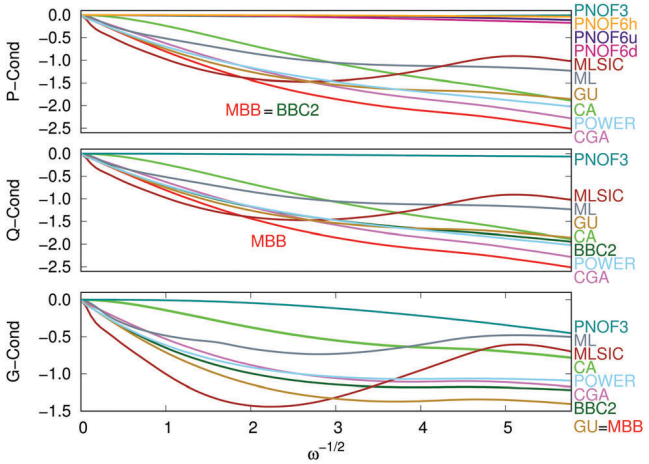

Fig. 5 Sum of all negative eigenvalues of P, Q and G matrices against $\omega^{-1/2}$. PNOF2, PNOF4 and SD have not been included because they satisfy the N-representability conditions studied.

eigenvalues of the P matrix that change depending on the definition of S_γ. In fact, if the wavefunction would correspond to a perfect-pairing situation (in which natural orbitals are coupled by pairs, each pair occupancy summing exactly to one electron) the P-condition would be satisfied for a two-electron closed-shell system regardless the definition of S_γ. All K-functionals show significant deviations from P-, Q- and G-conditions that rapidly increase with electron correlation. The largest errors are presented by MBB, but BBC2, CA, CGA, GU and POWER also present non-negligible errors. ML and MLSIC approximations show non-monotonic increase of the errors due to their parameterized nature.

4.5 Delocalization index

The difference between the approximate DI and the exact one is plotted in Fig. 6. In the present case, where the density is computed from exact ONs for both methods (see eqn (18)), the latter quantity also corresponds to the difference between the exact and the approximate number of electron pairs between two regions. Upon increase of electron correlation effects, the number of electron pairs between regions is expected to decrease, as found by other calculations of the DI in molecules under DMFAs (see the ESI‡ for the exact values).[57,60,95–97]

In general, the gross number of pairs is pretty well described by BCC2, MBB, PNOF4, PNOF6 and POWER (that present errors below 3%), whereas CA, GU, MLSIC, PNOF2, PNOF3 and SD present errors ranging between 20% to 75%. Interestingly, GU, MBB, MLSIC, PNOF3 and PNOF6u systematically underestimate the DI (*i.e.*, they overestimate the number of electron pairs) whereas BBC2, CA, CGA, PNOF2 and PNOF6d always overestimate it. In line with the results obtained in the sum rule and N-representability tests, PNOF6h provides better results than PNOF6u and PNOF6d.

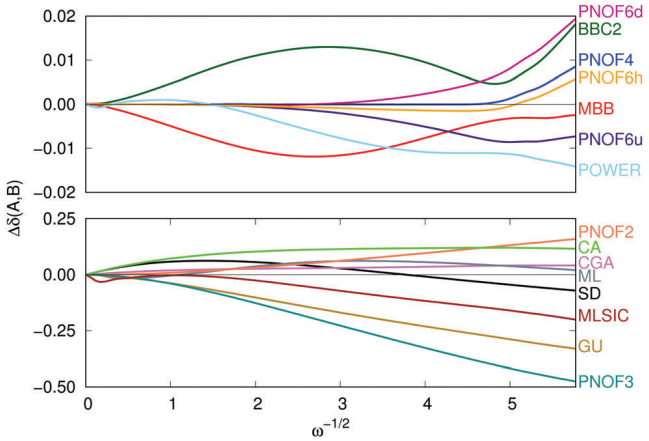

Fig. 6 Error in the DI against $\omega^{-1/2}$. (top) DMFAs with errors below 3% and (bottom) DMFAs with errors above 3%.

4.6 Interelectronic distance

In this section we analyze four quantities related to the interelectronic distance: (i) the mean value, $\langle r_{12}\rangle$, (ii) the variance, $\sigma^2 = \langle r_{12}^2\rangle - \langle r_{12}\rangle^2$, (iii) the interelectronic density distribution through radial intracule density profiles, and (iv) the V_{ee}. All these quantities can be calculated from the radial intracule density, eqn (16).

4.6.1 $\langle r_{12}\rangle$ and σ^2. The analysis of the $\langle r_{12}\rangle$ and the σ^2 reveals important aspects of the effects of electron correlation in DMFAs. Usually large $\langle r_{12}\rangle$ values go with smaller V_{ee}, but some exceptions exist.[98] Hence, large (small) $\Delta\langle r_{12}\rangle$ are common in methods that overestimate (underestimate) electron correlation, whereas the variance of the probability distribution measures the spread of the interelectronic distribution. Fig. 7 shows that all DMFAs deviate from the exact $\langle r_{12}\rangle$ as correlation increases. BBC2($\approx$MBB), PNOF3, PNOF6d and PNOF6h overestimate correlation effects, whereas CA, CGA, GU, ML, MLSIC, POWER, PNOF2, PNOF4, PNOF6u and SD underestimate electron correlation at all ω values. This is actually the only test (together with V_{ee}, *vide infra*) where SD performs clearly and systematically worse than the other DMFAs. The error of PNOF4 is small and only due to the choice of phase factors. PNOF6h performs somewhat better than the other two PNOF6 versions.

Fig. 8 plots the difference between the approximate variance, computed from DMFAs, and the exact one against ω^{-2}.

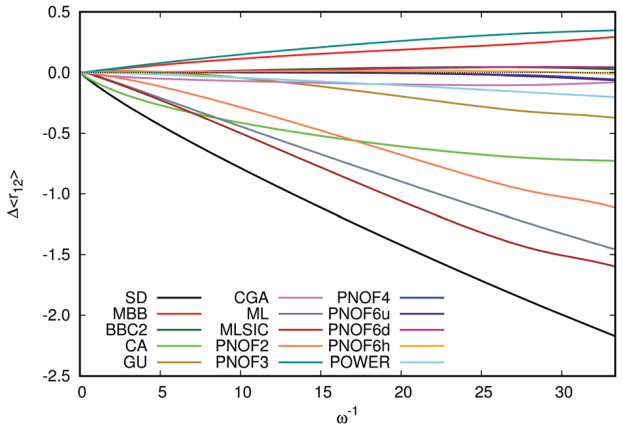

Fig. 7 Error in $\langle r_{12}\rangle$ against ω^{-1}.

Only PNOF4 and PNOF6 show a good agreement with both the exact $\langle r_{12}\rangle$ and σ^2. Interestingly, all DMFAs either underestimate or overestimate the distribution spread around the average value, the SD approximation showing the largest overestimation and MBB presenting the sharpest distribution among all DMFAs.

4.6.2 Radial intracule density. In Fig. 9 we have plotted the difference between the DMFA and the exact radial intracule density for three values of the ω parameter which cover low- (ω = 1000), medium- (ω = 0.5) and high-correlation (ω = 0.03) regimes. These profiles allow a range-separation analysis of electron correlation, the typical profile of the method that lacks electron correlation being negative at short distances and positive at large distances.[99] The negative and the positive regions compensate for all DMFAs that satisfy the sum rule. For ω = 1000 we observe that all DMFAs produce exact results except CA, CGA, ML, MLSIC and SD. One should keep in mind that there is residual correlation even at the limit of large ω,[48,78] however, thus far this is the only analyzed property that some DMFAs fail to reproduce at the weak correlation limit. CA and SD actually coincide because CA recovers the SD expression at this limit. At the medium-correlation regime, no functional is exact except PNOF4 and PNOF6, whereas at the high-correlation regime even PNOF4 and PNOF6 show some deviations. PNOF4 presents the smallest error while PNOF6h shows the best performance among PNOF6 versions. GU, ML, MLSIC, PNOF3 and SD exhibit larger negative values at short and medium ranges that are not compensated by positive ones at larger separations because these functionals do not satisfy the sum rule.

We may classify the functionals according to their profile. The only functionals that are not included in this classification are PNOF4 and PNOF6, which show the smallest errors, and MLSIC which presents the largest errors. In Fig. 9, for the medium-correlation regime (see the l.h.s. ω = 0.5 plot), there is a first type of profile including CA, ML, PNOF2 and SD, which consists in the typical profile of methods that underestimate electron correlation. Namely, CA and SD underestimate short-range correlation, whereas ML and PNOF2 underestimate mid-range correlation. These four DMFAs also underestimated importantly the value of $\langle r_{12}\rangle$. The r.h.s. of the ω = 0.5 plot, including BBC2, CGA, GU, MBB, PNOF3 and POWER, shows an unusual intracule density profile with overestimation of short-range correlation and underestimation of mid- and long-range correlation. The latter group of functionals actually provided quite accurate $\langle r_{12}\rangle$ for small and medium-correlation regimes and, at high correlation, either overestimated $\langle r_{12}\rangle$ or presented values that are not much smaller than the exact one (see Fig. 7). The profile of the intracule density at ω = 0.03 can be also used to classify the functionals. We first find a group of DMFAs (including BBC2, CA, CGA, MBB and POWER), which presents two maxima: one at short-range and the other at long-range (see ω = 0.03 r.h.s plot in Fig. 9). A second group of DMFAs includes GU and PNOF3 that underestimate the interelectronic separation at all ranges except at very short range (see also ω = 0.03 r.h.s plot in Fig. 9). The last group of DMFAs (ML, MLSIC, PNOF2 and SD) show large underestimation of short- and medium-range correlation (see ω = 0.03 l.h.s plot in Fig. 9).

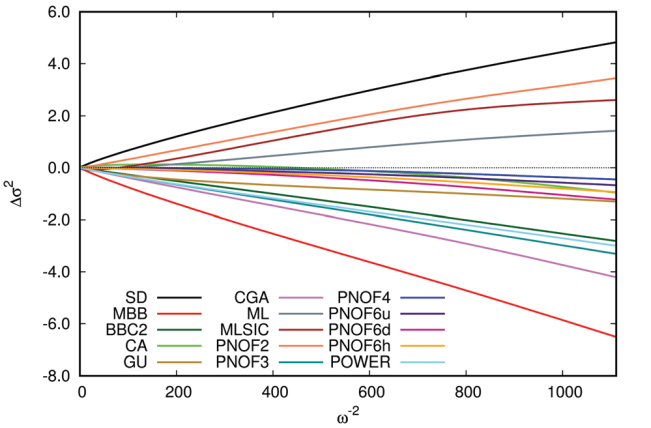

Fig. 8 Error in σ^2 against ω^{-2}.

Although most DMFAs show similar profiles at different electron correlation regimes, the values of r_{12} at which they underestimate/overestimate the interelectronic separation changes with ω. Hence, if one would use these functionals (at least those that preserve the profile with electron correlation) in a range-separation scheme[100,101] the attenuating parameter[102] should depend on ω.[103,104] An inspection of the intersection values at different ω puts forward that $\Delta I(r_{12})$ = 0 occurs at values of r_{12} that change with $\omega^{-1/2}$. Taking the latter point as the point at which short- and long-range separation functions coincide would ensure that errors are kept at different correlation regimes. If we choose the error function, erf(μr_{12}), as the range-separation function it is easy to prove that the attenuating parameter, μ, should be proportional to $\omega^{1/2}$, in line with the well-known fact that the attenuating parameter should change with electron correlation.[103–106]

The radial intracule density of harmonium atom at ω = 0.03 presents negative probabilities in the short-range region (Fig. S2 in the ESI‡). Hence, we are prompted to attribute the overestimation of short-range correlation at the high-correlation regime in a number of DMFAs (BBC2, CA, CGA, GU, MBB, PNOF3, PNOF6 and POWER) to the unphysical behavior of the associated pair density, which can be traced back to the violation of the P condition. The only functional that actually shows overestimation of short-range correlation at ω = 0.03 and it is not due to negative radial intracule density values is PNOF4. Despite their negative radial intracule density values, the $\langle r_{12}\rangle$ values computed with BBC2, CA, CGA, GU, MBB, POWER, PNOF3 and PNOF6 functionals are not among the worst ones.

4.6.3 Electron repulsion energy. Thus far, all the tests considered in this work did not measure the ability of DMFAs to reproduce the electronic energy. In this section, we analyze the performance of the DMFAs in reproducing the V_{ee}, the only fraction of the energy that is actually approximated in DMFT. See previous publications of our group for a similar analysis of DMFAs in other systems.[23,27]

Fig. 10 shows the relative error in the V_{ee} against $\omega^{-1/2}$. We have not included the POWER functional because it was

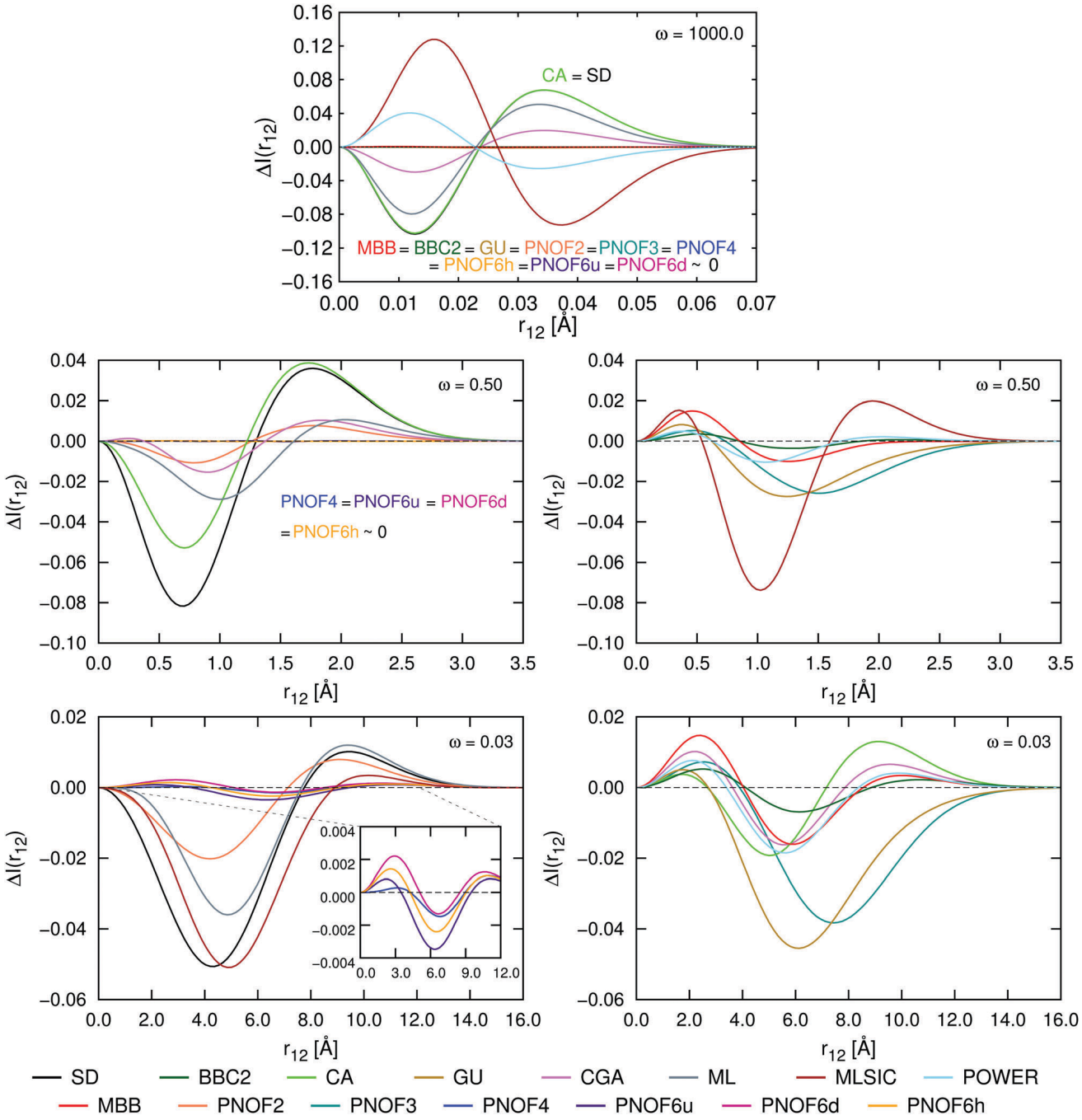

Fig. 9 Difference between the exact and the approximate radial intracule density (eqn (16)) for three values of ω (1000, 0.5 and 0.03).

optimized to reproduce the exact V_{ee}, yielding errors below 10^{-5} a.u. (see the ESI‡ for further details). CA, GU, ML, PNOF2, PNOF4, PNOF6u and PNOF6h underestimate correlation energy, whereas BBC2, CGA, MBB, MLSIC and PNOF6d overestimate it. SD performs very poorly with a relative correlation error that grows linearly with $\omega^{-1/2}$. Interestingly, despite the wrong behavior found in the previous tests, all other DMFAs perform better. Namely, BBC2, CA, CGA, PNOF4 and PNOF6 present errors below 10%. PNOF4 is virtually exact for all values of ω, whereas PNOF6h and PNOF6d provide very accurate estimates and only show some minor deviations at the high-correlation regime. This fact puts forward the need for tests not based in the energy to reveal some inherent important problems in DMFAs.

5 Discussion and conclusions

Despite its simplicity, the two-electron harmonium atom has proven an excellent model for benchmarking.[64,107] Even though two-electron systems should not pose a great challenge for DMFAs, the present paper has unveiled many problems and

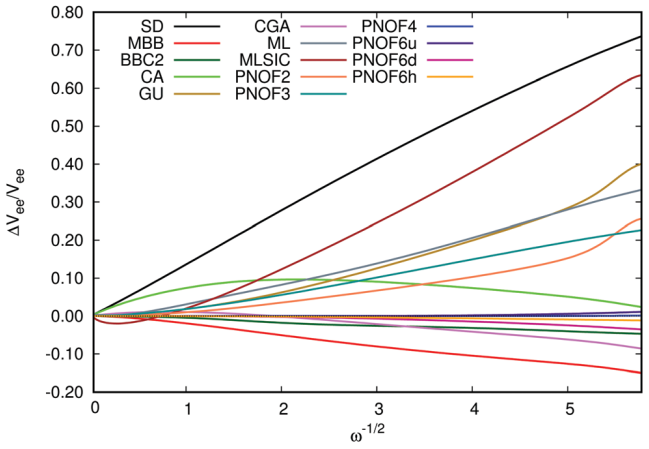

Fig. 10 Relative error in V_{ee} against $\omega^{-1/2}$.

strengths of current approximations. In the following we summarize these results and put forward various suggestions for the development of DMFAs.

The study of the diagonal and the antisymmetry of the 2-DM reveals the limited accuracy of *K*-functionals. The only *K*-functional that can satisfy the antisymmetry requirements of the 2-DM is the SD approximation, which, actually, performs better than (or equal to) any other *K*-functional in the calculation of the trace and the assessment of the CAE diagonal elements. These results evince that the construction of a DMFA needs to consider, at least, both *J* and *K* terms.

Results obtained with ML and MLSIC functionals, which present errors oscillating with the confinement strength in many tests, suggest caution in using fitted parameters for the construction of DMFAs.

The DI test warns against the use of the SD approximation in strongly correlated systems. The widely used MBB approximation remains a good approximation in any correlation regime[57] but we suggest the usage of PNOF6h or PNOF7 as they provide more accurate results. However, the performance of DMFAs in the DI for molecules is an open question that needs to be addressed.

As expected, the results of PNOF4 (equivalent to PNOF5, PNOF7 and FP) are significantly better than those obtained with other DMFAs with the only exception of PNOF6. PNOF4 test results reveal that the phase dilemma[36] reminds an open problem, which affects the energy in a lesser extent than other properties. Namely, at the high-correlation regime, non-negligible errors arise in the off-diagonal elements of the 2-DM that result in inaccurate DI, interelectronic distances, variances, and radial intracule densities.

The study of radial intracule densities unveils that many DMFAs present negative probabilities at short interelectronic distances, in connection with the violation of the *P* condition. On the other hand, numerical inspection indicates that most DMFAs present $\Delta I(r_{12}) = 0$ for r_{12} values that are proportional to $\omega^{-1/2}$. In this sense, it seems natural to choose the latter point as the crossing point between the attenuating functions that separate short- and long-range regions in range-separated functionals. Assuming that the attenuating functions are error functions depending on an attenuating parameter,[100,101] μ, it is easy to show that μ should be proportional to $\omega^{1/2}$. This fact can be exploited in the construction of new range-separation methods.

Let us notice that many functionals performed reasonably well in the calculation of the exact electronic energy but produce important errors in the calculation of other properties, supporting the claim that functional development should consider other properties besides the electronic energy.[30,31] In the calibration of DMFAs one can use properties such as the intracule pair density, which are particularly challenging for DMFAs, or other properties, such as the expected value of the interelectronic separation and its variance, which are convenient because they are easy to compute.

Finally, we can draw the conclusion that a DMFA should attain as many *N*-representable properties as possible because the best-performing functionals are those that satisfy most of these conditions. Some of these *N*-representable conditions can be imposed in the construction of the functional.

The results of this work suggest the construction of a DMFA following some simple and somewhat expected rules: (i) consider both *J* and *K* energy components beyond the single-determinant approximation, (ii) impose the known *N*-representability conditions, (iii) refrain from using empirical parameterization; and calibrate the functionals using (iv) the energy and other properties, (v) a model with tunable electron correlation to consider various correlation regimes.

In the present study we have suggested a battery of ten tests to analyze DMFAs, including several properties that the exact functional should satisfy. The tests are performed on a two-electron model system with varying electron correlation and carrying a very small computational effort. The test can be easily extended to a larger number of electrons, thus setting new challenges for DMFAs. We are confident that DMFA developers will benefit from the results obtained in this paper and will use this test set as a means to construct more robust approximations.

Conflicts of interest

There are no conflicts to declare.

Appendix I: *N*-representability conditions

The analysis of *P*, *Q* and *G* *N*-representability conditions, involves the diagonalization of the *P*, *Q* and *G* matrices (eqn (13)–(15)) for each spin case ($\alpha\alpha$, $\beta\beta$, $\alpha\beta$ and $\beta\alpha$). Some of these matrices render themselves to an analytic diagonalization, producing eigenvalues that can be used to constrain the 2-DM elements that enter DMFAs; other matrices cannot be diagonalized and they only impose conditions that can be checked *a posteriori*. In this section we present the eigenvalues

and the constraints associated to the P, Q and G conditions produced by K-functionals and PNOFs.

K-Functionals

These DMFAs assume that the opposite-spin cumulant terms are zero. Hence, the eigenvalues associated to the opposite-spin P, Q and G matrices are identical for all methods:

- P-condition (opposite-spin):

$$\bar{P}_{ij}^{\sigma\sigma'} = n_i^{\sigma} n_j^{\sigma'} \geq 0 \tag{23}$$

- G-condition (opposite-spin):

$$\bar{G}_{ij}^{\sigma\sigma'} = n_i^{\sigma}\left(1 - n_j^{\sigma'}\right) \geq 0 \tag{24}$$

- Q-condition (opposite-spin):

$$\bar{Q}_{ij}^{\sigma\sigma'} = \left(1 - n_i^{\sigma}\right)\left(1 - n_j^{\sigma'}\right) \geq 0 \tag{25}$$

These eigenvalues are necessarily non-negative and, therefore, the opposite-spin matrices do not impose additional constraints in these functionals. Conversely, the same-spin matrices depend on the definition of $f(n_i,n_j)$ and thus produce *ad hoc* eigenvalues. These eigenvalues are collected in the following matrices:

- P-condition (same-spin):

$$\bar{P}_{ij}^{\sigma\sigma} = \begin{cases} n_i^2 - f(n_i,n_i) & \text{if } i = j \\ n_i n_j + f(n_i,n_j) & \text{if } i < j \\ n_i n_j - f(n_j,n_i) & \text{if } i > j \end{cases} \tag{26}$$

- Q-condition (same-spin):

$$\bar{Q}_{ij}^{\sigma\sigma} = \begin{cases} n_i^2 - f(n_i,n_i) & \text{if } i = j \\ n_i n_j - f(n_i,n_j) & \text{if } i < j \\ 2\left(1 - n_i - n_j\right) + n_i n_j + f(n_i,n_j) & \text{if } i > j \end{cases} \tag{27}$$

- G-condition (same-spin):

$$\bar{G}_{ij}^{\sigma\sigma} = \begin{cases} \bar{\gamma}_i & \text{if } i = j \\ n_i - f(n_i,n_j) & \text{if } i < j \\ n_j - f(n_i,n_j) & \text{if } i > j \end{cases} \tag{28}$$

where $\bar{\gamma}_i$ are the (basis-set dependent) eigenvalues of the following matrix:

$$\gamma_{ij} = \begin{cases} n_i(n_i + 1) - f(n_i,n_i) & \text{if } i = j \\ n_i n_j & \text{if } i \neq j \end{cases} \tag{29}$$

where we have assumed that all occupancies n_i refer to σ-spin natural orbitals (*i.e.*, $n_i \equiv n_i^{\sigma}$). The latter matrices dimension is M, the size of the basis set. In the case of P and Q conditions, K-functionals produce two sets (one for each spin case: $\alpha\alpha$ and $\beta\beta$) of M^2 basis-set-independent eigenvalues, giving rise to some conditions that one can impose in the corresponding functional. The G condition, on the other hand, produces $M(M-1)$ basis-set independent eigenvalues (and some corresponding conditions on $f(n_i,n_j)$) and M basis-set-dependent eigenvalues that can only be checked *a posteriori*.

PNOF

In the case of PNOF, the matrices to diagonalize are given in terms of Δ and Π. The conditions will involve like- and opposite-spin components of the 2-DM because, unlike K-functionals, PNOFs construct all the spin-components of the cumulant. We collect below the eigenvalues of these matrices:

- P-condition (same-spin):

$$\bar{P}_{ij}^{\sigma\sigma} = \begin{cases} 2\left(n_i n_j - \Delta_{ij}\right) & \text{if } i > j \\ 0 & \text{if } i \leq j \end{cases} \tag{30}$$

- Q-condition (same-spin):

$$\bar{Q}_{ij}^{\sigma\sigma} = \begin{cases} 2\left(h_i h_j - \Delta_{ij}\right) & \text{if } i > j \\ 0 & \text{if } i \leq j \end{cases} \tag{31}$$

- G-condition (same-spin):

$$\bar{G}_{ij}^{\sigma\sigma} = \begin{cases} n_i h_j + \Delta_{ij} & \text{if } i \neq j \\ \bar{\gamma}_i & \text{if } i = j \end{cases} \tag{32}$$

where $h_i = (1 - n_i)$ and $\bar{\gamma}_i$ are the (basis-set dependent) eigenvalues of the following matrix:

$$\gamma_{ij} = \begin{cases} n_i & \text{if } i = j \\ n_i n_j - \Delta_{ij} & \text{if } i \neq j \end{cases} \tag{33}$$

where $n_i = n_i^{\sigma}$ for eqn (30)–(33).

The opposite-spin components of P, Q and G matrices produce the following eigenvalues:

- P-condition (opposite-spin):

$$\bar{P}_{ij}^{\sigma\sigma'} = \begin{cases} n_i n_j - \Delta_{ij} & \text{if } i \neq j \\ \bar{\gamma}_i & \text{if } i = j \end{cases} \tag{34}$$

where $\bar{\gamma}_i$ are the (basis-set dependent) eigenvalues of the following matrix:

$$\gamma_{ij} = \begin{cases} n_i & \text{if } i = j \\ \Pi_{ij} & \text{if } i \neq j \end{cases} \tag{35}$$

- Q-condition (opposite-spin):

$$\bar{Q}_{ij}^{\sigma\sigma'} = \begin{cases} h_i h_j - \Delta_{ij} & \text{if } i \neq j \\ \bar{\gamma}_i & \text{if } i = j \end{cases} \tag{36}$$

$\bar{\gamma}_i$ are the (basis-set dependent) eigenvalues of the following matrix:

$$\gamma_{ij} = \begin{cases} h_i & \text{if } i = j \\ \Pi_{ij} & \text{if } i \neq j \end{cases} \tag{37}$$

- *G*-condition (opposite-spin):

$$\bar{G}_{ij}^{\sigma\sigma'} = \begin{cases} \dfrac{n_i h_j + \Delta_{ij} + \Delta_{ji} + n_j h_i + \sqrt{\left(n_i h_j - n_j h_i\right)^2 + 4\Pi_{ij}^2}}{2} & \text{if } i < j \\ \dfrac{n_i h_j + \Delta_{ij} + \Delta_{ji} + n_j h_i - \sqrt{\left(n_i h_j - n_j h_i\right)^2 + 4\Pi_{ij}^2}}{2} & \text{if } i > j \\ n_i & \text{if } i = j \end{cases} \quad (38)$$

where $n_i = n_i^\sigma$ for eqn (34)–(38), which are only valid for a closed-shell restricted system.

Acknowledgements

This research has been funded by Spanish MINECO/FEDER Projects CTQ2014-52525-P and CTQ2015-67608-P, and the Basque Country Consolidated Group Project No. IT588-13. M. R. M. wants to acknowledge the Spanish Ministry of Education, Culture and Sports for the doctoral grant FPU-2013/00176. M. V. N. wants to acknowledge the Spanish Ministry of Economy, Industry and Competitiveness for the doctoral grant BES-2015-072734.

References

1 T. Gilbert, *Phys. Rev. B: Solid State*, 1975, **12**, 2111.
2 M. Piris and J. Ugalde, *Int. J. Quantum Chem.*, 2014, **114**, 1169–1175.
3 K. Pernal and K. J. H. Giesbertz, *Top. Curr. Chem.*, 2015, **368**, 125.
4 A. M. K. Müller, *Phys. Lett.*, 1984, **105A**, 446–452.
5 M. A. Buijse, PhD thesis, Vrije Universiteit, Amsterdam, The Netherlands, 1991.
6 S. Goedecker and C. J. Umrigar, *Phys. Rev. Lett.*, 1998, **81**, 866–869.
7 G. Csányi and T. A. Arias, *Phys. Rev. B: Condens. Matter Mater. Phys.*, 2000, **61**, 7348.
8 M. A. Buijse and E. J. Baerends, *Mol. Phys.*, 2002, **100**, 401–421.
9 G. Csányi, S. Goedecker and T. A. Arias, *Phys. Rev. A: At., Mol., Opt. Phys.*, 2002, **65**, 032510.
10 O. Gritsenko, K. Pernal and E. J. Baerends, *J. Chem. Phys.*, 2005, **122**, 204102.
11 M. Piris, *Int. J. Quantum Chem.*, 2006, **106**, 1093–1104.
12 M. Piris, X. Lopez and J. M. Ugalde, *J. Chem. Phys.*, 2007, **126**, 214103.
13 M. A. L. Marques and N. N. Lathiotakis, *Phys. Rev. A: At., Mol., Opt. Phys.*, 2008, **77**, 032509.
14 D. R. Rohr, K. Pernal, O. V. Gritsenko and E. J. Baerends, *J. Chem. Phys.*, 2008, **129**, 164105.
15 J. Cioslowski and K. Pernal, *J. Chem. Phys.*, 1999, **111**, 3396–3400.
16 J. Cioslowski and K. Pernal, *Phys. Rev. A: At., Mol., Opt. Phys.*, 2000, **61**, 034503.
17 S. Sharma, J. K. Dewhurst, N. N. Lathiotakis and E. K. Gross, *Phys. Rev. B: Condens. Matter Mater. Phys.*, 2008, **78**, 201103.
18 M. Piris, J. M. Matxain, X. Lopez and J. M. Ugalde, *J. Chem. Phys.*, 2010, **132**, 031103.
19 M. Piris, J. M. Matxain, X. Lopez and J. M. Ugalde, *J. Chem. Phys.*, 2010, **133**, 111101.
20 M. Piris, X. Lopez, F. Ruipérez, J. M. Matxain and J. M. Ugalde, *J. Chem. Phys.*, 2011, **134**, 164102.
21 M. Piris, *J. Chem. Phys.*, 2014, **141**, 044107.
22 M. Piris, *Phys. Rev. Lett.*, 2017, **119**, 063002.
23 J. Cioslowski, M. Piris and E. Matito, *J. Chem. Phys.*, 2015, **143**, 214101.
24 F. Ruipérez, M. Piris, J. Ugalde and J. Matxain, *Phys. Chem. Chem. Phys.*, 2013, **15**, 2055–2062.
25 X. Lopez, F. Ruipérez, M. Piris, J. M. Matxain, E. Matito and J. M. Ugalde, *J. Chem. Theory Comput.*, 2012, **8**, 2646–2652.
26 X. Lopez, M. Piris, M. Nakano and B. Champagne, *J. Phys. B: At., Mol. Opt. Phys.*, 2013, **47**, 015101.
27 E. Ramos-Cordoba, X. Lopez, M. Piris and E. Matito, *J. Chem. Phys.*, 2015, **143**, 164112.
28 E. Ramos-Cordoba, P. Salvador and E. Matito, *Phys. Chem. Chem. Phys.*, 2016, **18**, 24015–24023.
29 E. Ramos-Cordoba and E. Matito, *J. Chem. Theory Comput.*, 2017, **13**, 2705.
30 M. G. Medvedev, I. S. Bushmarinov, J. Sun, J. P. Perdew and K. A. Lyssenko, *Science*, 2017, **355**, 49–52.
31 E. Ramos-Cordoba, P. Salvador, M. Piris and E. Matito, *J. Chem. Phys.*, 2014, **141**, 234101.
32 E. Ramos-Cordoba, E. Matito, I. Mayer and P. Salvador, *J. Chem. Theory Comput.*, 2012, **8**, 1270–1279.
33 N. R. Kestner and O. Sinanoglu, *Phys. Rev.*, 1962, **128**, 2687.
34 E. Matito, D. Casanova, X. Lopez and J. M. Ugalde, *Theor. Chim. Acta*, 2016, **135**, 226.
35 P.-O. Löwdin and H. Shull, *Phys. Rev.*, 1956, **101**, 1730–1739.
36 K. Pernal and J. Cioslowski, *J. Chem. Phys.*, 2004, **120**, 5987–5992.
37 J. Cioslowski and K. Pernal, *Chem. Phys. Lett.*, 2006, **430**, 188–190.
38 K. J. H. Giesbertz and R. van Leeuwen, *J. Chem. Phys.*, 2013, **139**, 104110.
39 X. W. Sheng, Ł. M. Mentel, O. V. Gritsenko and E. J. Baerends, *J. Chem. Phys.*, 2013, **138**, 164105.
40 P.-O. Löwdin, *Phys. Rev.*, 1955, **97**, 1474–1489.
41 R. McWeeny, *Rev. Mod. Phys.*, 1960, **32**, 335–369.
42 A. J. Coleman and V. I. Yukalov, *Reduced density matrices: Coulson's challenge*, Springer Verlag, Berlin, 2000, vol. 72.
43 M. Piris, *J. Math. Chem.*, 1999, **25**, 47–54.
44 J. M. Herbert and J. E. Harriman, *J. Chem. Phys.*, 2003, **118**, 10835–10846.
45 W. Kutzelnigg and D. Mukherjee, *J. Chem. Phys.*, 1999, **110**, 2800–2809.
46 M. Piris, J. Matxain and X. Lopez, *J. Chem. Phys.*, 2013, **139**, 234109.
47 M. Piris and N. H. March, *J. Phys. Chem. A*, 2015, **119**, 10190–10194.
48 J. Cioslowski and K. Pernal, *J. Chem. Phys.*, 2000, **113**, 8434.
49 M. Piris, *Int. J. Quantum Chem.*, 2013, **113**, 620–630.
50 D. A. Mazziotti, *Phys. Rev. Lett.*, 2012, **108**, 263002.

51 A. J. Coleman, *Rev. Mod. Phys.*, 1963, **35**, 668–687.
52 C. Garrod and J. K. Percus, *J. Math. Phys.*, 1964, **5**, 1756–1776.
53 F. Weinhold and E. B. Wilson Jr, *J. Chem. Phys.*, 1967, **47**, 2298–2311.
54 A. S. Eddington, *Fundamental theory*, Cambridge University Press, Cambridge, 1946.
55 R. F. W. Bader and M. E. Stephens, *Chem. Phys. Lett.*, 1974, **26**, 445.
56 X. Fradera, M. A. Austen and R. F. W. Bader, *J. Phys. Chem. A*, 1999, **103**, 304–314.
57 E. Matito, M. Solà, P. Salvador and M. Duran, *Faraday Discuss.*, 2007, **135**, 325–345.
58 F. Feixas, E. Matito, M. Duran, M. Solà and B. Silvi, *J. Chem. Theory Comput.*, 2010, **6**, 2736–2742.
59 F. Feixas, J. Vandenbussche, P. Bultinck, E. Matito and M. Solà, *Phys. Chem. Chem. Phys.*, 2011, **13**, 20690–20703.
60 M. García-Revilla, E. Francisco, A. Costales and A. M. Pendás, *J. Phys. Chem. A*, 2012, **116**, 1237–1250.
61 F. Feixas, M. Solà, J. M. Barroso, J. M. Ugalde and E. Matito, *J. Chem. Theory Comput.*, 2014, **10**, 3055–3065.
62 F. Feixas, M. Rodrguez-Mayorga, E. Matito and M. Solà, *Comput. Theor. Chem.*, 2015, **1053**, 173–179.
63 M. Rodríguez-Mayorga, E. Ramos-Cordoba, P. Salvador, M. Solà and E. Matito, *Mol. Phys.*, 2016, **114**, 1345.
64 M. Rodríguez-Mayorga, E. Ramos-Cordoba, F. Feixas and E. Matito, *Phys. Chem. Chem. Phys.*, 2017, **19**, 4522.
65 E. Santos, *An. R. Soc. Esp. Fis. Quim.*, 1968, **64**, 117.
66 M. Taut, *Phys. Rev. A: At., Mol., Opt. Phys.*, 1993, **48**, 3561.
67 P. Hessler, J. Park and K. Burke, *Phys. Rev. Lett.*, 1999, **82**, 378.
68 P. M. Laufer and J. B. Krieger, *Phys. Rev. A: At., Mol., Opt. Phys.*, 1986, **33**, 1480–1491.
69 S. Kais, D. R. Hersbach, N. C. Handy, C. W. Murray and G. J. Laming, *J. Chem. Phys.*, 1993, **99**, 417.
70 C. Filippi, C. J. Umrigar and M. Taut, *J. Chem. Phys.*, 1994, **100**, 1290.
71 C.-J. Huang and C. J. Umrigar, *Phys. Rev. A: At., Mol., Opt. Phys.*, 1997, **56**, 290.
72 M. Taut, A. Ernst and H. Eschrig, *J. Phys. B: At., Mol. Opt. Phys.*, 1998, **31**, 2689.
73 Z. Qian and V. Sahni, *Phys. Rev. A: At., Mol., Opt. Phys.*, 1998, **57**, 2527.
74 S. Ivanov, K. Burke and M. Levy, *J. Chem. Phys.*, 1999, **110**, 10262.
75 E. V. Ludeña, V. Karasiev, A. Artemiev and D. Gómez, in *Functional N-representability in density Matrix and Density Functional Theory: An illustration for Hooke's Atom*, ed. J. Cioslowski, Kluwer Academic/Plenum Publishers, New York, 2000, ch. 10.
76 W. M. Zhu and S. B. Trickey, *J. Chem. Phys.*, 2006, **125**, 094317.
77 J. Cioslowski and E. Matito, *J. Chem. Theory Comput.*, 2011, **7**, 915.
78 J. Cioslowski and E. Matito, *J. Chem. Phys.*, 2011, **134**, 116101.
79 J. Cioslowski, K. Strasburger and E. Matito, *J. Chem. Phys.*, 2012, **136**, 194112.
80 J. Cioslowski, K. Strasburger and E. Matito, *J. Chem. Phys.*, 2014, **141**, 044128.
81 I. Mitxelena, M. Piris and M. Rodríguez-Mayorga, *J. Phys.: Condens. Matter*, 2017, in press, http://iopscience.iop.org/article/10.1088/1361-648X/aa80ca.
82 P.-F. Loos and P. M. Gill, *Phys. Rev. Lett.*, 2009, **103**, 123008.
83 P.-F. Loos and P. M. Gill, *Chem. Phys. Lett.*, 2010, **500**, 1.
84 P.-F. Loos and P. M. Gill, *Phys. Rev. Lett.*, 2012, **108**, 083002.
85 P.-F. Loos and P. M. Gill, *J. Chem. Phys.*, 2013, **138**, 164124.
86 E. Matito, J. Cioslowski and S. F. Vyboishchikov, *Phys. Chem. Chem. Phys.*, 2010, **12**, 6712.
87 P. J. Knowles and N. C. Handy, *Chem. Phys. Lett.*, 1984, **111**, 315–321.
88 P. J. Knowles and N. C. Handy, *Comput. Phys. Commun.*, 1989, **54**, 75.
89 E. Matito and F. Feixas, *DMn program*, University of Girona (Spain) and University of Szczecin (Poland), 2009.
90 M. Rodríguez-Mayorga, *RHO2-OPS: 2-DM Operations*, Institute of Computational Chemistry and Catalysis, University of Girona, Catalonia, Spain, 2016.
91 J. Cioslowski and G. Liu, *J. Chem. Phys.*, 1996, **105**, 4151–4158.
92 M. Rodríguez-Mayorga, *RHO-OPS: Density Operations*, Institute of Computational Chemistry and Catalysis, University of Girona, Catalonia, Spain, 2015.
93 E. Matito, *ESI-3D: Electron Sharing Indices Program for 3D Molecular Space Partitioning*, Institute of Computational Chemistry and Catalysis, University of Girona, Catalonia, Spain, 2015.
94 E. Matito, M. Duran and M. Solà, *J. Chem. Phys.*, 2005, **122**, 014109.
95 Y. G. Wang, C. Matta and N. H. Werstiuk, *J. Comput. Chem.*, 2003, **24**, 1720–1729.
96 F. Feixas, J. Jiménez-Halla, E. Matito, J. Poater and M. Solà, *J. Chem. Theory Comput.*, 2010, **6**, 1118–1130.
97 I. Ruiz, E. Matito, F. J. Holgun-Gallego, E. Francisco, Á. M. Pendás and T. Rocha-Rinza, *Theor. Chem. Acc.*, 2016, **135**, 209.
98 J. M. Mercero, M. Rodríguez-Mayorga, E. Matito, X. Lopez and J. M. Ugalde, *Can. J. Chem.*, 2017, **94**, 998–1001.
99 C. A. Coulson and A. H. Neilson, *Proc. Phys. Soc., London*, 1961, **78**, 831.
100 A. Savin, *Int. J. Quantum Chem.*, 1988, **34**, 59–69.
101 A. Savin, *Density functional methods in chemistry*, Springer, 1991, pp. 213–230.
102 P. M. Gill, R. D. Adamson and J. A. Pople, *Mol. Phys.*, 1996, **88**, 1005–1009.
103 T. M. Henderson, A. F. Izmaylov, G. E. Scuseria and A. Savin, *J. Chem. Theory Comput.*, 2008, **4**, 1254–1262.
104 B. G. Janesko, T. M. Henderson and G. E. Scuseria, *Phys. Chem. Chem. Phys.*, 2009, **11**, 443–454.
105 J. Jaramillo, G. E. Scuseria and M. Ernzerhof, *J. Chem. Phys.*, 2003, **118**, 1068–1073.
106 T. M. Henderson, A. F. Izmaylov, G. E. Scuseria and A. Savin, *J. Chem. Phys.*, 2007, **127**, 221103.
107 M. Rodriguez-Mayorga, MSc thesis, Univ. Girona, Girona, 2013.

Supplementary Information

Comprehensive Benchmarking for Density Matrix Functional Approximations

M. Rodríguez-Mayorga,[†,‡] Eloy Ramos-Cordoba,[†,¶] M. Via-Nadal,[†] M. Piris,[†,§] and Eduard Matito[*,†,§]

†*Kimika Fakultatea, Euskal Herriko Unibertsitatea, UPV/EHU, and Donostia International Physics Center (DIPC). P.K. 1072, 20080 Donostia, Euskadi, Spain*

‡*Institut de Química Computacional i Catàlisi (IQCC) and Departament de Química, University of Girona, 17071 Girona, Catalonia, Spain*

¶*Currently at Kenneth S. Pitzer Center for Theoretical Chemistry, University of California, Berkeley*

§*IKERBASQUE, Basque Foundation for Science, 48011 Bilbao, Spain.*

E-mail: ematito@gmail.com

1 $\alpha(\omega)$ optimization for the POWER[1–3] Functional

The best $\alpha(\omega)$ parameters were obtained by taking the two-electron integrals in the basis of natural orbitals and first scanning the interval $0 \leq \alpha \leq 1$. Then selecting the best alpha iteratively reducing the size of the interval until the error was $\leq 10^{-5}$. The exact V_{ee}, the best α and the errors are collected in Table 1.

Table 1: $\alpha(\omega)$ values which minimize the difference $V_{ee}^{POWER} - V_{ee}$

ω	V_{ee} (a.u.)	α
0.03	0.07564	0.540430
0.033	0.08052	0.539340
0.036	0.08524	0.538200
0.0365373	0.08607	0.538020
0.04	0.09132	0.537110
0.05	0.10563	0.536140
0.06	0.11891	0.536110
0.08	0.14319	0.535190
0.10	0.16523	0.534120
0.15	0.21376	0.531544
0.20	0.25600	0.529410
0.30	0.32880	0.526060
0.40	0.39157	0.523610
0.50	0.44762	0.521657
1.00	0.67184	0.516090
2.00	0.99493	0.511085
5.00	1.64342	0.506484
10.0	2.37889	0.502882
100.0	7.82805	0.493154
1000.0	25.0768	0.474605

2 Exact DI

The exact value of the DI between regions A and B is plotted in Figure 1. The decay of the DI with $\omega^{-1/2}$ is due to two effects: the less compact electronic density which is produced by the weakening of the harmonic confinement and the enhanced role of the electron-electron repulsion.

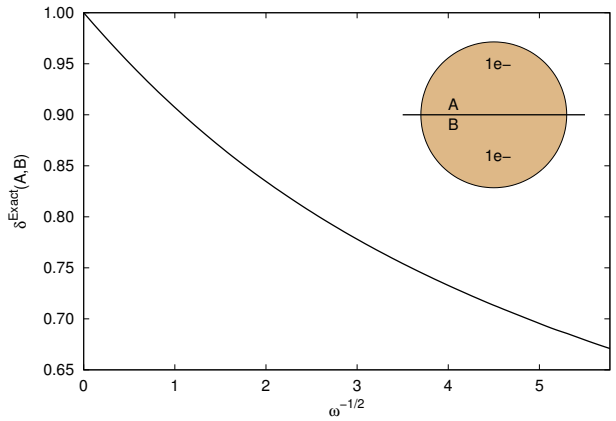

Figure 1: Exact delocalization index between regions A and B against $\omega^{-1/2}$.

3 Short-range radial intracule density for $\omega = 0.03$

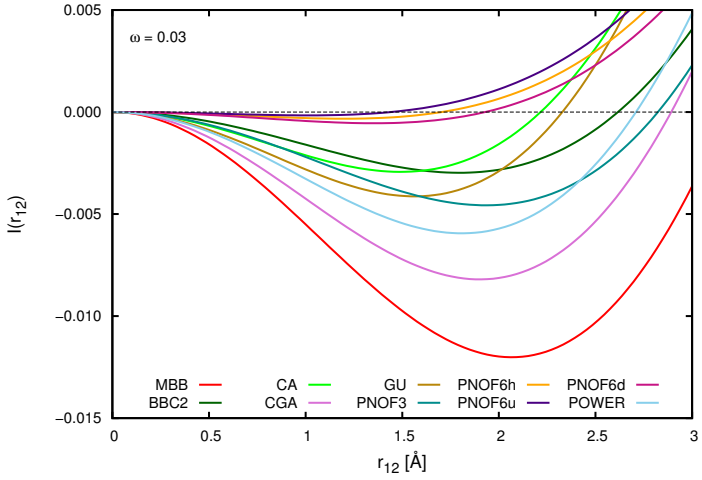

Figure 2: Radial intracule density (Eq. 16 in the text) against r_{12} for $\omega = 0.03$. ML, MLSIC, PNOF2, PNOF4 and SD have been not been included because they do not present negative radial intracule density values.

Where MBB, BBC2, CA, CGA, GU, PNOF3, PNOF6 and the POWER functionals produce negative radial intracule densities for small r_{12} values.

References

(1) Cioslowski, J.; Pernal, K. Constraints upon natural spin orbital functionals imposed by properties of a homogeneous electron gas. *J. Chem. Phys.* **1999**, *111*, 3396–3400.

(2) Cioslowski, J.; Pernal, K. Description of a homogeneous electron gas with simple functionals of the one-particle density matrix. *Phys. Rev. A* **2000**, *61*, 034503.

(3) Sharma, S.; Dewhurst, J. K.; Lathiotakis, N. N.; Gross, E. K. Reduced density matrix functional for many-electron systems. *Phys. Rev. B* **2008**, *78*, 201103.

VI) Characterization of Bonds from Electron-Pair Distributions

6.1) The Electron-Pair Density Distribution of the $^{1,3}\Pi_u$ Excited States of H_2

Mercero J.M., Mayorga-Rodríguez M., Matito E., Lopez X., Ugalde J.; The electron-pair density distribution of the 1,3Πu excited states of H2. *Can. J. Chem*. Vol. 94, issue 12 (December 2016) : 998-1001.

https://doi.org/10.1139/cjc-2016-0203

NRC Research Press

ARTICLE

The electron-pair density distribution of the $^{1,3}\Pi_u$ excited states of H_2

J.M. Mercero, M. Rodríguez-Mayorga, E. Matito, X. Lopez, and J.M. Ugalde

Abstract: The non-monotonic behavior of the electron repulsion energy and the inter-electronic distance, as a function of the internuclear separation, in the $^3\Pi_u$ excited state of the hydrogen molecule has been assessed by explicit calculation and analysis of the electron-pair density distribution functions from high level ab initio full configuration interaction wave functions, for both the $^3\Pi_u$ and the $^1\Pi_u$ states. Additionally, Hund's rule as applied to these two states has been accounted for in terms of simple electronic shielding effects induced by wave function antisymmetrization.

Key words: electron correlation, excited states, electron-pair density, intracular density, Hund's rule.

Résumé : Nous avons évalué le comportement non monotonique de l'énergie de répulsion électronique et de la distance interélectronique comme une fonction de la séparation internucléaire dans l'état excité 3u de la molécule d'hydrogène. Pour ce faire, nous avons effectué le calcul explicite et l'analyse des fonctions de distribution de la densité de sa paire d'électrons à partir des fonctions d'onde à pleine interaction de configuration issues de calculs *ab initio* au niveau élevé pour les états 3u et 1u. De plus, nous avons établi que la règle de Hund appliquée à ces deux états s'explique par de simples effets de blindage électronique induits par l'antisymétrie de la fonction d'onde. [Traduit par la Rédaction]

Mots-clés : corrélation électronique, états excités, densité de paire d'électrons, densité intraculaire, règle de Hund.

Introduction

Electron-pair densities describe the relative motion of any two electrons of a system and were first introduced by Coulson et al. to gain insight into the physical consequences of electron correlation.[1–3] Nowadays, however, interest in electron-pair densities stems from their usage to develop faster and more accurate computational methods within both molecular orbital theory[4] and density functional theory frameworks.[5] Additionally, electron-pair densities have recently been used to unveil the distinctive features of two-electron density in different types of chemical bonds.[6–10]

Electron-pair densities do also reveal, even for electronic ground states,[11–13] a number of features of quantum correlations between electrons that are challenging to predict at first sight because in many cases they are counterintuitive. Excited states, as expected, exhibit such counterintuitive effects more commonly. Thus, the double-well first and second excited states of $^1\Sigma_g^+$ symmetry, known respectively as the EF and GK excited states, of the hydrogen molecule show an intriguing non-monotonic behavior of the mean electron-electron distance with respect to increases in the internuclear distance. Indeed, at sharp variance with the ground state,[14] the mean electron-electron distance decreases as the internuclear distance increases in the transition from the E to the F minima[15] and in the transition from the G to the K minima,[16] respectively.

In this vein, Tal and Katriel[17] and Colbourn[18] reported the (counterintuitive) non-monotonic behavior of the electron repulsion energy in the $^3\Pi_u$ excited state of H_2. Indeed, based on their (crude) Hartree–Fock (HF) calculations, with a small basis set consisting of four uncontracted sp primitives, they found that an increase in the internuclear distance carries an increase of the electron repulsion energy and a concomitant decrease of the mean interelectronic distance, in the domain of the short internuclear distances. This remarkable counterintuitive feature is not seen in the parent, arising from the same $1\sigma^1 1\pi_u^1$ configuration, $^1\Pi_u$ excited state. For this state, the electron repulsion energy decreases monotonically as the internuclear separation increases, in the whole range of internuclear separations, in accordance with common (classical) intuition. One is naturally prone to attribute this unexpected counterintuitive behavior of the triplet state to the expected failure of HF method for states like these, which bear substantial multiconfigurational character, in spite of Tal and Katriel hypothesis: *…the non-monotonic trend is real rather than a Hartree–Fock artifact*.

In this paper, electron-pair densities obtained from high-level ab initio full configuration interaction calculations will be used to examine these issues and to put into proper perspective earlier

Received 4 May 2016. Accepted 2 June 2016.

J.M. Mercero. Kimika Fakultatea, Euskal Herriko Unibertsitatea (UPV/EHU) and Donostia International Physics Center (DIPC), P.K. 1072, 20080 Donostia, Euskadi, Spain; IZO-SGI SGIker Kimika Fakultatea, Euskal Herriko Unibertsitatea (UPV/EHU), P.K. 1072, 20080 Donostia, Euskadi, Spain.
M. Rodríguez-Mayorga. Kimika Fakultatea, Euskal Herriko Unibertsitatea (UPV/EHU) and Donostia International Physics Center (DIPC), P.K. 1072, 20080 Donostia, Euskadi, Spain; Institut de Química Computacional i Catàlisi (IQCC), Departament de Química, Universitat de Girona, Girona, Catalunya, Spain.
E. Matito. Kimika Fakultatea, Euskal Herriko Unibertsitatea (UPV/EHU) and Donostia International Physics Center (DIPC), P.K. 1072, 20080 Donostia, Euskadi, Spain; IKERBASQUE Basque Foundation for Science, 48011 Bilbao, Euskadi, Spain.
X. Lopez and J.M. Ugalde. Kimika Fakultatea, Euskal Herriko Unibertsitatea (UPV/EHU) and Donostia International Physics Center (DIPC), P.K. 1072, 20080 Donostia, Euskadi, Spain.

Corresponding author: J.M. Ugalde (email: jesus.ugalde@ehu.eus).

This paper is part of a Special issue dedicated to Professors Russell Boyd and Arvi Rauk.

Published at www.nrcresearchpress.com/cjc on 10 July 2016.

Fig. 1. Calculated potential energy curves for the $^{1,3}\Pi_u$ excited states of H_2. Energy and internuclear distance, R, in a.u.

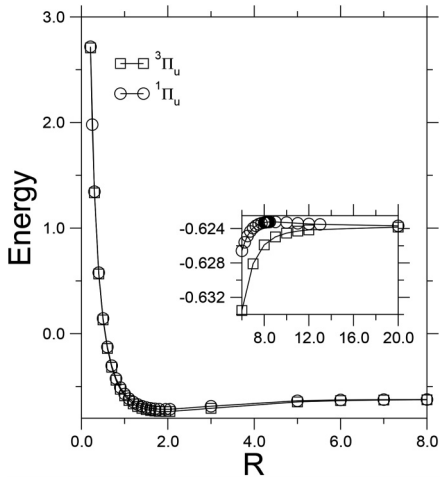

preliminary calculations,[19] demonstrating that the Tal and Katriel hypothesis is true.

Calculations

The radial electron-pair density distribution, $h(u)$, of an electronic state $|\Psi\rangle$ is

$$h(u) = u^2 \int I(\mathbf{u})\, d\Omega_{\mathbf{u}} \quad (1)$$

where $I(u)$, the so-called[20] intracule density

$$I(\mathbf{u}) = \langle\Psi| \sum_{i>j} \delta(\mathbf{u} - \mathbf{r}_i + \mathbf{r}_j)|\Psi\rangle \quad (2)$$

stands for the probability density of the coordinates $\mathbf{r}_i$ and $\mathbf{r}_j$ of any two electrons to be separated by the vector $\mathbf{u}$. $\Omega_{\mathbf{u}}$, in eq. 1, stands for the solid angle subtended by the interelectronic vector $\mathbf{u}$.

Observe that the moments of radial electron-pair density

$$\langle u^n\rangle = \int_0^\infty u^n h(u) du \quad (3)$$

yield various interesting two-electron properties, such as the electron repulsion for $n = -1$, the number of electron pairs, $n = 0$, and the mean interelectronic distance for $n = 1$. Additionally, it is worth noting that the intracule density can be inferred from accurate total X-ray intensities.[21]

Results

We have calculated the intracule density, $I(\mathbf{u})$, and its spherically averaged electron-pair density distribution function, $h(u)$, for both the $^3\Pi_u$ and the $^1\Pi_u$ states of H_2 from an accurate full configuration interaction (FCI) wave function, constructed from a large Gaussian basis set which is described in detail in Ref. 22.

The calculated potential energy curves resulting from the calculations are shown in Fig. 1, and Table 1 gives the spectroscopic constants calculated at the equilibrium geometries, along with the available experimental data. Observe that the equilibrium distance of both states and the harmonic vibrational frequencies, ω_e, are given rather accurately with respect to their experimental marks.

Table 1. Equilibrium distances are given in a.u, energies in a.u., vibrational frequencies in cm^{-1}, electron repulsion energies in a.u., and electron–electron coalescence densities in a.u for the $^{1,3}\Pi_u$ excited states of H_2.

	$^1\Pi_u$	$^3\Pi_u$
R_e	1.95	1.96
	(1.952)	(1.961)
E	−0.716055	−0.736850
ω_e	2446.2	2460.9
	(2442.7)	(2465.0)
$\langle u^{-1}\rangle$	0.229863	0.246438
$I(0)$	0.81×10^{-2}	0.26×10^{-6}

Note: Experimenatal values in parentheses are taken from Herzberg.[24]

The inset graph of Fig. 1 shows that the $^1\Pi_u$ state rises above the dissociation limit asymptote at $R = 7.17$ a.u., and reaches a tiny maximum at the large internuclear distance of $R = 9.0$ a.u. Its height with respect to the dissociation asymptote is 0.014 eV. These results are consistent with respect to earlier calculations of the potential energy curve of this state[23] and lend support to the accuracy of our calculated wave functions.

The calculated mean values ($n = \pm1$) of the intracular coordinate u, evaluated in eq. 3, are shown in Fig. 2 as a function of the internuclear separation, R. The counterintuitive bahavior of both the electron repulsion energy and the inter-electronic distance, within the domain of short internuclear separations, i.e.: $R \in [0.2 - 0.5]$ a.u., for the $^3\Pi_u$ state is readily seen upon inspection of Fig. 2, which is in sharp contrast with the smoothly monotonic behavior observed for its parent $^1\Pi_u$ state.

This demonstrates that the non-monotonic behavior of the electron repulsion and its associated interelectronic distance in the $^3\Pi_u$ state, in the domain of short internuclear distances, is not an artifact arising from the crudeness of its HF description.

Inspection of the difference between the electron-pair density distribution functions calculated at two internuclear distances

$$\Delta h(u; R, \Delta R) = h(u; R) - h(u; R + \Delta R) \quad \Delta R > 0 \quad (4)$$

provides an alternative view of these unusual correlation effects, relative to the more familiar $h(u) - h_{HF}(u)$ difference. Indeed, as seen in Fig. 3, we observe that for the $^1\Pi_u$ state, increasing the internuclear distance from $R = 0.2$ a.u. to $R = 0.5$ a.u., from $R = 0.5$ a.u. to $R = 0.75$ a.u., and from $R = 1.5$ a.u to $R = 1.95$ a.u. results in a decreased probability of finding the electrons at short distances and a concomitant increased probability of finding the electrons at larger distances. Notice that the three curves in the right panel of Fig. 3 are positive for small inter-electronic distances, hence the probability of finding two electrons within these short inter-electronic distances is larger for the small internuclear distance, and vice-versa for large inter-electronic distances.

However, for the $^3\Pi_u$ state, the probability of finding the electrons at short relative distances is larger for $R = 0.2$ a.u. than for $R = 0.5$ a.u. in spite of the tiny positive peak at $u \sim 1.25$ a.u., and clearly much larger for $R = 0.75$ a.u. than for $R = 0.5$ a.u. (see dotted curve in the left panel of Fig. 3), opposite to what is found for larger internuclear distances. For instance, the probability of finding the two electrons close to each other is larger at $R = 1.5$ a.u. than at $R = 1.95$ a.u., in accordance with intuition.

But, as mentioned above, at smaller internuclear distances, increasing the internuclear distance increases the probability of finding the electrons at short interelectronic distances. This behavior is *counterintuitive* and should be seen as one more (*unexpected*) effect of the symmetry constraints imposed by the Pauli principle.

Fig. 2. Dependence of the mean inter-electronic repulsion energy $\langle u^{-1}\rangle$, (left panel) and the mean interelectronic separation $\langle u^{+1}\rangle$, (right panel) in the $^3\Pi_u$ state (solid curve) and in the $^1\Pi_u$ state (dashed curve).

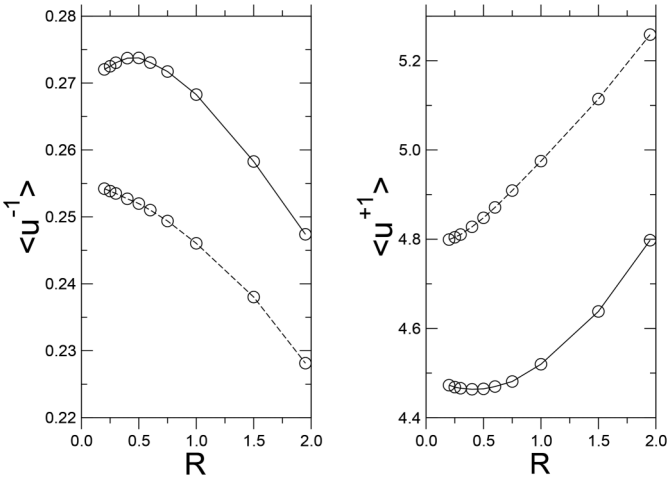

Fig. 3. Difference of the electron-pair density probability function for the $^3\Pi_u$ state (left panel) and for the $^1\Pi_u$ state (right panel). Solid curve: $h(u; R = 0.2) - h(u; R = 0.5)$, dotted curved: $h(u; R = 0.5) - h(u; R = 0.75)$, and dashed curve: $h(u; R = 1.5) - h(u; R = 1.95)$.

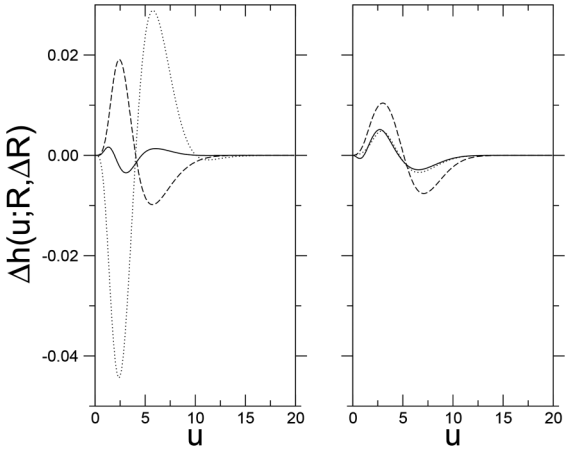

Hund's Rule in the $^{1,3}\Pi_u$ states of H_2

The parent $^{1,3}\Pi_u$ states of the hydrogen molecule differ because of the different symmetry constraints, which Pauli's principle imposes to the spatial part of their corresponding wave functions. Thus, while the singlet state transforms symmetrically with respect to exchanging the electronic coordinates, $\mathbf{r}_1 \leftrightarrow \mathbf{r}_2$, the triplet state's spatial part of the wave function must do it antisymmetrically:

$$\Psi(\mathbf{r}_1, \mathbf{r}_2) = -\Psi(\mathbf{r}_2, \mathbf{r}_1) \quad \forall(\mathbf{r}_1, \mathbf{r}_2) \tag{5}$$

and consequently:

$$\Psi(\mathbf{r}_1, \mathbf{r}_1) = 0 \quad \forall\mathbf{r}_1 \tag{6}$$

This allows for the straightforward evaluation of the electron–electron coalescence density,[25] namely: $I(\mathbf{u} = 0)$, for the triplet state as

Fig. 4. Difference between the electron-pair density probability functions of the $^3\Pi_u$ state and the $^1\Pi_u$ state. Solid curve: $R = 0.2$ a.u., dashed curve $R = 0.5$ a.u., dotted curve: $R = 1.5$ a.u., dotted and dashed curve: $R = 1.95$ a.u.

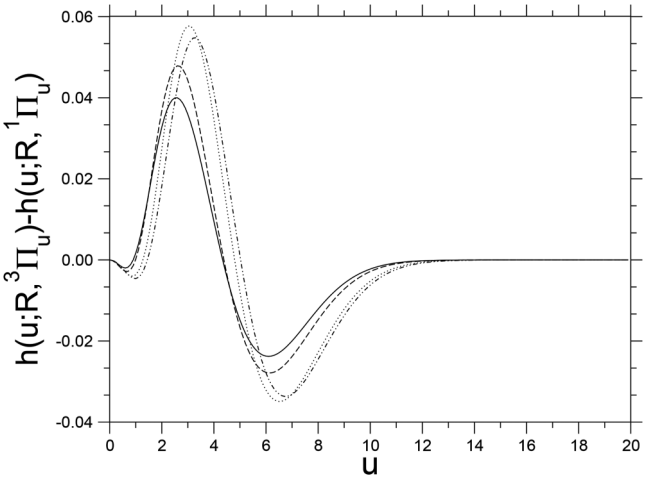

$$\begin{aligned} I(0) &= \langle\Psi|\delta(\mathbf{r}_1 - \mathbf{r}_2)|\Psi\rangle \\ &= \int d\mathbf{r}_1 d\mathbf{r}_2 \Psi^*(\mathbf{r}_1, \mathbf{r}_2)\Psi(\mathbf{r}_1, \mathbf{r}_2)\delta(\mathbf{r}_1 - \mathbf{r}_2) \\ &= \int d\mathbf{r}_1 \Psi^*(\mathbf{r}_1, \mathbf{r}_1)\Psi(\mathbf{r}_1, \mathbf{r}_1) = 0 \end{aligned} \tag{7}$$

Our explicitly calculated values for $I(0)$ for the $^3\Pi_u$ state, shown in Table 1, agree with this prediction and lend further support to our calculated intracule densities.

Furthermore, due to the continuity of the intracule density function, it is expected that the spherically averaged electron-pair density distribution function, $h(u)$, will start building up slower in the triplet state than in the singlet, because in the singlet state $I(0) > 0$ (see Table 1). Consequently, one expects that the probability of finding two electrons at short inter-electronic distances will be larger for the singlet than for the triplet.

The electron-pair density distribution function differences of the $^3\Pi_u$ state minus that of $^1\Pi_u$ state, at a number of selected internuclear distances, plotted in Fig. 4, confirm this assumption. That is, as stated above, $h(u)$ is smaller at small inter-electronic distances, u, for the triplet than for the singlet, hence the negative values shown in Fig. 4 at short inter-electronic distances u, irrespective of the internuclear distance.

The Pauli principle, therefore, prevents electrons from coming into close proximity of each other, as is well known. A natural consequence of this is (hypothesized) that the electron repulsion in the triplet state should be smaller than in its parent same-configuration singlet state, where electrons are not impeded from approaching each other, and consequently, due to associated decreased electron repulsion energy, the triplet (high) spin state is more stable that the singlet (low) spin state. This has been claimed to constitute the physical basis of the Hund's rule,[26–28] which the $^{1,3}\Pi_u$ excited states of H_2 strictly fulfill.

However, the data reported in Table 1 and in Fig. 2 show that this is not the case for the $^{1,3}\Pi_u$ excited states of H_2. Indeed, the electron repulsion energy for the triplet state is larger than for the singlet state, irrespective of the internuclear distance. Additionally, it is worth recalling that numerous explicit evaluations of the electron repulsion energy for the various spin states arising from the same configuration found, with no exception, that the electron repulsion energy is larger in the high-spin state (see Ref. 29, p. 234). This invalidates the explanation outlined above for Hund's

rule, as it was elegantly put forward by Boyd[30,31] and subsequently elaborated on by others.[32,33]

The physical basis of the lower energy of the $^3\Pi_u$, with respect to its parent $^1\Pi_u$ state, is shown in Fig. 4. Notice that although the probability of finding the electron in close proximity is smaller in the triplet than in the singlet state, the triplet favors intermediate inter-electronic distances, compared with the singlet state. Additionally, notice also that the probability of finding the electrons at large separation is larger in the singlet than in the triplet state, unlike the behavior found for short inter-electronic distances. The triplet state, therefore, favors intermediate inter-electronic distances, which makes the electronic cloud more compact in the triplet than in the singlet state, and consequently makes the electron–nucleus attraction energy larger in the triplet than in the singlet state, in such an amount that it outweighs the larger electron repulsion of the latter.[34–38]

In other words, since the electrons of the triplet state avoid each other in the vicinity of the nuclei, they screen less the nuclear charge and consequently the electron cloud becomes more compact than in the singlet state, for which the nuclear charge is screened more efficiently.[39] This leads ultimately to an increased electron–nucleus attraction for the triplet, which overweighs the larger electron repulsion of the triplet state, yielding, therefore, a more stable triplet state.

Summary

We have demonstrated, in accordance with Tal and Katriel,[17] that the non-monotonic behavior with respect to the internuclear separation of the electron repulsion energy and its associated mean inter-electronic distance in the $^3\Pi_u$ excited state of the hydrogen atom are real, *counterintuitive*, effects of the symmetry constraints imposed by the Pauli principle on the wave function of triplet states. High-level FCI calculations show that while in the $^1\Pi_u$ excited state the electron repulsion energy and its associated mean inter-electronic distance behave monotonically, in the $^3\Pi_u$ excited state, the electron repulsion energy increases and the mean inter-electronic distance decreases as the internuclear separation increases.

Finally, we have found that Hund's rule, which holds also for these $^{1,3}\Pi_u$ same-configuration $1\sigma_g^1\pi_u^1$ excited states, can be accounted for in terms of simple electronic shielding effects induced by wave function antisymmetrization, in accordance with the accepted interpretation.[31]

Acknowledgements

This research has been funded by Euskal Herriko Unibertsitatea (University of the Basque Country), Eusko Jaurlaritza (Basque Government), and the Spanish Office of Science and Technology (MINECO CTQ2014-52525-P). JMU wishes to thank Professor Russell J. Boyd for his continuous encouragement and dedicated guidance over the years in the exciting field of electron-pair densities.

References

(1) Coulson, C. A.; Neilson, A. H. *Proc. Phys. Soc.* **1961**, *78*, 831. doi:10.1088/0370-1328/78/5/328.
(2) Curl, R. F.; Coulson, C. A. *Proc. Phys. Soc.* **1965**, *85*, 647. doi:10.1088/0370-1328/85/4/303.
(3) Boyd, R. J.; Coulson, C. A. *J. Phys. B: At. Mol. Phys.* **1973**, *6*, 782. doi:10.1088/0022-3700/6/5/012.
(4) Kutzelnigg, W. In *Explicitly Correlated Wave Functions in Chemistry and Physics. Theory and Applications*; Rychlewski, J., Ed.; Kluwer Academic: Dordrecht, Netherlands, 2003; Vol. 13, Chapter 1, pp. 3–90. doi:10.1007/978-94-017-0313-0_1.
(5) Maitra, N. T.; Burke, K. In *Many-Electron Densities and Reduced Density Matrices*; Cioslowski, J., Ed.; Kluwer Academic/Plenum: New York, 2000; pp. 183–208. doi:10.1007/978-1-4615-4211-7_9.
(6) Piris, M.; Lopez, X.; Ugalde, J. M. *J. Chem. Phys.* **2008**, *128*, 214105. doi:10.1063/1.2937456.
(7) Hollett, J. W.; McKemmish, L. K.; Gill, P. M. W. *J. Chem. Phys.* **2011**, *134*, 224103. doi:10.1063/1.3599937.
(8) Zielinski, Z. A. M.; Pearson, J. K. *Comput. Theor. Chem.* **2013**, *1003*, 79. doi:10.1016/j.comptc.2012.08.033.
(9) Hennessey, D. C.; Sheppard, B. J. H.; Mackenzie, D. E. C. K.; Pearson, J. K. *Phys. Chem. Chem. Phys.* **2014**, *16*, 25548. doi:10.1039/C4CP02669A.
(10) Proud, A. J.; Mackenzie, D. E. C. K.; Pearson, J. K. *Phys. Chem. Chem. Phys.* **2015**, *17*, 20194. doi:10.1039/C5CP03280F.
(11) Pearson, J. K.; Gill, P. M. W.; Ugalde, J. M.; Boyd, R. J. *Mol. Phys.* **2009**, *107*, 1089. doi:10.1080/00268970902740563.
(12) Per, M. C.; Russo, S. P.; Snook, I. K. *J. Chem. Phys.* **2009**, *130*, 134103. doi:10.1063/1.3098353.
(13) Wang, J.; Kim, K. S.; Baerends, E. J. *J. Chem. Phys.* **2010**, *132*, 204102. doi:10.1063/1.3429608.
(14) Boyd, R. J.; Sarasola, C.; Ugalde, J. M. *J. Phys. B: At., Mol. Opt. Phys.* **1988**, *21*, 2555. doi:10.1088/0953-4075/21/14/008.
(15) Wang, J.; Mercero, J. M.; Silanes, I.; Ugalde, J. M. *Europhys. Lett.* **2006**, *76*, 808. doi:10.1209/epl/i2006-10335-x.
(16) Wang, J.; Wang, Y.; Lv, S.; Ugalde, J. M. *J. Chem. Phys.* **2007**, *127*, 074307. doi:10.1063/1.2768531.
(17) Tal, Y.; Katriel, J. *J. Phys. B: At. Mol. Phys.* **1974**, *7*, 2113. doi:10.1088/0022-3700/7/16/010.
(18) Colbourn, E. A. *J. Phys. B: At. Mol. Phys.* **1975**, *8*, 1926. doi:10.1088/0022-3700/8/11/027.
(19) Mercero, J. M.; Valderrama, E.; Ugalde, J. M. In *Metal-Ligand Interactions*; Russo, N.; Salahub, D. R.; Witko, M., Eds.; Kluwer Academic: New York, 2003; Vol. 116 of *NATO Science Series II. Mathematics, Physics and Chemistry*, pp. 205–239. doi:10.1007/978-94-010-0191-5_10.
(20) Thakkar, A. J. In *Density Matrices and Density Functionals*; Erdahl, R.; Smith, V. H., Jr., Eds.; Reidel: New York, 1987; pp. 553–581. doi:10.1007/978-94-009-3855-7_30.
(21) Watanabe, N.; Ten-no, S.; Iwata, S.; Udaguwa, Y. In *Reviews of Modern Quantum Chemistry*; Sen, K. D., Ed.; World Scientific: Singapore, 2002; Vol. 1, pp. 553–577.
(22) Mercero, J. M.; Fowler, J. E.; Sarasola, C.; Ugalde, J. M. *Phys. Rev. A* **1998**, *57*, 2550. doi:10.1103/PhysRevA.57.2550.
(23) Browne, J. C. *J. Chem. Phys.* **1964**, *40*, 43. doi:10.1063/1.1724891.
(24) Herzberg, G. *Molecular Structure and Spectra, I. Diatomic Molecules*; D. Van Nostrand: New York, 1950; pp. 531–532.
(25) Ugalde, J. M.; Sarasola, C. *Phys. Rev. A* **1994**, *49*, 3081. doi:10.1103/PhysRevA.49.3081.
(26) Hund, F. *Z. Phys.* **1925**, *33*, 345.
(27) Hund, F. *Z. Phys.* **1925**, *34*, 296.
(28) Hund, F. *Linienspektren und Periodisches System der Elemente*; Springer: Berlin, 1927; Vol. 4. doi:10.1007/978-3-7091-5695-7.
(29) Valderrama, E.; Ugalde, J. M.; Boyd, R. J. In *Many-Electron Densities and Reduced Density Matrices*; Cioslowski, J., Ed.; Kluwer Academic/Plenum: New York, 2000; Chapter 11, pp. 231–248. doi:10.1007/978-1-4615-4211-7_11.
(30) Boyd, R. J. *Nature* **1974**, *250*, 566. doi:10.1038/250566a0.
(31) Boyd, R. J. *Nature* **1984**, *310*, 480. doi:10.1038/310480a0.
(32) Katriel, J.; Pauncz, R. *Adv. Quantum Chem.* **1977**, *10*, 143. doi:10.1016/S0065-3276(08)60580-8.
(33) Warner, J. W.; Berry, R. S. *Nature* **1985**, *313*, 160. doi:10.1038/313160a0.
(34) Katriel, J. *Phys. Rev. A.* **1972**, *5*, 1990. doi:10.1103/PhysRevA.5.1990.
(35) Regier, P. E.; Thakkar, A. J. *J. Phys. B: At. Mol. Phys.* **1984**, *17*, 3391. doi:10.1088/0022-3700/17/17/011.
(36) Ugalde, J. M.; Boyd, R. J. *Chem. Phys. Lett.* **1985**, *114*, 197. doi:10.1016/0009-2614(85)85086-7.
(37) Thakkar, A. J. *J. Phys. B: At. Mol. Phys.* **1987**, *20*, 3939. doi:10.1088/0022-3700/20/16/007.
(38) Darvesh, K. V.; Boyd, R. J. *J. Chem. Phys.* **1987**, *87*, 5329. doi:10.1063/1.453651.
(39) Warner, J. W.; Bartell, L. S.; Blinder, S. M. *Int. J. Quantum Chem.* **1980**, *18*, 921. doi:10.1002/qua.560180403.

6.2) Electron-Pair Distribution in Chemical Bond Formation

Rodríguez-Mayorga M., Via-Nadal M., Solà M., Ugalde J. M., Lopez X., Matito E. “Electron-Pair Distribution in Chemical Bond Formation”. *J. Phys. Chem. A*. Vol. 122, issue 7-8 (2018) : 1916-1923.

https://doi.org/10.1021/acs.jpca.7b12556

THE JOURNAL OF PHYSICAL CHEMISTRY A

Article

Cite This: J. Phys. Chem. A 2018, 122, 1916−1923

pubs.acs.org/JPCA

Electron-Pair Distribution in Chemical Bond Formation

Published as part of The Journal of Physical Chemistry virtual special issue "Manuel Yáñez and Otilia Mó Festschrift".

M. Rodríguez-Mayorga,[†,‡] M. Via-Nadal,[†] M. Solà,[‡] J. M. Ugalde,[†] X. Lopez,[†] and E. Matito*[,†,§]

[†]Kimika Fakultatea, Euskal Herriko Unibertsitatea, UPV/EHU, and Donostia International Physics Center (DIPC). P.K. 1072, 20080 Donostia, Euskadi, Spain

[‡]Institut de Química Computacional i Catàlisi (IQCC) and Departament de Química, University of Girona, C/ Maria Aurèlia Capmany, 69, 17003 Girona, Catalonia, Spain

[§]IKERBASQUE, Basque Foundation for Science, 48013 Bilbao, Euskadi, Spain

Supporting Information

ABSTRACT: The chemical formation process has been studied from relaxation holes, $\Delta h(u)$, resulting from the difference between the radial intracule density and the nonrelaxed counterpart, which is obtained from atomic radial intracule densities and the pair density constructed from the overlap of the atomic densities. $\Delta h(u)$ plots show that the internal reorganization of electron pairs prior to bond formation and the covalent bond formation from electrons in separate atoms are completely recognizable processes from the shape of the relaxation hole, $\Delta h(u)$. The magnitude of $\Delta h(u)$, the shape of $\Delta h(u)$ $\forall$ $u < R_{eq}$, and the distance between the minimum and the maximum in $\Delta h(u)$ provide further information about the nature of the chemical bond formed. A computational affordable approach to calculate the radial intracule density from approximate pair densities has been also suggested, paving the way to study electron-pair distributions in larger systems.

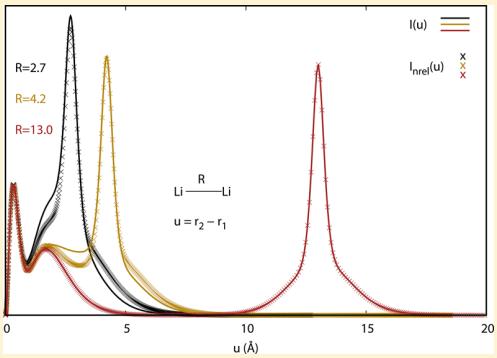

INTRODUCTION

Understanding chemical processes requires a proper characterization of bond formation. The formation of bonds is usually analyzed from the energy gain or loss, through the study of potential energy surfaces,[1] suggested by René Marcelin in 1913. Since the advent of quantum mechanics, the chemical bond has been also investigated from descriptors based on the electron density.[2−4] Many tools have been designed to this aim, the quantum theory of atoms in molecules[5] (QTAIM) of Bader probably being the most popular one. Another avenue consists in the study of electron pair formation in chemical bond, as pioneered by the classical work of Lewis in 1916.[6] Since the landmark paper of Lewis, there have been many attemps to fit the classic idea of electron pairs in the chemical bond within the framework of quantum mechanics, mostly using electron-pair distributions.[7−21] The electron-pair distribution or *pair density* provides a quantum-mechanical description of the distribution of electron pairs in the space.[22,23] Although the pair density has a simple probabilistic interpretation, it is a complicated six-coordinate function that is not easy to analyses. Most analysis of the pair density employ transformations that reduce the dimensionality,[10,24,25] use statistical quantities such the average number of pairs,[7−9,11−14,16,18,26,27] or employ two-electron expectation values such as the energy[28−35] or the square of the total spin angular momentum.[36−39] One of the most convenient transformations of the pair density is the so-called *intracule density*, which results from the integration of the pair density over the extracule coordinate. The radial or isotropic intracule density depends only on one coordinate, the interelectronic distance, but it still retains information about the electron-pair distribution and it is also the simplest quantity in terms of which an explicit expression of the electron−electron energy is known. Interestingly, the intracule density is related to an experimental observable, as it can be obtained from X-ray scattering techniques.[40−42] The intracule density has been previously used to analyze the electronic structure and electron correlation of some molecular systems,[24,43−59] but very few studies of the intracule density have been devoted to the investigation of bond formation.[60−62]

The aim of this paper is to understand the changes occurring in the intracule density during the chemical bond formation. To this aim, we have chosen three simple molecules: (i) H_2 and (ii) HeH^+, which have a chemical bond consisting of a single electron pair, and (iii) BH, which contains several electron pairs, only one of which is involved in the chemical bond. The study is complemented with molecules presenting more

Received: December 21, 2017
Revised: January 29, 2018
Published: January 30, 2018

DOI: 10.1021/acs.jpca.7b12556
J. Phys. Chem. A 2018, 122, 1916−1923

complicated bonding situations such as CO, Li_2, F_2, or the ground and first excited states of LiH. Finally, we consider the cost of the intracule density plots and suggest a means to obtain it at a reduced computational overhead.

METHODOLOGY

The pair probability density or simply *pair density*[25,63] (2-PD) is defined as

$$\rho_2(\mathbf{r}_1, \mathbf{r}_2) = \frac{N(N-1)}{2} \int |\Psi(\mathbf{r}_1, \mathbf{r}_2, \mathbf{r}_3, \ldots, \mathbf{r}_N)|^2 \, d\mathbf{r}_3 \ldots d\mathbf{r}_N \tag{1}$$

for any electronic wave function Ψ of a N-electron system. It is proportional to the probability of finding a pair of electrons at $\mathbf{r}_1$ and at $\mathbf{r}_2$, regardless the position of the other $N-2$ electrons. Among all electron-pair distributions, we may select the ones that satisfy $\mathbf{u} = \mathbf{r}_2 - \mathbf{r}_1$ for a fixed $\mathbf{u}$,

$$I(\mathbf{u}) = \int \rho_2(\mathbf{r}_1, \mathbf{r}_2) \, \delta(\mathbf{u}-\mathbf{r}_1+\mathbf{r}_2) \, d\mathbf{r}_1 \, d\mathbf{r}_2 \tag{2}$$

which is known as the intracule probability density or simply *intracule density*. Upon integration over the solid angle Ω_u we obtain the *radial* or isotropic intracule density,

$$I(u) = u^2 \int I(\mathbf{u}) \, d\Omega_u \tag{3}$$

This function only depends on the interelectronic distance, and therefore it provides a simple visualization of the distribution of electron−electron separations. By monitoring the changes of this distribution as we stretch a chemical bond, we should observe the formation and breaking of electron pairs and the electron reorganization in the molecule. Unfortunately, the radial intracule density contains all the information on the $N(N-1)$ electron pairs in the molecule, most of which is superflous to explain the chemical bond formation. To select the chemical important information within the radial intracule density, some of us[62] defined the *relaxation hole*,

$$\Delta h(u) \equiv \Delta h_{\mathrm{rel}}(u) = I(u) - I_{\mathrm{nrel}}(u) \tag{4}$$

as the difference between the actual radial intracule density and the *nonrelaxed* one,

$$I_{\mathrm{nrel}}(u) = \sum_{\mathrm{A}} I_{\mathrm{A}}(u) + \sum_{\mathrm{A>B}} I_{\mathrm{AB}}(u) \tag{5}$$

where the first term at the right-hand side accounts for the atomic contribution and is computed from isolated atoms, and the second term involves the summation of all interatomic contributions computed using nonrelaxed densities,

$$I_{\mathrm{AB}}(u) = u^2 \int \rho_{\mathrm{A}}(\mathbf{r}_1) \, \rho_{\mathrm{B}}(\mathbf{r}_2) \, \delta(\mathbf{u}-\mathbf{r}_1+\mathbf{r}_2) \, d\mathbf{r}_1 \, d\mathbf{r}_2 \, d\Omega_u \tag{6}$$

where $\rho_{\mathrm{A}}(\mathbf{r}_1)$ is the density of the isolated atom A. The nonrelaxed density is thus the intracule density that can be obtained using atomic information only. Notice that the nonrelaxed density considers the distribution of electron pairs within the atoms but also the electron pairs generated from the two individual atomic densities, $\rho_{\mathrm{A}}\rho_{\mathrm{B}}$. $I_{\mathrm{nrel}}(u)$ was proven to be a "poor man's approach to the real $I(u)$",[62] and insufficient to characterize van der Waals interactions.[54,62] However, the structure of $\Delta h_{\mathrm{rel}}(u)$ was shown to provide valuable information about the bonding nature of small few-electron systems.[62] In this work we are concerned with the *bond formation* process in species with larger numbers of electrons, which we will study through the analysis of $\Delta h_{\mathrm{rel}}(u)$ at different bond lengths for various diatomic molecules.

The computational cost of the intracule density is quite high because it involves the calculation of the second-order reduced density matrix (2-RDM) from a highly accurate wave function (typically a full-configuration interaction, FCI) and the numerical integration with a Gauss−Hermite quadrature of eq 2 and a surface integration using a Lebedev quadrature (eq 3). In this paper we will consider two different approximations that can reduce the computational cost (see Supporting Information for performance values). First of all, we will substitute the FCI calculation with a sufficiently accurate wave function. Namely, we will consider coupled-cluster single and doubles (CCSD) and complete active space self-consistent field (CASSCF) wave functions as substitutes of the FCI calculation in the presence of dynamic and nondynamic correlation effects, respectively.[64,65] Second, we will use an approximation of the 2-RDM that only includes two-index elements[66,67] and, therefore, reduces the 2-RDM from the exact four-index quantity to an approximate two-index one.

CCSD wave functions do not satisfy the Hellmann−Feynman theorem and usually the expensive energy-derivative 2-RDM are employed.[35,68−70] To reduce the cost, several authors[14,20,71−73] have used 2-PD approximations extracted from the reduced density matrix functional theory (RDMFT).[53,74−76] In this paper we opt for the same solution to reduce the cost of CASSCF and CCSD 2-RDM. Among the different RDMFT approximations, we have chosen the simple Müller approximation[66] (also known as Baerends−Buijse approximation[67,77]) that provides reliable results in the calculation of chemical bonding descriptors.[14,20,53]

FCI calculations of the potential energy curves (PECs) have been performed for H_2, HeH^+, BH, Li_2, and LiH (for LiH both ground and first excited states are considered) with a modified version of the code developed by Knowles and Handy.[78,79] For F_2 and CO, CASSCF calculations of the PEC were performed using Gaussian 09[80] taking ten electrons in six orbitals for F_2 and six electrons in six orbitals, including a state average of six energy levels, for CO. The Gaussian 09 package was employed to perform CCSD calculations for all diatomics but CO and two-electron molecules. The computation of approximate $\Delta h(u)$ using CCSD wave functions employed the unrestricted formalism to compute the total radial intracule density and the nonrelaxed ones (which often involve open-shell species) in the same grounds. All CCSD calculations included the correlation of all the electrons except for F_2, for which we performed frozen-core calculations to produce a meaningful comparison between CCSD and CASSCF results. In all cases the aug-cc-pVDZ basis was used. PECs of all the studied systems are collected in Figure S1. 2-RDMs were produced from the expansion coefficients of CASSCF and FCI wave functions using the in-house DMn code.[81,82] Intracule densities were computed with the *RHO2_OPS*[83] code using the algorithm of Cioslowski and Liu.[84]

RESULTS

H_2, HeH^+, and BH. All the equilibrium distances at the corresponding level of theory are collected in Table 1. The formation of the covalent bond in H_2 is due to a partial deformation of the electron density of the two isolated atoms, which is relocated between them. The same phenomenon can be studied in terms of the pair density, by comparing the radial intracule density of H_2 to the nonrelaxed radial intracule

DOI: 10.1021/acs.jpca.7b12556
J. Phys. Chem. A 2018, 122, 1916−1923

Table 1. First Maximum (M) and Minimum (m) of $\Delta h(u)$ for All the Systems Studied[a]

molecule	R_{eq}	u_M	u_m	$\Delta h(u_M)$	$\Delta h(u_m)$
H_2	0.7	0.76	1.86	0.113	−0.071
HeH^+	0.8	0.84	0.31	0.026	−0.014
BH	1.3	1.16	2.17	0.192	−0.067
Li_2	2.7	2.02	4.08	0.344	−0.239
CO	1.1	0.69	1.19	1.287	−1.038
F_2	1.5	0.77	1.32	0.516	−0.903
LiH ($X^1\Sigma^+$)	1.6	1.37	3.04	0.322	−0.185
LiH ($A^1\Sigma^+$)	2.6	6.05	2.21	0.263	−0.409

[a] u and R_{eq} (the equilibrium distance) are in Å.

density described in the previous section. The formation of an electron pair between the two atoms is evident from the plots in Figure 1, where we observe that $\Delta h(u)$ peaks at the bond length or at shorter distances and is negative at larger distances. In other words, the electron-pair distance shrinks upon the formation of the chemical bond. The distance between the maximum and minimum of $\Delta h(u)$ provides information about the deformation of the electron-pairs length (Table 1). In H_2, this length systematically reduces as the molecule is formed, increasing the probability of having the electron pair at shorter distances.

HeH^+ is formed from He and H^+, and therefore, the nonrelaxed intracule density of this diatomic molecule is rather simple because H^+ does not contribute to atomic or diatomic components of the nonrelaxed intracule density (the density and the pair density of H^+ are zero). Hence, $\Delta h(u)$ only has contributions from the atomic He component and it results from the difference of the radial intracule density of HeH^+ and He. The redistribution of the electron-pair probability density upon bond formation is less important than in the hydrogen molecule, as the values of $\Delta h(u)$ are 1 order of magnitude smaller. The formation of the covalent bond in this molecule is actually completely opposite to the latter case, as we can see in Figure 1. First, as the helium atom approaches the proton, the electron pair within He stretches, reducing the probability of having the electrons separated ca. 0.5 Å and increasing it around the bond length. Only at the equilibrium, R = 0.8 Å, is the electron-pair density at larger distances reduced. The fact that the pair density is dragged from short distances always around the same position (around 0.3−0.5 Å) is in accord with the fact that this molecule is just experiencing an internal pair reorganization of the electrons within He.

The formation of BH from B and H is an intermediate case where a bonding electron pair is formed from two electrons that come one from each atom, and there is simultaneously an internal reorganization of the electron pairs in B. At large atomic separations, as a result of the deformation of the electron density within B atom, electrons move toward H and, hence, the electron-pair distribution shifts to larger distances (Figure 2). Eventually, the two atoms get quite close and the

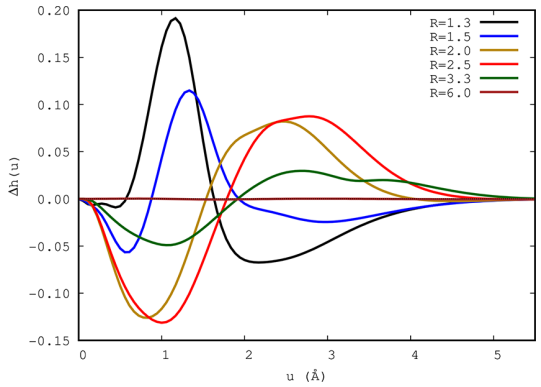

Figure 2. $\Delta h(u)$ of BH along the bond formation process. All R and u in Å.

profile of $\Delta h(u)$ reverses: the electron-pair distribution increases around the bond length by reducing the density of electron pairs at shorter and longer distances. Finally, the bond is completely formed and the peak of $\Delta h(u)$ is entirely due to the reduction of the distance of electron pairs. As we can see, the internal reorganization of electron pairs prior to bond formation and the covalent bond formation from electrons in separate atoms are completely recognizable processes from the shape of the relaxation hole.

Li_2, CO, F_2, and LiH. In this section we analyze the intracule densities during the bond formation of Li_2, CO, F_2 and LiH from the neutral atoms in gas phase. In the latter case we study both the ground and the first excited states, $X^1\Sigma^+$ and $A^1\Sigma^+$, respectively. All these diatomic molecules dissociate into neutral atoms in the gas phase and there is, at least, some partial covalent character in the bonds of these molecules at equilibrium.[85]

In F_2 the reorganization of electron pairs occurs faster than in BH (Figure 3). Indeed, the first appreciable variation of the electron pair distribution does not occur until the atoms are

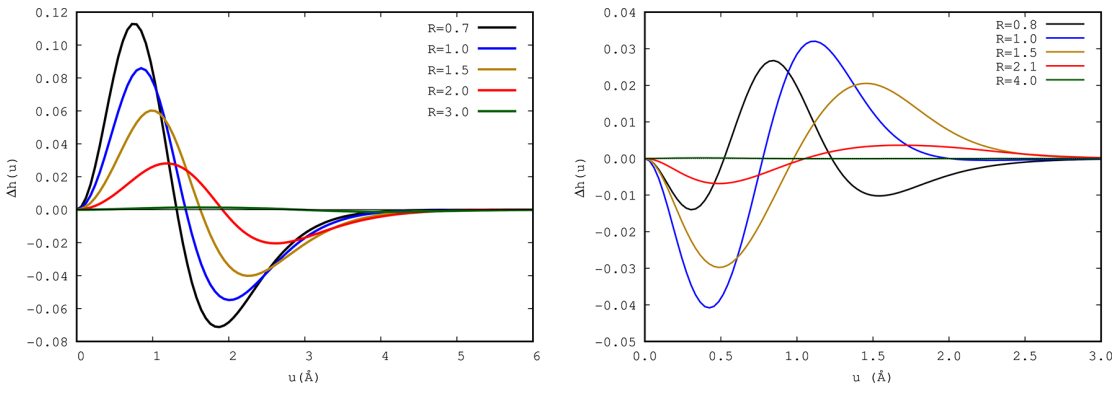

Figure 1. $\Delta h(u)$ of H_2 (left) and HeH^+ (right) at different bond lengths. All R and u in Å.

DOI: 10.1021/acs.jpca.7b12556
J. Phys. Chem. A 2018, 122, 1916−1923

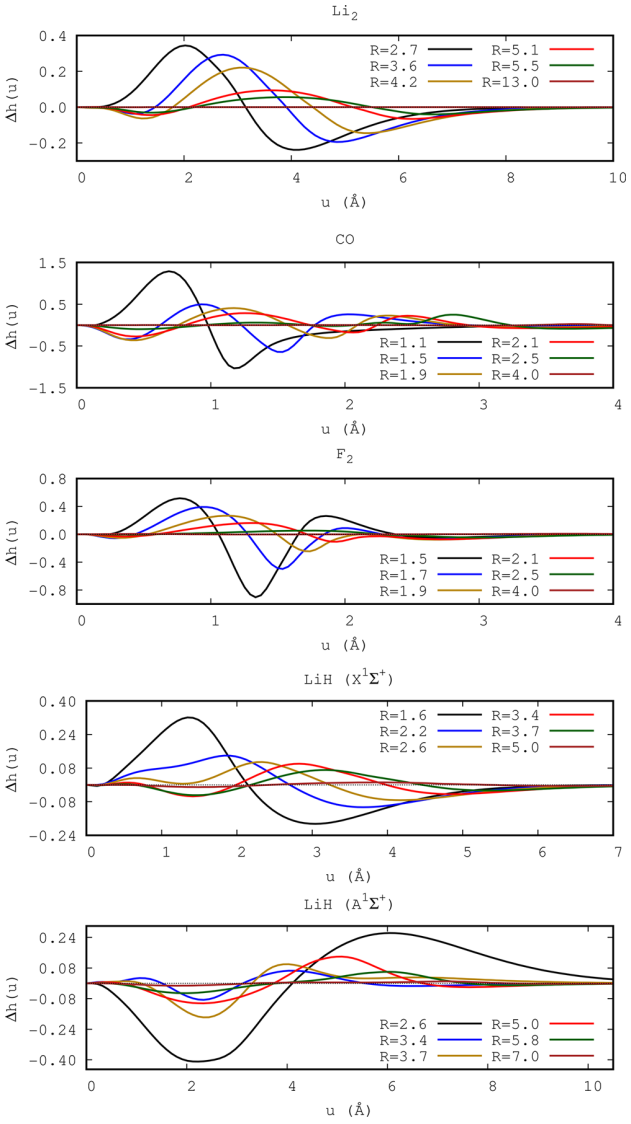

Figure 3. Relaxation holes for Li_2, CO, F_2, and LiH at different bond lengths (R). The ground ($X^1\Sigma^+$) and excited ($A^1\Sigma^+$) states of LiH were analyzed. The minimal bond length corresponds to the equilibrium geometry in all cases. All R and u in Å.

separated 2.5 Å, i.e., at 1.2 Å from the equilibrium distance. The first significant values of $\Delta h(u)$ occur at R = 2.1 Å, where the electron-pair distribution is shifted to shorter distances, augmenting the probability of finding electron pairs between the F atoms. Unlike H_2 or BH, the maximum of the relaxation hole, $\Delta h(u)$, occurs at values of u significantly shorter than the equilibrium distance (Table 1), suggesting that two bonding electrons lie in the bonding region as opposed to the situation in which the electrons of the bonding pair are sitting close to the nuclei. The same situation is reproduced in Li_2 and CO, and therefore, we are deemed to conclude that this profile is typical in covalent bonds. Obviously, H_2 constitutes an exception because there are no core electrons in this molecule and, therefore, the electrons in the bonding pair are highly attracted toward the closest nucleus.

Let us now examine Li_2, which presents a non-nuclear attractor (NNA) in the middle of the bond at various bond lengths ($R_{LiLi} \in [2.7-3.3]$ Å)[86] and is the smallest electride documented thus far.[87] At equilibrium, we find that $\Delta h(u) > 0$ for all $u < R_{eq}$ and significant large $\Delta h(u)$ at $u = R_{eq}/2$, indicating the additional formation of electron pairs between the electrons at the NNA and the ones at each Li atom. In this case, the formation of the molecule occurs less abruptly than in F_2 and involves the reorganization of electron pairs at larger distances.

The $\Delta h(u)$ evolution with the bond length in CO has also some resemblance with the latter two cases. There are, however, three important differences. The first one is that the CO bond formation takes place in a shorter span than in Li_2 but larger than in F_2, the first important electron-pair redistribution occurring only at about 1 Å from the equilibrium distance. The second one is the long-range peaks of $\Delta h(u)$, showing at distances larger than the bond length, suggesting a non-negligible reorganization of the lone pairs prior to bond formation. Finally, we find that $\Delta h(u)$ is systematically larger than in Li_2 and F_2, as it corresponds to the formation of three electron pairs in CO. Interestingly, CO and F_2 have the shortest distance between the maximum and the minimum of $\Delta h(u)$ (Table 1), indicating that these molecules experience a less drastic deformation of the electron-pair length upon bond formation. This fact is in agreement with the more electronegative character of the composing atoms, conferring them with a lower capacity to be deformed.

A most interesting electron reorganization occurs in LiH ground and first excited states.[85] The $X^1\Sigma^+$ and $A^1\Sigma^+$ states dissociate into $H(^2S)$ + $Li(^2S)$ and $H(^2S)$ + $Li(^2P)$, respectively. The adiabatic ground state, $X^1\Sigma^+$, is dominated by a diabatic ionic state at the equilibrium but, as the molecule stretches, the PEC passes through an avoided crossing and the state is predominantly covalent in nature. In this sense, the character of the bond in LiH changes from covalent to ionic as the molecule is formed. This change of bond character is accompanied by an electron transfer from hydrogen to lithium, which is commonly known as the *harpoon mechanism*. This peculiar mechanism is given by the crossing between two diabatic states, the ionic and the lowest-lying covalent ones, around 3 Å. The $A^1\Sigma^+$ state is even more complicated because it results from the crossing of three diabatic states, the ionic and the two lowest-lying covalent diabatic states, giving rise to two avoided crossings (the first of which obviously is shared with the ground state). Hence, when the molecule is formed, the bonding character of $A^1\Sigma^+$ LiH changes from covalent to ionic and, then, back to covalent. The second avoided crossing takes places when Li and H are separated about 6 Å. The electron transfers occur in the regions close to the avoided crossings and were fully characterized in our previous work.[85]

The profile of $\Delta h(u)$ for $X^1\Sigma^+$ at equilibrium resembles BH, peaking not far from the equilibrium distance. However, as we stretch the bond, one does not observe electron-pair depletion at short distances. In fact, it is only after we have passed the avoided crossing that we start to observe an increase of the probability at short electron−electron distances. In other words, the typical profile of covalent bond dissociation is only reproduced when we are in the part of the potential energy surface that is purely covalent. Although the profiles of $\Delta h(u)$ for large R are very similar for the ground and excited states, the situation at short bond lengths is reversed for the $A^1\Sigma^+$ state. As we approach the equilibrium distance, the profile does not reverse and we barely observe the formation of short-range electron pairs. This plot puts forward the rather polarized character of this bond, which is characterized by significant

DOI: 10.1021/acs.jpca.7b12556
J. Phys. Chem. A 2018, 122, 1916−1923

electron-pair stretching upon bond formation, i.e., completely opposite to all the molecules studied in this work. Even HeH^+ is a quite different case because in this molecule there was only internal reorganization of the electron pairs, which were never shifted to distances much larger than the bond length.

Approximate Radial Intracule Densities. In this section we assess the performance of approximate radial intracule densities in reproducing the plots of the previous sections. Thus far, we have employed CASSCF wave functions for F_2 and CO, and FCI for H_2, HeH^+, BH, Li_2, and LiH (both states). Both FCI and CASSCF yield *N*-representable 2-RDMs.

First of all, we replace the FCI/CASSCF calculation by CCSD for all the systems, except CO, for which a multideterminant calculation is mandatory. Second, we use an approximate 2-RDM calculated from CCSD natural orbital occupancies. Namely, we apply the Müller approximation[66,67,77] using the energy-derivative CCSD 1-RDMs obtained from Gaussian. The latter are not *N*-representable and, thus, might present natural occupancies outside the physical range [0,1]. However, in the present cases, only a few populations did not meet this condition and the deviations from the occupation boundaries were small, producing no quantitative effect on the results presented.

We did not include H_2 and HeH^+ because, for these two-electron systems, the CCSD wave functions actually correspond to the exact solution and, therefore, only the 2-RDM could be approximated. In addition, as we have just recently proven, the Müller approximation performs quite accurately in a weakly correlated regime.[53] Accordingly, our calculations on these systems confirm this finding, producing intracule plots that are indistinguishable from the exact ones, and therefore, we have omitted them in the manuscript. We have also omitted the excited state of LiH. The approximate $\Delta h(u)$ plots for the rest of the molecules are plotted in Figure 4 (see Supporting Information for error plots). In all cases there is a very good agreement between the original calculations using FCI/CASSCF and the exact 2-RDM and these approximate wave functions using CCSD and Müller's approximation. The small difference occurs for the short-range part of $\Delta h(u)$ of F_2, which can be attributed to the fact that CASSCF calculations did not include the 2σ orbital in the active space whereas the CCSD wave function takes the correlation effects of this orbital into account. We also collect the information on the minima and the maxima of $\Delta h(u)$ in Table 2. Comparison with the numbers in Table 1 reveals very small differences between the original and the approximate $\Delta h(u)$, validating the use of the approximations to retrieve information about the electron pairing in electronic structures.

CONCLUSIONS

In this paper we have studied the chemical formation process from the study of radial intracule densities. We have analyzed the relaxation holes, $\Delta h(u)$, resulting from the difference between the actual radial intracule density and the nonrelaxed one constructed from atomic radial intracule densities and the pair density obtained from the overlap of the atomic densities. Our results show that the mechanism of electron-pair formation is contained in $\Delta h(u)$. In particular, the internal reorganization of electron pairs prior to bond formation and the covalent bond formation from electrons in separate atoms are completely recognizable processes from the shape of the relaxation hole, $\Delta h(u)$. The magnitude of $\Delta h(u)$, the shape of $\Delta h(u)$ $\forall$ $u < R_{eq}$, and the distance between the minimum and the maximum in $\Delta h(u)$ provide information about the nature of the chemical bond formed.

We have also suggested a computational affordable approach to calculate the radial intracule density from approximate pair densities and adequate wave functions such as CCSD or CASSCF as replacements of FCI in regimes of dynamic and

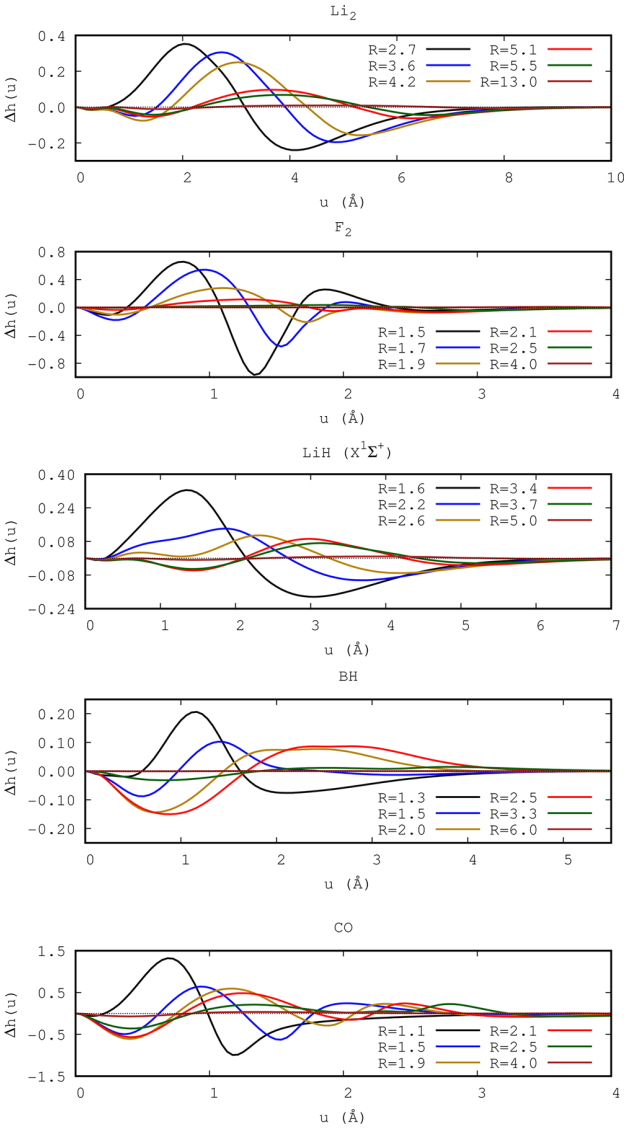

Figure 4. Approximate $\Delta h(u)$ for Li_2, F_2, LiH, BH, and CO at different bond lengths (R). The 2-RDM uses the Müller approximation from CCSD (Li_2, F_2, BH, and LiH) and CASSCF (CO) wave functions. All R and u in Å.

Table 2. First Maximum (M) and Minimum (m) of $\Delta h(u)$ for the Systems Analyzed with the Approximate Relaxation Hole at the Equilibrium Distance (Table 1)[a]

molecule	u_M	u_m	$\Delta h(u_M)$	$\Delta h(u_m)$
BH	1.15	2.08	0.207	−0.076
Li_2	2.04	4.10	0.353	−0.241
CO	0.70	1.19	1.322	−1.000
F_2	0.80	1.35	0.657	−0.970
LiH ($X^1\Sigma^+$)	1.36	3.03	0.325	−0.184

[a] u in Å.

DOI: 10.1021/acs.jpca.7b12556
J. Phys. Chem. A 2018, 122, 1916−1923

nondynamic correlation, respectively. In all cases, there is a qualitative agreement with the reference calculation and, quite often, the relaxation holes produced from both methodologies are barely distinguishable. This approach paves the way to study electron-pair distributions in larger systems.

■ ASSOCIATED CONTENT

Supporting Information

The Supporting Information is available free of charge on the ACS Publications website at DOI: 10.1021/acs.jpca.7b12556.

Potential energy curves, error analysis, and computational saving of the approximate relaxation holes (PDF)

■ AUTHOR INFORMATION

Corresponding Author

*E. Matito. E-mail: ematito@gmail.com.

ORCID

M. Solà: 0000-0002-1917-7450

J. M. Ugalde: 0000-0001-8980-9751

E. Matito: 0000-0001-6895-4562

Notes

The authors declare no competing financial interest.

■ ACKNOWLEDGMENTS

This research has been funded by the Spanish MINECO/FEDER Projects CTQ2014-52525-P (E.M.), CTQ2017-85341-P (M.S.), CTQ2015-67608-P (X.L.), CTQ2015-67660-P (J.M.U.), and EUIN2017-88605 (E.M.), the Basque Country Consolidated Group Project No. IT588-13, the Generalitat de Catalunya (Project 2014SGR931, Xarxa de Referència en Química Teòrica i Computacional, and the ICREA Academia 2014 prize (M.S.)). The FEDER grant UNGI10-E10-801 (European fund for Regional Development) has also supported this research. M.R.M. acknowledges the Spanish Ministry of Education, Culture and Sports for the doctoral grant FPU-2013/00176 and M.V.N. the Spanish Ministry of Economy, Industry and Competitiveness (MINECO) for the doctoral grant BES-2015-072734. The authors acknowledge the computational resources and technical and human support provided by the DIPC and the SGI/IZO-SGIker UPV/EHU.

■ REFERENCES

(1) Marcelin, M. R. Contribution à l'étude de la cinétique physico-chimique. *Ann. Phys.* **1915**, *9*, 120−231.

(2) Coulson, C. A. The electronic structure of some polyenes and aromatic molecules. VII. Bonds of fractional order by the molecular orbital method. *Proc. R. Soc. London, Ser. A* **1939**, *169*, 428.

(3) Mulliken, R. S. Electronic Population Analysis on LCAO-MO Molecular Wavefunctions. *J. Chem. Phys.* **1955**, *23*, 1833−1840.

(4) Daudel, R. *Quantum Theory of The Chemical Bond*; Reidel: Dordrecht, The Netherlands, 1974.

(5) Bader, R. F. W. *Atoms in Molecules: A Quantum Theory*; Oxford University Press: Oxford, 1990.

(6) Lewis, G. N. The Atom and the Molecule. *J. Am. Chem. Soc.* **1916**, *38*, 762−786.

(7) Bader, R. F. W.; Stephens, M. E. Fluctuation and correlation of electrons in molecular systems. *Chem. Phys. Lett.* **1974**, *26*, 445−449.

(8) Bader, R. F. W.; Stephens, M. E. Spatial localization of the electronic pair and number distributions in molecules. *J. Am. Chem. Soc.* **1975**, *97*, 7391−7399.

(9) Fradera, X.; Austen, M. A.; Bader, R. F. W. The Lewis Model and Beyond. *J. Phys. Chem. A* **1999**, *103*, 304−314.

(10) Becke, A. D.; Edgecombe, K. E. A simple mesure of electron localization in atomic and molecular systems. *J. Chem. Phys.* **1990**, *92*, 5397−5403.

(11) Ponec, R.; Strnad, M. Population analysis of pair densities: A link between quantum chemical and classical picture of chemical structure. *Int. J. Quantum Chem.* **1994**, *50*, 43−53.

(12) Ponec, R. Electron pairing and chemical bonds. Chemical structure, valences and structural similarities from the analysis of the Fermi holes. *J. Math. Chem.* **1997**, *21*, 323−333.

(13) Silvi, B. The Spin Pair Compositions as Local Indicators of the Nature of the Bonding. *J. Phys. Chem. A* **2003**, *107*, 3081−3085.

(14) Matito, E.; Solà, M.; Salvador, P.; Duran, M. Electron sharing indexes at the correlated level. Application to aromaticity calculations. *Faraday Discuss.* **2007**, *135*, 325−345.

(15) Matito, E.; Silvi, B.; Duran, M.; Solà, M. Electron localization function at the correlated level. *J. Chem. Phys.* **2006**, *125*, 024301.

(16) Francisco, E.; Martín Pendás, A.; Blanco, M. A. Electron number probability distributions for correlated wave functions. *J. Chem. Phys.* **2007**, *126*, 094102.

(17) Matito, E.; Solà, M. The role of electronic delocalization in transition metal complexes from the electron localization function and the quantum theory of atoms in molecules viewpoints. *Coord. Chem. Rev.* **2009**, *253*, 647−665.

(18) Kohout, M. A Measure of Electron Localizability. *Int. J. Quantum Chem.* **2004**, *97*, 651−658.

(19) Matito, E.; Poater, J.; Solà, M.; Duran, M.; Salvador, P. Comparison of the AIM Delocalization Index and the Mayer and Fuzzy Atom Bond Orders. *J. Phys. Chem. A* **2005**, *109*, 9904−9910.

(20) Feixas, F.; Matito, E.; Duran, M.; Solà, M.; Silvi, B. Electron localization function at the correlated level: a natural orbital formulation. *J. Chem. Theory Comput.* **2010**, *6*, 2736−2742.

(21) Ponec, R.; Cooper, D. L.; Savin, A. Analytic Models of Domain-Averaged Fermi Holes: A New Tool for the Study of the Nature of Chemical Bonds. *Chem. - Eur. J.* **2008**, *14*, 3338−3345.

(22) Löwdin, P.-O. Quantum theory of many-particle systems. I. Physical interpretations by means of density matrices, natural spin-orbitals, and convergence problems in the method of configurational interaction. *Phys. Rev.* **1955**, *97*, 1474−1489.

(23) Born, M. Quantenmechanik der stoßvorgänge. *Eur. Phys. J. A* **1926**, *38*, 803−827.

(24) Coulson, C. A.; Neilson, A. H. Electron correlation in the ground state of helium. *Proc. Phys. Soc., London* **1961**, *78*, 831−837.

(25) McWeeny, R. Some recent advances in density matrix theory. *Rev. Mod. Phys.* **1960**, *32*, 335−369.

(26) Bochicchio, R. C.; Ponec, R.; Lain, L.; Torre, A. On the Physical Meaning of Bond Indices from the Population Analysis of Higher Order Densities. *J. Phys. Chem. A* **1998**, *102*, 7176−7180.

(27) Ponec, R.; Roithova, J. Domain-averaged Fermi holes - a new means of visualization of chemical bonds. Bonding in hypervalent molecules. *Theor. Chem. Acc.* **2001**, *105*, 383−392.

(28) Blanco, M. A.; Martín Pendás, A.; Francisco, E. Interacting quantum atoms: a correlated energy decomposition scheme based on the quantum theory of atoms in molecules. *J. Chem. Theory Comput.* **2005**, *1*, 1096−1109.

(29) Francisco, E.; Martín Pendás, A.; Blanco, M. A. A molecular energy decomposition scheme for atoms in molecules. *J. Chem. Theory Comput.* **2006**, *2*, 90−102.

(30) Mayer, I.; Hamza, A. Energy decomposition in the topological theory of atoms in molecules and in the linear combination of atomic orbitals formalism: a note. *Theor. Chem. Acc.* **2001**, *105*, 360−364.

(31) Salvador, P.; Duran, M.; Mayer, I. One-and two-center energy components in the atoms in molecules theory. *J. Chem. Phys.* **2001**, *115*, 1153−1157.

(32) Vyboishchikov, S. F.; Salvador, P.; Duran, M. Density functional energy decomposition into one-and two-atom contributions. *J. Chem. Phys.* **2005**, *122*, 244110.

(33) Tognetti, V.; Joubert, L. Density functional theory and Bader's atoms-in-molecules theory: towards a vivid dialogue. *Phys. Chem. Chem. Phys.* **2014**, *16*, 14539−14550.

(34) Salvador, P.; Mayer, I. Energy partitioning for "fuzzy" atoms. *J. Chem. Phys.* **2004**, *120*, 5046−5052.
(35) Ruiz, I.; Matito, E.; Holguín-Gallego, F. J.; Francisco, E.; Pendás, Á. M.; Rocha-Rinza, T. Fermi and Coulomb correlation effects upon the interacting quantum atoms energy partition. *Theor. Chem. Acc.* **2016**, *135*, 209.
(36) Mayer, I.; Matito, E. Calculation of local spins for correlated wave functions. *Phys. Chem. Chem. Phys.* **2010**, *12*, 11308−11314.
(37) Ramos-Cordoba, E.; Matito, E.; Mayer, I.; Salvador, P. Toward a Unique Definition of the Local Spin. *J. Chem. Theory Comput.* **2012**, *8*, 1270−1279.
(38) Ramos-Cordoba, E.; Matito, E.; Salvador, P.; Mayer, I. Local spins: improved Hilbert-space analysis. *Phys. Chem. Chem. Phys.* **2012**, *14*, 15291−15298.
(39) Ramos-Cordoba, E.; Salvador, P.; Piris, M.; Matito, E. Two new constraints for the cumulant matrix. *J. Chem. Phys.* **2014**, *141*, 234101.
(40) Thakkar, A. J.; Tripathi, A.; Smith, V. H., Jr Molecular x-ray- and electron-scattering intensities. *Phys. Rev. A: At., Mol., Opt. Phys.* **1984**, *29*, 1108.
(41) Thakkar, A. J.; Tripathi, A.; Smith, V. H. Anisotropic electronic intracule densities for diatomics. *Int. J. Quantum Chem.* **1984**, *26*, 157−166.
(42) Watanabe, N.; Kamata, Y.; Yamaguchi, K.; Udawa, Y.; Miller, T. Calculation of X-ray scattering intensities by means of the coupled cluster singles and doubles model. *J. Comput. Chem.* **2001**, *22*, 1315−1320.
(43) Curl, R. F.; Coulson, C. A. Coulomb hole in the ground state of two electron atoms. *Proc. Phys. Soc., London* **1965**, *85*, 647−652.
(44) Boyd, R. F.; Coulson, C. A. Coulomb hole in some excited states of helium. *J. Phys. B: At. Mol. Phys.* **1973**, *6*, 782−793.
(45) Boyd, R. J.; Sarasola, C.; Ugalde, J. M. Intracule densities and electron correlation in the hydrogen molecule. *J. Phys. B: At., Mol. Opt. Phys.* **1988**, *21*, 2555.
(46) Besley, N. A.; Gill, P. W. Atomic and molecular intracules for excited states. *J. Chem. Phys.* **2004**, *120*, 7290−7297 (and references therein).
(47) Fradera, X.; Duran, M.; Mestres, J. The relevance of the Laplacian of intracule and extracule density distributions for analyzing electron−electron interactions in molecules. *J. Chem. Phys.* **1997**, *107*, 3576−3583.
(48) Fradera, X.; Duran, M.; Mestres, J. The mapping of the local contributions of Fermi and Coulomb correlation into intracule and extracule density distributions. *J. Chem. Phys.* **2000**, *113*, 2530−2543.
(49) Fradera, X.; Sarasola, C.; Ugalde, J. M.; Boyd, R. J. The topological features of the intracule density of the uniform electron gas. *Chem. Phys. Lett.* **1999**, *304*, 393−398.
(50) Ugalde, J. M.; Sarasola, C.; Dominguez, L.; Boyd, R. J. The evaluation of electronic extracule and intracule densities and related probability functions in terms of Gaussian basis functions. *J. Math. Chem.* **1991**, *6*, 51−61.
(51) Sarasola, C.; Ugalde, J. M.; Boyd, R. J. The evaluation of extracule and intracule densities in the first-row hydrides, LiH, BeH, BH, CH, NH, OH and FH, from self-consistent field molecular orbital wavefunctions. *J. Phys. B: At., Mol. Opt. Phys.* **1990**, *23*, 1095.
(52) Sarasola, C.; Dominguez, L.; Aguado, M.; Ugalde, J. The Laplacian of the intracule and extracule densities and their relationship to the shell structure of atoms. *J. Chem. Phys.* **1992**, *96*, 6778−6783.
(53) Rodríguez-Mayorga, M.; Ramos-Cordoba, E.; Via-Nadal, M.; Piris, M.; Matito, E. Comprehensive benchmarking of density matrix functional approximations. *Phys. Chem. Chem. Phys.* **2017**, *19*, 24029−24041.
(54) Via-Nadal, M.; Rodríguez-Mayorga, M.; Matito, E. A Salient Signature of van der Waals Interactions. *Phys. Rev. A: At., Mol., Opt. Phys.* **2017**, *96*, 050501.
(55) Via-Nadal, M.; Rodríguez-Mayorga, M.; Ramos-Cordoba, E.; Matito, E. Singling out Weak and Strong Correlation, submitted for publication.
(56) Piris, M.; Lopez, X.; Ugalde, J. Correlation holes for the helium dimer. *J. Chem. Phys.* **2008**, *128*, 134102.
(57) Gori-Giorgi, P.; Seidl, M.; Savin, A. Intracule densities in the strong-interaction limit of density functional theory. *Phys. Chem. Chem. Phys.* **2008**, *10*, 3440−3446.
(58) Cioslowski, J.; Liu, G. Topology of electron-electron interactions in atoms and molecules. II. The correlation cage. *J. Chem. Phys.* **1999**, *110*, 1882−1887.
(59) Rodríguez-Mayorga, M.; Ramos-Cordoba, E.; Lopez, X.; Solà, M.; Ugalde, J. M.; Matito, E. The Coulomb Hole of the Ne Atom, submitted for publication.
(60) Mercero, J. M.; Valderrama, E.; Ugalde, J. M. In *Metal-Ligand Interactions*; Russo, N., Salahub, D. R., Witko, M., Eds.; Kluwer Academic Publishers: The Netherlands, 2003; pp 205−239.
(61) Mercero, J. M.; Rodríguez-Mayorga, M.; Matito, E.; Lopez, X.; Ugalde, J. M. The electron-pair density distribution of the $^{1,3}\Pi_u$ excited states of H_2. *Can. J. Chem.* **2016**, *94*, 998−1001.
(62) Piris, M.; Lopez, X.; Ugalde, J. M. Electron-pair density relaxation holes. *J. Chem. Phys.* **2008**, *128*, 214105.
(63) Eddington, A. S. *Fundamental theory*; Cambridge University Press: Cambridge, 1946.
(64) Ramos-Cordoba, E.; Salvador, P.; Matito, E. Separation of dynamic and nondynamic correlation. *Phys. Chem. Chem. Phys.* **2016**, *18*, 24015−24023.
(65) Ramos-Cordoba, E.; Matito, E. Local Descriptors of dynamic and nondynamic correlation. *J. Chem. Theory Comput.* **2017**, *13*, 2705−2711.
(66) Müller, A. M. K. Explicit approximate expression between reduced two- and one-particle density matrices. *Phys. Lett. A* **1984**, *105*, 446−452.
(67) Buijse, M. A. Thesis: Electron Correlation. Fermi and Coulomb holes, dynamical and nondynamical correlation. *Ph.D. thesis*, Vrije Universiteit, Amsterdam, The Netherlands, 1991.
(68) Helgaker, T.; Jorgensen, P.; Olsen, J. *Molecular Electronic Structure Theory*; Wiley: Chichester, 2000.
(69) Chávez-Calvillo, R.; García-Revilla, M.; Francisco, E.; Martín Pendás, A.; Rocha-Rinza, T. Dynamical correlation within the Interacting Quantum Atoms method through coupled cluster theory. *Comput. Theor. Chem.* **2015**, *1053*, 90−95.
(70) Holguín-Gallego, F. J.; Chávez-Calvillo, R.; García-Revilla, M.; Francisco, E.; Martín Pendás, A.; Rocha-Rinza, T. Electron correlation in the interacting quantum atoms partition via coupled-cluster lagrangian densities. *J. Comput. Chem.* **2016**, *37*, 1753−1765.
(71) Wang, Y. G.; Matta, C.; Werstiuk, N. H. Comparison of localization and delocalization indices obtained with Hartree−Fock and conventional correlated methods: Effect of Coulomb correlation. *J. Comput. Chem.* **2003**, *24*, 1720−1729.
(72) García-Revilla, M.; Francisco, E.; Costales, A.; Martín Pendás, A. Performance of the density matrix functional theory in the quantum theory of atoms in molecules. *J. Phys. Chem. A* **2012**, *116*, 1237−1250.
(73) Feixas, F.; Vandenbussche, J.; Bultinck, P.; Matito, E.; Solà, M. Electron delocalization and aromaticity in low-lying excited states of archetypal organic compounds. *Phys. Chem. Chem. Phys.* **2011**, *13*, 20690−20703.
(74) Piris, M.; Ugalde, J. Perspective on natural orbital functional theory. *Int. J. Quantum Chem.* **2014**, *114*, 1169−1175.
(75) Cioslowski, J.; Piris, M.; Matito, E. Robust validation of approximate 1-matrix functionals with few-electron harmonium atoms. *J. Chem. Phys.* **2015**, *143*, 214101.
(76) Pernal, K.; Giesbertz, K. J. H. Reduced Density Matrix Functional Theory (RDMFT) and Linear Response Time-Dependent RDMFT (TD-RDMFT). *Top. Curr. Chem.* **2015**, *368*, 125−183.
(77) Buijse, M. A.; Baerends, E. J. An approximate exchange-correlation hole density as a functional of the natural orbitals. *Mol. Phys.* **2002**, *100*, 401−421.
(78) Knowles, P. J.; Handy, N. C. A new determinant-based full configuration interaction method. *Chem. Phys. Lett.* **1984**, *111*, 315−321.
(79) Knowles, P. J.; Handy, N. C. A determinant based full configuration interaction program. *Comput. Phys. Commun.* **1989**, *54*, 75.

DOI: 10.1021/acs.jpca.7b12556
J. Phys. Chem. A 2018, 122, 1916−1923

(80) Frisch, M. J. et al.. *Gaussian 09* Revision D.01; Gaussian Inc.: Wallingford, CT, 2009.
(81) Matito, E.; Feixas, F. *DMn program*; University of Girona (Spain) and University of Szczecin (Poland), 2009.
(82) Feixas, F.; Solà, M.; Barroso, J. M.; Ugalde, J. M.; Matito, E. New Approximation to the Third-Order Density. Application to the Calculation of Correlated Multicenter Indices. *J. Chem. Theory Comput.* **2014**, *10*, 3055−3065.
(83) Rodríguez-Mayorga, M. *RHO2-OPS: 2-DM Operations*; Institute of Computational Chemistry and Catalysis, University of Girona: Catalonia, Spain,.
(84) Cioslowski, J.; Liu, G. Fast evaluation of electron intracule and extracule densities on large grids of points. *J. Chem. Phys.* **1996**, *105*, 4151−4158.
(85) Rodríguez-Mayorga, M.; Ramos-Cordoba, E.; Salvador, P.; Solà, M.; Matito, E. Bonding description of the Harpoon Mechanism. *Mol. Phys.* **2016**, *114*, 1345.
(86) Martín Pendás, A.; Blanco, M. A.; Costales, A.; Mori Sánchez, P.; Luaña, V. Non-nuclear Maxima of the Electron Density. *Phys. Rev. Lett.* **1999**, *83*, 1930−1933.
(87) Postils, V.; Garcia-Borrás, M.; Solà, M.; Luis, J. M.; Matito, E. *Chem. Commun.* **2015**, *51*, 4865−4868.

DOI: 10.1021/acs.jpca.7b12556
J. Phys. Chem. A 2018, 122, 1916−1923

Supporting Information

Electron-Pair Distribution in Chemical Bond Formation

M. Rodríguez-Mayorga,[†,‡] M. Via-Nadal,[†] M. Solà,[‡]

J. M. Ugalde,[†] X. Lopez,[†] and E. Matito[*,†,¶]

†*Kimika Fakultatea, Euskal Herriko Unibertsitatea, UPV/EHU, and Donostia International Physics Center (DIPC). P.K. 1072, 20080 Donostia, Euskadi, Spain*

‡*Institut de Química Computacional i Catàlisi (IQCC) and Departament de Química, University of Girona, 17071 Girona, Catalonia, Spain*

¶*IKERBASQUE, Basque Foundation for Science, 48013 Bilbao, Euskadi, Spain.*

E-mail: ematito@gmail.com

1 Potential Energy Curves

1.1 Reference

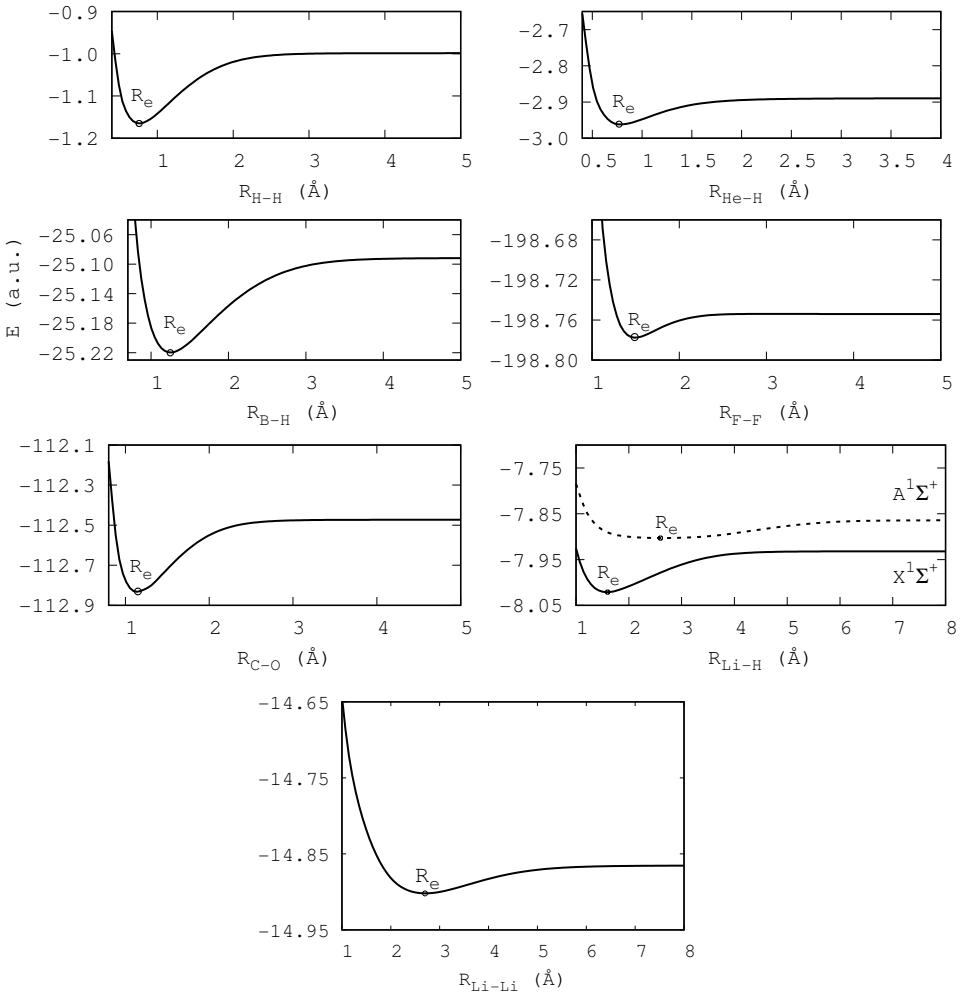

Figure S1: Potential energy curves for all systems studied obtained with FCI or CASSCF.

1.2 CCSD

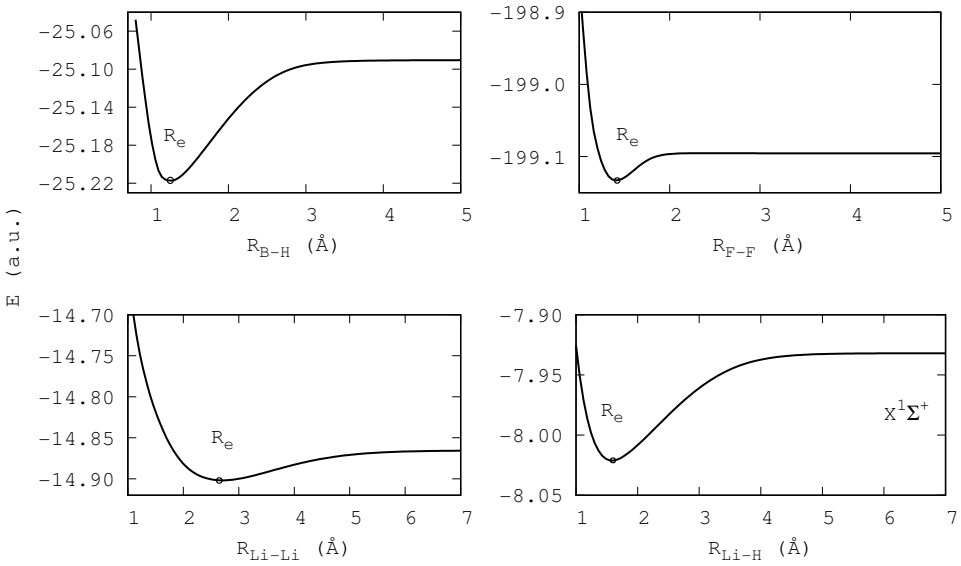

Figure S2: Potential energy curves obtained with CCSD.

2 $\Delta[\Delta h(u)]$

Analysis of the error between the reference $\Delta h(u)$ and the approximated one $\tilde{\Delta} h(u)$, obtained from CCSD or CASSCF natural occupancies using the MBB approximation.

$$\Delta[\Delta h(u)] = \tilde{\Delta} h(u) - \Delta h(u) \tag{1}$$

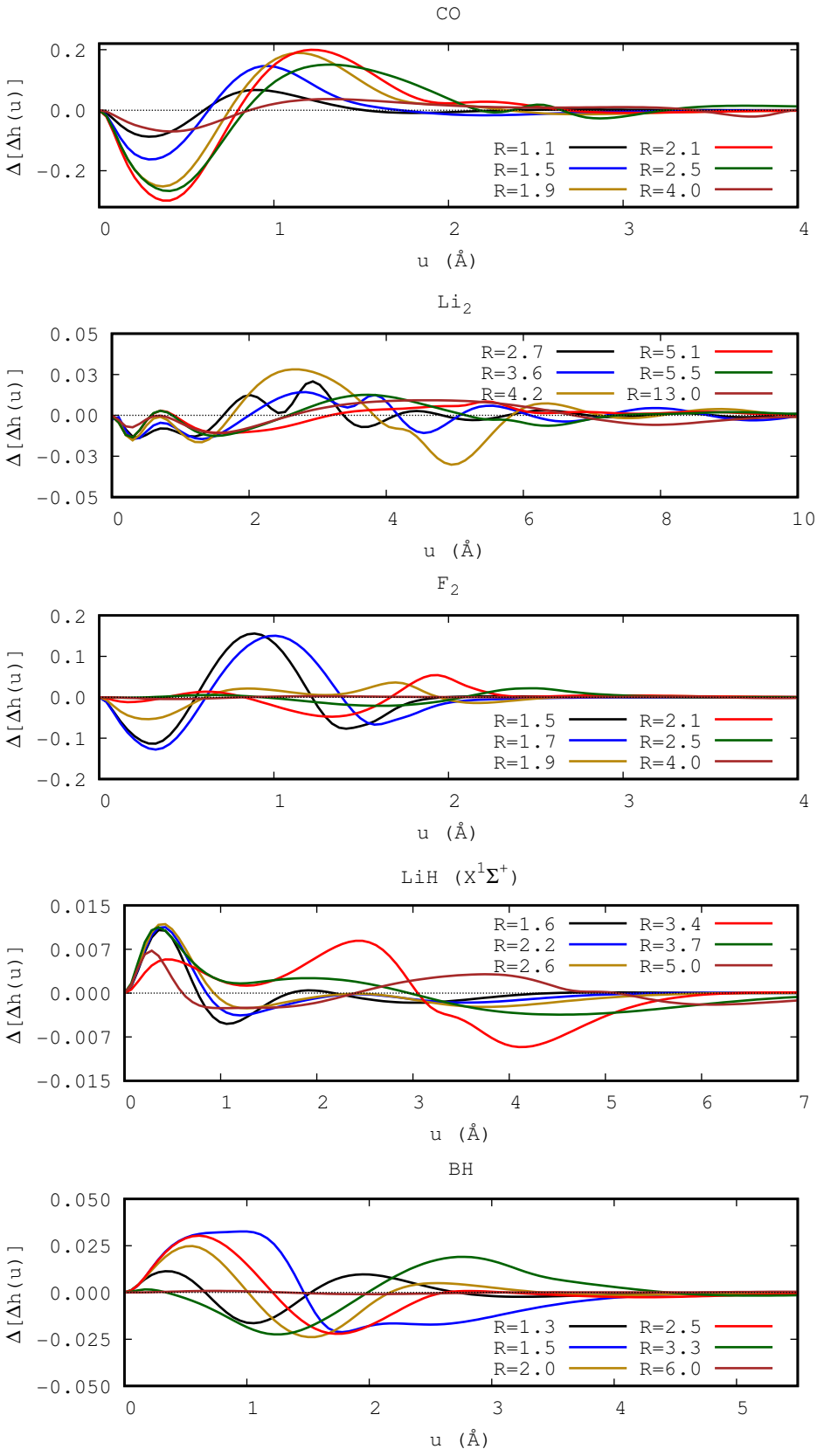

Figure S3: $\Delta[\Delta h(u)]$ using MBB and natural orbital occupancies. CCSD natural occupancies were used in all cases but CO, for which CASSCF natural occupancies were employed.

In Fig. S3 we observe small differences between the exact and approximate $\Delta h(u)$. F_2 presents the largest deviations because CCSD involves many more non-zero natural orbital occupancies than CASSCF (for which only the active space orbitals are correlated).

3 Computational saving using the approximation

Table S1 collects the memory needs to store the second order reduced density matrix (2-RDM). As we can observe the memory requirements are very similar for small molecules, but as the size of the *exact* 2-RDM matrix grows, the size of the approximate 2-RDM reduces significantly. The larger the memory matrix, the larger computational time needed to perform the calculation of the relaxation hole.

Table S1: Average memory in Kb required to store the *exact* and the approximate 2-RDM for the studied systems.

	Memory in Kb	
Molecule	FCI/CASSCF	CCSD or CASSCF in MBB
H_2	76	60
HeH^+	270	260
LiH	3900	3400
BH	75000	20000
Li_2	2500	1900
F_2	30	100
CO	4000	3200

VII) Some Feature of the Coulomb Hole of Neon Atom

7.1) The Coulomb Hole of the Ne Atom

The Coulomb Hole of the Ne atom

Mauricio Rodríguez-Mayorga,[1,2] Eloy-Ramos-Cordoba,[1,3]
Xabier Lopez,[1] Miquel Solà,[2] Jesus M. Ugalde,[1] and Eduard Matito[1,4*]
[1]*Kimika Fakultatea, Euskal Herriko Unibertsitatea (UPV/EHU), and Donostia International Physics Center (DIPC), P.K. 1072, 20080 Donostia, Euskadi, Spain.*
[2]*Institut de Química Computacional i Catàlisi (IQCC) and Departament de Química, University of Girona, C/ Maria Aurèlia Capmany, 69, 17003 Girona, Catalonia, Spain,*
[3]*Department of Chemistry, University of California Berkeley, Berkeley, USA and*
[4]*IKERBASQUE, Basque Foundation for Science, 48011 Bilbao, Euskadi, Spain.*

We analyze the Coulomb hole of Ne from highly-accurate CISD wave functions obtained from optimized even-tempered basis sets. Using a two-fold extrapolation procedure we obtain highly accurate results that recover 97% of the correlation energy. We confirm the existence of a shoulder in the short-range region of the Coulomb hole of the Ne atom, which is due to the correlation of the core electrons in the K shell. The feature is not displayed in the Coulomb hole calculated with certain basis sets, such as the cc-pVnZ basis set of Dunning, proving that a proper description of the core electrons requires the usage of, at least, the cc-pCVnZ basis set. The shoulder is due to an internal reorganization of the K shell, where electrons are pushed towards the K-shell boundary. A short-range feature of the Coulomb hole is not exclusive to Ne atom and it is also present in most of second-row atoms, suggesting that it is due to the core correlation effects.

I. INTRODUCTION

Electron correlation is still a central problem in physics and chemistry. Its study often provides physical insights to develop new computational methods to tackle the electronic structure of molecules. The primitive description provided by the Hartree-Fock (HF) wave function has been improved by consideration of different types of electron correlation, such as dynamic and nondynamic correlation, in the so-called post-HF methods as well as in methods that do not employ wave functions, such as the density and reduced-density matrix functional theories (DFT[1] and RDMFT[2–4]). The improvement of computational methods, the correct choice of a computational protocol to address a given problem, and our understanding of the electron correlation, hinge on the development of appropriate descriptors of electron correlation.[5–13] Lately, our efforts have concentrated in this direction, resulting in the development of simple electron correlation descriptors capable of separating dynamic and nondynamic correlation.[10–12]

The Coulomb hole stands among the classical descriptors that are used to study the electron correlation due to its conceptual simplicity and its connection with the electron-electron interaction energy.[14–17] The Coulomb hole provides a practical picture of how the electron correlation affects the interelectronic separation. Namely, it reflects the change of the electron-electron distance distribution upon the inclusion of electron correlation. From this quantity the correlation effects on the average interelectronic distance, its variance, and the electron-electron repulsion are easily assessed. The topological features of the Coulomb hole have also been studied, leading to some relevant conclusions about the nature of electron correlation.[18–20] Some of us have also recently used the long-range part of the Coulomb hole to characterize van der Waals interactions.[12,21]

In this work, we analyze a key feature of the Coulomb hole of the Ne atom that, thus far, has been largely ignored by many quantum mechanics practitioners. In 1969, Bunge and coworkers identified a shoulder structure in the short-range part of the Coulomb hole of the Ne atom,[22] which was corroborated by Cioslowski and Liu thirty years later.[23] Bunge attributed this peculiarity to the K-shell electrons, whereas Cioslowski did not comment on this feature. We have found that the shoulder is very sensible to the quality of the basis sets employed in the calculation, turning into a mininum or vanishing depending on the basis set. In order to confirm the presence of the shoulder we have performed CISD and FCI calculations employing large optimized even-tempered basis sets, which provide energy estimates that compare well with the most accurate values obtained by Bunge.[22,24–26] Our results provide a thorough study on the origin of the shoulder, identifying the causes that are responsible for its presence. Finally, we prove that this feature is not exclusive to Ne atom.

II. METHODOLOGY

There are two different ways to define correlation holes: McWeeny's[15] and Coulson's.[14] The former is statistically motivated and it does not employ reference wave functions, whereas Coulson's definition uses HF as the uncorrelated reference. In this work, we are concerned with Coulson's definition, which is connected with an experimental observable. Coulson's Coulomb hole is obtained from the difference between the exact and the HF intracule densities. The radial intracule density provides a distribution of the electron-electron distances,

$$I(u) = \int\int d\mathbf{r}_1 d\mathbf{r}_2\, n_2(\mathbf{r}_1,\mathbf{r}_2)\delta(u - r_{12})\,, \qquad (1)$$

where $n_2(\mathbf{r}_1, \mathbf{r}_2)$ is the pair density and r_{12} is the module of the intracule coordinate, $\mathbf{r}_{12} = \mathbf{r}_1 - \mathbf{r}_2$.

Recall that the electron correlation hole studied in the present work differs from the exchange-correlation hole of Kohn-Sham DFT.[27] The latter represents the rearrangement of a test electron's density arround a reference electron due to the DFT exchange-correlation, which includes some non negligible excess kinetic energy contribution. Our intracule based Coulomb hole averages the position of the reference electron and, consequently, reflects the effect of the electron correlation due to Coulomb like interactions within an averaged electron pair.

The X-ray scattering intensity is essentially determined by the Fourier-Bessel transform of the intracule pair density[28,29] and it is employed in the study of elastic and inelastic scattering of electrons.[22] The total X-ray scattering intensity for short wavelengths is actually governed by the value of the intracule at the coalescence points, $I(0)$.[30]

The difference between the exact pair density and an uncorrelated reference, represents the change in electron pair distribution upon the introduction of electron correlation. Coulson's Coulomb hole[14] sets HF intracule pair density as the uncorrelated reference,

$$h_C(u) = I(u) - I_{\rm HF}(u) \tag{2}$$

giving negative (positive) values for the interelectronic separations u that are increased (decreased) upon the inclusion of correlation. The integration of $h_C(u)$ over u gives zero.

The optimization of the basis sets employs an analoguous procedure to the one developed elsewhere.[31] This procedure has been successfully used to generate highly-accurate basis functions to test model systems and calibrate a number of methods.[31–35] First of all, a family of uncontracted basis sets consisting of spherical Gaussian primitives is constructed by selecting the optimized exponents that minimize the CISD energies (the coefficients that multiply the primitives are equal to 1 and do not enter the optimization procedure). From these values, the complete-basis set (CBS) estimate of Ne CISD energies are obtained by a two-fold extrapolation procedure.

The family of basis sets employs functions with exponents $\zeta^k_{L,N}$ that are even-tempered[36] according to the expression

$$\zeta^k_{L,N} = \alpha_{L,N} \left[\beta_{L,N}\right]^{k-1}, \quad 1 \le k \le N. \tag{3}$$

Each basis set is characterized by the maximum angular momentum, L, and the number of basis functions for each function type, N. For instance, 6SP ($L = 1, N = 6$) basis set consists of six groups of functions containing one S and three P functions (p_x, p_y and p_z) sharing the same exponent. The exponent assigned to each group is given by k in Eq.3, which runs from 1 to N. $\alpha_{L,N}$ and $\beta_{L,N}$ are, therefore, unique for each basis set and determined by minimization of the CISD energy of Ne with a simplex method (minimal accuracy 10^{-7} a.u.). The family includes basis sets with angular momentum between 0 and L ($1 \le L \le 4$) and involve equal numbers N ($6 \le N \le 16$) of spherical Gaussian primitives with exponents $\zeta^k_{L,N}$, giving rise to 44 different basis sets.

The computed energies $E_{L,N}$ have been extrapolated to the respective $N \to \infty$ limits E_L by fitting the actual energy values for $N = 12, 13, 14, 15$ and 16 with the double-exponential expression

$$E_{L,N} = E_L + a_L e^{-\alpha_{L,N} N} + b_L e^{-\beta_{L,N} N}, \tag{4}$$

which generalizes the Dunning extrapolation.[37] The resulting system of five non-linear equations has been solved analytically with Mathematica[38] employing the Ramanujan algorithm.[39]

In turn, the estimates E_L have been extrapolated to the respective CBS limits E by fitting the values of E_L for $L = 2, 3$, and 4 to the expression[40–42]

$$E_L = E + \frac{B}{[L+1]^3}. \tag{5}$$

These extrapolations, E_L and E, provide lower-energy estimates of the total energy that are not variational.

In the case of HF, the energy results are almost converged using only S and P basis functions. Therefore, we take the SP-energy limit as a good estimate of the CBS-extrapoled result. The numerical estimate is obtained from $N = 16, 17, 18, 19$ and 20 calculations applying the fitting of Eq. 5.

The full-configuration interaction (FCI) calculations have been carried out with a modified version of the FCI program of Knowles and Handy[43] and the CISD calculations have been performed with Gaussian.[44] The calculations of the second-order reduced density matrices (2-RDM) have been calculated from the FCI/CISD expansions coefficients using the in-house DMN code.[45,46] The radial intracule density was computed with the in-house RHO2_OPS code,[47] which uses the algorithm proposed by Cioslowski and Liu.[48]

III. RESULTS

A. Benchmark data

Following the procedure described in the previous section we have obtained a CISD extrapolated energy of -128.9254609 a.u., which represents an energy lowering of -0.0143843 a.u. with respect to the best variational estimate, $E_{4,16}$ (see Table I). These results compare well with the best non-relativistic FCI estimate available in the literature, -128.937588 a.u.[26]

Our CISD SPDF-energy limit, -128.8984284 a.u., is in good agreement with the FCI value -128.897 ± 0.002 a.u. calculated by Bunge.[24] This and the other partial waves reported in Table I are also in accord with the second-order correlation energies of Lindgren and Salomonson.[49]

TABLE I. CISD energies (a.u.) for the basis set family developed in this work and the corresponding partial waves.

N	$E_{1,N}$	$E_{2,N}$	$E_{3,N}$	$E_{4,N}$
5	-127.8146757	-127.9311638	-127.9638254	-127.9755176
6	-128.3326841	-128.4543077	-128.4887366	-128.5010355
7	-128.5692718	-128.6923709	-128.7272631	-128.7395973
8	-128.6612022	-128.7855792	-128.8209903	-128.8335145
9	-128.6987672	-128.8240698	-128.8598984	-128.8725885
10	-128.7176209	-128.8433421	-128.8794251	-128.8922251
11	-128.7265782	-128.8526131	-128.8888882	-128.9017858
12	-128.7304973	-128.8567898	-128.8932237	-128.9062091
13	-128.7323966	-128.8588808	-128.8954410	-128.9085010
14	-128.7334758	-128.8600836	-128.8967326	-128.9098489
15	-128.7340477	-128.8607425	-128.8974582	-128.9106198
16	-128.7343430	-128.8611063	-128.8978764	-128.9110766
∞	-128.7346499	-128.8615534	-128.8984284	-128.9117007

Our extrapolated HF energy, −128.547100 a.u., which also corresponds to the SP-energy limit, is in excellent agreement with the numerical HF results, −128.547098 a.u., reported elsewhere.[50] Our best CISD estimate of the correlation energy is, therefore, −0.378361 a.u., which represents 97% of the correlation energy of Ne.[51] Our best variational estimate of the correlation energy, based on the CISD/16SPDFG calculation (including 400 basis functions), recovers 93% of the correlation energy. Our calculations on the angular and the radial correlation[52] indicators of Kutzelnigg[53] show no qualitivative improvement in the description of correlation beyond the 11SPDF basis set (see Figs. S1 and S2) and Bunge and coworkers report very small effects upon introduction of the triple and quadruple excitations (less than 0.01% change on the density).[54] Therefore, we conclude that our CISD calculations provide an accurate description of electron correlation in Ne.

We have also explored the convergence of certain properties related to the Coulomb hole with the size of the basis set. Our results indicate that the average interelectronic distance and its variance are much more affected by the number of basis functions than by the inclusion of functions of large angular momentum. In this respect, the use of 9SP basis functions provides a reasonable description of these indicators (see Figs. S3 and S4). For this reason, we have chosen the CISD/9SP wave function to provide a qualitative explanation of the Coulomb hole in Ne atom. In some selected cases, analysis with larger basis sets have been performed to confirm our conclusions.

B. The Coulomb hole of the Ne atom

In his seminal paper, Bunge[22] reported a small shoulder of the Coulomb hole of Ne in the short interelectronic distances domain that he attributed to the electron correlation within the K-shell. This calculation was based on a FCI wave function that yield an electronic energy of −128.8602 a.u. and, thus, only retrieved 85% of the correlation energy.[24] Thirty years later, Cioslowski and Liu confirmed this result using 2-RDMs obtained from energy derivatives of MP2 calculations with a non-optimized even-tempered basis set of 50 functions ($20s10p$).[23] We have tried to reproduce the results of Bunge and Cioslowski and have encountered a major difficulty choosing the appropriate basis set. We have performed over hundred CISD calculations (and some FCI calculations as well) using different basis with and without the frozen core approximation, finding that the shoulder is only reproduced in about half of the cases (see Tables S1 and S2). No frozen-core calculation could reproduce the shoulder structure regardless the size of the basis set, supporting the idea that this feature, if real, is a result of the correlation of the core K-shell electrons. The basis set families show similar results among its members. Pople's 6-311G and larger basis of this family as well as the first family of basis sets developed by Dunning (nZ) and the core correlated-consistent basis sets cc-pCVnZ display the shoulder structure.[55,56] Conversely, the family of correlated-consistent basis sets of Dunning[57] (cc-pVnZ) and the series of basis sets of Petersson[58] (nZaP) cannot reproduce the shoulder structure (see Fig. 1 for some examples).

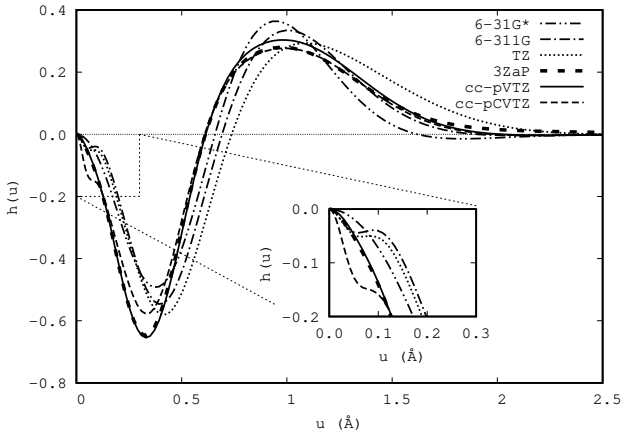

FIG. 1. The CISD Coulomb hole of Ne for some selected basis sets.

In order to solve this controversy, we have built a series of even-tempered basis sets following the procedure described above. For all these basis sets, regardless the size, the shoulder structure shows at ca. 0.1Å (see Fig. 2). For small basis sets, including only S and P functions, the shoulder is actually a minimum, in accord with the

results presented by Cioslowski and Liu that also employed only S and P functions.[23] The shoulder structure, as reported by Bunge and Cioslowski[22,23] shows using S, P and D functions. Augmenting with F functions does not produce a large change, and the addition of G functions barely changes the Coulomb hole, thus suggesting that the presence of the shoulder is not due to a basis set completeness problem (see Fig. 2). Actually, the presence of the shoulder structure was also reported using Monte Carlo calculations.[59] The role of core orbitals is evident because the corresponding frozen-core CISD (fc-CISD) calculations do not show any shoulder structure (see Fig. S5 in the Supporting Information).

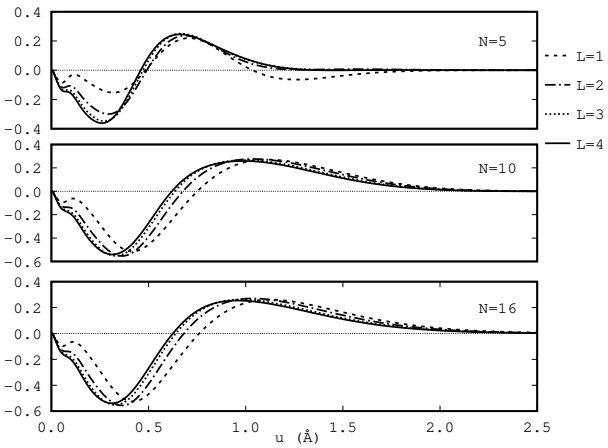

FIG. 2. The CISD Coulomb hole of Ne for some even-tempered basis sets.

C. The origin of the shoulder

In this section we analyze the reasons for the existence of the shoulder in the Coulomb hole of Ne. We have already established that the correlation of core electrons is responsible for it. Let us now consider the importance of different configurations by removing some of them from the CISD expansion calculated with the 9SP basis set. In Fig. 3 we have plotted the Coulomb hole generated with this wave function and other wave functions in which we have deleted various excitations from the core orbital ($1s$). The CISD expansion in which we have removed all the excitations from the core orbital except the single excitations (CISD(nc)+A in Fig. 3) produces a Coulomb hole that is virtually identical to the fc-CISD one. The double excitations involving only one electron in $1s^2$ produce likewise a Coulomb hole qualitatively similar to the fc-CISD wave function (CISD(nc)+B). Among the double excitations the most important ones are those exciting simultaneously both $1s^2$ electrons as evidenced from the shoulder structure of the Coulomb hole of the CISD wave function where only these excitations from the core orbital are retained (CISD(nc)+C). A detailed analysis of the double excitations from the $1s$ orbital shows that the preferred virtual orbitals are $4s$, $5s$, $5p$, and $6p$ (see CISD(nc)+D Coulomb hole in Fig. 3). These results have been qualitatively confirmed with the CISD/16SPDFG wave function (see Fig. S9 in the Supporting Information).

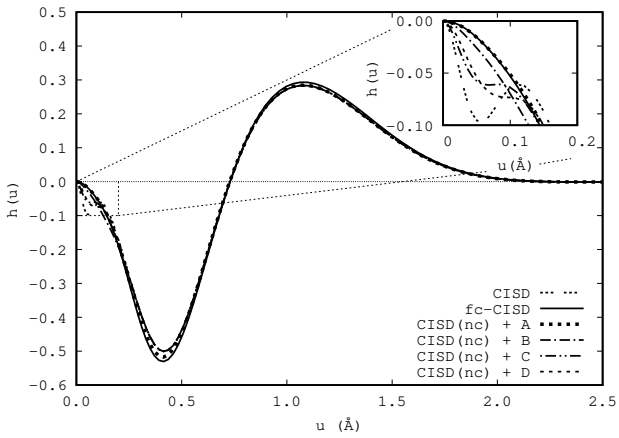

FIG. 3. The CISD/9SP Coulomb hole in terms of several expansions. fc-CISD calculations were obtained from a CISD calculation in which no excitations from core orbitals were allowed, whereas CISD(nc) is a regular CISD calculation in which the configurations involving excitations from the core orbital have been removed *a posteriori*. A-C are groups of configurations including various excitations from the core orbital: (A) single excitations, (B) double excitations involving only one electron in the core orbital, (C) double excitations involving the two electrons in the core orbital excited to one single orbital, and (D) double excitations involving the two electrons in the core orbital excited to orbitals $4s$, $5s$, $5p$ and $6p$. After removal and addition of these configurations, the expansion coefficients have been rescaled to attain the normalization of the wave function.

Fig. 4 plots the Coulomb hole for CISD expansions that only include the HF configuration and some chosen configurations involving excitations from the $1s$ orbital. Unlike the previous CISD expansions, these ones only include correlation effects due to the core electrons in Ne and, therefore, should reflect the importance of certain configurations in retrieving the shoulder. The inclusion of double excitations from the core orbitals gives rise to a hole structure (see HF+E in Fig. 4) that is responsible for the shoulder structure of the complete CISD expansion. From this plot is also evident that double excitations and particularly those involving $4s$, $5s$, $5p$ and $6p$ are mostly responsible for the shoulder structure.

Thus far, we have firmly established that the presence of the shoulder in the Coulomb hole of Ne is due to the electron correlation of the core electrons. In the following, we will analyze how the correlation affects the electronic structure of Ne and the particular role that the core electrons play in this context using the CISD/16SP wave function. First of all, we will con-

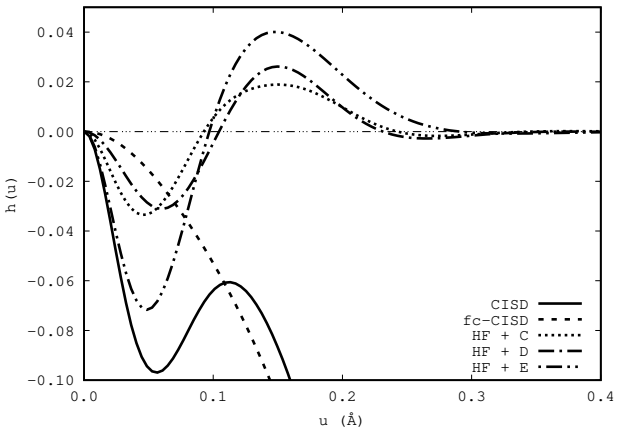

FIG. 4. The CISD/9SP Coulomb hole in terms of several expansions. The groups of configurations allowed involve excitations from the core orbitals to some particular virtual orbitals (see the caption of Fig. 3 for C and D). The E group includes configurations involving double excitations from 1s to all virtual orbitals.

sider the shell-structure of Ne. There has been some controversy in the literature concerning the descriptor that should be employed to identify the shell structure and shell numbers in atoms,[60–62] in our opinion, the one-electron potential (OEP) of Kohout being the most robust suggestion made thus far.[63] According to the OEP, we find that the radius of the K shell does not change upon inclusion of electron correlation effects ($r_K = 0.138$Å) and the K-shell number only increases $3 \cdot 10^{-3}$ electrons due to correlation ($n_K^{\rm HF} = 2.0019$ e.). Therefore, according to the shell structure determined by the OEP, we conclude that electron correlation does not cause an expansion or contraction of the K shell, but a small reorganization within the K shell, pushing some electron density towards the K-shell boundary with the L shell.

We have also checked the convergence of the electron-electron repulsion and the electron-nucleus attraction to see how these quantities are affected by the frozen-core approximation. These energy components show a convergence pattern that alternates fc-CISD results with CISD results, suggesting that wave functions that do not show the shoulder structure do not converge these properties differently (see Figs. S6 and S7). Conversely, as one could expect, we have found that the intracule of the pair density at the coalescence point divided by the charge-concentration index, $\int \rho^2(\mathbf{r}) d\mathbf{r}$,[20,64] is affected by the inclusion of core correlation (see Fig. S8).

Finally, let us assess the type of correlation affecting the shoulder structure. We will use our recently introduced separation of dynamic and nondynamic correlation scheme[10,11] that we have lately extended to separate the correlation in Coulomb holes.[12] In Fig. 5 we can see that the short-range part of the Coulomb hole corresponds mostly to dynamic correlation and that the shoulder structure is also present in this part of the Coulomb hole.

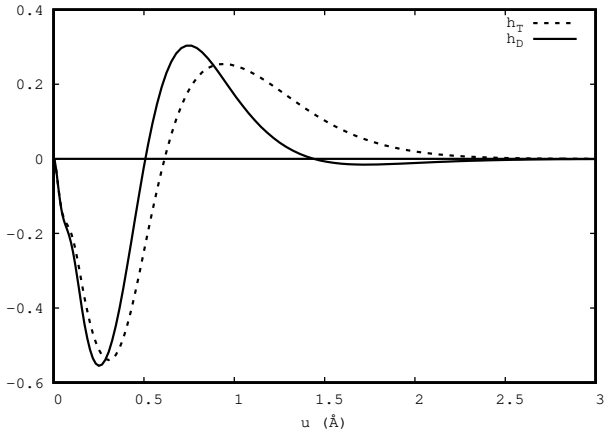

FIG. 5. The dynamic part (h_D) and the total (h_T) Coulomb hole of Ne at the CISD/16SPDFG level of theory.

D. Second-row atoms and molecules.

It is well known that the Coulomb holes of He and Li do not present such a shoulder.[65,66] However, the rest of atoms of the second row in their ground states always some feature is obtained for small interelectronic separations as we shown in Fig. 6 (the complete holes can be found in Fig. S10). In Fig. 6 we plot the Coulomb hole divided by the square of the atomic charge (Z^2) in order to make all the holes fit in the same scale. The Coulomb holes reported for the open-shell systems were obtained using an unrestricted formalism (i.e. they correspond to the difference between the UCISD and the UHF radial intracule densities). Our study reveals that for Be, B and F atoms, a maximum of the Coulomb hole is observed, while for C, N, and O atoms, a shoulder is produced. When fc-CISD wave functions are used the shoulder or the maximum vanish (see Fig. S10), which proves that the features observed correspond to correlation effects of the core $1s^2$ electrons. The analysis of the OEP reveals that in all cases, the radius of the K shell does not change upon inclusion of electron correlation effects, and only an internal small reorganization within the K shell is produced (see Table S4 for more details). Interestingly, the shoulder is also present in the short-range part of the Coulomb hole of noble-gas molecules, such as Ne_2 (see Fig. S12).

IV. CONCLUSIONS

We have analyzed the Coulomb hole of Ne from highly-accurate CISD wave functions. Our energy estimates have been obtained from a two-fold extrapolation of optimized even-tempered basis sets and compare well with the best estimates available in the literature (we recover 97% of the correlation energy of Ne).

We have confirmed the existence of a shoulder in the short-range region of the Coulomb hole of the Ne atom, which is due to the correlation of the core electrons in the K shell. Double excitations from the core orbital give rise to the most important configurations in the CISD expansion that contribute to the shoulder. The shoulder is due to an internal reorganization of the K shell, where electrons are pushed towards the K-shell boundary. The correlation nature of the shoulder is dynamic, as one would expect.

The feature is not displayed in the Coulomb hole calculated with certain basis sets, such as the cc-pVnZ basis set of Dunning, proving that a proper description of the core electrons requires the usage of, at least, the core correlated-consistent cc-pCVnZ basis set.

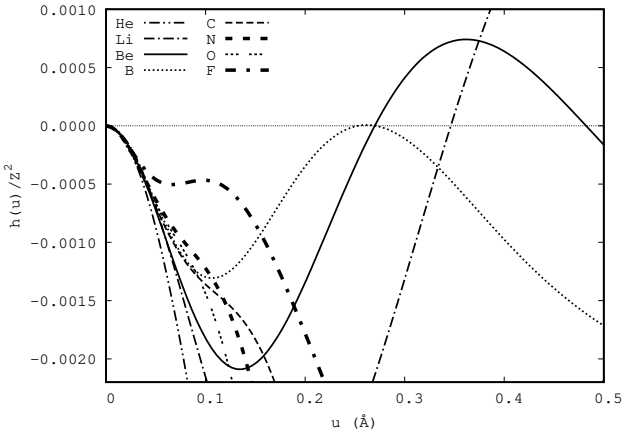

FIG. 6. Zoom of the short-range CISD/6-311G* Coulomb holes of the second-row atoms.

Finally, we have proven that for the rest of second-row atoms, except Li, a shoulder or a maximum in the short-range region of the Coulomb hole is obtained, which is due to the correlation of the core electrons in the K shell. In all cases, the shoulder or the maximum corresponds to an internal reorganization of the K shell.

ACKNOWLEDGMENTS

This research has been funded by the Spanish MINECO/FEDER Projects CTQ2014-52525-P (E.M.), CTQ2017-85341-P (M.S.), CTQ2015-67608-P (X.L.), CTQ2015-67660-P (J.M.U.) and EUIN2017-88605 (E.M.), the Basque Country Consolidated Group Project No. IT588-13, the Generalitat de Catalunya (Project 2017SGR39, Xarxa de Referència en Química Teòrica i Computacional, and the ICREA Academia 2014 prize (M.S.)). The FEDER grant UNGI10-4E-801 (European fund for Regional Development) has also supported this research. M.R.M. acknowledges the Spanish Ministry of Education, Culture and Sports for the doctoral grants FPU-2013/00176. E.R.C. and E.M. acknowledge funding from the European Union's Horizon 2020 research and innovation programme under the Marie Sklodowska-Curie grant agreement (No. 660943). The authors acknowledge the computational resources and technical and human support provided by the DIPC (especially to Daniel Franco and Diego Lasa) and the SGI/IZO-SGIker UPV/EHU.

* To whom the correspondence should be addressed: ematito@gmail.com

[1] R. G. Parr and W. Yang, *Density-Functional Theory of Atoms and Molecules* (Oxford University Press, 1989).
[2] M. Piris and J. Ugalde, Int. J. Quant. Chem. **114**, 1169 (2014).
[3] J. Cioslowski, M. Piris, and E. Matito, J. Chem. Phys. **143**, 214101 (2015).
[4] K. Pernal and K. J. H. Giesbertz, Top. Curr. Chem. **368**, 125 (2015).
[5] E. Ramos-Cordoba, P. Salvador, M. Piris, and E. Matito, J. Chem. Phys. **141**, 234101 (2014).
[6] E. Ramos-Cordoba, X. Lopez, M. Piris, and E. Matito, J. Chem. Phys. **143**, 164112 (2015).
[7] F. Feixas, J. Jiménez-Halla, E. Matito, J. Poater, and M. Solà, J. Chem. Theory Comput. **6**, 1118 (2010).
[8] E. Matito, M. Solà, P. Salvador, and M. Duran, Faraday Discuss. **135**, 325 (2007).
[9] I. Ruiz, E. Matito, F. J. Holguín-Gallego, E. Francisco, Á. M. Pendás, and T. Rocha-Rinza, Theor. Chem. Acc. **135**, 209 (2016).
[10] E. Ramos-Cordoba, P. Salvador, and E. Matito, Phys. Chem. Chem. Phys. **18**, 24015 (2016).
[11] E. Ramos-Cordoba and E. Matito, J. Chem. Theory Comput. **13**, 2705 (2017).
[12] M. Via-Nadal, M. Rodríguez-Mayorga, E. Ramos-

Cordoba, and E. Matito, (submitted).
[13] E. Ramos-Cordoba, E. Matito, I. Mayer, and P. Salvador, J. Chem. Theory Comput. **8**, 1270 (2012).
[14] C. A. Coulson and A. H. Neilson, Proc. Phys. Soc. London **78**, 831 (1961).
[15] R. McWeeny, Rev. Mod. Phys. **32**, 335 (1960).
[16] E. J. Baerends and O. V. Gritsenko, J. Phys. Chem. A **101**, 5383 (1997).
[17] M. A. Buijse and E. J. Baerends, Mol. Phys. **100**, 401 (2002).
[18] J. Cioslowski, in *Many-Electron Densities and Reduced Density Matrices* (Springer, New York, 2000) pp. 249–265.
[19] X. Fradera, M. Duran, and J. Mestres, J. Chem. Phys. **113**, 2530 (2000).
[20] E. Valderrama, X. Fradera, and J. M. Ugalde, J. Chem. Phys. **115**, 1987 (2001).
[21] M. Via-Nadal, M. Rodríguez-Mayorga, and E. Matito, Phys. Rev. A **96**, 050501 (2017).
[22] E. M. A. Peixoto, C. F. Bunge, and R. A. Bonham, Phys. Rev. **181**, 322 (1969).
[23] J. Cioslowski and G. Liu, J. Chem. Phys. **109**, 8225 (1998).
[24] C. F. Bunge and E. M. A. Peixoto, Phys. Rev. A **1**, 1277 (1970).
[25] C. F. Bunge, J. Chem. Phys. **125**, 014107 (2006).
[26] C. F. Bunge, Mol. Phys. **108**, 3279 (2010).
[27] R. O. Jones, Rev. Mod. Phys. **87**, 897 (2015).
[28] A. J. Thakkar, A. Tripathi, and V. H. Smith, Int. J. Quant. Chem. **26**, 157 (1984).
[29] A. J. Thakkar, A. Tripathi, and V. H. Smith Jr, Phys. Rev. A **29**, 1108 (1984).
[30] A. J. Thakkar and V. H. Smith Jr, J. Phys. B: Atom. Molec. Phys. **11**, 3803 (1978).
[31] E. Matito, J. Cioslowski, and S. F. Vyboishchikov, Phys. Chem. Chem. Phys. **12**, 6712 (2010).
[32] J. Cioslowski and E. Matito, J. Chem. Theory Comput. **7**, 915 (2011).
[33] M. Rodríguez-Mayorga, E. Ramos-Cordoba, F. Feixas, and E. Matito, Phys. Chem. Chem. Phys. **19**, 4522 (2017).
[34] M. Rodríguez-Mayorga, E. Ramos-Cordoba, M. Via-Nadal, M. Piris, and E. Matito, Phys. Chem. Chem. Phys. **19**, 24029 (2017).
[35] X. Telleria, M. Piris, J. M. Ugalde, E. Matito, and X. Lopez, in preparation.
[36] K. Ruedenberg, R. C. Raffenetti, and R. D. Bardo, *Energy, Structure, and Reactivity. Proceedings of the 1972 Boulder Seminar Research Conference on Theoretical Chemistry*, edited by D. W. Smith (Wiley, New York, 1973) p. 164.
[37] D. E. Wood and T. H. Dunning Jr., J. Chem. Phys. **99**, 1914 (1993).
[38] S. Wolfram, Inc., Champaign, Illinois (2014).
[39] S. Ramanujan, J. Ind. Math. Soc. **4**, 94 (1912).
[40] R. N. Hill, J. Chem. Phys. **83**, 1173 (1985).
[41] W. Kutzelnigg and J. D. Morgan, J. Chem. Phys. **96**, 4484 (1992).
[42] W. Kutzelnigg and J. D. Morgan, J. Chem. Phys. **97**, 8821 (Erratum) (1992).
[43] P. J. Knowles and N. C. Handy, Comput. Phys. Commun. **54**, 75 (1989).
[44] M. Frisch, G. Trucks, H. Schlegel, G. Scuseria, M. Robb, J. Cheeseman, G. Scalmani, V. Barone, B. Mennucci, G. Petersson, *et al.*, Available: www. gaussian. com/g_tech/g_ur/m_citation. htm. Accessed **9** (2014).
[45] E. Matito and F. Feixas, "DMn program," (2009), university of Girona (Spain) and University of Szczecin (Poland).
[46] F. Feixas, M. Solà, J. M. Barroso, J. M. Ugalde, and E. Matito, J. Chem. Theory Comput. **10**, 3055 (2014).
[47] M. Rodríguez-Mayorga, "RHO2-OPS: 2-dm operations." (2016), Institute of Computational Chemistry and Catalysis, University of Girona, Catalonia, Spain.
[48] J. Cioslowski and G. Liu, J. Chem. Phys. **105**, 4151 (1996).
[49] I. Lindgren and S. Salomonson, Physica Scripta **21**, 335 (1980).
[50] J. Kobus, Comput. Phys. Comm. **184**, 799 (2013).
[51] The correlation energy fraction is calculated from the estimates provided in Ref. 26.
[52] J. E. Lennard-Jones, J. Chem. Phys. **20**, 1024 (1952).
[53] W. Kutzelnigg, G. Del Re, and G. Berthier, Phys. Rev. **172**, 49 (1968).
[54] A. V. Bunge and R. O. Esquivel, Phys. Rev. A **34**, 853 (1986).
[55] T. H. Dunning Jr. and P. J. Hay, in *Modern Theoretical Chemistry*, Vol. 3, edited by H. F. Schaefer III (Plenum, New York, 1977) pp. 1–28.
[56] D. E. Woon and T. H. Dunning Jr, J. Chem. Phys. **103**, 4572 (1995).
[57] T. H. Dunning Jr., J. Chem. Phys. **90**, 1007 (1989).
[58] D. S. Ranasinghe and G. A. Petersson, J. Chem. Phys. **138**, 144104 (2013).
[59] A. Sarsa, F. Gálvez, and E. Buendıa, J. Chem. Phys. **109**, 7075 (1998).
[60] H. Schmider, R. P. Sagar, and V. H. Smith Jr, J. Chem. Phys. **94**, 8627 (1991).
[61] M. Kohout and A. Savin, Int. J. Quant. Chem. **60**, 875 (1996).
[62] E. Matito, B. Silvi, M. Duran, and M. Solà, J. Chem. Phys. **125**, 024301 (2006).
[63] M. Kohout, Int. J. Quant. Chem. **83**, 324 (2001).
[64] M. Solà, J. Mestres, J. M. Oliva, M. Duran, and R. Carbó, Int. J. Quant. Chem. **58**, 361 (1996).
[65] J. M. Mercero, E. Valderrama, and J. M. Ugalde, in *Metal-Ligand Interactions*, edited by N. Russo and et al. (Kluwer Academic Publishers, The Netherlands, 2003) pp. 205–239.
[66] J. K. Pearson, P. M. Gill, J. M. Ugalde, and R. J. Boyd, Mol. Phys. **107**, 1089 (2009).

Supporting Information: The Coulomb Hole of Ne atom

Mauricio Rodríguez-Mayorga,[1,2] Eloy-Ramos-Cordoba,[1,3]
Xabier Lopez,[1] Miquel Solà,[2] Jesus M. Ugalde,[1] and Eduard Matito[1,4,*]
[1]*Kimika Fakultatea, Euskal Herriko Unibertsitatea (UPV/EHU),*
and Donostia International Physics Center (DIPC), P.K. 1072, 20080 Donostia, Euskadi, Spain.
[2]*Institut de Química Computacional i Catàlisi (IQCC) and Departament de Química,*
University of Girona, 17071 Girona, Catalonia, Spain,
[3]*Kenneth S. Pitzer Center for Theoretical Chemistry, University of California, Berkeley and*
[4]*IKERBASQUE, Basque Foundation for Science, 48011 Bilbao, Euskadi, Spain.*

Eduard Matito
(Dated: June 15, 2018)

TABLE S1: CISD energies (a.u.) with a large variety of basis sets.

Basis	CISD Energy	Orbitals	Total Orb.	Shoulder
fc-5SP	-127.77104975	5s,5p	20	no
5SP	-127.81467566	5s,5p	20	yes
fc-5SPD	-127.87192601	5s,5p,5d	45	no
fc-5SPDF	-127.90213928	5s,5p,5d,5f	80	no
fc-5SPDFG	-127.91318231	5s,5p,5d,5f,5g	125	no
5SPD	-127.93116378	5s,5p,5d	45	yes
5SPDF	-127.96382539	5s,5p,5d,5f	80	yes
5SPDFG	-127.97551756	5s,5p,5d,5f,5g	125	yes
fc-6SP	-128.28775711	6s,6p	24	no
6SP	-128.33268410	6s,6p	24	yes
fc-6SPD	-128.39354873	6s,6p,6d	54	no
fc-6SPDF	-128.42545039	6s,6p,6d,6f	96	no
fc-6SPDFG	-128.43707561	6s,6p,6d,6f,6g	150	no
6SPD	-128.45430770	6s,6p,6d	54	yes
6SPDF	-128.48873660	6s,6p,6d,6f	96	yes
6SPDFG	-128.50103554	6s,6p,6d,6f,6g	150	yes
fc-7SP	-128.52405361	7s,7p	28	no
7SP	-128.56927176	7s,7p	28	yes
fc-8SP	-128.61574220	8s,8p	32	no
fc-DZ Dunning	-128.62188366	4s,2p	10	no
fc-7SPD	-128.63140882	7s,7p,7d	63	no
DZ Dunning	-128.63462232	4s,2p	10	yes
fc-6-311g	-128.65111350	4s,3p,1d	13	no
fc-9SP	-128.65316089	9s,9p	36	no
8SP	-128.66120220	8s,8p	32	yes
fc-7SPDF	-128.66373571	7s,7p,7d,7f	112	no
6-311G	-128.66668345	4s,3p,1d	13	yes
fc-DZP Dunning	-128.66863312	4s,2p,1d	15	no
fc-10SP	-128.67193945	10s,10p	40	no
fc-TZ Dunning	-128.67379599	5s,3p	14	no
fc-7SPDFG	-128.67536095	7s,7p,7d,7f,7g	175	no
fc-cc-pCVDZ	-128.67795662	4s,3p,1d	18	no
fc-11SP	-128.68084555	11s,11p	44	no
DZP Dunning	-128.68152560	4s,2p,1d	15	yes
fc-12SP	-128.68473222	12s,12p	48	no
fc-13SP	-128.68660915	13s,13p	52	no
fc-14SP	-128.68767247	14s,14p	56	no
fc-15SP	-128.68823406	15s,15p	60	no
fc-16SP	-128.68852202	16s,16p	64	no
TZ Dunning	-128.68913475	5s,3p	14	yes
7SPD	-128.69237085	7s,7p,7d	63	yes
9SP	-128.69876715	9s,9p	36	yes
10SP	-128.71762085	10s,10p	40	yes
cc-pCVDZ	-128.71587097	4s,3p,1d	18	yes
fc-8SPD	-128.72426761	8s,8p,8d	72	no
11SP	-128.72657815	11s,11p	44	yes
7SPDF	-128.72726305	7s,7p,7d,7f	112	yes
fc-6-311G*	-128.72839556	4s,3p,1d	18	no
12SP	-128.73049730	12s,12p	48	yes
13SP	-128.73239655	13s,13p	52	yes
14SP	-128.73347579	14s,14p	56	yes
15SP	-128.73404767	15s,15p	60	yes
16SP	-128.73434299	16s,16p	64	yes
fc-6-311+G*	-128.73530543	5s,4p,1d	22	no
7SPDFG	-128.73959732	7s,7p,7d,7f,7g	175	yes
6-311G*	-128.74683538	4s,3p,1d	18	yes
6-311+G*	-128.75395221	5s,4p,1d	22	yes
fc-8SPDF	-128.75707242	8s,8p,8d,8f	128	yes
8SPD	-128.78557924	8s,8p,8d	72	yes
fc-9SPD	-128.76254609	9s,9p,9d	81	no
fc-8SPDFG	-128.76886845	8s,8p,8d,8f,8g	200	no

fc-10SPD	-128.78172130	10s,10p,10d	90	no
fc-11SPD	-128.79091465	11s,11p,11d	99	no
fc-12SPD	-128.79503587	12s,12p,12d	108	no
fc-9SPDF	-128.79573424	9s,9p,9d,9f	144	no
fc-TZP Dunning	-128.79603876	5s,3p,2d,1f	34	no
fc-13SPD	-128.79708854	13s,13p,13d	117	no
fc-14SPD	-128.79826515	14s,14p,14d	126	no
fc-cc-pCVTZ	-128.79868187	6s,5p,3d,1f	43	no
fc-15SPD	-128.79890557	15s,15p,15d	135	no
fc-16SPD	-128.79925598	16s,16p,16d	144	no
cc-pVTZ	-128.80416500	4s,3p,2d,1f	30	no
fc-9SPDFG	-128.80767786	9s,9p,9d,9f,9g	225	no
TZP Dunning	-128.81472950	5s,3p,2d,1f	34	yes
fc-10SPDF	-128.81513872	10s,10p,10d,10f	160	no
8SPDF	-128.82099029	8s,8p,8d,8f	128	yes
fc-11SPDF	-128.82450725	11s,11p,11d,11f	176	no
fc-10SPDFG	-128.82717723	10s,10p,10d,10f,10g	250	no
9SPDF	-128.85989837	9s,9p,9d,9f	144	yes
3ZaP	-128.82273667	5s,4p,2d,1f	34	no
9SPD	-128.82406981	9s,9p,9d	81	yes
fc-12SPDF	-128.82877381	12s,12p,12d,12f	192	no
fc-13SPDF	-128.83094175	13s,13p,13d,13f	208	no
fc-14SPDF	-128.83219920	14s,14p,14d,14f	224	no
fc-QZP Dunning	-128.83229798	6s,4p,3d,2f,1g	56	no
fc-15SPDF	-128.83290033	15s,15p,15d,15f	240	no
fc-16SPDF	-128.83329990	16s,16p,16d,16f	256	no
8SPDFG	-128.83351449	8s,8p,8d,8f,8g	200	yes
fc-11SPDFG	-128.83663377	11s,11p,11d,11f,11g	275	no
fc-12SPDFG	-128.84097997	12s,12p,12d,12f,12g	300	no
fc-13SPDFG	-128.84321506	13s,13p,13d,13f,13g	325	no
10SPD	-128.84334214	10s,10p,10d	90	yes
fc-14SPDFG	-128.84452306	14s,14p,14d,14f,14g	350	no
fc-15SPDFG	-128.84526482	15s,15p,15d,15f,15g	375	no
fc-16SPDFG	-128.84569969	16s,16p,16d,16f,16g	400	no
11SPD	-128.85261311	11s,11p,11d	99	yes
cc-pCVTZ	-128.85525663	6s,5p,3d,1f	43	yes
12SPD	-128.85678981	12s,12p,12d	108	yes
13SPD	-128.85888080	13s,13p,13d	117	yes
14SPD	-128.86008359	14s,14p,14d	126	yes
15SPD	-128.86074254	15s,15p,15d	135	yes
16SPD	-128.86110629	16s,16p,16d	144	yes
QZP Dunning	-128.86242743	6s,4p,3d,2f,1g	56	yes
4ZaP	-128.86918690	6s,4p,3d,2f,1g	56	no
9SPDFG	-128.87258845	9s,9p,9d,9f,9g	225	yes
10SPDF	-128.87942505	10s,10p,10d,10f	160	yes
10SPDFG	-128.89222510	10s,10p,10d,10f,10g	250	yes
11SPDF	-128.88888815	11s,11p,11d,11f	176	yes
12SPDF	-128.89322368	12s,12p,12d,12f	192	yes
13SPDF	-128.89544100	13s,13p,13d,13f	208	yes
14SPDF	-128.89673260	14s,14p,14d,14f	224	yes
15SPDF	-128.89745823	15s,15p,15d,15f	240	yes
16SPDF	-128.89787641	16s,16p,16d,16f	256	yes
11SPDFG	-128.90178579	11s,11p,11d,11f,11g	275	yes
12SPDFG	-128.90620911	12s,12p,12d,12f,12g	300	yes
13SPDFG	-128.90850103	13s,13p,13d,13f,13g	325	yes
14SPDFG	-128.90984894	14s,14p,14d,14f,14g	350	yes
15SPDFG	-128.91061975	15s,15p,15d,15f,15g	375	yes
16SPDFG	-128.91107662	16s,16p,16d,16f,16g	400	yes

TABLE S2: FCI energies (a.u.) with different basis sets.

Basis	FCI Energy	Orbitals	Total Orbs	Shoulder
STO-3G	-126.60452509	2s,1p	5	no
3-21G	-127.91898852	3s,2p	9	no
3-21+G	-127.98028596	4s,3p	13	no
6-31G	-128.58980235	3s,2p	9	no
fc-DZ Dunning	-128.62579080	4s,2p	10	no
6-31G*	-128.62995598	3s,2p,1d	15	no
DZ Dunning	-128.63880898	4s,2p	10	yes
6-31+G*	-128.64536419	4s,3p,1d	18	no
fc-6-311G	-128.65597963	4s,3p,1d	13	no
6-311G	-128.67188511	4s,3p	13	yes
fc-DZP Dunning	-128.67403307	4s,2p,1d	15	no
fc-TZ Dunning	-128.67884748	5s,3p	14	no
cc-pVDZ	-128.68088113	3s,2p,1d	14	no
DZP Dunning	-128.68730452	4s,2p,1d	15	yes
TZ Dunning	-128.69455258	5s,3p	14	yes
aug-cc-pVDZ	-128.71147489	4s,3p,2d	23	no
fc-6-311G*	-128.73538842	4s,3p,1d	18	no
2ZaP	-128.73640663	4s,3p,1d	18	no
6-311G*	-128.75434359	4s,3p,1d	18	yes
6-311+G*	-128.76220259	5s,4p,1d	22	yes
cc-pVTZ	-128.81521344	4s,3p,2d,1f	30	no

TABLE S3. Optimized $\alpha_{L,N}$ and $\beta_{L,N}$ parameters for the even-tempered basis.

	L=1		L=2		L=3		L=4	
N	$\alpha_{L,N}$	$\beta_{L,N}$	$\alpha_{L,N}$	$\beta_{L,N}$	$\alpha_{L,N}$	$\beta_{L,N}$	$\alpha_{L,N}$	$\beta_{L,N}$
5	0.7447008	4.987933	0.7468682	4.975678	0.7481146	4.970626	0.7486768	4.968260
6	0.5855851	4.235044	0.5879834	4.226252	0.5896187	4.221960	0.5896036	4.221960
7	0.4331290	3.827501	0.4372306	3.816989	0.4396631	3.811919	0.4408068	3.809588
8	0.3832597	3.540438	0.3868512	3.527534	0.3887524	3.521848	0.3898830	3.519020
9	0.3295404	3.268363	0.3335108	3.255642	0.3353360	3.249659	0.3365048	3.246530
10	0.2685024	3.067461	0.2746154	3.053101	0.2771096	3.045830	0.2786413	3.042154
11	0.2432995	2.923246	0.2483912	2.906247	0.2511414	2.896871	0.2521809	2.891937
12	0.2267954	2.791407	0.2310510	2.771277	0.2330325	2.759503	0.2341548	2.753617
13	0.2051878	2.665739	0.2089870	2.644094	0.2114696	2.631279	0.2126607	2.624009
14	0.1836303	2.564108	0.1886687	2.540909	0.1916617	2.526210	0.1937285	2.517031
15	0.1705574	2.482135	0.1768171	2.452739	0.1794341	2.435215	0.1821470	2.423519
16	0.1624894	2.405121	0.1677557	2.371700	0.1707450	2.349419	0.1721495	2.336306

TABLE S4. One electron potential of Kohout.[1] Radii of the K shell (r_K), Hartree-Fock K shell density (n_K^{HF}) and change in the density due to electron correlation ($\Delta n_K = n_K^{\mathrm{FCI}} - n_K^{\mathrm{HF}}$).

Atom	r_K (a.u.)	n_K^{HF} (e.)	Δn_K (e.)
Li	1.37	1.9940	$< 10^{-3}$
Be	1.00	2.0069	$< 10^{-3}$
B	0.61	1.9986	0.003
C	0.49	2.0044	0.002
N	0.41	1.9909	$< 10^{-3}$
O	0.35	2.0000	$< 10^{-3}$
F	0.31	1.9982	0.002

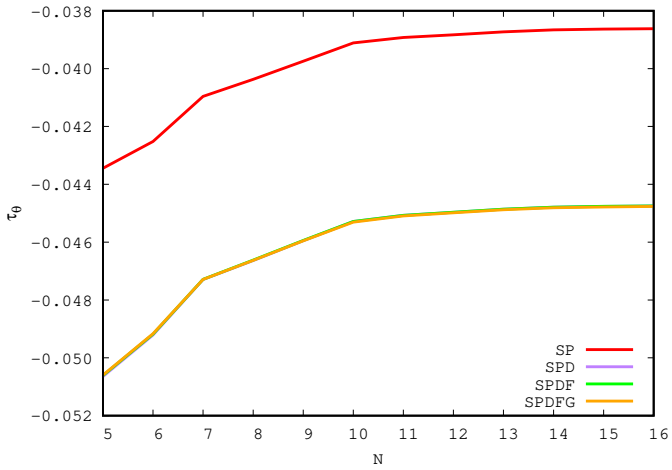

FIG. S1. The angular correlation descriptor of Kutzelnigg[2] in terms of the total number of basis functions (per angular momentum), N, and the maximum angular momentum, L.

[1] M. Kohout, Int. J. Quant. Chem. **83**, 324 (2001).

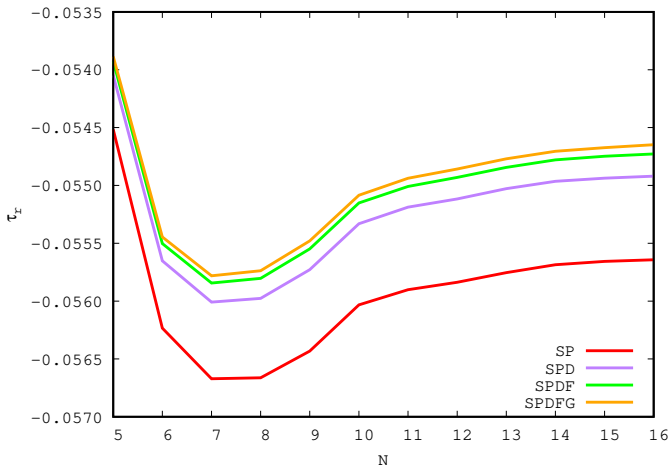

FIG. S2. The radial correlation descriptor of Kutzelnigg[2] in terms of the total number of basis functions (per angular momentum), N, and the maximum angular momentum, L.

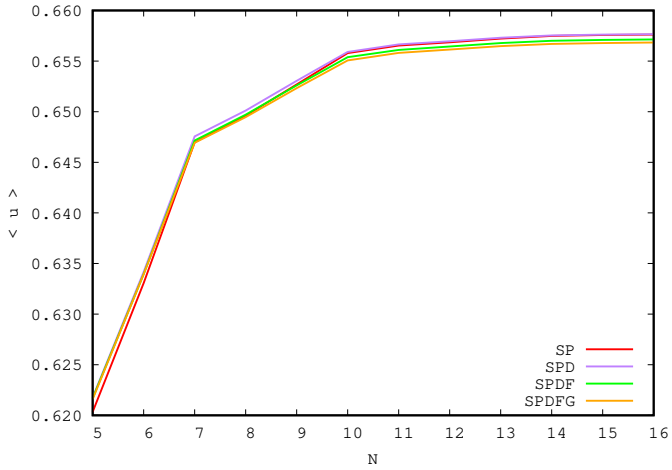

FIG. S3. The average interelectronic distance in terms of the total number of basis functions (per angular momentum), N, and the maximum angular momentum, L.

[2] W. Kutzelnigg, G. Del Re, and G. Berthier, Phys. Rev. **172**, 49 (1968).

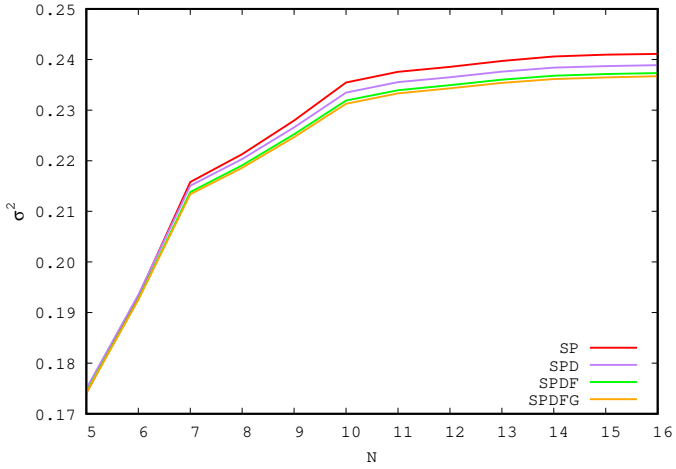

FIG. S4. The variance of the interelectronic distance in terms of the total number of basis functions (per angular momentum), N, and the maximum angular momentum, L.

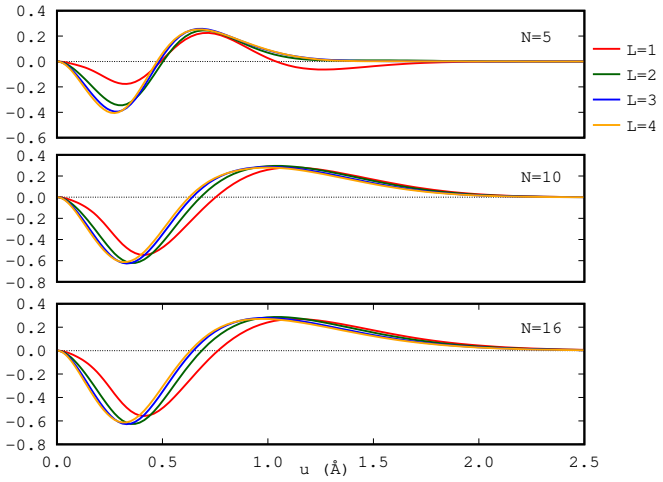

FIG. S5. The frozen-core CISD Coulomb hole for some even-tempered basis sets.

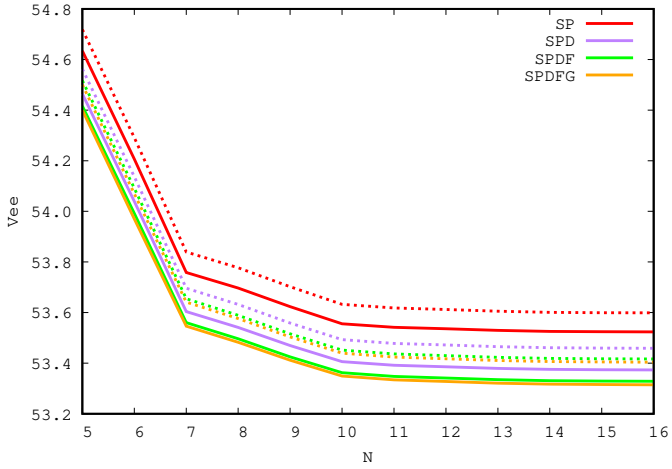

FIG. S6. The electron-electron repulsion energy in terms of the total number of basis functions (per angular momentum), N, and the maximum angular momentum, L. Dashed lines are frozen-core CISD calculations, whereas solid lines are full CISD calculations.

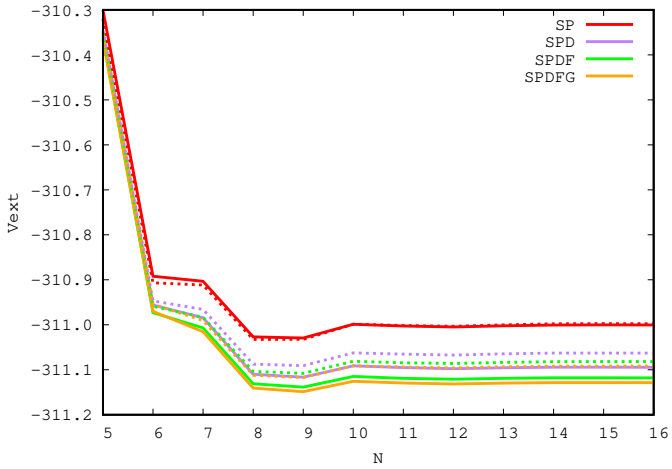

FIG. S7. The electron-nucleus attraction energy in terms of the total number of basis functions (per angular momentum), N, and the maximum angular momentum, L. Dashed lines are frozen-core CISD calculations, whereas solid lines are full CISD calculations.

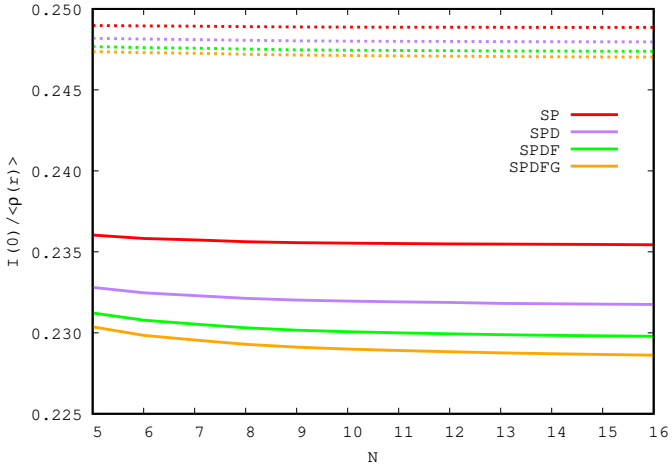

FIG. S8. The intracule at the coalescence point divided by the charge-concentration index, $I(0)/\langle\rho(r)\rangle$, in terms of the total number of basis functions (per angular momentum), N, and the maximum angular momentum, L. Dashed lines are frozen-core CISD calculations, whereas solid lines are full CISD calculations. For comparison let us recall that $I_{\mathrm{HF}}(0)/\langle\rho_{\mathrm{HF}}(r)\rangle = 1/4$.

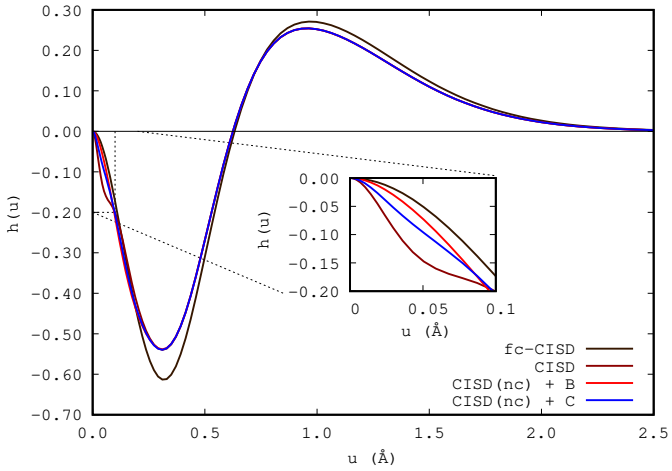

FIG. S9. The CISD/16SPDFG, fc-CISD/16SPDFG, CISD(nc)+B/16SPDFG and CISD(nc)+C/16SPDFG pair densities of Ne. The CISD(nc) is a regular CISD calculation in which the configurations involving excitations from the core orbital have been removed *a posteriori*. B and C is a group of configurations including various excitations from the core orbital: (B) double excitations involving only one electron in the core orbital and (C) double excitations involving the two electrons in the core orbital excited to one single orbital.

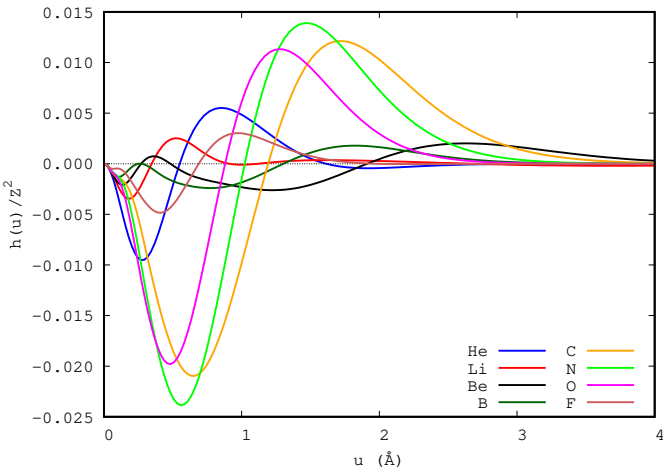

FIG. S10. CISD/6-311G* Coulomb holes for all second row atoms. For the open-shell atoms an unrestricted formalism was employed (i.e. they correspond to the difference between the UCISD and the UHF radial intracule densities). We have plotted the holes divided by the square of the atomic charge (Z^2) in order to make all the holes fit in the same scale.

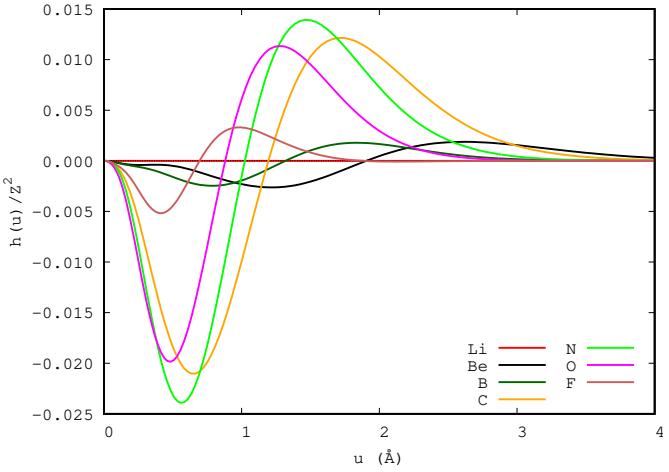

FIG. S11. Frozen core CISD/6-311G* Coulomb holes for all second row atoms. For the open-shell atoms an unrestricted formalism was employed (i.e. they correspond to the difference between the UCISD and the UHF radial intracule densities). We have plotted the holes divided by the square of the atomic charge (Z^2) in order to make all the holes fit in the same scale.

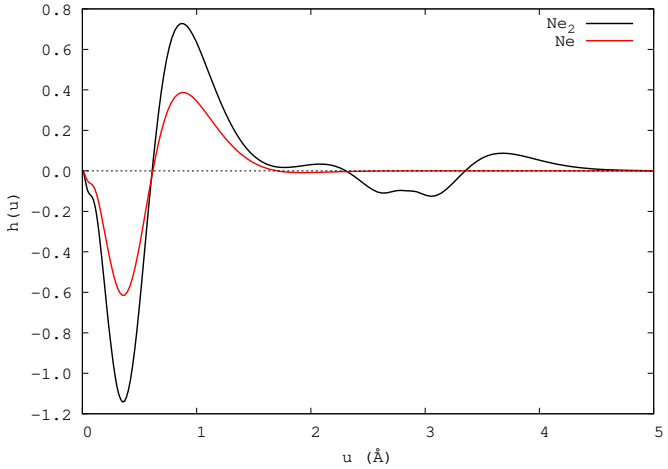

FIG. S12. The Coulomb hole of Ne atom and Ne_2 molecule at the 6-311G* level of theory show the shoulder at the short-range region.

VIII) The Harpoon Mechanism: An Approach from Bonding Descriptors

8.1) Bonding Description of the Harpoon Mechanism

Rodríguez-Mayorga M., Ramos-Cordoba E., Salvador P., Solà M., Matito. E. “Bonding description of the Harpoon Mechanism”. *Mol. Phys*. Vol., issue 7-8 (2016) : 1345-1355.

http://doi.org/10.1080/00268976.2015.1121297

Received 26 October 2015 /Accepted 4 November 2015

Abstract

The lowest lying states of LiH have been widely used to develop and calibrate many different methods in quantum mechanics. In this paper, we show that the electron-transfer processes occurring in these two states are a difficult test for chemical bonding descriptors and can be used to assess new bonding descriptors on its ability to recognise the harpoon mechanism. To this aim, we study the bond formation mechanism in a series of diatomic molecules. In all studied electron reorganisation mechanisms, the maximal electron-transfer variation point along the bond formation path occurs when about half electron has been transferred from one atom to another. If the process takes place through a harpoon mechanism, this point of the reaction path coincides with the avoided crossing. The electron sharing indices and one-dimensional plots of the electron localisation function and the Laplacian of the electron density along the molecular axis can be used to monitor the bond formation in diatomics and provide a distinction between the harpoon mechanism and a regular electron reorganisation process.

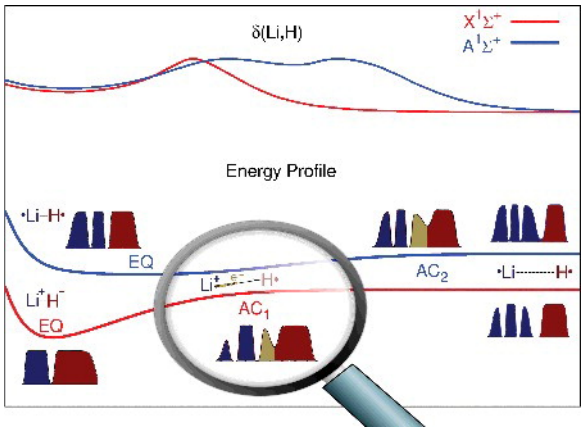

Keywords

Chemical bonding, harpoon mechanism, excited states, ionic bond, QTAIM

Bonding Description of the Harpoon Mechanism

Supporting Information

M. Rodríguez-Mayorga, E. Ramos-Cordoba, P. Salvador, M. Solà and E. Matito

November 9, 2015

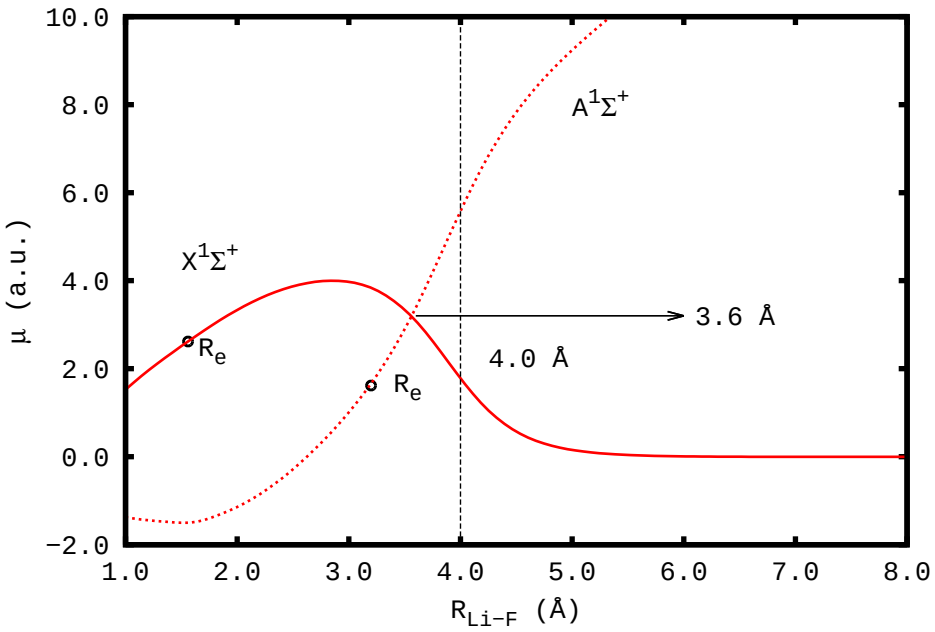

Figure S1: Dipole moment (in a.u.) along the internuclear axis for the $X^1\Sigma^+$ and the $A^1\Sigma^+$ states of LiF as function of the interatomic distance.

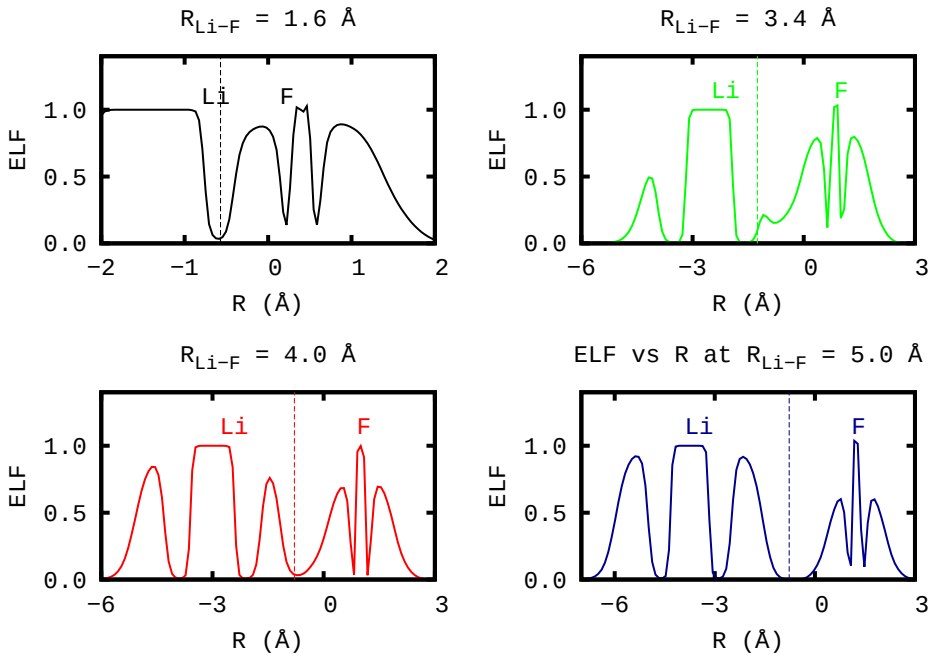

Figure S2: The ELF profile of the $A^1\Sigma^+$ state of LiF along the internuclear axis for several values of the interatomic distance. The zero is located at the center of mass and the vertical dashed line indicates the bond critical point.

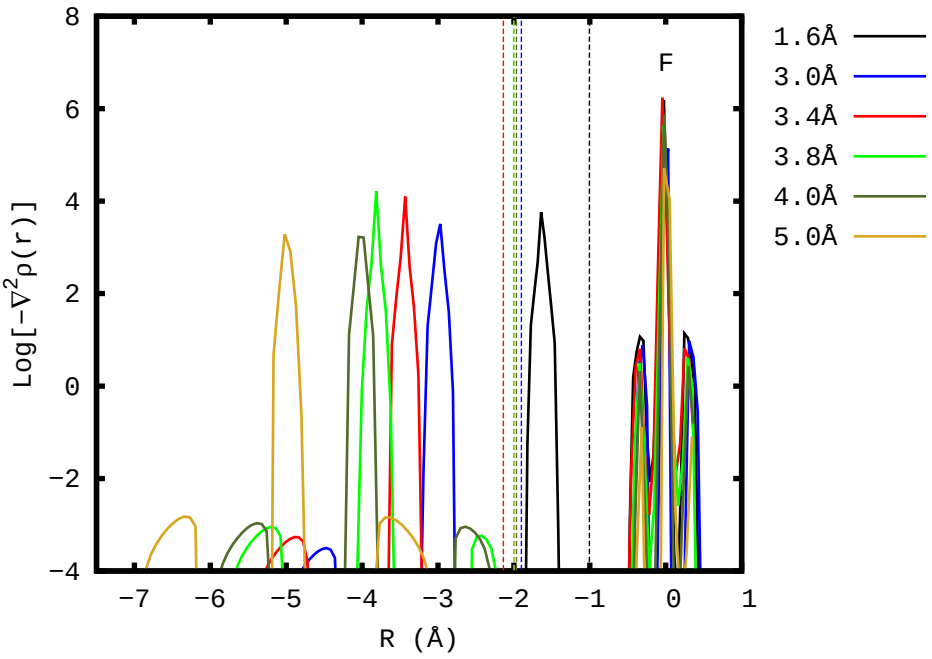

Figure S3: The negative values of the Laplacian of the electron density of LiF's $X^1\Sigma^+$ state along the internuclear axis as function of the interatomic distance for several interatomic distances All molecules locate Li atom in the z-axis at zero for comparison. The vertical dashed line indicates the bond critical point. Laplacian units are a.u.

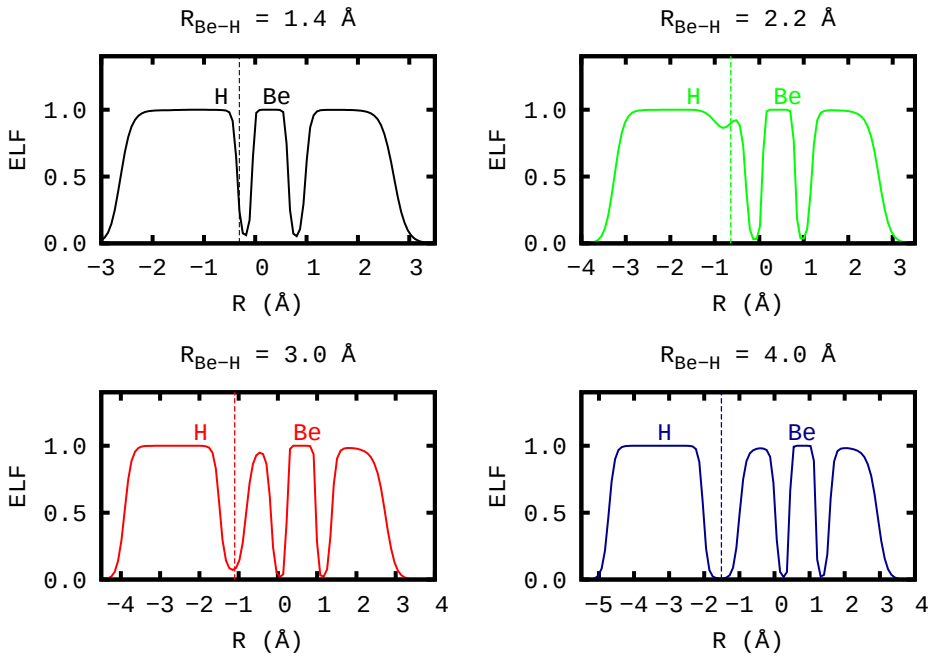

Figure S4: The ELF profile of the $X^2\Sigma^+$ state of BeH along the internuclear axis for several values of the interatomic distance. The zero is located at the center of mass and the vertical dashed line indicates the bond critical point.

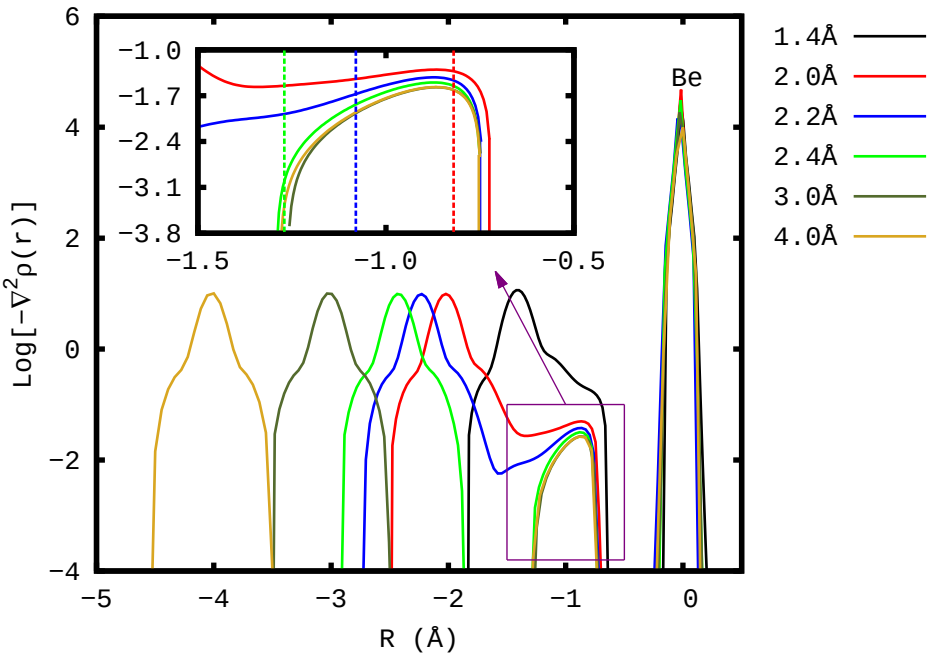

Figure S5: The negative values of the Laplacian of the electron density of BeH along the internuclear axis for several interatomic distances. All molecules locate Be atom in the z-axis at zero for comparison. The vertical dashed line indicates the bond critical point. Laplacian units are a.u.

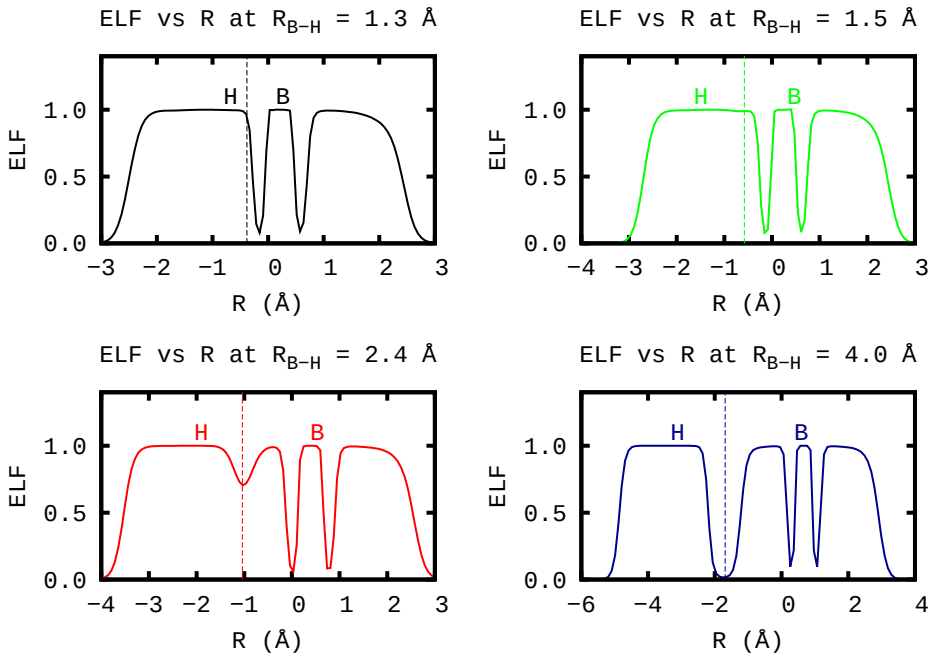

Figure S6: The ELF profile of the $X^1\Sigma^+$ state of BH along the internuclear axis for several values of the interatomic distance. The zero is located at the center of mass and the vertical dashed line indicates the bond critical point.

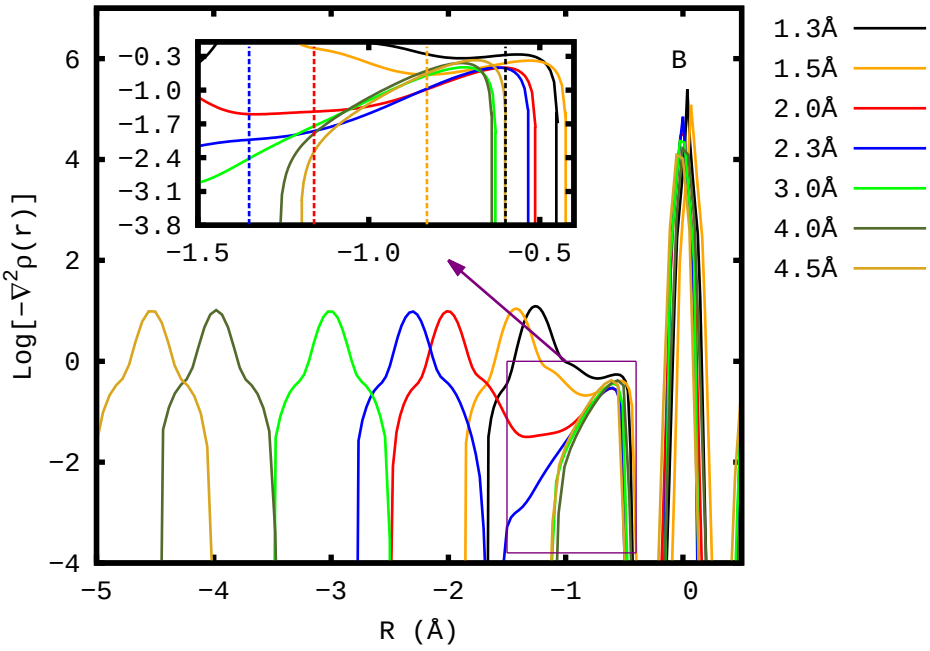

Figure S7: The negative values of the Laplacian of the electron density of BH along the internuclear axis for several interatomic distances. All molecules locate B atom in the z-axis at zero for comparison. The vertical dashed line indicates the bond critical point. Laplacian units are a.u.

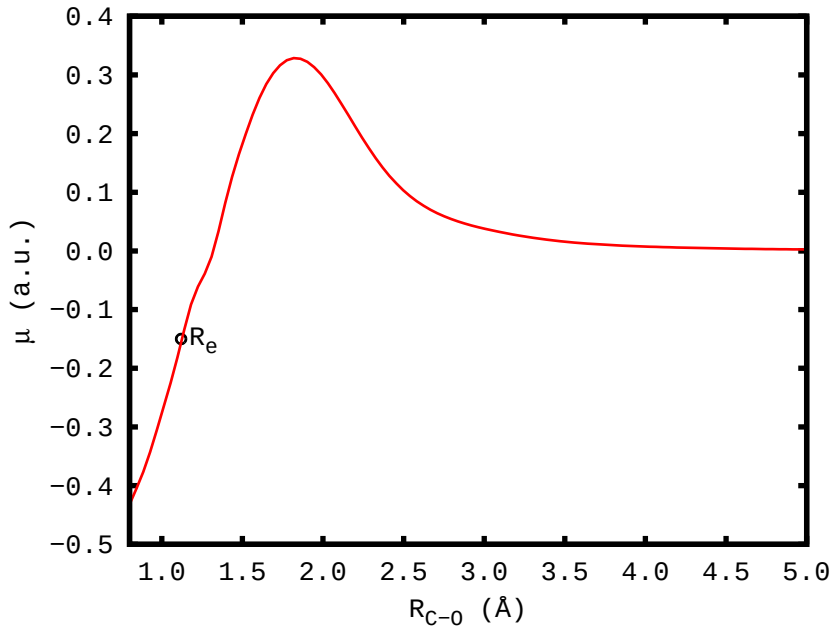

Figure S8: Dipole moment (in a.u.) along the internuclear axis for CO as function of the interatomic distance.

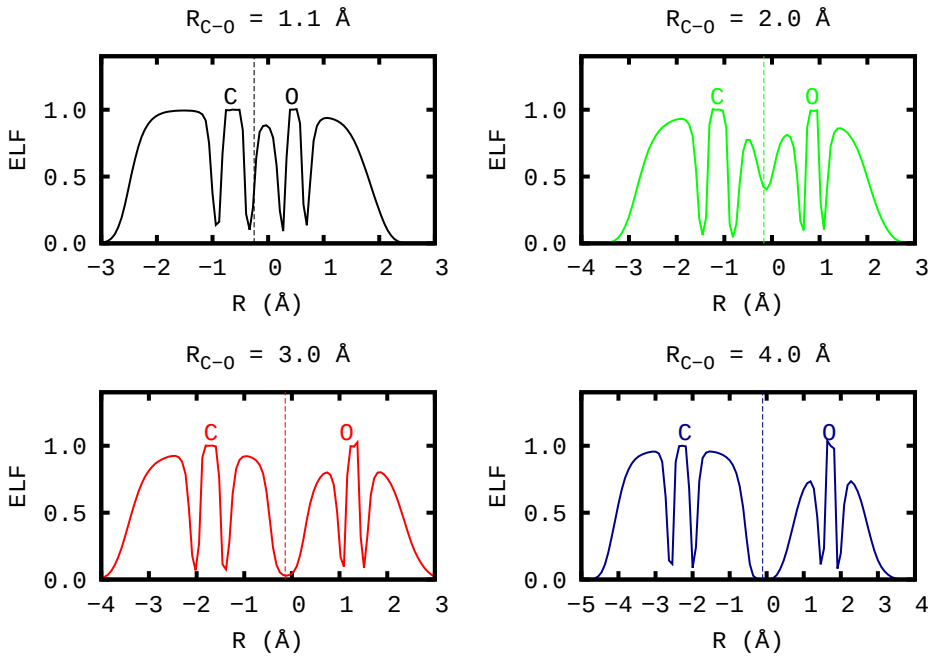

Figure S9: The ELF profile of CO along the internuclear axis for several values of the interatomic distance. The zero is located at the center of mass and the vertical dashed line indicates the bond critical point.

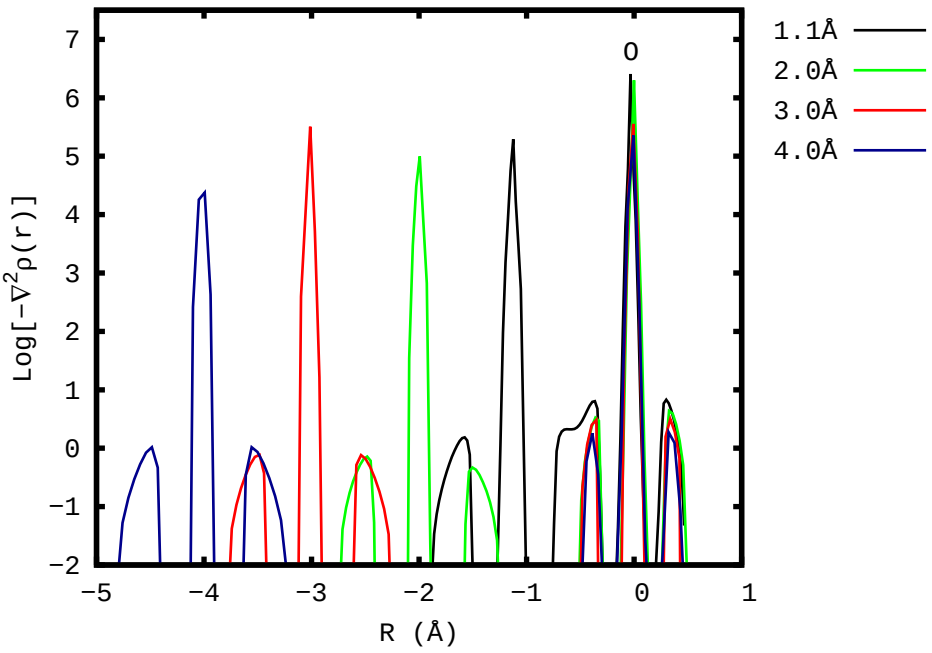

Figure S10: The negative values of the Laplacian of the electron density of CO along the internuclear axis for several interatomic distances. All molecules locate O atom in the z-axis at zero for comparison. The vertical dashed line indicates the bond critical point. Laplacian units are a.u.

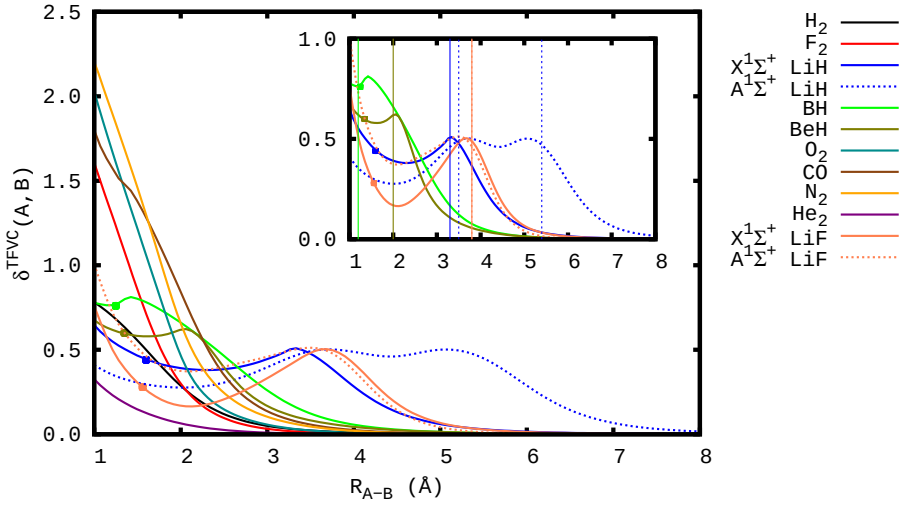

Figure S11: Electron sharing indices calculated using TFVC partition for the series of diatomic molecules. Solid and dotted lines are used for ground states and excited states, respectively. The solid points indicate the position of the equilibrium distance and the vertical lines in the inset plot mark the position of the maximal transfer variation points (see text). ESI units are electron pairs.

IX) Results and Discussions

In order to summarize the results of this thesis, we will briefly comment the most important results obtained in chapters IV-VIII. We have divided this section into four parts. The first part is devoted to 3-RDM approximations, where we analyze how electron correlation affects these approximations but we also analyze the performance of these approximations for describing electron sharing among three centers. In the second section, the most important results from the analysis of correlation effects in 2-RDM approximations are commented. The robustness of 2-RDM and 3-RDM is tested using the two-electron and three-electron Harmonium atom models, by tuning electron correlation effects playing with the ω parameter, and we also provide clues for developing more robust n-RDM approximations. Following, the third section is dedicated to a function linked to 2-RDM approximations, the radial intracule probability density ($I(s)$). We focus in three important aspects: a) the analysis of how the $I(s)$ evolves during the bond formation/cleavage of some simple but representative diatomic molecules, b) provide an approximation to the exact $I(s)$ that reduces the computational cost by using the MBB 2-RDM approximation and CCSD or CASSCF natural orbital occupancies, c) analyze the open question about the shoulder present in the Coulomb hole, $h(s)$, of Ne atom. Finally, the last section is purely descriptive of some chemical issue. The topic is the proper description of the harpoon mechanism, which is based on magnitudes that we previously used merely as benchmark tools but can also be employed as chemical descriptors. In this part, we analyze the ability of these indicators to provide an explanation of the electronic rearrangements leading to the formation of ionic species from neutral ones for some diatomic systems in gas phase.

9.1) 3-RDM Approximations Benchmark

9.1.1) Benchmark of Electron Correlation Effects

In chapter IV, we first analyze how electron correlation affects 3-RDM density matrix approximations. Actually, it is easy to prove that all suggested 3-RDM reduce to the Hartree-Fock approximation (also known as Hartree-Fock like approximation (HFl)) in the weak-correlation regime. But the open question was: How these approximations perform when correlation effects are not negligible? Thus, in this chapter we used the states ^2P and ^3P of the 3e-Harmonium Atom model system. We use this model because varying the ω parameter allows us to easily tune correlation effects. We used 12 ω values ($\omega \in [0.1, 1000]$) for which Cioslowski and coworkers [186] developed a set of even-tempered basis.[26] In this work we used the 7SPDF basis which involves 7s, 7p, 7d and 7f basis functions. For large-ω values it is known [186, 187, 199] that the correlation energy, E_{corr}, is not zero but correlation effects are negligible. On the other hand, for small-ω values, a good account of correlation effects is fundamental for a correct description of the system (even more than in many molecular systems). Therefore, the three-electron harmonium atom using ω values in the interval $[0.1, 1000]$ allows us to cover a wide range of correlation regimes (the interval is large enough to cover part of the strong-correlation regime but also most of the weak-correlation regime). Actually, for $\omega = 1000$, the Hartree-Fock approximation is an excellent approximation that obviously deteriorates when correlation increases. In this chapter, we used as benckmark tools: a) the 3c-ESI, b) the trace of the approximate 3-RDM, $^3\mathbf{D}^X$, c) the N-representability conditions, and d) the cumulative absolute error. The 3c-ESI was computed among three

[26] It is worth to mention that the electronic density of the correlated Harmonium Atom model is different to the density of Coulombic systems (e.g. of atoms) in the strong-correlation regime because the electron-nucleus cusp is not present in the Harmonium Atom model [151]. Thus, the usual basis used for Coulombic systems are not accurate enough and need to be reoptimize for this model system. Actually, it is easy to prove that the one-electron Harmonium Atom Hamiltonian reduces to the usual 3D oscillator problem, and thus the Hermite polynomials are a better basis than the Slater orbitals for this system.

regions A, B and C, which are delimited by two spheres centered at the origin, whose radius (r_A and r_B) were adjusted to make each region contain only one electron $\overline{N}_A = \overline{N}_B = \overline{N}_C = 1$, as illustrated in Fig. 4.

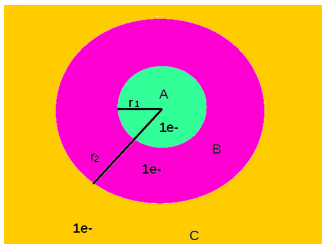

Figure 4 – Partition of the three-electron Harmonium atom using the radius r_A and r_B to generate regions A, B and C, that contain only one electron $\overline{N}_A = \overline{N}_B = \overline{N}_C = 1$.

The cumulative absolute error (called the termwise error in chapter IV) defined as

$$\mathrm{CAE}[{}^3\mathbf{D}^X] = \sum_{(i<j<k)\leq(l<m<n)} |{}^3D^X_{ijk,lmn} - {}^3D_{ijk,lmn}|, \tag{104}$$

where we subtract the approximate terms ${}^3D^X_{ijk,lmn}$ to the exact ones. In this study, we worked with Valdemoro's [95], Mazziotti's [178] and Nakatsuji's [179] approximations to the 3-RDM and analyzed the four properties above mentioned. For the approximate 3-RDM elements proposed by Matito and coworkers [102], we only analyzed the approximated 3c-ESI and trace of the 3-RDM produced. The main conclusion from this battery of tests is that all approximations deteriorate when correlation effects become more and more important. The second most important result is that Fermi correlation seems to be easier to be modeled than the Coulomb one; our results for the ${}^4P$ state compared to the ones obtained for the ${}^2P$ state support this statement.[27] In general, the sum rule, the N-representability conditions (the P-, Q- and two G-like conditions) and the cumulative absolute error test show a linear increase of the errors with respect to ω^{-1} in the $\omega \to \infty$ limit (see Fig 5). On the other hand, the deviation of the 3c-ESI is logarithmic ($\mathrm{Log}_{10}[\omega]$) in this limit (see Fig. 6), which means

[27] Recall that the Fermi correlation is smaller than Coulomb correlation.

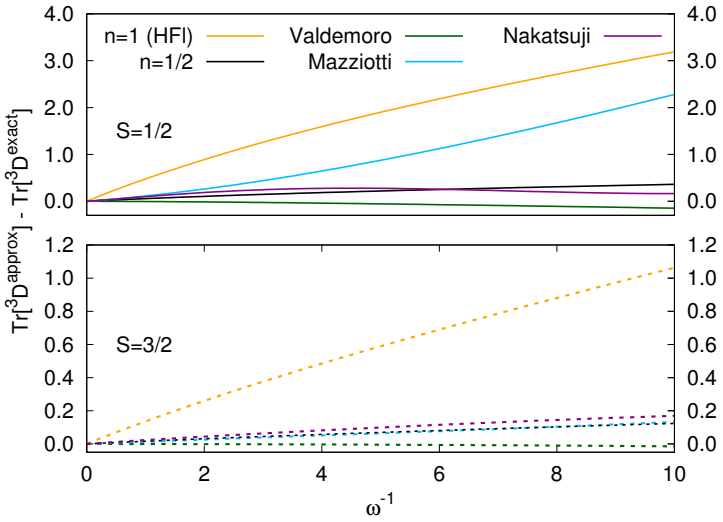

Figure 5 – Error in the trace for all 3-RDM approximations. Solid lines correspond to the doublet state whereas dotted ones correspond to the quartet state.

that 3c-ESI is less affected by correlation effects than the rest of properties here analyzed. In all tests, we have always subtracted the approximated value to the exact one. Notice that the Hartree-Fock approximation is retrieved by setting $a = 1$ in Matito and coworkers approximation (in this section the letter n was used instead of a in this work to denote the exponent) see Eq. 101.

Only the Hartree-Fock approximation satisfies the N-representability conditions here analyzed but it fulfills them by construction because its starting point is a single-determinant wavefunction. Unfortunately, the trace of the Hartree-Fock approximation is only correct when the occupancies are either 0 or 1, hence, the trace deviates from the exact value when fractional occupancies are used, which occurs in the presence of electron correlation. Actually, the worst traces are produced by this approximation; the violation of the sum rule makes the Hartree-Fock approximation not N-representable when fractional occupancies are used. In view of the results obtained, Nakatsuji approximation provides a much better 3-RDMs than the rest of approximations despite its clear violations

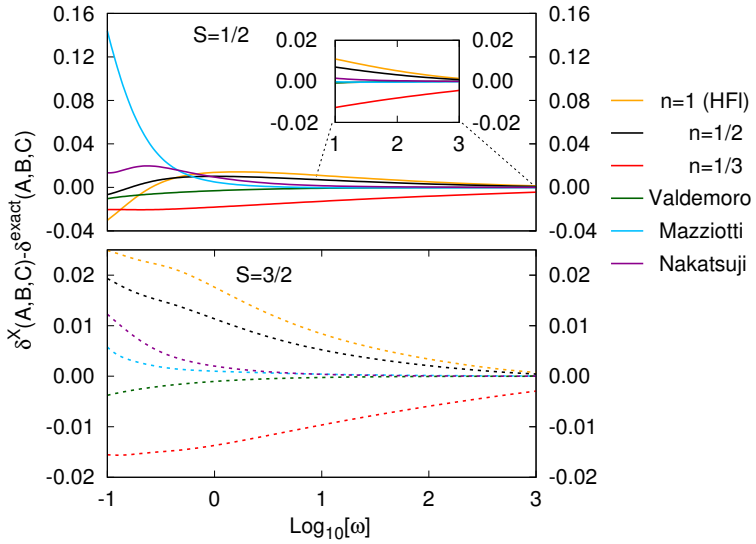

Figure 6 – Error in the 3c-ESI for all 3-RDM approximations. Solid lines correspond to the doublet state whereas dotted ones correspond to the quartet state.

of the P, Q and G N-representability conditions and its incorrect trace (see Fig. 3 in section 4.1). Surprisingly, the Nakatsuji 3-RDM is much closer to the exact one than the rest of approximated 3-RDMs (see Fig. 5 in section 4.1). Despite the similarity of their expressions (see Eqs. 97 and 98), Nakatsuji and Mazziotti approximations differ a lot in many tests, which suggests that the phase factor σ_p is clearly responsible for this fact. Recall that the phase factor is only present in Nakatsuji approximation and that it depends on the Fermi level (it is $+1$ for orbitals below the Fermi level and -1 otherwise). This observation introduces the question of whether more attention should be put to the selection of these phases when developing 3-RDM approximations. Finally, from the 3c-ESI and trace tests, it is clear that the $a = 1/3$ approximation produces excellent results in good agreement with the exact ones because these two quantities are known to be intimately related (a good trace seems to be a necessary condition to obtain accurate 3c-ESI).

9.1.2) Benchmark in Molecular Systems

In the second part of chapter IV, we analyzed the performance of the above mentioned approximations to the 3-RDM for the computation of the 3c-ESI as well as the average number of three particles (i.e. $\langle \widehat{A}_1 \widehat{A}_2 \widehat{A}_3 \rangle$) for a set of molecules. Also in the second part of chapter IV, we focused on two aspects to consider when computing the 3c-ESI: a) the difference between the 3c-ESI computed from uncorrelated wavefunctions and the 3c-ESI computed from correlated wavefunctions, and b) the change in the partition scheme from QTAIM to topological fuzzy Voronoi cells (TFVC). In all cases, CASSCF calculations and QTAIM partitions were taken as reference. As we did with the 3e-Harmonium model, all 3-RDM approximations (Hartree-Fock, Valdemoro, Mazziotti, Nakatsuji, and Matito and coworkers (setting $a = 1/2$ and $a = 1/3$ in Eq. 101)) were used to compute the 3c-ESI and compared it against the reference one. For the set of chosen molecules, our results demonstrate that Valdemoro's approximation is again, as it was for Harmonium, the most competitive approximation closely followed by the $a = 1/3$ approximation. Since the average number of three particles is the only component of the 3c-ESI with an explicit dependence to the 3-RDM, we checked the mean absolute deviation from the average number of three particles committed by the approximations. We checked the errors committed for: $\langle \widehat{A}_1 \widehat{A}_1 \widehat{A}_1 \rangle$, $\langle \widehat{A}_1 \widehat{A}_1 \widehat{A}_2 \rangle$ and $\langle \widehat{A}_1 \widehat{A}_2 \widehat{A}_3 \rangle$ type of terms for $A_1 \neq A_2 \neq A_3$ (which allows us to test not only the electron sharing but also the electron localization[28]). The first expectation value corresponds to the number of three particles within the same atom, the second one between two different atoms and the last one among three atoms (which contributes to the 3c-ESI). Our results for the average number of three particles demonstrate that Valdemoro's approx-

[28] Notice that $\langle \widehat{A}_1 \widehat{A}_1 \widehat{A}_1 \rangle$ accounts for the expected number of groups of three particles in region A_1 and $\langle \widehat{A}_1 \widehat{A}_1 \widehat{A}_2 \rangle$ considers groups of three particles, two located in region A_1 and one in region A_2, thus, these two expectation values account for localization of electrons in some specific regions. Whereas the last expectation value, $\langle \widehat{A}_1 \widehat{A}_2 \widehat{A}_3 \rangle$, considers the expected number of three particles each lying in a different region (i.e. $\langle \widehat{A}_1 \widehat{A}_2 \widehat{A}_3 \rangle$ is related to the sharing of particles instead of localization).

imation was the best approximation for this test but again closely followed by the $a = 1/3$ approximation. Due to the good results obtained by the latter approximation, we also computed the 3c-ESI using the $a = 1$, $a = 1/2$ and $a = 1/3$ schemes employing the natural orbitals and occupancies obtained from MP2 and CCSD calculations (recall that for these methods the n-RDMs are not uniquely defined). From these tests, we may argue that the $a = 1/3$ approximation provides reliable results which match well with the reference ones (i.e. the CASSCF ones), opening an avenue for computing 3c-ESI from MP2 and CCSD calculations specially in the weak-correlation regime. In the strong-correlation regime, MP2 and CCSD approximations will dramatically fail for many systems even if an unrestricted formalism is adopted, therefore, we suggest the usage of CASSCF occupancies and the $a = 1/3$ approximation in the strong-correlation regime.

The study of how electron correlation affects the 3c-ESI was performed comparing CASSCF wave functions and single-determinant Hartree-Fock ones. In all cases we observed that electron correlation reduces the 3c-ESI values. Nevertheless, the single-determinant wavefunction retains the classical description of the three-center indices [200], which can be distinguished by the 3c-ESI sign.[29] Conversely, the CASSCF wavefunction provides positive values (apart from some exceptions like FHF^-) which precludes the identification of the type of bond. Finally, our study suggested that TFCV and QTAIM partition results are in good agreement except for bonds involving Li and S atoms. For example, for the H-S-H bond, the reference QTAIM value is 0.0549 whereas with TFVC is 0.1359. Further studies must be carried out to clarify the differences obtained between TFVC and QTAIM for bonds including Li and S atoms.

[29] Where positive values of the 3c-ESI correspond to 3c-2e bonds while negative values correspond to 3c-4e bonds.

9.2) 2-RDM Approximations Benchmark

In chapter V, we studied how electron correlation affects the 2-RDM approximations introduced in the *Methodology* section. As we did for 3-RDM approximations, we used the Harmonium atom model as benchmarking system due to the simplicity of tuning correlation effects through its confinement parameter (ω). In this study, we worked with the two-electron Harmonium atom in the ^1S state which corresponds to the ground state of the system. We worked with a set of 20 optimized even-tempered 7SDPF basis [189], and the range of ω values taken was from 0.03 to 1000 in order to cover the strong- and the weak-correlation regimes, respectively. The α parameter of the POWER [160,162,169] functional was properly optimized in order to produce an approximate V_{ee} that differs from the exact one in less than 10^{-5} a.u. for each ω.

Before we start our analysis, it is worth to mention that for a closed-shell two-electron system, PNOF4, PNOF5 and PNOF7 approximations recover the exact FP expression. Thus, the results presented in chapter V for the FP approximation are also valid for PNOF4, PNOF5 and PNOF7 approximations. Hence, in this study we have just reported the results of PNOF4.

In chapter V, we developed a battery of tests for 2-RDM approximations, considering 10 tests: (i) the calculation of the trace, (ii) cumulative absolute error for the diagonal elements, i.e.,

$$\mathrm{CAE}_D[^2\mathbf{D}^X] = \sum_{ij,\sigma\sigma'} |^2D^{X,\sigma\sigma'}_{ij,ij} - {}^2D^{\sigma\sigma'}_{ij,ij}|, \tag{105}$$

(iii) cumulative absolute error for the whole matrix

$$\mathrm{CAE}[^2\mathbf{D}^X] = \sum_{ijkl,\sigma\sigma'} |^2D^{X,\sigma\sigma'}_{ij,kl} - {}^2D^{\sigma\sigma'}_{ij,kl}|, \tag{106}$$

(iv) the correct antisymmetry of the 2-RDM, i.e.,

$$Err_A[^2\mathbf{D}^X] = \sum_{ijkl,\sigma} |^2D^{X,\sigma\sigma}_{ij,kl} + {}^2D^{X,\sigma\sigma}_{ij,lk} + {}^2D^{X,\sigma\sigma}_{ji,lk} + {}^2D^{X,\sigma\sigma}_{ji,kl}|, \tag{107}$$

(v) the P, Q and G N-representability conditions, (vi) the DI between two symmetric regions generated by a bisecting plane passing through the center of mass, (vii) the average interelectronic distance $\langle s\rangle = \int sI(s)ds$ (denoted as $\langle u\rangle$ in chapter V) and (viii) its variance $\sigma^2 = \langle s^2\rangle - \langle s\rangle^2$ (where $\langle s^2\rangle = \int s^2 I(s)ds$), (ix) the interelectronic repulsion, V_{ee}, and (x) the radial intracule density profile. Notice that we have used ${}^2\mathbf{D}^X$ to refer to the approximated 2-RDM.

From this battery of tests, we obtained that all approximations deteriorate when the electron correlation increases. Even PNOF4, which is exact for closed-shell two-electron systems except for some phases, fails to reproduce the exact results for all tests, failing for the DI, the $\langle u\rangle$, variance, the V_{ee} and the radial intracule density profile. This approximation only fails due to the incorrect selection of the phases in the strong-correlation regime. Nevertheless, our results suggest that this functional expression must be a cornerstone when developing 2-RDM approximations.

9.2.1) The Sum Rule

First of all, we focus on the diagonal elements and the analysis of the sum rule and the $\mathrm{CAE}_D[{}^2\mathbf{D}^X]$. The exact trace is $N(N-1)$ in McWeeny's normalization, which for a two-electron system is equal to 2. Only BBC2, CA, CGA, MBB, PNOF2 and PNOF4 satisfy the sum rule. In Fig. 7 we have plotted the error in the trace with respect to $\omega^{-1/2}$, thus, correlation effects increase from the left to right; it is clear that the increase of correlation affects some approximations that deteriorate and produce incorrect traces. The GU and MLSIC approximations coincide with the HFl approximation for this test because their diagonal elements are the same for a closed-shell two-electron system. Let us remark that many JK-only approximations considered in this work produce unphysical elements like ${}^2D^{\sigma\sigma}_{ii,ii}$, which correspond to probabilities of finding like-spin electron pairs in the same spatial orbital. Recall that MLSIC and GU approximations

do not produce these unphysical elements (GU is simply MBB approximation removing the unphysical elements). Unfortunately, these unphysical elements are responsible for correcting the trace with respect to the initial HFl approximation in BBC2, CA, CGA and MBB approximations. Therefore, GU and MLSIC do not include the unphysical elements but introduce errors in the trace which proves that this kind of self-interaction correction is not satisfactory in the development of 2-RDM approximations. PNOF3 approximation produces the same trace as HFl approximation because the former only modifies the opposite-spin elements in the cumulant with respect to the HFl approximation. Only PNOF6 approximation slightly deviates from the correct trace in the strong-correlation limit due to the S_γ parameter, being PNOF6h the best among the three PNOF6s.

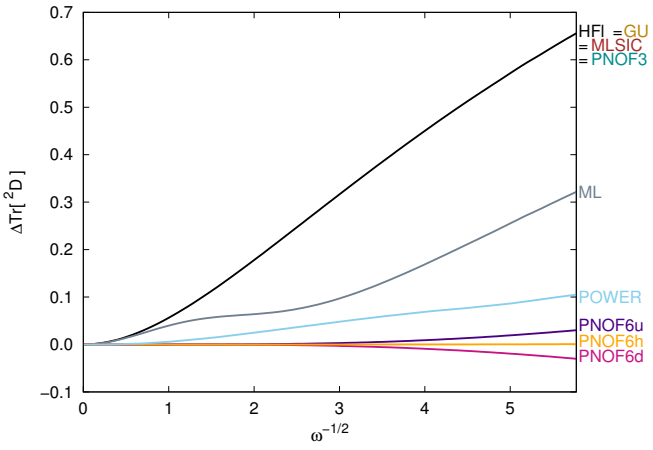

Figure 7 – Trace error for all 2-RDM approximations. BBC2, CA, CGA, MBB, PNOF2 and PNOF4 have not been included because they satisfy the sum rule by definition.

10.2.2) CAE for the Diagonal Elements

The analysis of the trace was complemented by the analysis of the $\mathrm{CAE}_D[^2\mathbf{D}^X]$, which is plotted in Fig. 8, where we observe that only PNOFi approximations produce elements in good agreement with the exact ones. Indeed, all

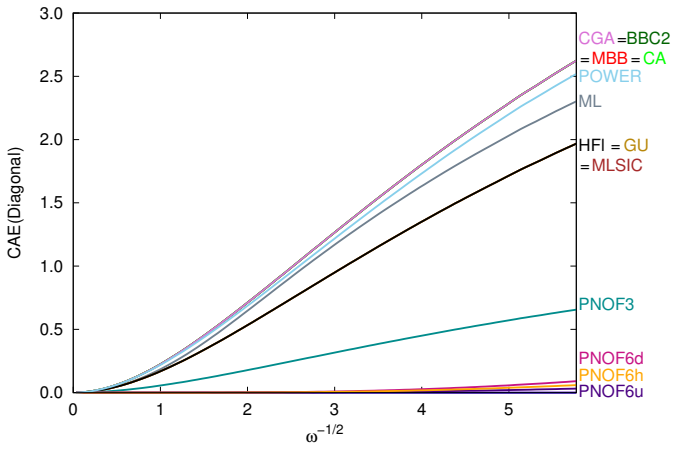

Figure 8 – Cumulative absolute error in the trace for the diagonal elements of all 2-RDM approximations. PNOF4 and PNOF2 have not been included because they present errors lower than 10^{-4}.

JK-only approximations that produce unphysical elements, ${}^2D^{\sigma\sigma}_{ii,ii}$, obviously correct the trace but introduce large $\mathrm{CAE}_D[{}^2\mathbf{D}^X]$ errors. The aforedescribed self-interaction correction done for GU and MLSIC reduces the diagonal elements to the HFl approximation. Among the approximations that do not attain the sum rule, only PNOF6 approximation produces small deviations but mainly in the strong-correlation regime. To complement the study of $\mathrm{CAE}_D[{}^2\mathbf{D}^X]$, we also studied the whole cumulative absolute error. This study proved that all 2-RDM approximations deviate from the exact 2-RDM in the strong-correlation regime. Even PNOF4 deviates due to some phases, Φ_{kl}, that reverse the sign (for $\omega \leq 0.1$) when correlation effects become more important. Nevertheless, the most remarkable result is that only PNOFs improve over the HFl approximation, whereas all JK-only approximations produce elements that are clearly worse than the HFl ones (see Fig. 9).

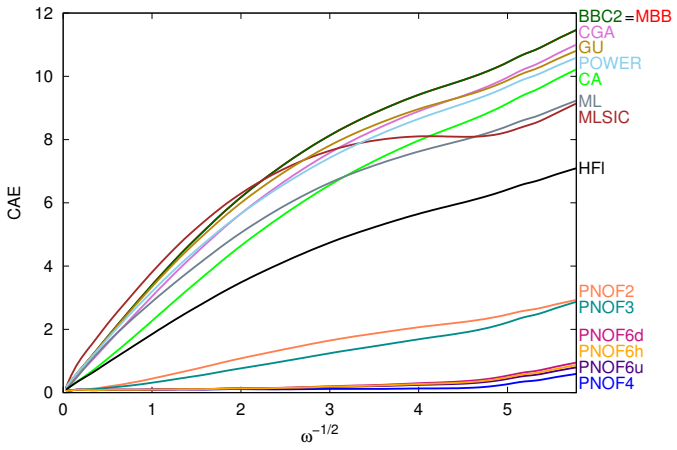

Figure 9 – Cumulative absolute error for all 2-RDM approximations.

9.2.3) Antisymmetry of the 2-RDM

Our next test consists in checking that the proper antisymmetry of the 2-RDM was produced by these approximations. Only all JK-only approximations violate the antisymmetry condition and the error produced increases with correlation. Let us point out that ML and MLSIC were developed using Padé approximants employing some parameters, thus it is not surprissing that ML approximation does not present a monotonic increase. These parameterization casts doubts on the use of parameterized approximations in the development of 2-RDM approximations.

9.2.4) The Fulfillment of N-Representability Conditions

In the benchmark of 3-RDM approximations we used the fulfillment of N-representability conditions (i.e. P, Q and G conditions) as benchmark tools, here, for the benchmark of 2-RDM approximations we have also included the fulfillment of these conditions in the battery of tests. In contrast to our work with 3-RDM, where we only checked these conditions in the canonical basis,

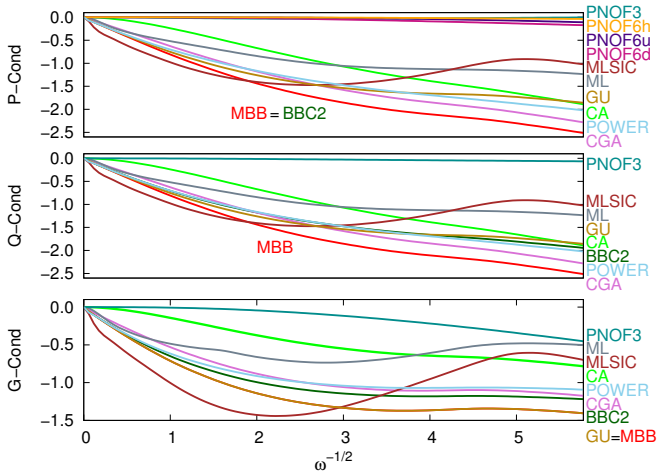

Figure 10 – Sum of all negative eigenvalues of **P**, **Q** and **G** matrices. PNOF2 and PNOF4 are not included since they satisfy these three conditions.

in this study we have analyzed the actual positive semidefinite character of **P**, **Q** and **G** matrices (i.e. checking whether the eigenvalues produced from the diagonalization of these matrices are greater than or equal to zero). All approximations considered in this work are built using only two indices (see Eqs. 82, 85 and 86), thus, it is easy to demonstrate that the **P**, **Q** and **G** matrices present blocks which simplify the diagonalization procedure. Some blocks are basis-set dependent (M×M blocks) and we used a Jacobi diagonalization procedure to obtain the corresponding eigenvalues, while some other blocks are not basis-set dependent (see Ref. [201] for some examples) and analytic eigenvalues[30] can be obtained. In Fig. 10 we have collected the sum of all negative eigenvalues of **P**, **Q** and **G** matrices. HFl, PNOF2 and PNOF4 are not included since they satisfy these three conditions. In agreement with previous findings, our results demonstrate that PNOFs that were built attending to some N-representability conditions, perform well in general for this test, except PNOF3 which is known to violate the G condition when correlation effects are more important [173].

[30] Analytic eigenvalues that depend either on the $f(n_i, n_j)$ functions for JK-only functionals or on $\mathbf{\Delta}$ and $\mathbf{\Pi}$ matrix elements for PNOFs.

Clearly, all JK-only approximations deviate from the N-respresentability and only negligible errors are present in the weak-correlation limit. But, as soon as correlation effects are important, the number of violations of the conditions is increased. Lastly, let us remark that the analytic eigenvalues of $\mathbf{P}$, $\mathbf{Q}$ and $\mathbf{G}$ matrices [202] impose bounds on the elements of $\mathbf{\Delta}$ and $\mathbf{\Pi}$ matrices of PNOFs. Unfortunately, for all PNOFs there are always blocks that are basis-set dependent precluding from a complete knowledge of the bounds imposed on the elements of $\mathbf{\Delta}$ and $\mathbf{\Pi}$ matrices. Nevertheless, our results suggest that, for a closed-shell two-electron system, imposing the analytic bounds in the construction of PNOFs is sufficient to produce a functional that fulfills the P, Q and G conditions.

9.2.5) The Delocalization Index

The next test focused on the analysis of the DI, where we also noticed that all approximations deviate from the exact DI when correlation effects are increased. In these tests, PNOF6h was proven to be the best approximation followed by PNOF4 and MBB. Notice that PNOF6h was the best among the three PNOF6s in the trace test; thus, it was reasonable that it should perform better than the previous ones for the DI test. BBC2, MBB, PNOF4, PNOF6 and the fitted POWER functional describe well the gross number of pairs with errors below 3%. The rest on approximations presented errors ranging between 20 to 75%.

9.2.6) Properties Dependent of the Interelectronic Distance

Finally, we studied properties that are dependent on the interelectronic distance. The first test consisted in the analysis of the $I(s)$ distribution, where we checked the mean value ($\langle s \rangle$) and the variance (σ^2). For all 2-RDM approximations $\langle s \rangle$ and σ^2 deviate from the exact values when correlation increases. The HFl approximation produces the worst values when correlation increases,

whereas PNOF4 fails only due to the incorrect phases. PNOF6h produces very accurate $\langle s \rangle$ and σ^2 values for all correlation regimes and is the best approximation among the three PNOF6 approximations. Here, we observed that there is a quasi-linear dependence of the error with respect to the mean value and, likewise for the variance with respect to ω^{-1} and ω^{-2}, respectively (see Figs. 7 and 8 of Ref. [184]). Hence, the variance of the $I(s)$ distribution is more affected by correlation than the mean value. The rest of tests analyzed in chapter V show a quasi-linear dependence with respect to $\omega^{-1/2}$ in the $\omega \to \infty$ limit, which means that they are less affected by correlation than the mean value.

The analysis of the profile of the radial intracule probability density and the comparison with respect to the exact profile can be plotted in a simple 2D plot ($\Delta I(s) = I^X(s) - I(s)$). Let us start with HFl approximation, it lacks many correlation effects due to the absence of the cumulant (recall that ${}^2\mathbf{D} = {}^1\mathbf{D}^2 + {}^2\mathbf{\Gamma}$ and ${}^2\mathbf{\Gamma} = 0$ in HFl approximation). Thus, it is expected that the difference between the exact and the HFl radial intracule probability densities produces first a decrease to a minimum and then an increase to a maximum in the plot of $h(s)$ vs s ($s \equiv r_{12}$). This shape resembles the so-called Coulomb hole. In Fig. 11 we have plotted the difference between the approximate and the exact radial intracule probability densities for three ω values, covering from the weak- ($\omega = 1000$) to the strong-correlation ($\omega = 0.03$) regimes.

For $\omega = 1000$, correlation effects are negligible and many approximations produce almost exact results. Nevertheless, the HFl approximation misses correlation effects contained in the cumulant and the shape of a Coulomb hole is retrieved. CA approximation recovers exactly the HFl approximation in this limit. Notice that even in the weak-correlation limit HFl, CA, ML, CGA, POWER and MLSIC are unable to reproduce the correct intracule.

In the medium correlation regime ($\omega = 0.5$), only PNOF4 and PNOF6s approximations are able to produce accurate radial intracule probability densities.

From the shape of the profile, we may argue that there are two types of approximations: a) approximations that underestimate correlation effects like HFl, and b) approximations that overestimate correlation effects and produce "inverted Coulomb holes" (in Fig. 11 is easy to distinguish between the two types). We have separated the approximations on the l.h.s and on the r.h.s according to the shape of the Coulomb hole produced. Notice that the usual Coulomb hole integrates to zero because the integration of $I(s)$ should be $N(N-1)/2$, but, we have seen that some approximations do not show a proper trace thus, their $I(s)$ integrates to an incorrect number and the positive and negative differences do not compensate (see for example MLSIC for $\omega = 0.5$).

Lastly, in the strong-correlation limit ($\omega = 0.03$), none of the approximations retrieves the exact intracule. Only PNOF4 and PNOF6s approximations provide the most reliable results. The Coulomb holes of MBB, BBC2, CA, CGA, GU, PNOF3, PNOF4, PNOF6s, and the POWER approximations show a maximum for small r_{12} values, thus, these approximations seem to overestimate correlation effects in the strong-correlation limit. Nonetheless, we have plotted the $I(s)$ for these approximations to confirm that they overestimate correlation effects. When we plotted the radial intracule probability density we noticed that negative probabilities were produced by some approximations (see Fig. 12). Clearly, these approximations produce unphysical profiles. The exact profile should never be negative since probabilities cannot be negative. Moreover, this incorrect profile should be obviously related to the violation of the P N-representability condition which causes this unphysical behavior. The only approximation that truly overestimates correlation effects is PNOF4 (because of the incorrect phases).

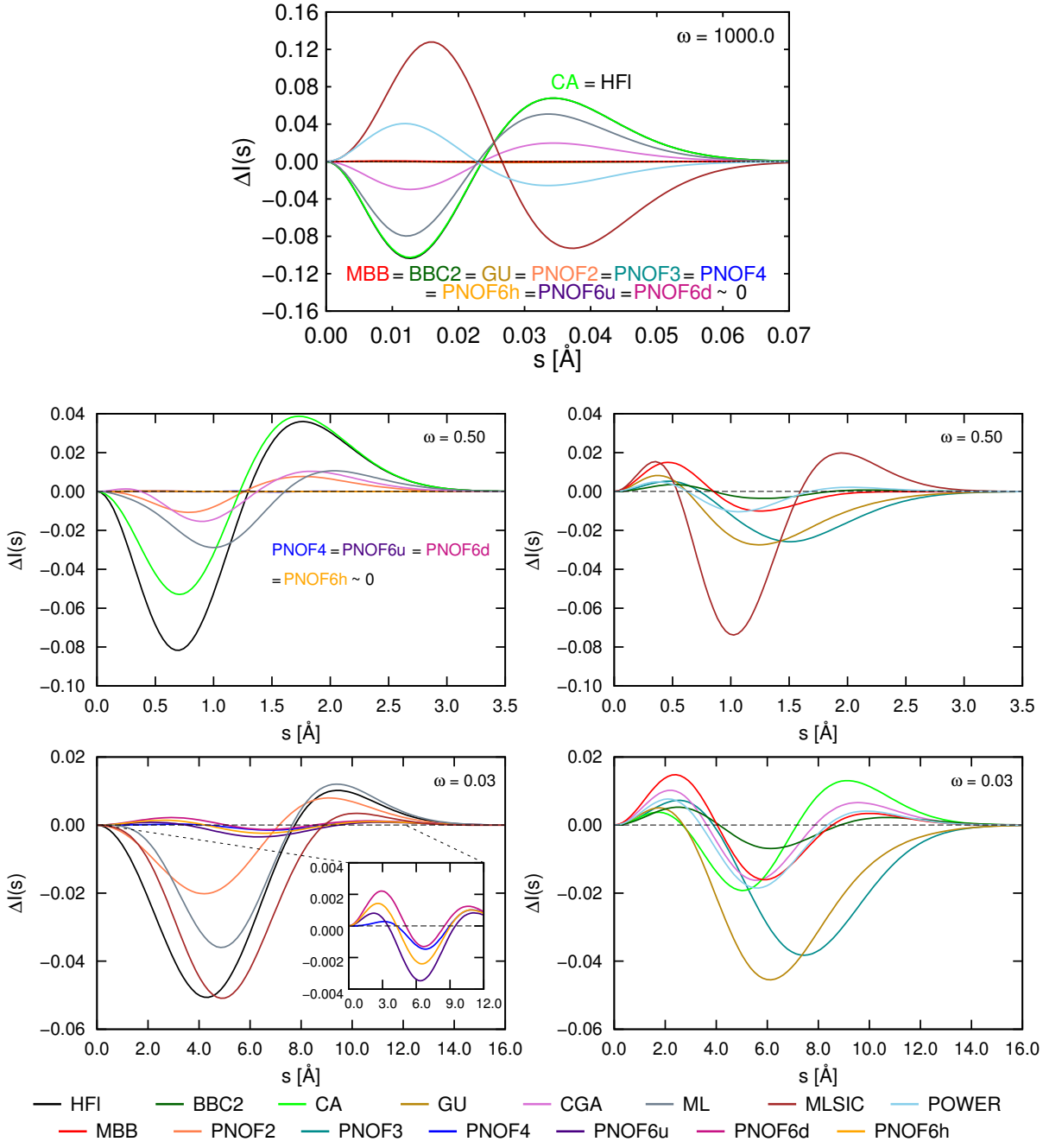

Figure 11 – Difference between the exact and the approximate radial intracule density for three values of ω (1000, 0.5 and 0.03).

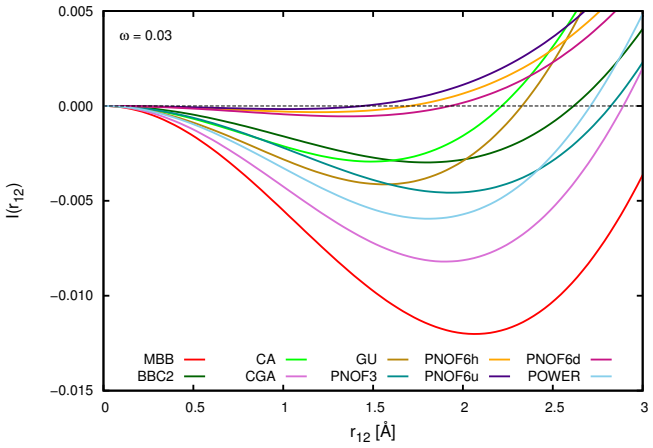

Figure 12 – Approximated radial intracule probability densities for $\omega = 0.03$ in the small r_{12} region.

9.2.7) The V_{ee} Energy

Our last test consisted in the analysis of the V_{ee} energy produced using these approximations. Recall that this component is the only one that is approximated by all the functionals here studied. Our results demonstrate that the relative error in the V_{ee} energy increases with correlation but, in general, all approximations perform relatively well in reproducing the V_{ee} energy. The POWER functional was fitted to produce V_{ee} that differs in less than 10^{-5} a.u. with respect to the exact V_{ee}, therefore, it was not included in the analysis.

9.3) Characterization of Bonds from Electron-Pair Distributions

9.3.1) The $^{1,3}\Pi_u$ Excited States of H_2

In chapter VI, we studied the evolution of electron-pair distributions along the bond formation/cleavage process. Our first analysis focused on the electron-pair distribution of the $^{1,3}\Pi_u$ excited states of H_2. Correlations between electrons are sometimes counterintuitive, a rather simple but counterintuitive case given by the $^3\Pi_u$ electronic excited state of H_2. Tal and Katriel [203], and Colbourn [204] found and reported the counterintuitive non-monotonic behavior of the electron repulsion energy in the $^3\Pi_u$ excited state of H_2 as a function of the internuclear separation. It was observed by comparison with some Hartree-Fock calculations an increase of the V_{ee}, accompanied by a decrease of the $\langle s \rangle$, when the H-H bond is stretched. The configuration $1\sigma^1 1\pi_u^1$ produces the $^3\Pi_u$ state and also the $^1\Pi_u$ state, but the latter does not present any counterintuitive effect when the bond is stretched. In order to confirm this effect, we performed FCI calculations to obtain potential energy curves for $^3\Pi_u$ and $^1\Pi_u$ excited states and we checked that the computed data matched well with the available experimental data (see Table 3). Then, we observed that for the geometries which lie in the interval $R_{HH} \in [0.2, 0.5]$, the counterintuitive effect in the $^3\Pi_u$ was confirmed at the FCI level of theory. From the Pauli principle it is well known that the spatial part of the electronic wavefunction for the triplet state must be antisymmetric with respect to the exchange of the electronic coordinates $\mathbf{r}_1 \leftrightarrow \mathbf{r}_2$. Thus, it is easy to prove that $I(0) = 0$ for the triplet state. Our computed values for the $I(0)$ lend further support to the accuracy of our calculated intracule densities. For the singlet state $I(0) > 0$ was obtained (see Table 3) and we know that the intracule density is a continuous function. Therefore, one expects that the probability for finding electrons close to each other should be larger in the singlet than in the triplet. Following Hund's rule, the triplet should be much more stable than the singlet due to the reduction of repulsion that is imposed

by the Pauli principle. Nevertheless, this is not the case if we look at the V_{ee} reported in Table 3. Actually, it is well-established that the V_{ee} is larger for high spin states than lower spin ones for the same configuration. The only reason for the triplet to be lower in energy than the singlet is that the triplet state favors intermediate interelectronic distance with respect to the singlet (that shows non null probabilities for larger interelectronic distances). When intermediate interelectronic distances are favored, the electronic cloud is more compact and the screening of the external potential, produced by the nuclei, is less strong; the electron-nucleus attraction is much larger in the triplet than in the singlet, compensating, the larger V_{ee} obtained for the triplet state.

Table 3 – Equilibrium distances given in a.u., energies in a.u., vibrational frequencies in cm^{-1}, V_{ee} in a.u. and electron-electron coalescence densities in a.u. for $^3\Pi_u$ and $^1\Pi_u$ excited states. In parentheses we provide the experimental data taken from Herzberg [4].

	$^1\Pi_u$	$^3\Pi_u$
R_e	1.95	1.96
	(1.952)	(1.961)
E	-0.716055	-0.736850
ω_e	2446.2	2460.9
	(2442.7)	(2465.0)
V_{ee}	0.229863	0.246438
$I(0)$	0.81×10^{-2}	0.26×10^{-6}

9.3.2) The Electron-Pair Density Distribution Along the Bond Formation Process

Our second study covers the changes of the electron-pair density distribution along the bond formation process. A set of diatomic molecules is used to understand the rearrangements that lead to changes on the electron-pair density distribution. In order to follow these rearrangements, we decided to work with the $I(s)$ but subtracting from it the non-relaxed one, $I_{nrel}(s)$, the latter being defined as

$$I_{nrel}(s) = \sum_{A} I_A(s) + \sum_{A<B} I_{AB}(s), \tag{108}$$

where the first term at the r.h.s accounts for atomic contributions and is computed from isolated atoms, and the second term involves the summation of all interatomic contributions computed from nonrelaxed densities,

$$I_{AB}(s) = s^2 \int \rho_A(\mathbf{r}_1)\rho_B(\mathbf{r}_2) d\mathbf{r}_1 d\mathbf{r}_2 d\Omega_s, \tag{109}$$

where $\rho_A(\mathbf{r}_1)$ is the density of the isolated atom A. The $I_{nrel}(s)$ was proven to be a "poor man's" approach to the real $I(s)$ by Piris et al. [205], and not enough to capture many electronic effects such as the ones producing van der Waals interactions. The difference $I(s) - I_{nrel}(s) = \Delta h(s)$ was computed for several geometries in an interval that covers from the nearly isolated species till the equilibrium distance (R_e) for the following set of diatomic molecules: H_2, HeH^+, BH, Li_2, CO, F_2 and LiH (in its ground state $X^1\Sigma^+$ and its first excited state $A^1\Sigma^+$).

The first bond formation studied was the covalent bond of H_2 molecule (in the ground state). For this purpose, we performed FCI calculations using aug-cc-pVDZ basis, then we computed the $\Delta h(s)$ (called the $\Delta h(u)$ in this work) and plotted it in Fig. 13 for some different bond lengths. We observed that the pair density shrinks upon the formation of the chemical bond increasing the probability of having the electron pair at shorter distances. The bond of HeH^+ ion was also used to study the changes in the electron-pair probability density.

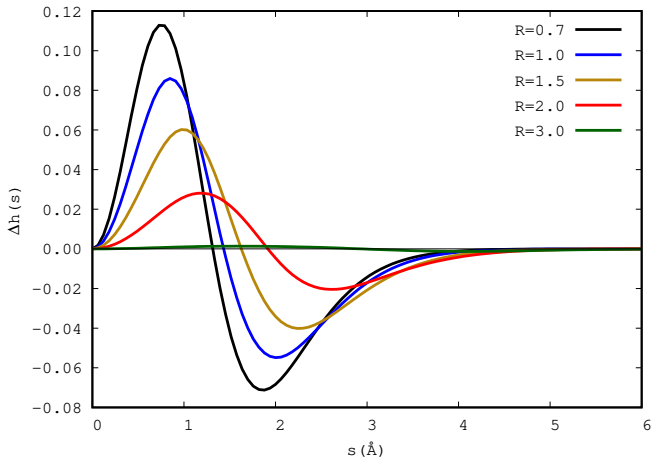

Figure 13 – $\Delta h(s)$ of H_2 at different bond lengths (all R in Å).

This two-electron system is formed from a He atom and a proton (H^+), and the $I_{nrel}(s)$ is always that of the isolate He atom. In Fig. 14, we have plotted $\Delta h(s)$ for this system, and observed that the redistribution of the electron-pair probability density is less important than in H_2 because the values of $\Delta h(s)$ are one order of magnitude lower than in the previous case. We know that when the He atom approaches the proton, the electronic density, $\rho(\mathbf{r})$, is redistributed between the two centers. We observed a maximum of the $\Delta h(s)$ which lies near the interatomic distance and a minimum around ca. 0.5 Åthat allows us to conclude that $I_{nrel}(s)(\equiv I_{\mathrm{He}}(s))$ puts more electron-pair probability density at smaller interelectronic distance than the actual $I(s)$. Only at the equilibrium distance, there is a decease of the electron-pair probability at small and at large interelectronic distance with respect to the isolated He atom. The decrease, in this latter case, is accompanied by an increase in the neighborhood of the interatomic distance. The minimum observed around 0.3-0.5 Åis in accord with the fact that only an internal pair reorganization of He atom electrons is produced within this molecule.

The next bond we analyzed was the covalent bond of BH molecule. In this system the bond is formed with two electrons, one that belongs to the B atom

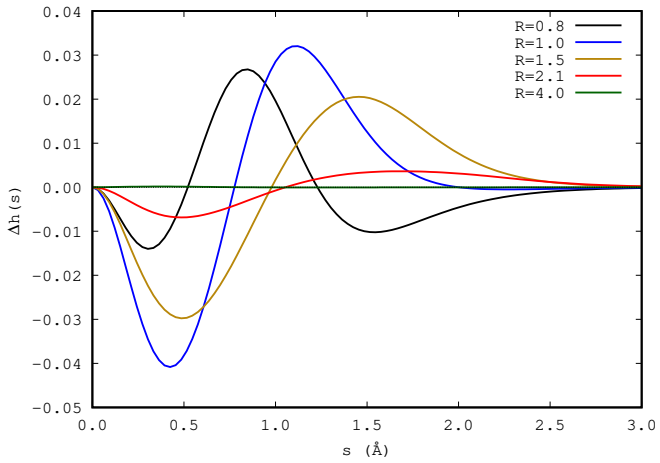

Figure 14 – $\Delta h(s)$ of HeH^+ at different bond lengths (all R in Å).

and the second one, which belongs to the H atom. As we can see in Fig. 15, at large interatomic distances, the B atom electronic cloud is distorted making the electrons move towards the H atom, hence the electron pair density shifts to larger distances. Near the equilibrium geometry, the profile of $\Delta h(s)$ changes because the electron-pairs are located around the bond length. The previous example makes clear that the internal reorganization is easily followed from the analysis of $\Delta h(s)$.

The rest of systems studied were F_2, Li_2, CO and LiH (in the latter, we studied two states as we mentioned above). We observed that the reorganization for F_2 takes places in a shorter span than for BH but the maximum of the relaxation hole in this case lies at smaller interelectronic values, suggesting that the two bonding electrons lie in the bonding region instead of on the top of the atoms. The same trending outcome was observed for Li_2 and CO, which allows us to conclude that this must be a feature of covalent bonds. In regard of Li_2, the change is less abrupt and we could appreciate an additional formation of electrons pairs between the electrons of each Li atom and the electron localized in the middle of the two Li atoms (in the non-nuclear attractor). Regarding CO, at large interatomic distances, a first reorganization of the lone pairs is observed

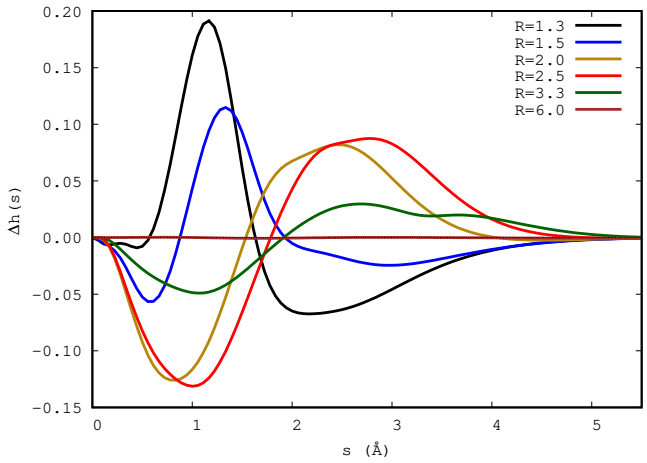

Figure 15 – $\Delta h(s)$ of BH at different bond lengths (all R in Å).

and only at around $R_e + 1$ Å, occurs the most important electron-pair reorganization before the bond is formed. The distance between the maximum of $\Delta h(s)$ and its minimum is the shortest among those studied in this work, only followed by F_2, which is due to the more electronegative character of the C and O atoms, preventing these atoms to experience larger deformations on the electron pair density. Finally, the last system under study is LiH in its ground $X^1\Sigma^+$ and excited $A^1\Sigma^+$ states. These states dissociate to H(^2S) and Li(^2S), and H(^2S) and Li(^2P), respectively. We have used them to characterize the so-called harpoon mechanism,[31] where an electron is transferred from the H to the Li atom to form the bond. In this mechanism, the adiabatic potential energy curve passes through an avoided crossing and changes the character from covalent (when the system is dissociated) to ionic (when the systems is bonded). In the ground state, the avoided crossing happens at around $R_{\mathrm{LiH}} = 3.6$ Å, whereas in the excited state, the avoided crossing lies around $R_{\mathrm{LiH}} = 6$ Å. Our results shown that the $\Delta h(s)$ profile of the ground state only resembles the usual profile of covalent bonds for large R_{LiH} distances (where the covalent character is dominant). On

[31] We will focus on this mechanism in more detail in the last part of the *Results and Discussions* section.

the other hand, near the equilibrium distance the $\Delta h(s)$ profile resembles the profile of BH. Actually, for large R_{LiH} distances the $X^1\Sigma^+$ and $A^1\Sigma^+$ states produce similar $\Delta h(s)$ profiles. Only for small interatomic distances, the profile for the $A^1\Sigma^+$ is different to the rest due to the rather polarized character of this bond with little formation of short-range electron pairs.

In this study, we also explored the usage of approximate intracules for visualizing the changes in the electron-pair distribution along the bond formation process. In the results presented above, we used highly accurate wavefunctions (FCI or CASSCF) and exact 2-RDMs extracted from these wavefunctions. Nevertheless, to make this kind of analysis much more affordable (from the computational cost perspective) for large and complex systems, it is mandatory to suggest alternatives to the exact FCI wavefunction. Thus, we suggested in this work the usage of the unrestricted coupled-cluster with singles and doubles included (UCCSD) approximation to replace the FCI wavefunction in systems where dynamic correlation effects are dominant. Unfortunately, (U)CCSD wavefunctions do not satisfy the Hellmann-Feynman theorem [206] and usually an expensive energy-derivative procedure is employed to obtain 2-RDMs from CCSD wavefunctions [67]. Thus, in this work we also decided to approximate the 2-RDM construction and we chose MBB approximation to this end because this approximation is being widely used for computing some other chemical descriptors like the DI [115]. From our UCCSD calculation, natural orbitals and natural orbitals occupancies were built and later used to construct the 2-RDM needed for computing the $I(s)$. An unrestricted formalism was chosen because for the isolated species usually the ground state was an open-shell atom (that is better described by an unrestricted formalism) and, to be consistent, we were forced to compute the $I(s)$ also using an UCCSD wavefunction. Also, our tests proved that at the $R_{\mathrm{AB}} \to \infty$, the $\Delta h(s)$ did not tend to zero as we would expect. Our results demonstrated that using UCCSD and MBB produces results practically indistinguishable from the reference ones. Interestingly, even if we take the CASSCF occupancies and natural orbitals for CO, and use the MBB ap-

proximation instead of the exact 2-RDM, the results are in good agreement with the reference CASSCF exact ones; proving that even in this system dominated by nondynamic correlation effects, using MBB approximation is indeed a good approximation to the exact 2-RDM.

9.4) Some Feature of the Coulomb Hole of Neon Atom

In this thesis, in chapter VII, we used the electron-pair distribution density to understand a certain feature produced by correlations that is present in the Coulomb hole of Neon atom. Bunge and coworkers [207], in 1969, and Cioslowski and Liu [208], thirty years later, obtained the Coulson's Coulomb hole for Neon atom. Both Coulomb holes showed an intriguing shoulder (or a minimum) ca. 0.1 Å, in the short-range region of the hole. Only Bunge intended to attribute it some meaning, suggesting it was due to the K-shell electrons. In order to confirm this observation, we obtained FCI wavefunctions for some basis sets of Pople, Dunning and Petersson (when a FCI calculation was computationally affordable). Then, we noticed that Pople's basis 6-311G and cc-pCVTZ basis were able to reproduce the shoulder. We knew from Bunge's work that most of correlation effects could be retrieved by including only singles and doubles excitations. Thus, we performed CISD calculations and confirmed that only little differences between the hole computed with the exact FCI and the hole computed with CISD approximate wavefunctions were observed. The advantage of using a CISD approximation is that larger basis can be used due to the reduction of the number of determinants involved in the construction of the wavefunction. In an attempt to confirm that the shoulder was not merely an artifact of Pople's basis, we optimized our own set of even-tempered [209] basis at the CISD level. Even-tempered basis contain groups of basis functions classified with respect to the exponents $\chi^k_{L,N}$, that are even-tempered according to the expression

$$\chi^k_{L,N} = \alpha_{L,N} \left[\beta_{L,N}\right]^{k-1}, \qquad 1 \leq k \leq N, \tag{110}$$

the exponent assigned to each group is given by k, while $\alpha_{L,N}$ and $\beta_{L,N}$ are determined by minimization of the CISD energy and are unique for each basis set. From Eq. 110, we observe that even-tempered basis are defined using two numbers: the angular momentum, L, and the number of basis functions of each type, N. For instance, if we set $N = 6$ and $L = 1$ then, this basis is labeled as 6SP and it contains 6s and 6p uncontracted basis functions (notice that each p function includes three Cartesian functions: p_x, p_y and p_z). We covered the ranges of $1 \leq L \leq 4$ and $6 \leq N \leq 16$ meaning that the largest basis optimized was 16SPDFG (which contains a total of 400 basis functions). Our CISD and HF energies extrapolated to infinite basis were -128.9254609 a.u. and -128.547100 a.u., respectively. Being both results in good agreement with all previous studies found in the literature [207, 210, 211]. Our best CISD estimate of the correlation energy is -0.378361 a.u., which represents 97% of the correlation energy of Ne. Our best variational result obtained with the 16SPDFG basis recovers up to 93% of the correlation energy. For the whole set of wavefunctions, we checked the convergence of some properties with respect to L and N, and the 9SP basis set seemed to provide a reasonable description of the system. Therefore, the 9SP basis set was an excellent candidate to understand the nature of this shoulder. Let us point out that for all CISD wavefunctions computed with our optimized even-tempered basis, the shoulder was always observed, as we can see in Fig. 16 (in fact, a minimum instead of a shoulder is observed for all $L = 1$ basis set).

Nevertheless, when a frozen-core approach was used and the $1s^2$ electrons of Ne were not correlated, the shoulder (minimum) vanished as we can see in Fig. 17. Also, we noticed that for any basis set for which the shoulder was present, like 6-311G, the frozen-core approximation of the Coulomb hole does not show any shoulder. Thus, we were able to conclude that the shoulder appears due to correlation effects of the core electrons.

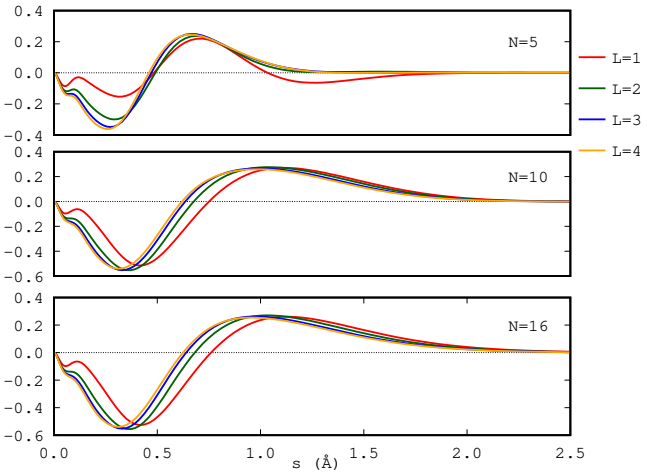

Figure 16 – The CISD Coulomb hole of Ne for some even-tempered basis.

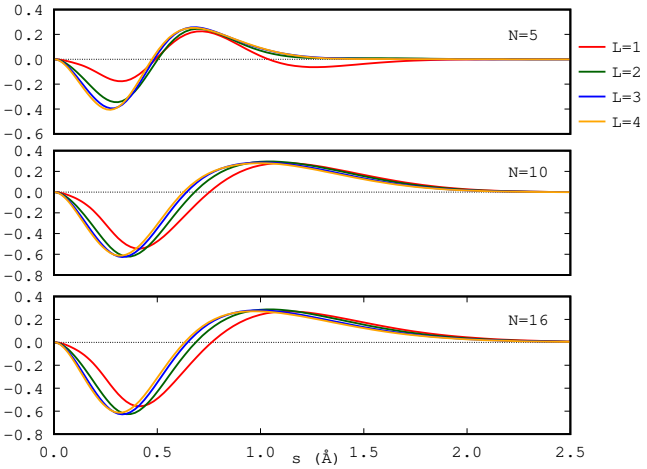

Figure 17 – The frozen-core CISD Coulomb hole of Ne for some even-tempered basis.

Our analysis of the shoulder was done with the CISD wavefunction built using the 9SP basis but removing some excitation. In Fig. 18 we have plotted the Coulomb holes for the fc-CISD and CISD wavefunctions but also: A) the Coulomb hole obtained with the CISD wavefunction but where all the excitations of the core electrons except the singles ones were removed (CISD(nc)+A), B) including all singles excitations of the core electrons but also the double ex-

citations where only one of the $1s^2$ electrons is involved (CISD(nc)+B), C) the wavefunction including all previous excitations plus the most important simultaneous double excitations of the $1s^2$ core electrons, which from Fig. 18 seem to be the most important for producing the shoulder (CISD(nc)+C), and D) Finally, a detailed analysis allowed us to conclude that the most important excitations that contribute to the shoulder are the doubles excitations from the $1s^2$ to the 4s, 5s, 5p and 6p orbitals (CISD(nc)+D). These results were also confirmed qualitatively with the wavefunction obtained using the 16SPDFG basis. Our analysis of the one electron potential of Kohout [212], allowed us to define the radius of the K-shell ($r_K = 0.138$ Å) which remains invariant under inclusion of correlation effects. We also proved that there was a little difference in the K-shell number which only increases by $3{\cdot}10^{-3}$ electrons due to correlation. Therefore, we concluded that there is only a reorganization of the electron density which is pushed to the boundary of the K-shell with the L-shell. Finally, our analysis of the type of correlation demonstrated that this effect is purely produced by short-range dynamic correlation.

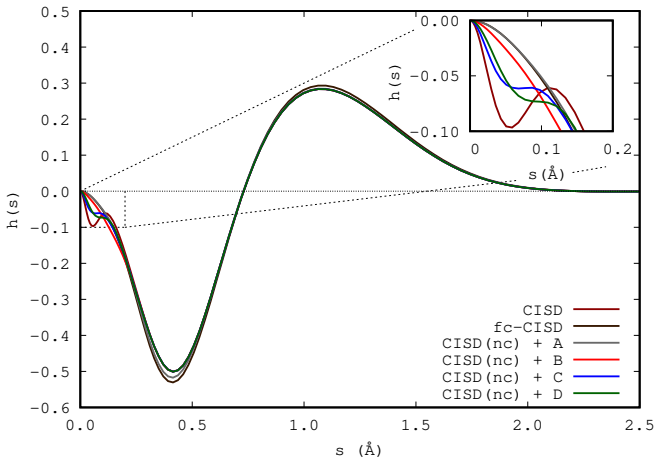

Figure 18 – The CISD/9SP Coulomb hole in terms of several expansions. fc-CISD calculations were obtained from a CISD calculation in which no excitations from core orbitals were allowed, whereas CISD(nc) is a regular CISD calculation in which the configurations involving excitations from the core orbital have been removed *a posteriori*. A-C are groups of configurations including various excitations from the core orbital: (A) single excitations, (B) double excitations involving only one electron in the core orbital, (C) double excitations involving the two electrons in the core orbital excited to one single orbital, and (D) double excitations involving the two electrons in the core orbital excited to orbitals 4s, 5s, 5p and 6p. After removal and addition of these configurations, the expansion coefficients have been rescaled to attain the normalization of the wavefunction.

9.5) The Harpoon Mechanism: An Approach from Bonding Descriptors

In chapter VIII, we studied the harpoon mechanism using bonding descriptors. This mechanism was proposed by Polanyi as an attempt to justify the large cross-sections in the formation of alkali halides. In these systems, the Coulomb attraction needed to favor the electron-transfer process is usually small due to the similar ionization potential of the alkali and the electron affinity of the halogen, which favors the electron transfer at large separations. On the other hand, for alkali hydrides the process takes place at shorter distance separations than for alkali halides because of the electron affinity of H is smaller than the ion-

ization potential of alkali. The goal of this chapter is visualizing the electron transfer using bonding descriptors (like the ELF, the Laplacian of the electronic density) and highly accurate wavefunctions. Ponec and coworkers [213] had shown before that the DI for LiF and BeH shows a peak in the vicinity of an avoided crossing of two adiabatic states. The DI should be able to recognize the electron transfer due to the changes in the bond order that the electron transfer produces, because, the bond order is zero at the dissociation limit, then, it increases up to the avoided crossing (due to the formation of the covalent bond) and, finally, after the avoided crossing the bond order should decrease due to the change of character of the bond (i.e. the change from mostly covalent to nearly ionic, which reduces the bond order). Interestingly, the DI computed using QTAIM definition of atoms produces the peak in the vicinity of the avoided crossing whereas Mulliken atomic partition does not produce it. In this study we also analyzed which atomic partitions are able to produce the peak near the avoided crossing.

The systems that we selected for this work were LiH, LiF and BeH dimers, which are expected to follow the harpoon mechanism because their adiabatic potential energy curves pass through an avoided crossing in the ground state, BH whose potential energy curve does not show any avoided crossing but its bond is very similar to the previous ones and, finally, some counter examples that should not follow the harpoon mechanism: H_2, He_2, CO, F_2, N_2 and O_2. Notice that the last group contains different types of bonds (i.e. single, double, triple but also covalent and weak bonds). FCI wavefunctions were computed for H_2, He_2, LiH, BH and BeH. For the rest of systems, appropriate CASSCF wavefunctions were used. In all cases, we worked with the aug-cc-pVDZ basis set.

The smallest system formed by the harpoon mechanism is LiH. The electron transfer in this case occurs at a short distance comparing to alkali halides. The ground state, $X^1\Sigma^+$, and the first excited state, $A^1\Sigma^+$, produce an avoided

crossing at around R_{HH} =3.7 Å(see Fig. 19). In the ground state, on the l.h.s. of the avoided crossing, the nature of the wavefunction is ionic but on the r.h.s its nature is covalent. Thus, at the equilibrium distance the ionic bond is formed between Li^+H^-, while at the dissociated limit neutral atoms are formed ($H(^2S)$+$Li(^2S)$). The $A^1\Sigma^+$ state shows a second avoided crossing with the $B^1\Sigma^+$ state at about 5.9 Å. The $A^1\Sigma^+$ bond is covalent at the equilibrium then becomes ionic after the avoided crossing at 3.7 Åand, finally, it becomes covalent again when atoms are dissociated ($H(^2S)$+$Li(^2P)$).

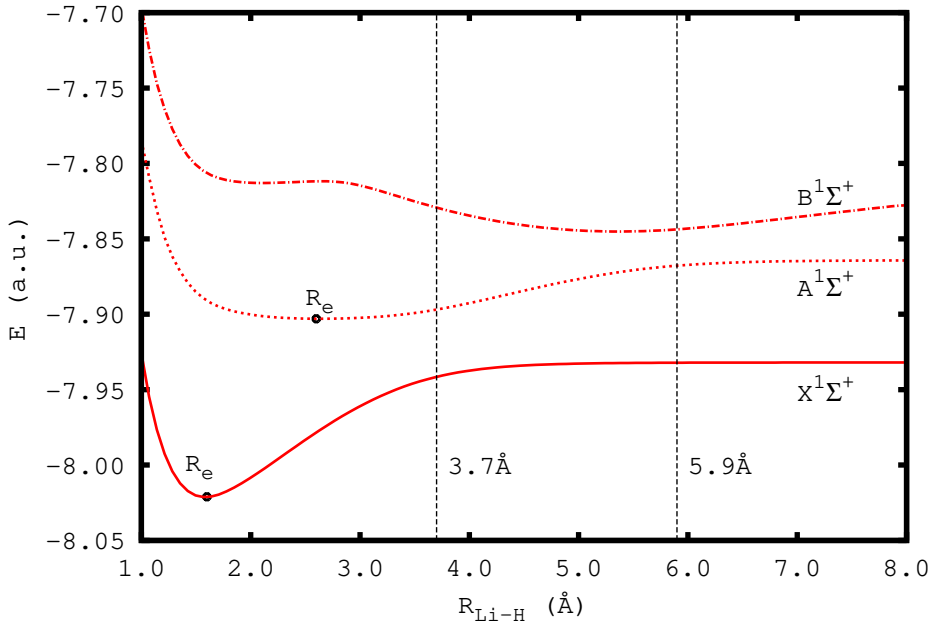

Figure 19 – Potential energy curve of LiH for the ground state ($X^1\Sigma^+$) and the two lowest lying $^1\Sigma^+$ states. Energy in a.u. The vertical dashed lines mark the corresponding avoided crossings.

Our first analysis was of the changes of the atomic QTAIM populations due to the electronic density transfer. In Fig. 20 we have plotted the changes in the atomic QTAIM population of the most electropositive atom for all systems here

studied. Firstly, we notice that for LiH in the ground state there is a transfer of about 0.9 electrons from H to Li near the avoided crossing, which changes the bond character from ionic to covalent. In the case of the $A^1\Sigma^+$ excited state, with respect to the equilibrium distance there is a transfer of about 0.5 electrons from Li to H, which changes the character of the bond from mostly covalent to nearly ionic. Nevertheless, near the second avoided crossing the electronic density transfer is from H to Li, which ends up gaining ca. 0.2 electrons in the end (when the fully covalent picture is recovered). Notwithstanding, it is evident from Fig. 20 that some molecules not formed through the harpoon mechanism, like CO, also experience important changes in their atomic QTAIM populations when their bond is stretched, thus, large changes of the atomic QTAIM populations do not ensure that a system is formed through the harpoon mechanism.

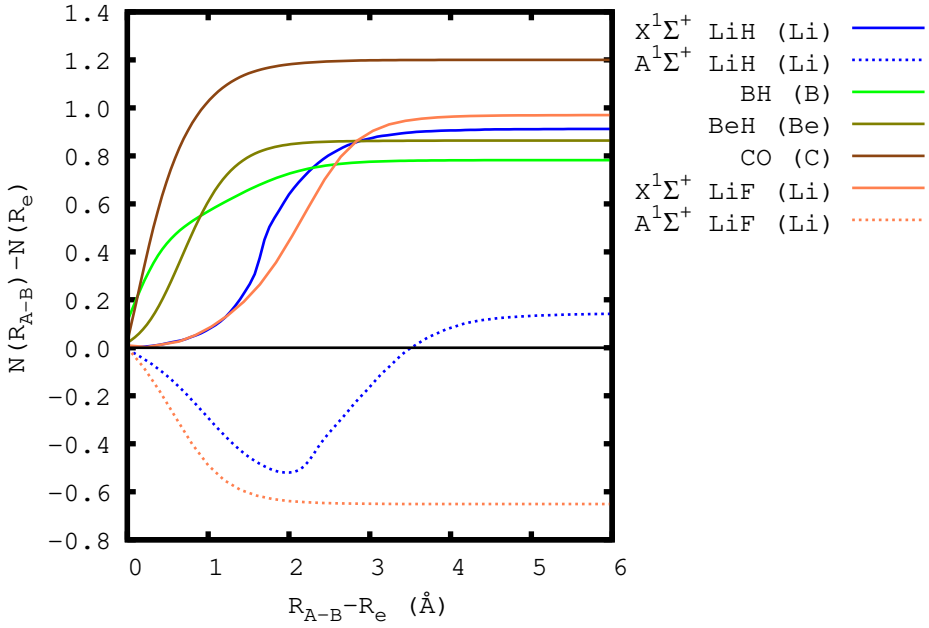

Figure 20 – Change in the atomic QTAIM population of the most electropositive atom along the bond stretching in the series of studied molecules that present electron reorganization. Population units are in electrons.

It is much more convenient to use the DI to follow the electron density transferred as some authors previously demonstrated [213]. In Fig. 21 we have plotted the DI for LiH $X^1\Sigma^+$ state. The plot of the DI shows that near the equilibrium region the DI starts at a very low value (i.e. ca. 0.19 that is in good agreement with the ionic character system near the equilibrium geometry) and slightly decays when the bond is stretched. But the DI then increases up to a maximum at 3.3 Åin the vicinity where the avoided crossing is located. The increase of the DI is produced due to the rise of the covalent character of the wavefunction, the peak being produced at the geometry where the largest variation of the electron population takes place; we know that at this point 0.5 electrons were already transferred from Li to H. From the analysis of the DI we have identified the position where the electron remains in *no one's land* which is easily identified with the avoided crossing. For the $A^1\Sigma^+$, the covalent character is larger in this state and the DI is larger than the DI of the ground state. The DI for the excited state increases towards a maximum that is localized near the first avoided crossing but then remains almost constant, only slightly decaying and growing again, until it reaches a second maximum in the region where the second avoided crossing lies (between the $A^1\Sigma^+$ and $B^1\Sigma^+$ states). Finally, the DI decays to 0 for large interatomic distances. These two maxima obtained for the DI correspond to the points where a maximal transfer variations takes place between the Li and the H atoms.

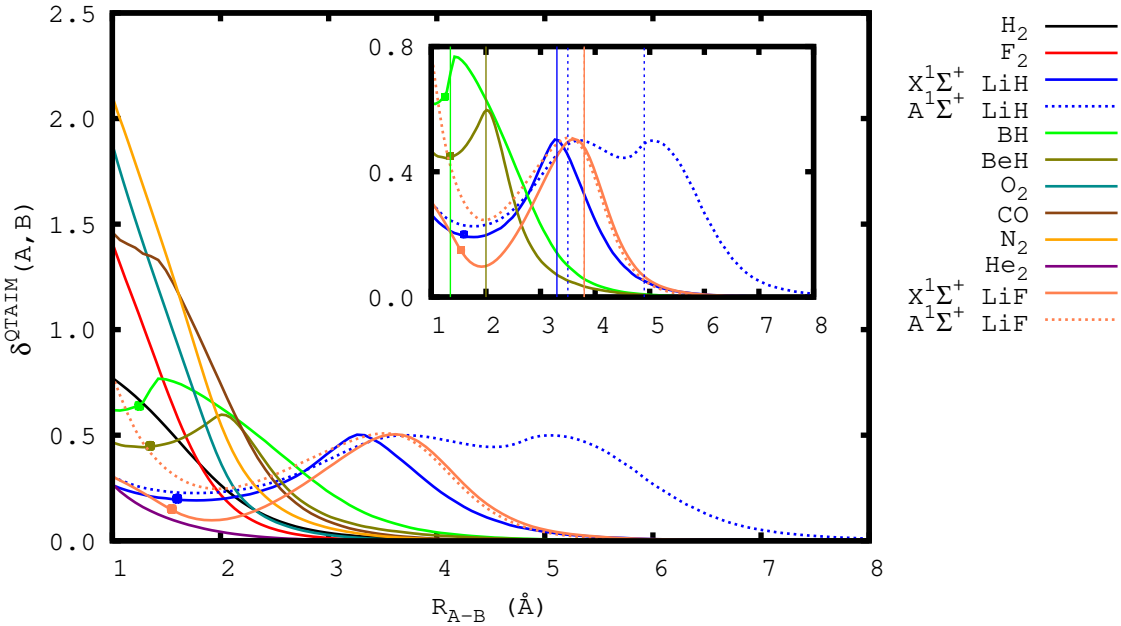

Figure 21 – Delocalization index from QTAIM partition. Solid lines are used for ground state and dotted lines for the excited states. The solid point indicates the equilibrium distance and vertical lines in the inset mark the geometries at which the maximal electron-transfer variation points (see text) is observed. DI units are electron pairs.

In an attempt to visualize this electron transfer we also used the ELF and the Laplacian of the electronic density in this work. As we said in the *Methodology* section, the ELF allows us to characterize localized electrons. Our analysis of the ELF does not reveal the presence of a separate basin that corresponds to the electron transferred. Only a progressive elongation of H's valence basin that splits and is finally absorbed by Li's basin was observed. 3D plots of the ELF do not allow an easy visualization of the electron transferred but 2D plots along the interatomic axis do. Fig. 22 includes several profiles of the ELF along the interatomic axis of LiH's ground state. The vertical dashed line marks the QTAIM bond critical point between Li and H. From this plot, we observe that about the avoided crossing the Li basin emerges at one end of the molecule, while the H basin splits into two that still belong to H. At 3.3 Å, the H peak

splits and part of H basin is transferred to Li QTAIM atomic basin. At 5 Å, the process is almost complete and Li valence basin is fully formed. Similarly, for the $A^1\Sigma^+$, only the formation of a peak in H basin appears and is completely transferred to Li only after the second avoided crossing.

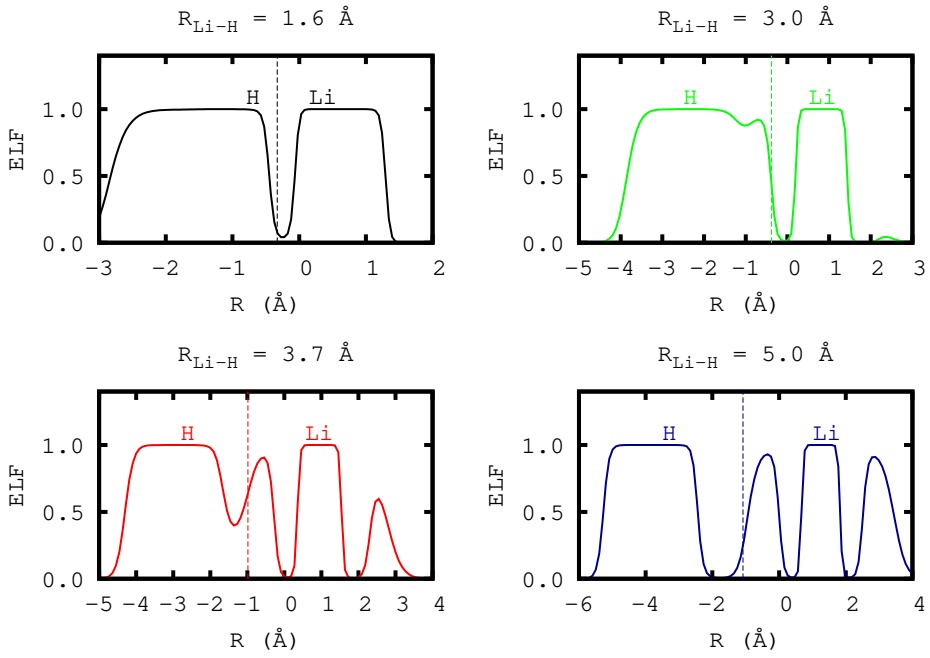

Figure 22 – The ELF profile for $X^1\Sigma^+$ state of LiH along the interatomic axis for several R_{LiH} distances. The zero is always located at the center of mass and the vertical dashed lines represents the bond critical point.

Likewise, the scan of the Laplacian of the electron density, $-\nabla^2\rho(\mathbf{r})$, at different interatomic distances reveals the harpoon mechanism. In Fig. 23, we present in logarithmic scale the scan of the negative values of the Laplacian and we used dashed vertical lines to indicate the bond critical points. For the $X^1\Sigma^+$ state, at 2 Åthe peak corresponding to H expands and later splits into two peaks at $R_{\mathrm{LiH}} = 2.5$ Åthat still belong to H basin. Later, the small peak crosses the bond critical point border and becomes the valence basin of Li at about 3.7 Å. In this work, we also proved that the electron transfer in the $A^1\Sigma^+$ state (according to

the Laplacian of the electron density) occurs between the two avoided crossings.

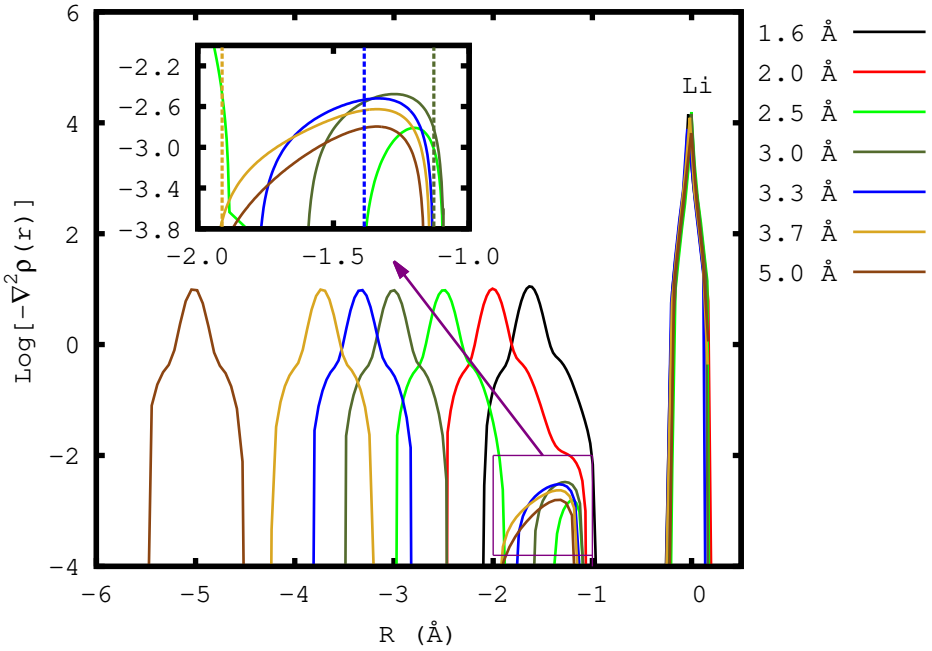

Figure 23 – Negative values of the Laplacian of the electron density (in a.u.) for the $X^1\Sigma^+$ state of LiH along the interatomic axis for several R_{LiH} distances. The Li atom is located at the origin. Vertical dashed lines indicate the bond critical point.

Our study using the DI, the ELF and the Laplacian demonstrated that the formation of BeH and LiF is also through the harpoon mechanism. In the case of BeH, the ionization potential of Be is larger than the Li one and, hence, the electron transfer takes place at short distances. On the contrary, in LiF the difference between the ionization potential and the electron affinity makes the transfer to take place at large interatomic distances. Among the counterexamples used in this work, for CO we observed large changes of the populations of the species (see Fig. 20), nonetheless, there was no maximum of the DI, suggesting that this molecule was not formed through the harpoon mechanism. Also, the analysis of the ELF and the Laplacian in the CO molecule revealed

that there is only a bond dissociation process, where the electron density that was forming the bond is splitted among the two atoms (see Fig. 24 for example). Only for BH there is a maximum at very short interatomic distances (ca. 1.5 Å) for the DI but there is no avoided crossing. Therefore, there must be an important electron reorganization when BH bond is formed. The ground state DI is rather large ($\delta(B,H) = 0.6$) for ionic species and the valence bond description assigns a covalent bond for this system. The profile of the ELF and the Laplacian coincides with the results obtained for molecules that follow the harpoon mechanism, but the absence of an avoided crossing suggests that BH is formed through the harpoon mechanism without the existence of the avoided crossing.

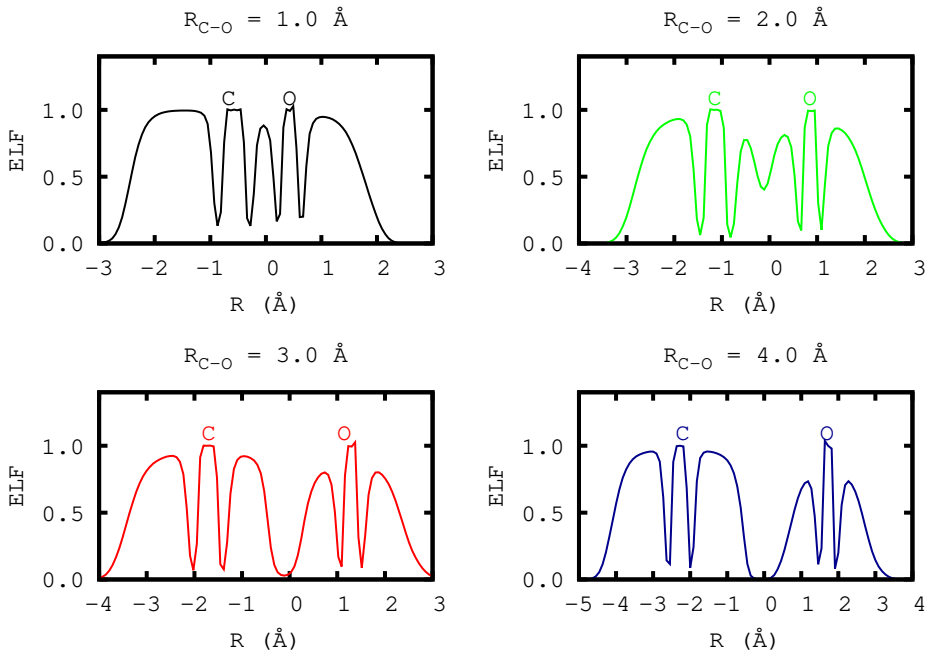

Figure 24 – The ELF profile for $X^1\Sigma^+$ state of CO along the interatomic axis for several R_{CO} distances. The zero is always located at the center of mass.

Information theory indicators (Shannon entropies and Fisher integrals) were also used in this study in an attempt to follow the electron transfer process.

To do so, we took the values at infinity minus its value at different interatomic distances ($\Delta X = X^{\infty} - X$). Among these properties, Shannon entropy (S_ρ and S_π) profiles do not allow to distinguish the type of bond because all systems produce similar plots. On the contrary, Fisher integrals presented distinctive profiles for molecules following the harpoon mechanism (see Figs. 25a and 25b). ΔF_π presents large values around the equilibrium region for molecules following the harpoon mechanism (only H_2 provides unexpected large ΔF_π values near the equilibrium distance). Using ΔF_ρ it was easy to distinguish molecules following the harpoon mechanism (see Fig. 25b) because a maximum near the avoided crossing was observed for those molecules. Again, only H_2 presents an unexpected maximum, making ΔF_ρ not a sufficient condition for the harpoon mechanism.

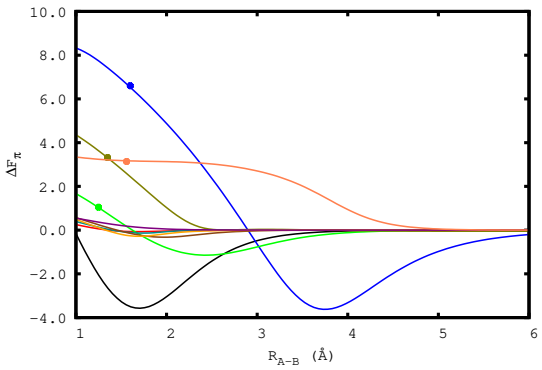

(a) $\Delta F_\pi = F_\pi^\infty - F_\pi^{R_{\mathrm{AB}}}$ plots against the interatomic distance.

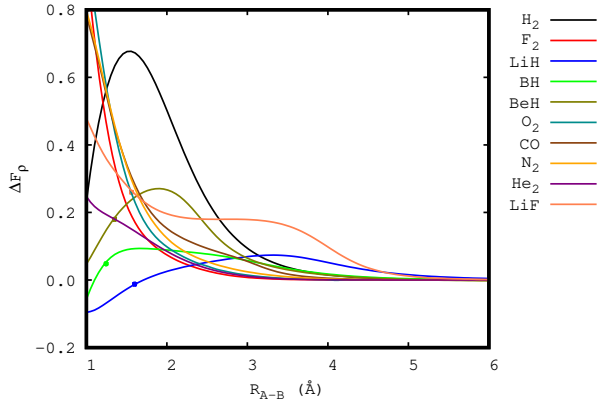

(b) $\Delta F_\rho = F_\rho^\infty - F_\rho^{R_{\mathrm{AB}}}$ plots against the interatomic distance.

Figure 25 – $\Delta F_{\pi,\rho}$ plots against the interatomic distance.

Finally, in this work we also analyzed some other partitions in order to compare them with QTAIM. In Fig. 26 we have plotted the DI computed using TFVC partition. TFVC partition provides a maximum of the DI despite the DI fails to identify the LiH's $A^1\Sigma^+$ as more covalent than the $X^1\Sigma^+$ bond. But it is worth to remark that many other partitions failed to identify the DI maximum characteristic of the harpoon mechanism.

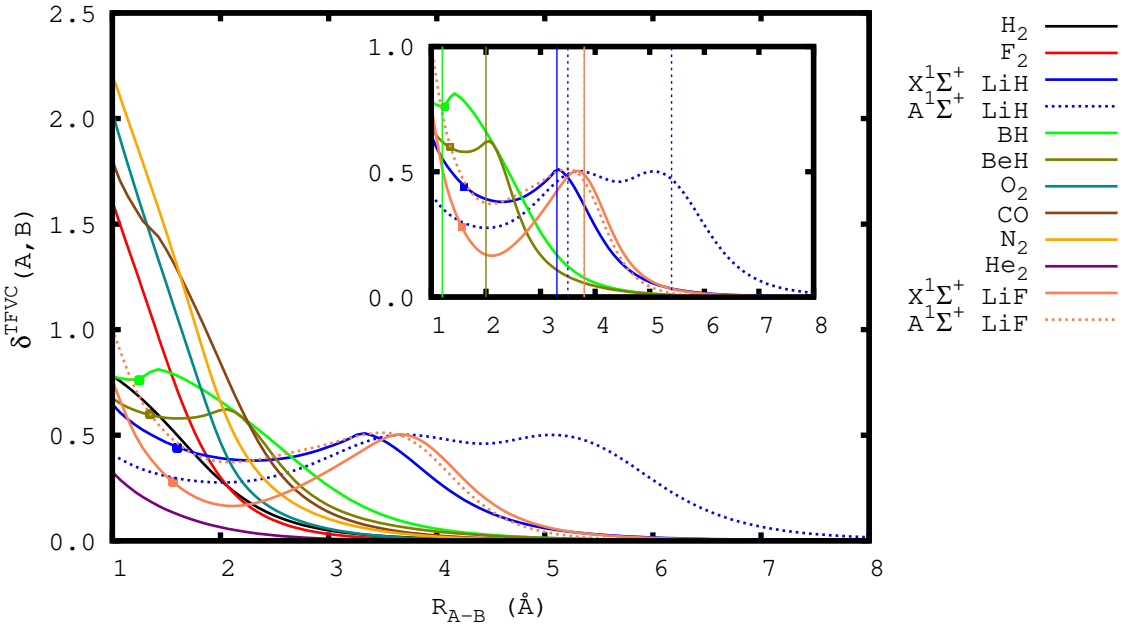

Figure 26 – Delocalization index from TFVC partition. Solid lines are used for ground state and dotted lines for the excited states. The solid point indicates the equilibrium distance. DI units are electron pairs.

X) Conclusions

In this thesis we have seen that the approximations to the 3-RDM perform reasonably well for the computation of the 3c-ESI (specially Valdemoro's approximation), despite they present important deviations for the diagonal elements (which are known to be fundamental for the computation of the 3c-ESI). We have also seen that these approximations fail to satisfy the N-representability conditions. Fermi correlation is the most important contribution to the total electron correlation in the quartet state, while in the doublet state Coulomb correlation, which is also present, is more challenging for the 3-RDM approximations than Fermi correlation. Surprisingly, Mazziotti's approximation performed worse for the doublet state than Nakatsuji's approximation (recall that both approximations are similar by construction, differing only on the phase factor σ_p). Since Mazziotti's approximation gave large deviations to the G N-representability condition, one is prompted to attribute the erratic behavior of this 3-RDM approximation to the violation of this condition. We expect that the construction of new 3-RDM approximations will benefit from the deficiencies shown by the present benchmark.

In our second benchmark we focused on the computation of the 3c-ESI in molecules using the 3-RDM approximations. We have seen that for single-determinant wavefunctions, it is possible to distinguish between 3c-2e and 3c-4e bonds, unfortunately, for correlated wavefunctions it is not possible to classify the bond types attending to the number of electrons. If one wants a clear-cut classification of three-center bonds into 3c-2e and 3c-4e, we recommend the calculation of the 3c-ESI using the Hartree-Fock-like approximation. As we also obtained in the previous benchmark, **Valdemoro approximation provides the most reliable results for the computation of the 3c-ESI and the average numbers of three electrons when compared to the exact values** (i.e. the reference values obtained from the exact wavefunction). On the

other hand, Matito and coworkers' approximation was the second best for the computation of the 3c-ESI and it is much cheaper than Valdemoro's approximation, thus we suggest the usage of the latter for the computation of the 3c-ESI. From the analysis of the atomic partitioning we have seen that TFVC produces values comparable to QTAIM ones. Finally, we have proven that the 3c-ESI computed using the occupancies obtained from MP2 and CCSD (and using the 3-RDM approximations) are comparable to the reference ones in the weak-correlation regime, which opens the avenue for computing approximated 3c-ESI from MP2 and CCSD calculations (in the strong-correlation regime it is better to use CASSCF occupancies for the computation of the 3c-ESI).

The last benchmark of this thesis is devoted to 2-RDM approximations. In this study, we have shown that the two-electron harmonium atom is an excellent model for benchmarking this kind of approximations. The JK-functionals only differ on the K terms and, among them, only the Hartree-Fock-like approximation can satisfy the antisymmetry requirements of the 2-RDM. The Hartree-Fock-like approximation performs better than (or equal to) any other JK-functional in the calculation of the trace and the assessment of the cumulative absolute error for the diagonal elements. These results evidence that **the construction of an approximation needs to consider, at least, both J and K terms**.

The test based on the DI for 2-RDM approximations warns against the use of the Hartree-Fock-like approximation in strongly correlated systems. Although the widely used MBB approximation remains a good approximation in any correlation regime, **from the results obtained in this work we suggest the usage of PNOF6h**.

From the 2-RDM approximations benchmark we have seen that the FP approximation results are significantly better than those obtained with any other approximation, only failing in the strong-correlation regime due to the phase

dilemma.

Our analysis of the radial intracule probability density revealed the presence of **negative probabilities at short interelectronic distances, in clear connection with the violation of the P condition**. It is worth to mention that many functionals performed reasonably well in the calculation of the exact electronic energy (V_{ee}) but produced errors in the calculation of other properties, supporting the claim that functional development should consider other properties besides the electronic energy. Finally, we can draw the conclusion that any approximate 2-RDM should attain as many N-representable properties as possible because the best-performing functionals are those that satisfy most of these conditions. **Some of these N-representable conditions can be imposed in the construction of the functional**.

In the study of the radial IPD of $^3\Pi_u$ state of H_2, **we have demonstrated (at FCI level) that the non-monotonic behavior of the electron repulsion energy with respect to the interatomic separation is real**. There, we proved that the electron repulsion energy increases and the mean interelectronic distance decreases as the interatomic separation increases for the $^3\Pi_u$ state. The $^{1,3}\Pi_u$ states are both generated by the $1\sigma_g^1\pi_u^1$ configuration, thus according to Hund's rule the triplet state must be lower in energy than the singlet state. We have seen that Hund's rule can be explained for these two states due to the shielding effects produced by the corresponding wavefunctions.

We have also worked with the radial IPD in the analysis of the relaxation holes, $\Delta h(s)$, resulting from the difference between the actual radial intracule density and the nonrelaxed one constructed from atomic radial intracule densities and the pair density obtained from the overlap of the atomic densities. Our results established that **the electron-pair formation can be followed from the analysis of $\Delta h(s)$**. The electron reorganization that leads to the bond formation can also be followed using $\Delta h(s)$. The magnitude of $\Delta h(s)$, the shape of

$\Delta h(s) \forall s < R_{eq}$, and the distance between the minimum and the maximum provide information about the nature of the chemical bond formed. **We have also suggested an affordable approach to calculate the radial IPD** from approximate pair densities and using CCSD or CASSCF occupancies and orbitals in MBB approximation to the 2-RDM. Our approximate approach produces relaxation holes almost indistinguishable from the reference ones.

In the last study devoted to the radial IPD, we have analyzed the Coulomb hole of Ne from highly-accurate CISD wavefunctions. The even-tempered basis sets developed recover 97% of the correlation energy of Ne, thus we have used highly accurate wavefunctions for the computation of the Coulomb hole. **We have confirmed the existence of a shoulder for small r_{12} distances in the Coulomb hole of the Ne atom**, which is due to the correlation of the core electrons in the K shell. The double excitations of the CISD wavefunction are responsible for the shoulder, where the latter occurs due to internal reorganization of the K shell (the electrons are pushed towards the K-shell boundary). Some basis sets, such as the correlated-consistent basis set of Dunning, do not display the shoulder, which showed the poor quality of the description of the core electrons when using these basis sets.

Finally, our last work focused on the harpoon mechanism and its characterization using chemical descriptors based on reduced quantities. We have shown that the lowest lying states of LiH can be use to develop and calibrate: a) chemical bonding descriptors, and b) to evaluate the goodness of new atomic partitions. The chemical descriptors must be able to recognize the electron-transfer processes (as it happens in the harpoon mechanism), while the atomic partitions should be able to reproduce the maximum in the DI observed for systems formed by this mechanism. From this study, we concluded that the atomic population can be used to monitor the electron density exchange between atoms, but it cannot be used to discriminate the reaction mechanism (i.e. it is not sufficient to guarantee that a system is formed by the harpoon mecha-

nism). In the majority of cases, the maximal transfer variation point along the bond formation occured when about half electron has been transferred from one atom to another. If the process takes places through a harpoon mechanism, the maximal transfer variation point of the reaction path coincides with the avoided crossing. **Only the DI is able to identify this mechanism, but it does not ensure the existence of an avoided crossing as we have seen for BH**. The DI computed using QTAIM partition was taken as reference in this work, but we showed that TFVC was also able to reproduce the maximum of the DI near the avoided crossing. Unfortunately, TFCV was not able to recognize the $A^1\Sigma^+$ state as more covalent than the $X^1\Sigma^+$ state. The ELF and Laplacian plotted along the interatomic axis at different interatomic distances permitted to monitor the bond formation process better than its three-dimensional counterparts. The transferred electron was seen as a one-dimensional peak in the direction of bond stretching that moved from one atom to another (i.e. crossing the QTAIM atomic boundary). The information theory indicators did not provide a convincing description that allowed a clear-cut separation between the different chemical bond formation mechanisms.

References

[1] E. Matito. *Master in Advanced Catalysis and Molecular Modeling, Subject:"New tools for chemical bonding analysis", classroom notes.* University of Girona, 2018.

[2] M. Rodríguez-Mayorga. RHO-OPS: Density operations., 2015. Institute of Computational Chemistry and Catalysis, University of Girona, Catalonia, Spain.

[3] M. Rodríguez-Mayorga. RHO2-OPS: 2-DM Operations., 2016. Institute of Computational Chemistry and Catalysis, University of Girona, Catalonia, Spain.

[4] G. Herzberg. *Molecular Spectra and Molecular Structure. II. Infrared and Raman Spectra of Polyatomic Molecules.* Van Nostrand, Princeton, 1945.

[5] G. Galilei. *On Motion, and On Mechanics: Comprising De Motu (ca. 1590)*, volume 5. University of Wisconsin Press, 1960.

[6] I. Newton. *Philosophiae naturalis principia mathematica*, volume 1. S. PEPYS, Reg. Soc. PRAESES, London, 1686.

[7] J. C. Maxwell. A treatise on electricity and magnetism, Clarendon Press, Oxford, 1873.

[8] T. Lyman. The spectrum of hydrogen in the region of extremely short wave-lengths. *Astrophys. J.*, 23:181, 1906.

[9] T. Lyman. An extension of the spectrum in the extreme ultra-violet. *Nature*, 93:241, 1914.

[10] J. J. Balmer. Notiz über die spectrallinien des wasserstoffs. *Ann. d. Physik*, 261:80, 1885.

[11] F. Paschen. Zur Kenntnis ultraroter Linienspektra. I.(Normalwellenlängen bis 27000 Å.-E.). *Ann. d. Physik*, 332:537, 1908.

[12] G. U. Kirchhoff. Ber das verhaltnis zwischen dem emissionsvermogen und dem absorptionsvermogen der korper fur warme und licht. *Poggendorfs Ann. d. Physik und Chemie*, 109:275, 1860.

[13] H. Hertz. Ueber einen einfluss des ultravioletten lichtes auf die electrische entladung. *Ann. d. Physik*, 267:983, 1887.

[14] T. Young et al. The bakerian lecture. on the theory of light and colours. In *Abstracts of the Papers Printed in the Philosophical Transactions of the Royal Society of London*, volume 1, pages 63–67. The Royal Society, 1832.

[15] M. Planck. On the law of distribution of energy in the normal spectrum. *Ann. d. physik*, 4:1, 1901.

[16] E. Schrödinger. An undulatory theory of the mechanics of atoms and molecules. *Phys. Rev.*, 28:1049, 1926.

[17] W. Heisenberg. *Über quantentheoretische Umdeutung kinematischer und mechanischer Beziehungen*. Springer, 1985.

[18] M. Born, W. Heisenberg, and P. Jordan. Zur quantenmechanik. ii. *Zeitschrift für Physik*, 35:557, 1926.

[19] N. Bohr. Über die serienspektra der elemente. *Z. Phys.*, 2:423, 1920.

[20] J. P. Klinman and A. Kohen. Hydrogen tunneling links protein dynamics to enzyme catalysis. *Annu. Rev. Biochem.*, 82:471, 2013.

[21] C. H. Bennett and D. P. DiVincenzo. Quantum information and computation. *Nature*, 404:247, 2000.

[22] W. Heisenberg. *Über den anschaulichen Inhalt der quantentheoretischen Kinematik und Mechanik*. Springer, 1985.

[23] L. De Broglie. *Recherches sur la théorie des quanta*. PhD thesis, Sorbone, 1924.

[24] R. Boyle. *The Sceptical Chymist.* J. Cadwell, London, 1661.

[25] P. Pomper. Lomonosov and the discovery of the law of the conservation of matter in chemical transformations. *Ambix*, 10:119, 1962.

[26] A. L. Lavoisier. *Traité élémentaire de chimie: présenté dans un ordre nouveau et d'après les découvertes modernes; avec figures*, volume 1. Cuchet, 1793.

[27] J. Dalton. *A new system of chemical philosophy*, volume 1. W. Dawson, 1808.

[28] C. C. W. Taylor et al. *The atomists, Leucippus and Democritus: fragments: a text and translation with a commentary*, volume 5. University of Toronto Press, 2010.

[29] W. Heitler and F. London. Wechselwirkung neutraler atome und homoöpolare bindung nach quantenmechanik. *Z. Physik*, 44:455, 1927.

[30] R. S. Mulliken. Electronic population analysis on lcao-mo molecular wavefunctions. i. *J. Chem. Phys.*, 23:1833, 1955.

[31] R. S. Mulliken. The assignment of quantum numbers for electrons in molecules. I. *Phys. Rev.*, 32:186, 1928.

[32] F. Hund. Zur deutung der molekelspektren. iv. *Z. Physik*, 51:759, 1928.

[33] M. Born. Quantenmechanik der stoßvorgänge. *Z. Physik*, 38:803, 1926.

[34] M. Born and R. Oppenheimer. Zur quantentheorie der molekeln. *Ann. d. physik*, 389:457, 1927.

[35] E. Hückel. Quantentheoretische beitraäge zum benzolproblem, i: Die elektronenkonfiguration des benzols und verwandter verbindungen. *Z. Physik*, 70:104, 1931.

[36] E. Hückel. Quantentheoretische beiträge zum benzolproblem, ii: Quantentheorie der induzierten polaritäten. *Z. Physik*, 72:310–337, 1931.

[37] E. Hückel. Beiträge zum problem der aromatischen und ungesättigten verbingungen. iii. *Z. Physik*, 76:628, 1932.

[38] E. Hückel. Grundzüge der theorie ungesättigter und aromatischer verbindungen. *Z. Elektrochemie*, 43:752, 827, 1937.

[39] L. Pauling. The nature of the chemical bond. ii. the one electron bond and the three-electron bond. *J. Am. Chem. Soc.*, 53:3225, 1931.

[40] L. Pauling. The nature of the chemical bond. iii. the transition from one extreme bond type to another. *J. Am. Chem. Soc.*, 54:988, 1932.

[41] L. Pauling and G. W. Wheland. The nature of the chemical bond, v: The quantum-mechanical calculation of the resonance energy of benzene and naphthalene and the hydrocarbon free radicals. *J. Chem. Phys.*, 1:362, 1933.

[42] L. Pauling. *The Nature of the Chemical Bond*. Cornell University Press, Ithaca, 1948.

[43] L. Pauling. Modern structural chemistry. Nobel Lecture, December 1954.

[44] W. J. Hehre, R. F. Stewart, and J. A. Pople. Self-Consistent Molecular-Orbital Methods. I. Use of Gaussian Expansions of Slater-Type Atomic Orbitals. *J. Chem. Phys.*, 51:2657, 1969.

[45] R. Ditchfield, W. J. Hehre, and J. A. Pople. Self—Consistent Molecular Orbital Methods. XII. Further Extensions of Gaussian—Type Basis Sets for Use in Molecular Orbital Studies of Organic Molecules . *J. Chem. Phys.*, 54:724, 1971.

[46] W. J. Hehre, R. Ditchfield, and J. A. Pople. Self-consistent molecular-orbital methods. XII. Further extensions of gaussian-type basis sets for use in molecular orbital studies of organic molecules. *J. Chem. Phys.*, 56:2257, 1972.

[47] J. S. Binkley, J. A. Pople, and W. J. Hehre. Self-consistent molecular orbital methods. 21. Small split-valence basis sets for first-row elements. *J. Am. Chem. Soc.*, 102:939, 1980.

[48] R. Krishnan, J. S. Binkley, R. Seeger, and J. A. Pople. Self-consistent molecular orbital methods. XX. A basis set for correlated wave functions. *J. Chem. Phys.*, 72:650, 1980.

[49] W. J. Pietro, M. M. Francl, W. J. Hehre, D. J. Defrees, J. A. Pople, and J. S. Binkley. Self-consistent molecular orbital methods. 24. Supplemented small split-valence basis sets for second-row elements. *J. Am. Chem. Soc.*, 104:5039, 1982.

[50] M. J. Frisch, J. A. Pople, and J. S. Binkley. Self-consistent molecular-orbital methods. XXV: Supplementary Functions for Gaussian Basis Sets. *J. Chem. Phys.*, 80:3265, 1984.

[51] J. A. Pople, M. Head-Gordon, D. J. Fox, K. Raghavachari, and L. A. Curtiss. Gaussian-1 theory: A general procedure for prediction of molecular energie. *J. Chem. Phys.*, 90:5622, 1989.

[52] W. Kohn. Theory of the insulating state. *Phys. Rev.*, 133:A171, 1964.

[53] P. Hohenberg and W. Kohn. Inhomogeneous electron gas. *Phys. Rev.*, 136:B864, 1964.

[54] W. Kohn and L. J. Sham. Self-consistent equations including exchange and correlation effects. *Phys. Rev.*, 140:A1133, 1965.

[55] W. Kohn. Density functional/wannier function theory for systems of very many atoms. *Chem. Phys. Lett.*, 208:167–172, 1993.

[56] R. Marcelin. *J. de Chim. Phys.*, 10:1913, 1913.

[57] K. J. Laidler. Just what is a transition state? *J. Chem. Educ.*, 65:540, 1988.

[58] M. Rodríguez-Mayorga, E. Ramos-Cordoba, P. Salvador, M. Solà, and E. Matito. Bonding description of the harpoon mechanism. *Mol. Phys.*, 114:1345, 2016.

[59] P. A. M. Dirac. Quantum mechanics of many-electron systems. *Proc. Roy. Soc. A*, 123:714, 1929.

[60] S. K. Berberian, J. Sánchez-Guillén, and A. Plans. *Introducción al espacio de Hilbert*. Teide, Barcelona, 1977.

[61] J. C. Slater. The theory of complex spectra. *Phys. Rev.*, 34:1293, 1929.

[62] J. C. Slater. A Simplification of the Hartree-Fock Method. *Phys. Rev.*, 81:385, 1951.

[63] P.-O. Löwdin. Quantum theory of many-particle systems. i. physical interpretations by means of density matrices, natural spin-orbitals, and convergence problems in the method of configurational interaction. *Phys. Rev.*, 97:1474, 1955.

[64] J. A. Pople and J. S. Binkley. Correlation energies for AHn molecules and cations. *Mol. Phys.*, 29:599, 1975.

[65] P.-O. Löwdin. The historical development of the electron correlation problem. *Int. J. Quant. Chem.*, 55:77, 1995.

[66] I. N. Levine. *Quantum chemistry*, volume 5. Prentice Hall Upper Saddle River, NJ, New Jersey, 2000.

[67] T. Helgaker, P. Jorgensen, and J. Olsen. *Molecular Electronic Structure Theory*. Wiley, Chichester, 2000.

[68] A. Szabo and N. S. Ostlund. *Modern quantum chemistry: introduction to advanced electronic structure theory*. Courier Corporation, New York, 2012.

[69] M. Via-Nadal, M. Rodríguez-Mayorga, and E. Matito. Salient signature of van der waals interactions. *Phys. Rev. A*, 96:050501, 2017.

[70] M. Via-Nadal, M. Rodríguez-Mayorga, E. Ramos-Cordoba, and E. Matito. Singling out weak and strong correlation. (submitted).

[71] E. Schrödinger. Quantisierung als eigenwertproblem. *Ann. d. Physik*, 385:437, 1926.

[72] C. Møller and M. S. Plesset. Note on an approximation treatment for many-electron systems. *Phys. Rev.*, 46:618, 1934.

[73] P. Jurečka, J. Šponer, J. Černỳ, and P. Hobza. Benchmark database of accurate (MP2 and CCSD (T) complete basis set limit) interaction energies of small model complexes, DNA base pairs, and amino acid pairs. *Phys. Chem. Chem. Phys.*, 8:1985, 2006.

[74] A. K. Dutta, F. Neese, and R. Izsák. Accelerating the coupled-cluster singles and doubles method using the chain-of-sphere approximation. *Mol. Phys.*, 116:1428, 2018.

[75] K. Burke and friends. *The ABC of DFT*. Department of Chemistry, University of California, Irvine, California, 2007.

[76] E. K. U. Gross and R. M. Dreizler. *Density functional theory*, volume 337. Springer Science & Business Media, Wurzburg, Germany, 2013.

[77] W. Koch and M. C. Holthausen. *A chemist's guide to density functional theory*. John Wiley & Sons, Marburg, Germany, 2015.

[78] M. Solà and J. M. Ugalde. *Quantum Chemistry Methods: II Density Functional Theory. Theoretical and Computational Chemistry: Foundations, Methods and Techniques, J. Andrés and J. Bertrán.* Publicacions de la Universitat Jaume I, Castelló de la Plana, 2007.

[79] N. Mardirossian and M. Head-Gordon. Thirty years of density functional theory in computational chemistry: an overview and extensive assessment of 200 density functionals. *Mol. Phys.*, 115:2315, 2017.

[80] J. Sun, A. Ruzsinszky, and J. P. Perdew. Strongly constrained and appropriately normed semilocal density functional. *Phys. Rev. Lett.*, 115:036402, 2015.

[81] Y. Zhao and D. G. Truhlar. A density functional that accounts for medium-range correlation energies in organic chemistry. *Org. lett.*, 8:5753, 2006.

[82] Y. Zhao and D. G. Truhlar. Density functionals with broad applicability in chemistry. *Acc. Chem. Res.*, 41:157, 2008.

[83] Y. Zhao and D. G. Truhlar. The M06 suite of density functionals for main group thermochemistry, thermochemical kinetics, noncovalent interactions, excited states, and transition elements: two new functionals and systematic testing of four M06-class functionals and 12 other functionals. *Theor. Chim. Acta (Berlin)*, 120:215, 2008.

[84] M. G. Medvedev, I. S. Bushmarinov, J. Sun, J. P. Perdew, and K. A. Lyssenko. Density functional theory is straying from the path toward the exact functional. *Science*, 355:49, 2017.

[85] M. Rodriguez-Mayorga. Improved hybrid functionals for an accurate description of doublet-quartet splitting in three-electron harmonium atom. Master's thesis, Univ. Girona, Girona, September 2013.

[86] N. R. Kestner and O. Sinanoglu. Study of electron correlation in helium-like systems using an exactly soluble model. *Phys. Rev.*, 128:2687, 1962.

[87] T. L. Gilbert. Hohenberg-Kohn theorem for nonlocal external potentials. *Phys. Rev. B*, 12:2111, 1975.

[88] R. A. Donnelly and R. G. Parr. Elementary properties of an energy functional of the first-order reduced density matrix. *J. Chem. Phys.*, 69:4431, 1978.

[89] M. Levy. Universal variational functionals of electron densities, first-order density matrices, and natural spin-orbitals and solution of the v-representability problem. *Proc. Natl. Acad. Sci. USA*, 76:6062, 1979.

[90] S. M. Valone. Consequences of extending 1-matrix energy functionals from pure–state representable to all ensemble representable 1 matrices. *J. Chem. Phys.*, 73:1344, 1980.

[91] D. A. Mazziotti. Variational two-electron reduced density matrix theory for many-electron atoms and molecules: Implementation of the spin- and symmetry-adapted T 2 condition through first-order semidefinite programming. *Phys. Rev. A*, 72:032510, 2005.

[92] A. J. Coleman and V. I. Yukalov. *Reduced density matrices: Coulson's challenge*, volume 72. Springer Verlag, Berlin, 2000.

[93] F. Colmenero, C. Perez del Valle, and C. Valdemoro. Approximating q-order reduced density matrices in terms of the lower-order ones. I. General relations. *Phys. Rev. A*, 47:971, 1993.

[94] F. Colmenero and C. Valdemoro. Approximating q-order reduced density matrices in terms of the lower-order ones. II. Applications. *Phys. Rev. A*, 47:979, 1993.

[95] F. Colmenero and C. Valdemoro. Self-consistent approximate solution of the second-order contracted Schrödinger equation. *Int. J. Quant. Chem.*, 51:369, 1994.

[96] C. Valdemoro, L. M. Tel, and E. Pérez-Romero. The contracted Schrödinger equation: some results. *Adv. Quant. Chem.*, 28:33, 1997.

[97] D. A. Mazziotti. Contracted Schrödinger equation: Determining quantum energies and two-particle density matrices without wave functions. *Phys. Rev. A*, 57:4219, 1998.

[98] C. Valdemoro, L. M. Tel, and E. Pérez-Romero. Critical questions concerning iterative solution of the contracted Schrödinger equation. In *Many-Electron Densities and Reduced Density Matrices*. Springer, 2000.

[99] D. A. Mazziotti. Anti-Hermitian contracted Schrödinger equation: Direct determination of the two-electron reduced density matrices of many-electron molecules. *Phys. Rev. Lett.*, 97:143002, 2006.

[100] J. Cioslowski, M. Piris, and E. Matito. Robust validation of approximate 1-matrix functionals with few-electron harmonium atoms. *J. Chem. Phys.*, 143(21):214101, 2015.

[101] V. N. Staroverov and G. E Scuseria. Assessment of simple exchange-correlation energy functionals of the one-particle density matrix. *J. Chem. Phys.*, 117:2489, 2002.

[102] F. Feixas, M. Solà, J. M. Barroso, J. M. Ugalde, and E. Matito. New Approximation to the Third-Order Density. Application to the Calculation of Correlated Multicenter Indices. *J. Chem. Theory Comput.*, 10:3055, 2014.

[103] F. Feixas, M. Rodríguez-Mayorga, E. Matito, and M. Solà. Three-center bonding analyzed from correlated and uncorrelated third-order reduced density matrices. *Comput. Theor. Chem.*, 1053:173, 2015.

[104] M. García-Revilla, E. Francisco, A. Costales, and A. M. Pendás. Performance of the density matrix functional theory in the quantum theory of atoms in molecules. *J. Phys. Chem. A*, 116:1237, 2012. ibid, 9216 (2012).

[105] R. McWeeny. *Methods of Molecular Quantum Mechanics*. Academic Press, London, second edition, 1989.

[106] A. Pais. Max Born's statistical interpretation of quantum mechanics. *Science*, 218:1193, 1982.

[107] A. J. Coleman. Structure of Fermion Density Matrices. *Rev. Mod. Phys.*, 35:668, 1963.

[108] G. N. Lewis. The Atom and the Molecule. *J. Am. Chem. Soc.*, 38:762, 1916.

[109] R. F. W. Bader and T. T. Nguyen-Dang. Quantum Theory of Atoms in Molecules –Dalton Revisited. In *Advances in Quantum Chemistry*, volume 14, pages 63–124. Academic Press, New York, 1981.

[110] R. F. W. Bader and M. E. Stephens. Fluctuation and correlation of electrons in molecular systems. *Chem. Phys. Lett.*, 26:445, 1974.

[111] R. F. W. Bader. Molecular Fragments or Chemical Bonds? *Acc. Chem. Res.*, 8:34, 1975.

[112] R. F. W. Bader and M. E. Stephens. Spatial localization of the electronic pair and number distributions in molecules. *J. Am. Chem. Soc.*, 97:7391–7399, 1975.

[113] X. Fradera, M. A. Austen, and R. F. W. Bader. The Lewis Model and Beyond. *J. Phys. Chem. A*, 103:304, 1999.

[114] X. Fradera, J. Poater, S. Simon, M. Duran, and M. Solà. Electron-pairing analysis from localization and delocalization indices in the framework of the atoms-in-molecules theory. *Theor. Chem. Acc.*, 108:214, 2002.

[115] E. Matito, M. Solà, P. Salvador, and M. Duran. Electron sharing indexes at the correlated level. application to aromaticity calculations. *Faraday Discuss.*, 135:325–345, 2007.

[116] R. F. W. Bader. Binding Regions in Polyatomic Molecules and Electron Density Distributions. *J. Am. Chem. Soc.*, 86:5070, 1964.

[117] I. Mayer. Charge, Bond Order, and Valence in the ab initio SCF Theory. *Chem. Phys. Lett.*, 97:270, 1983.

[118] K. C. Mundim, M. Giambiagi, and M. S. de Giambiagi. Multicenter Bond Index: Grassmann Algebra and N-Order Density Functional. *J. Phys. Chem.*, 98:6118, 1994.

[119] Michael George Bulmer. *Principles of statistics*. Courier Corporation, Oxford, 1979.

[120] A. D. Becke and K. E. Edgecombe. A simple mesure of electron localization in atomic and molecular systems. *J. Chem. Phys.*, 92:5397, 1990.

[121] A. D. Becke. Hartree–Fock exchange energy of an inhomogeneous electron gas. *Int. J. Quant. Chem.*, 23:1915, 1983.

[122] C. A. Coulson and A. H. Neilson. Electron correlation in the ground state of helium. *Proc. Phys. Soc. London*, 78:831, 1961.

[123] A. Savin. A combined density functional and configuration interaction method. *Int. J. Quant. Chem.*, 34:59, 1988.

[124] J. Toulouse, I. C. Gerber, G. Jansen, A. Savin, and J. G. Angyán. Adiabatic-connection fluctuation-dissipation density-functional theory based on range separation. *Phys. Rev. Lett.*, 102:096404, 2009.

[125] M. A. Buijse. *Thesis: Electron Correlation. Fermi and Coulomb holes, dynamical and nondynamical correlation*. PhD thesis, Vrije Universiteit, Amsterdam, The Netherlands, 1991.

[126] E. J. Baerends and O. V. Gritsenko. A quantum chemical view of density functional theory. *J. Phys. Chem. A*, 101:5383, 1997.

[127] A. J. Thakkar and V. H. Smith Jr. Form factors and total scattering intensities for the helium-like ions from explicitly correlated wavefunctions. *J. Phys. B: Atom. Molec. Phys.*, 11:3803, 1978.

[128] A. J. Thakkar, A. N. Tripathi, and V. H. Smith. Anisotropic electronic intracule densities for diatomics. *Int. J. Quant. Chem.*, 26:157, 1984.

[129] A. J. Thakkar, A. N. Tripathi, and V. H. Smith. Molecular x-ray- and electron-scattering intensities. *Phys. Rev. A*, 29:1108, 1984.

[130] M. Plancherel and M. Leffler. Contribution à l̆étude de la représentation d'une fonction arbitraire par des intégrales définies. *Rendiconti del Circolo Matematico di Palermo (1884-1940)*, 30:289, 1910.

[131] J. B. M. Uffink and J. Hilgevoord. New bounds for the uncertainly principle. *Physics Letters A*, 105:176, 1984.

[132] W. Beckner. Inequalities in Fourier analysis. *Ann. of Math.*, page 159, 1975.

[133] I. Bialynicki-Birula and J. Mycielsky. Uncertainty relations for information entropy in wave mechanics. *Commun. Math. Phys.*, 44:129, 1975.

[134] D. A. Mazziotti. Structure of fermionic density matrices: complete n-representability conditions. *Phys. Rev. Lett.*, 108:263002, 2012.

[135] A. A. Klyachko. Quantum marginal problem and N-representability. In *Journal of Physics: Conference Series*, volume 36, page 72. IOP Publishing, 2006.

[136] I. Theophilou, N. N. Lathiotakis, M. A. L. Marques, and N. Helbig. Generalized Pauli constraints in reduced density matrix functional theory. *J. Chem. Phys.*, 142:154108, 2015.

[137] A. E. DePrince III. Variational optimization of the two-electron reduced-density matrix under pure-state N-representability conditions. *J. Chem. Phys.*, 145:164109, 2016.

[138] D. A. Mazziotti and R. M. Erdahl. Uncertainty relations and reduced density matrices: Mapping many-body quantum mechanics onto four particles. *Phys. Rev. A*, 63:042113, 2001.

[139] H. Nakatsuji. Equation for the direct determination of the density matrix. *Phys. Rev. A*, 14:41, 1976.

[140] K. Yasuda and H. Nakatsuji. Direct determination of the quantum-mechanical density matrix using the density equation. II. *Phys. Rev. A*, 56:2648–2657, 1997.

[141] M. Ehara, M. Nakata, H. Kou, K. Yasuda, and H. Nakatsuji. Direct determination of the density matrix using the density equation: potential energy curves of HF, CH_4, BH_3, NH_3, and H_2O. *Chem. Phys. Lett.*, 305:483, 1999.

[142] M. Nakata, M. Ehara, K. Yasuda, and H. Nakatsuji. Direct determination of second-order density matrix using density equation: Open-shell system and excited state. *J. Chem. Phys.*, 112:8772, 2000.

[143] J. Cioslowski. *Many-electron densities and reduced density matrices.* Kluwer Academic, New York, 2000.

[144] B. Verstichel, H. van Aggelen, D. Van Neck, P. W. Ayers, and P. Bultinck. Variational determination of the second-order density matrix for the iso-electronic series of beryllium, neon, and silicon. *Phys. Rev. A*, 80:032508, 2009.

[145] M. Piris and J. Ugalde. Perspective on natural orbital functional theory. *Int. J. Quant. Chem.*, 114:1169, 2014.

[146] K. Pernal and K. J. H. Giesbertz. Reduced Density Matrix Functional Theory (RDMFT) and Linear Response Time-Dependent RDMFT (TD-RDMFT). *Top. Curr. Chem.*, 368:125, 2015.

[147] N. N. Lathiotakis, N. I. Gidopoulos, and N. Helbig. Size consistency of explicit functionals of the natural orbitals in reduced density matrix functional theory. *J. Chem. Phys.*, 132:084105, 2010.

[148] P.-O. Löwdin and H. Shull. Natural orbitals in the quantum theory of two-electron systems. *Phys. Rev.*, 101:1730–1739, 1956.

[149] K. Pernal and J. Cioslowski. Phase dilemma in density matrix functional theory. *J. Chem. Phys.*, 120:5987, 2004.

[150] S. Goedecker and C. J. Umrigar. Natural orbital functional for the many-electron problem. *Phys. Rev. Lett.*, 81:866, 1998.

[151] J. Cioslowski and K. Pernal. The ground state of harmonium. *J. Chem. Phys.*, 113:8434, 2000.

[152] K. J. H. Giesbertz and R. van Leeuwen. Long-range interactions and the sign of natural amplitudes in two-electron systems. *J. Chem. Phys.*, 139:104110, 2013.

[153] X. W. Sheng, Ł. M. Mentel, O. V. Gritsenko, and E. J. Baerends. A natural orbital analysis of the long range behavior of chemical bonding and van der Waals interaction in singlet H_2: The issue of zero natural orbital occupation numbers. *J. Chem. Phys.*, 138:164105, 2013.

[154] J. Cioslowski. Solitonic natural orbitals. *J. Chem. Phys.*, 148:134120, 2018.

[155] M. A. Buijse and E. J. Baerends. An approximate exchange-correlation hole density as a functional of the natural orbitals. *Mol. Phys.*, 100:401, 2002.

[156] A. M. K. Müller. Explicit approximate expression between reduced two- and one-particle density matrices. *Phys. Lett.*, 105A:446, 1984.

[157] I. Mitxelena, M. Piris, and M. Rodríguez-Mayorga. On the performance of natural orbital functional approximations in the Hubbard model. *J. Phys. Condens. Matter*, 29:425602, 2017.

[158] R. L. Fulton. Sharing of electrons in molecules. *J. Phys. Chem.*, 97:7516, 1993.

[159] I. Ruiz, E. Matito, F. J. Holguín-Gallego, E. Francisco, A. Martín Pendás, and T. Rocha-Rinza. Fermi and coulomb correlation effects upon the interacting quantum atoms energy partition. *Theor. Chem. Acc.*, 135:209, 2016.

[160] J. Cioslowski and K. Pernal. Constraints upon natural spin orbital functionals imposed by properties of a homogeneous electron gas. *J. Chem. Phys.*, 111:3396, 1999.

[161] E. H. Lieb and S. Oxford. Improved lower bound on the indirect Coulomb energy. *Int. J. Quant. Chem.*, 19:427, 1981.

[162] S. Sharma, J. K. Dewhurst, N. N. Lathiotakis, and E. K. U. Gross. Reduced density matrix functional for many-electron systems. *Phys. Rev. B*, 78:201103, 2008.

[163] E. Kamil, R. Schade, T. Pruschke, and P. E. Blöchl. Reduced density-matrix functionals applied to the Hubbard dimer. *Phys. Rev. B*, 93:085141, 2016.

[164] O. Gritsenko, K. Pernal, and E. J. Baerends. An improved density matrix functional by physically motivated repulsive corrections. *J. Chem. Phys.*, 122:204102, 2005.

[165] G. Csányi and T. A. Arias. Tensor product expansions for correlation in quantum many-body systems. *Phys. Rev. B*, 61:7348, 2000.

[166] G. Csányi, S. Goedecker, and T. A. Arias. Improved tensor-product expansions for the two-particle density matrix. *Phys. Rev. A*, 65:032510, 2002.

[167] M. A. L. Marques and N. N. Lathiotakis. Empirical functionals for reduced-density-matrix-functional theory. *Phys. Rev. A*, 77:032509, 2008.

[168] C. Kittel. *Quantum Theory of Solids*. John Wiley and sons, New York, 1963.

[169] J. Cioslowski and K. Pernal. Description of a homogeneous electron gas with simple functionals of the one-particle density matrix. *Phys. Rev. A*, 61:034503, 2000.

[170] R. Kubo. Generalized Cumulant Expansion Method. *J. Phys. Soc. Jpn.*, 17:1100, 1962.

[171] M. Piris, X. Lopez, and J. M. Ugalde. Dispersion interactions within the Piris natural orbital functional theory: The helium dimer. *J. Chem. Phys.*, 126:214103, 2007.

[172] M. Piris, J. M. Matxain, X. Lopez, and J. M. Ugalde. Communications: Accurate description of atoms and molecules by natural orbital functional theory. *J. Chem. Phys.*, 132:031103, 2010.

[173] M. Piris, J. M. Matxain, X. Lopez, and J. M. Ugalde. Communication: The role of the positivity N-representability conditions in natural orbital functional theory. *J. Chem. Phys.*, 133:111101, 2010.

[174] M. Piris, X. Lopez, F. Ruipérez, J. M. Matxain, and J. M. Ugalde. A natural orbital functional for multiconfigurational states. *J. Chem. Phys.*, 134:164102, 2011.

[175] M. Piris. Interacting pairs in natural orbital functional theory. *J. Chem. Phys.*, 141:044107, 2014.

[176] M. Piris. A Global Method For The Electron Correlation. *Phys. Rev. Lett.*, 119:063002, 2017.

[177] H. Grassmann. *Die lineale Ausdehnungslehre ein neuer Zweig der Mathematik: dargestellt und durch Anwendungen auf die übrigen Zweige der Mathematik, wie auch auf die Statik, Mechanik, die Lehre vom Magnetismus und die Krystallonomie erläutert.* Cambridge University Press, 2012.

[178] D. A. Mazziotti. Comparison of contracted Schrödinger and coupled-cluster theories. *Phys. Rev. A*, 60:4396, 1999.

[179] H. Nakatsuji and K. Yasuda. Direct determination of the quantum-mechanical density matrix using the density equation. *Phys. Rev. Lett.*, 76:1039, 1996.

[180] J. Cioslowski and K. Strasburger. Harmonium atoms at weak confinements: The formation of the Wigner molecules. *J. Chem. Phys.*, 146:044308, 2017.

[181] E. Santos. Cálculo aproximado de la energía de correlación entre dos electrons. *An. R. Soc. Esp. Fís. Quím.*, 64:117, 1968.

[182] M. Taut. Two electrons in an external oscillator potential: Particular analytic solutions of a coulomb correlation problem. *Phys. Rev. A*, 48:3561, 1993.

[183] P.-F. Loos and P. M. Gill. A tale of two electrons: Correlation at high density. *Chem. Phys. Lett.*, 500:1, 2010.

[184] M. Rodríguez-Mayorga, E. Ramos-Cordoba, M. Via-Nadal, M. Piris, and E. Matito. Comprehensive benchmarking of density matrix functional approximations. *Phys. Chem. Chem. Phys.*, 19:24029, 2017.

[185] M. Rodríguez-Mayorga, E. Ramos-Cordoba, F. Feixas, and E. Matito. Electron correlation effects in third-order densities. *Phys. Chem. Chem. Phys.*, 19:4522, 2017.

[186] J. Cioslowski and E. Matito. Benchmark Full Configuration Interaction Calculations on the Lowest-Energy 2P and 4P States of the Three-Electron Harmonium Atom. *J. Chem. Theory Comput.*, 7:915, 2011.

[187] J. Cioslowski, K. Strasburger, and E. Matito. The three-electron harmonium atom: The lowest-energy doublet and quadruplet states. *J. Chem. Phys.*, 136:194112, 2012.

[188] J. Cioslowski, K. Strasburger, and E. Matito. Benchmark calculations on the lowest-energy singlet, triplet, and quintet states of the four-electron harmonium atom. *J. Chem. Phys.*, 141:044128, 2014.

[189] E. Matito, J. Cioslowski, and S. F. Vyboishchikov. Properties of harmonium atoms from FCI calculations: Calibration and benchmarks for the ground state of the two-electron species. *Phys. Chem. Chem. Phys.*, 12:6712, 2010.

[190] E. Matito, M. Solà, M. Duran, and J. Poater. Comment on the "Nature of Bonding in the Thermal Cyclization of (Z)-1,2,4,6-Heptatetraene and Its Heterosubstituted Analogues". *J. Phys. Chem. B*, 109:7591, 2005.

[191] F. Feixas, J. Vandenbussche, P. Bultinck, E. Matito, and M. Solà. Electron delocalization and aromaticity in low-lying excited states of archetypal organic compounds. *Phys. Chem. Chem. Phys.*, 13:20690, 2011.

[192] F. Feixas, E. Matito, J. Poater, and M. Solà. Understanding Conjugation and Hyperconjugation from Electronic Delocalization Measures. *J. Phys. Chem. A*, 115:13104, 2011.

[193] F. Feixas, J. O. C. Jiménez-Halla, E. Matito, J. Poater, and M. Solà. A Test to Evaluate the Performance of Aromaticity Descriptors in All-Metal and Semimetal Clusters. An Appraisal of Electronic and Magnetic Indicators of Aromaticity. *J. Chem. Theory Comput.*, 6:1118, 2010.

[194] F. Feixas, E. Matito, J. Poater, and M. Solà. Metalloaromaticity. *WIREs, Comput. Mol. Sci.*, 3:105, 2013.

[195] F. Feixas, E. Matito, J. Poater, and M. Solà. Quantifying aromaticity with electron delocalisation measures. *Chem. Soc. Rev.*, 44:6389, 2015.

[196] I. Casademont-Reig, T. Woller, J. Contreras-García, M. Alonso, M. Torrent-Sucarrat, and E. Matito. New electron delocalization tools to describe the aromaticity in porphyrinoids. *Phys. Chem. Chem. Phys.*, 20:2787, 2018.

[197] F. Feixas, E. Matito, J. Poater, F. Maseras, and M. Solà. Agostic bonding. (unpublished).

[198] P. L. A. Popelier. On the full topology of the Laplacian of the electron density. *Coord. Chem. Rev.*, 197:169, 2000.

[199] J. Cioslowski and E. Matito. Note: The weak-correlation limit of the three-electron harmonium atom. *J. Chem. Phys.*, 134:116101, 2011.

[200] R. Ponec and I. Mayer. Investigation of some properties of multicenter bond indices. *J. Phys. Chem. A*, 101:1738, 1997.

[201] J. M. Herbert and J. E. Harriman. N-representability and variational stability in natural orbital functional theory. *J. Chem. Phys.*, 118:10835, 2003.

[202] M. Piris. A natural orbital functional based on an explicit approach of the two-electron cumulant. *Int. J. Quant. Chem.*, 113:620, 2013.

[203] Y. Tal and J. Katriel. Some unusual electronic precorrelation and correlation effects in the $^{1,3}\Pi_u$ states of the hydrogen molecule. *J. Phys. B*, 7:2113, 1974.

[204] E. A. Colbourn. The interelectronic distribution in the lowest ^{1,3} Π_u states of H_2. *J. Phys. B*, 8:1926, 1975.

[205] M. Piris, X. Lopez, and J. M. Ugalde. Electron-pair density relaxation holes. *J. Chem. Phys.*, 128:214105, 2008.

[206] R. P. Feynman. Forces in molecules. *Phys. Rev.*, 56:340, 1939.

[207] E. M. A. Peixoto, C. F. Bunge, and R. A. Bonham. Elastic and inelastic electron scattering by He and Ne atoms in their ground states. *Phys. Rev.*, 181:322, 1969.

[208] J. Cioslowski and G. Liu. Electron intracule densities and coulomb holes from energy-derivative two-electron reduced density matrices. *J. Chem. Phys.*, 109:8225, 1998.

[209] K. Ruedenberg, R. C. Raffenetti, and R. D. Bardo. Energy, structure and reactivity. In *Proceedings of the 1972 Boulder Seminar Research Conference on Theoretical Chemistry*, page 164. Wiley: New York, 1973.

[210] C. F. Bunge and E. M. A. Peixoto. Electronic Wave Functions for Atoms. IV. Ground State of Ne. *Phys. Rev. A*, 1:1277, 1970.

[211] J. Kobus. A finite difference Hartree-Fock program for atoms and diatomic molecules. *Comput. Phys. Commun.*, 184:799, 2013.

[212] M. Kohout. Occupation numbers for atomic shells in direct space bounded by the maxima of the one-electron potential. *Int. J. Quant. Chem.*, 83:324, 2001.

[213] R. Ponec and D. L. Cooper. Anatomy of bond formation. bond length dependence of the extent of electron sharing in chemical bonds. *J. Mol. Struct. (Theochem)*, 727:133, 2005.